Elucidating the molecular mechanism of drug binding and translocation by the multidrug transporter ABCG2

Parth Kapoor

Thesis submitted to the University of Nottingham for the degree of Doctor of Philosophy

January 2020

Abstract

Many drug resistant tumours express one or more of the three main drug efflux transporters, P-glycoprotein (ABCB1), multidrug resistance protein 1 (MRP1; ABCC1) and breast cancer resistance protein (ABCG2). These transporters facilitate the export of diverse range of structurally unrelated compounds from the cell. ABCG2, is widely distributed in tissues, contributes towards normal physiology and pharmacokinetic profiles of many exogenous drugs. It is this promiscuous drug binding and transport that makes it an appealing target for research. The aim of this project is to better understand the molecular mechanism of multidrug binding and transport by ABCG2. Here we focus on two specific regions of the protein: transmembrane helix 3 (TM3) and the NBD: NBD (nucleotide binding domain) interface to elucidate their role in the function of ABCG2 transporter.

Earlier research associated residues R482 and P485 located within TM3 helix, with drug binding and/or transport. HEK293T stable cell lines for wild type protein and point mutants along the length of TM3 (residues D477- L497) were generated and characterized for cell surface expression using confocal microscopy and flow cytometry. The transport function of all mutants was investigated using flow cytometry to determine the efflux of three fluorescent substrates (mitoxantrone, pheophorbide A and daunorubicin). This revealed at least 16 isoforms of ABCG2 protein associated with altered transport for one of the three fluorescent substrates. The majority of the mutants showed reduced efflux for the fluorescent substrates mitoxantrone and pheophorbide A. D477A showed impaired efflux for pheophorbide A and M496A showed increased efflux for mitoxantrone. However, R482A showed significant gain in function for daunorubicin efflux, in accordance with the published literature, suggesting substrate specificity. Only three mutants altered both Mx and pheophorbide A transport, suggesting overlapping sites for substrate interaction. T490A showed altered phenotypic effects for mitoxantrone and pheophorbide A transport, indicating the importance of drug specific interactions. The recognition and transport mechanism is distinct for daunorubicin compared to mitoxantrone and pheophorbide A. On the basis of these results we hypothesise TM3 helix as a putative gatekeeper for hydrophobic substrates. We propose a tentative drug recognition/transport mechanism at a groove site, involving potential interactions with

TM3 residues by means of molecular docking, thereby reinstating the importance of TM3 in substrate recognition and translocation.

The structural revolution for ABCG2 and its related family members (ABCG5/G8) enabled us to focus on the NBDs close contact interface. The structures revealed two interfaces between the NBDs, one being the canonical ATP sandwich dimer interface and the other, a unique constant contact interface at the NPXDF motif and in its close proximity. We explore the importance of this unique NBD interface motif and some surrounding residues of ABCG2 in forming a closed conformation at the cytoplasmic interface between the NBD: NBD interface. Point mutations at this interface showed altered drug specificity (E285K), altered drug transport (E285K, D292A and D292K) and loss of ATPase activity (E285K, D292A and D292K). The study demonstrates the importance of this interface with impact on local NBD events (ATP hydrolysis) and allosteric communication to the transmembrane domains and drug transport.

This research forms the basis to further investigate substrate and inhibitor binding of ABGC2 using complementary techniques such as fluorescence correlation spectroscopy, microscale thermophoresis and carbene footprinting - mass spectrometry in order better understand its mechanistic details and potentially lead to therapeutic approaches towards drug resistant cancers.

Papers published

Papers published during the course of this PhD study:

Research papers:

Kapoor, P., Briggs, D.A., Cox, M.H., Kerr, I.D., 2020. Disruption of the unique ABCG-family NBD:NBD interface impacts both drug transport and atp hydrolysis. Int. J. Mol. Sci.

Cox, M.H., Kapoor, P., Briggs, D.A., Kerr, I.D., 2018. Residues contributing to drug transport by ABCG2 are localised to multiple drug-binding pockets. Biochem. J. 475, 1553–1567.

Review articles:

Heyes, N., Kapoor, P., Kerr, I.D., 2018. Polymorphisms of the Multidrug Pump ABCG2: A Systematic Review of Their Effect on Protein Expression, Function, and Drug Pharmacokinetics. Drug Metab. Dispos. 46, 1886–1899.

Kapoor, P., Horsey, A.J., Cox, M.H., Kerr, I.D., 2018. ABCG2: does resolving its structure elucidate the mechanism? Biochem. Soc. Trans. 46, 1485–1494.

Declaration

The thesis entitled, “Elucidating the molecular mechanism of drug binding and translocation by the multidrug transporter ABCG2”, is the result of my own work undertaken during my period of registration at the University of Nottingham under the supervision of Dr Ian Kerr.

Parth Kapoor
Student ID: 4247012
January 2020

Acknowledgement

Pursuing a PhD degree at the University of Nottingham has been a life changing experience for me, main reason behind this is being a part of such a positive and enthusiastic group. I would like to express my sincere gratitude to my supervisor Dr. Ian Kerr, under whose guidance I have been able to sail through the ups and downs of my PhD life with ease. I have been grateful and fortunate to have such a brilliant, encouraging mentor through the most integral part of my career development, which I shall cherish throughout my life. I would like to thank him for believing in me and supporting me, while always pushing me to succeed. His immense support, not just professionally but also personally in the most difficult phase of my life and making sure that I am alright has touched me deeply. I would also like to thank him for allowing me to move on in my career during the writing phase and supporting me through the transition period. I would also like to acknowledge Prof. Robert Layfield, my second supervisor for being there for me and guiding me through. I also offer my deepest gratitude to the University of Nottingham Vice Chancellor's scholarship for allowing me to pursue my reach career at the University.

The other best part of being in such an amazing lab is to be able to understand the importance of a lab fairy or rather lab mommy; Deborah Briggs. No words can describe the generosity and care with which she has nurtured this lost soul in the lab. She truly is magical and still amazes me with the ease with which she gets anything and everything to work. Well, all thanks to the golden touch or magical fingers. My PhD would not have been possible without her valuable contribution towards its development. How can I not mention Will and Milo, the cute little munchkins. They are amazing. A big thank you to her and Jon for standing by me in my most difficult times. Thank you for the lovely trips to Oxford and Cirencester and many more to come along with some botheration.

I have been honoured to share my PhD life with Aaron Horsey and Megan Cox. Our long walks and coffee journeys have been immense part of our PhD life. It is a great bond that we have developed over the years that will last a lifetime. Thank you both for being there and helping me through my PhD. It has been a pleasure to work and build a good friendship with Simon Caulton. He is an amazing person at heart and

genuinely cares for you. Though we barely got to know each other over short span of time but the friendship developed for a lifetime, more with his cute son, precisely. He is lovely.

I would like to thank our true lab fairies- Sue and Carol, both are genuinely caring and helpful. I would also like to thank David Onion, Nicola Croxall (Flow Cytometry Facility), and Tim Self, Seema Rajani (School of Life Sciences Imaging facility) for giving me their valuable time, advice and training on relevant equipment. I would also like to thank Dr. Alistair Hume (UoN), Dr. Sally Wheatley (UoN) and Dr. Claire Friel (UoN) for allowing me to work in their labs and use their reagents and equipment. I would also like to thank Dr. Csilla Ozvegy Laczka (Hungarian Academy of Sciences) for the collaborative work in insect cells.

I would also like to thank Alex Rathbone, Sonali Singh and Dan Scott for their immense guidance and support through my PhD career. The never-ending tissue culture and office talks with them have been valuable.

I would like to thank the members of Kerr lab, James Mitchell and Hannan. Our lovely lunches together over period of few months have been amazing and it has been a pleasure to know and work with you both.

A special mention to the laughter bomb of our floor, Hannah Jackson. Thank you for being there always and a big shout out to your mom for the delicious food. Thank you for being a special friend. Our nonstop chats in your warm office have been amazing. I am glad to have met you as a true friend here. Cherish forever. I know I will always have your back.

A big thank you to my supporting family and extended family for being there in the most difficult phase. I would like to dedicate this PhD to my amazing dad, my champ. Dad, your dream is almost there, hope you are happy and content. Need your blessings and continuous support. Losing you, grandad and our family dog (my baby Casper) during this time completely shattered me and not even one day has gone by when I have not thought about you, but I am trying to achieve what we had thought about our stable future. Hopefully I take care of everybody and become the humble, kind and generous person that you were. I really miss you and love you to bits. A big thank you to my grandmom, mom, Kabir (lovely brother) and my aunt (Neelam Bhatia) without whom I wouldn't have been able to reach here in life. Lots of love to the new bundle of joy in the family, Archie. They all have been instrumental in teaching me in every step of my life. Lots of love and a big thank you to my amazing aunt Dr. Jyotsna

Chander. She and her family have been kind and have made me a part of their lovely family. They have always made me feel comfortable and at home. She truly has been a god mother in this new world for me. Lots of love to my elder sister (Smiti Talwar) and her family for being there for me. My trips to Ireland will finally start.

Lastly, I would like to thank all my friends, especially Nishtha Gulati (and her lovely family) for being there for me in every step of the way and putting up with me through the difficult phase in life and thesis writing. I know I will always have your back, come what may. Thank you for the special bond we share and have started to build for our future. Also, Samarth, for supporting and guiding me through my PhD life. I truly look up to his hard work and dedication. Special mention here goes to my childhood friend Ashmeet Singh (and his loving family), who has been instrumental in showing me the way forward and always aiming for a better life in future. His continuous support has been my key strength throughout. Lastly, Rudra Dutta (and his lovely family) has been more than a brother to me, and his continuous support and faith throughout has been key.

I would like to thank people from my workplace, OMass therapeutics for allowing me to work and write my PhD thesis at the same time.

Abbreviations

ABC	ATP binding cassette transporters
ABCB1	ATP binding cassette transporter B family
ABCC1	ATP binding cassette transporter C family
ABCG2	ATP binding cassette transporter G subfamily
ABCP	Human placenta-specific ATP-binding cassette gene
AcMNPV polyhedrin (PH)	*Autographa californica* nuclear polyhedrosis virus
ADE	Absorption, distribution and elimination
ADP	Adenosine diphosphate
AdrVp	
AHR	Aryl hydrocarbons
AML	Acute myeloid leukaemia
ATP	Adenosine triphosphate
BCRP	Breast cancer resistance protein
BIIC	Baculovirus infected insect cells
CFTR	Cystic fibrosis transmembrane conductance regulator
CMV	Cytomegalovirus
CO_2	Carbon dioxide
DLS	Dynamic light scattering
DMEM	Dulbecco's Modified Eagle Medium
DMSO	Dimethyl sulfoxide
DMPC	1, 2-Dimethyl-sn-glycero-3-phosphocholine
DNR	Daunorubicin
E_1S	Estrone-1- sulfate
EGF	Epidermal growth factor
EM	Electron microscopy
ERK1/2	extracellular signal-regulated kinases
ER	Endoplasmic reticulum
FCS	Foetal calf serum
FCS	Fluorescence Correlation Spectroscopy
FGF	fibroblast growth factors
FS	Forward scatter
GAPDH	Glyceraldehyde 3- phosphate dehydrogenase
GFP	Green fluorescent protein
HBSS	Hank's balanced salt solution
HEK	Human embryonic kidney cells
HisP	Histidine permease
Hly	Haemolysin
HSP90	heat shock protein 90
IOV	Inside out vesicles
JAK3	Janus kinase 3
LB	Luria-Bertoni

LY	Lucifer yellow
m-AB	Monoclonal antibody
MAPK	A mitogen-activated protein kinase
MATE	Multidrug and toxic compound extrusion
MBP	Maltose binding protein
MCF-7	Michigan Cancer Foundation-7
MDCKII	Madin-Darby canine kidney cell line
MDR1	Multidrug resistance protein 1
MEK1/2	Mitogen-activated protein kinase kinase
MGMT	O-6-methylguanine- DNA methyltransferase (MGMT) - mediated temozolomide resistance
MRE	Mirna response element
MRP	Membrane resistance protein
MST	Microscale thermophoresis
MβCD	Methyl-β cyclodextrin
Mx	Mitoxantrone
NBD	Nucleotide binding domain
NSCLC	Non-small-cell lung carcinoma
O_2	Oxygen
OAT	Organic anion transporter
OATP	Organic anion transporter polypeptide
OCT	Organic cation transporter
PBS	Phosphate buffered saline
PCH	Photon counting histogram
PCR	Polymerase chain reaction
PEI	Polyethylenimine
P-gp	P glycoprotein
PheoA	Pheophorbide A
PH	Polyhedrin
PhIP	Phenylimidazo (4,5-b) pyridine
Pi	Orthophosphate
Pim-1	Proto-Oncogene, Serine/Threonine Kinase
PMTs	Photomultiplying tubes
PRA	Prazosin
SAR	Structure activity relationship
SBE	Steroid binding element
SBP	Solute binding protein
SEM	Standard error mean
SDS	Sodium dodecyl sulphate
SDS-PAGE	Sodium dodecyl sulphate-Polyacrylamide gel electrophoresis
sf9	*Spodoptera fugiperda*
sfGFP	Superfolder GFP
SLC	Solute carriers
SS	Side scatter
SV40	Simian vacuolating virus 40

TAP	Transporter of antigenic peptides
TMD	Transmembrane domain
TMH	Transmembrane helices
TNF	Tumour necrosis factor
UDP	Uridine diphosphate
UTR	Untranslated regions
VTA	Vesicular transport assay
3D	3- dimensional

Table of Contents

Chapter 1: Introduction 1

1.1 Cell membrane 1

1.2 Transport across the membrane barrier 2

1.3 ABC transporters 4

1.4 ABC transporter domain organisation 5

1.5 Nucleotide Binding Domains (NBDs) 7

1.6 NBD crystal structure, dimer formation and ATP binding 7

1.7 Conserved NBD motifs 9

1.8 TMD topology of an ABC transporter 12

1.9 ABC transporter mechanism 14

1.10 Multidrug resistance and ABC transporters 17

1.11 Discovery of a multidrug resistance transporter: ABCG2 22

1.12 Molecular ABCG2 gene expression regulation 23

1.13 ABCG2 tissue distribution, sub-cellular localization and physiological role 25

1.14 ABCG2 pharmacology: substrates and inhibitors 27

1.15 Role of ABCG2 in multidrug resistance (MDR) 30

1.16 ABCG2 overall topology 31

1.17 Oligomerization state for a functional ABCG2 transporter 33

1.18 Molecular mechanism of ABCG2: do naturally occurring SNPs help? 34

1.19 Site directed mutagenesis 36

1.20 Multiple drug binding sites 39

1.21 Conformational change associated with ATP hydrolysis, drug binding and translocation by ABCG2 39

1.22 ABCG2 structure advances from past to current with the cryo-EM revolution . 40

1.23 Project Objectives and outlines 45

Chapter 2: Experimental design: methods 48

2.1 Molecular biology 48

2.1.1 Primer designing for site directed mutagenesis 48

2.1.2 Site directed mutagenesis 50

2.1.3 DpnI digestion 50

2.1.4 Transformation 50

2.1.5 Plasmid mini preparations and long-term storage of bacterial stocks 51

2.1.6 Restriction digestion, agarose gel electrophoresis and visualization of DNA 51

2.1.7 DNA Sequencing 52

2.2 ABCG2 expression in mammalian cells 52

2.2.1 Human embryonic Kidney cells maintenance (HEK293T cells) 52

2.2.2 Cell seeding 53

2.2.3 Polyethyleneimine (PEI) mediated transfection 53

2.2.4 Generation and maintenance of stable cell lines 54
2.2.5 Freezing cells for long term storage 54
2.2.6 Cell culture for membrane preparation, generation of crude membranes 55

2.3 ABCG2 protein expression: Sf9 cells 55
2.3.1 Generation and maintenance of insect cells 55
2.3.2 Insect cell infection 55
2.3.3 Preparation of BIIC stocks 56
2.3.4 Cell Viability 56
2.3.5 Cholesterol hemisuccinate doping 56

2.4 Protein expression: SDS PAGE and Western Blot 57

2.5 Live cell Imaging 59
2.5.1 Confocal plate reader-ImageXpress 59
2.5.2 Immunostaining and fixing mammalian cells 59

2.6 Membrane based assays 60
2.6.1 Preparation of crude membrane fractions 60
2.6.2 Vesicular transport assays 61
2.6.3 ATPase assay 62

2.7 Live cell assays 62
2.7.1 Flow cytometry, Drug efflux assays 62
2.7.2 Flow cytometry data analysis (Kaluza analysis version 1.5) 64
2.7.3 Data analysis 65
2.7.4 Cell surface expression 65
2.7.5 Data analysis using Kaluza 66
2.7.6 Mitoxantrone efflux assay in intact Sf9 cells 67

2.8 Molecular drug docking and visualisation 68

Chapter 3: Insect expression system as a model for heterologous production of ABCG2 70

3.1 Introduction 70

3.2 Optimising the heterologous expression system 72

3.3 Monitoring ABCG2 function in intact membrane vesicles 74

3.4 Monitoring ABCG2 function in Sf9 cells expressing ABCG2 78

3.5 Cholesterol and its role in potentiating activity in heterologous system 82

3.6 Summary and conclusion 87

Chapter 4: Generation, expression and localisation of transmembrane (TM) helix 3 mutant isoforms 89

4.1 Introduction 89

4.2 Plasmid construct 91

4.3 Generation of TM3 helix mutant isoforms 92

4.4 R482 and M496 case study- incorporation revealed by restriction enzyme digestion 93

4.5 Sequence analysis confirms all mutations 97

4.6 Generation of stable cell lines 98

4.7 Expression characterisation of TM3 helix mutant isoforms 100

4.8 Cell surface localisation and expression 101

4.9 Cell surface expression and localisation of ABCG2 mutant isoforms 104

4.10 Conclusion and summary 108

Chapter 5: Functional characterisation of ABCG2 mutant isoforms- role of transmembrane helix 3 in drug binding and/ or translocation 109

5.1 Introduction 109

5.2 Introduction to flow cytometry 110

5.3 Single cell ABCG2 expression profile using flow cytometry 113

5.4 Functional analysis of ABCG2 TM3 helix mutant isoforms- drug accumulation assays 115

5.5 Structural interpretation of the potential drug binding sites 126

5.6 Discussion and summary 129

Chapter 6: Importance of the highly conserved, unique NBD: NBD interface region in ABCG2 133

6.1 Introduction 133

6.2 Construct generation 137

6.3 Generation of stable cell lines for NBD interface mutants 137

6.4 Cell surface expression and localisation 138

6.5 Cell surface expression and localisation of NBD interface mutants using a two-channel spectrum 141

6.6 Defects in protein folding, trafficking affecting cellular localisation 143

6.7 Functional characterisation of NBD interface mutants 146

6.8 Functional characterisation of NBD interface mutants using the ATPase assay 150

6.9 Discussion and summary 154

Chapter 7: Discussion and future work 159

7.1 Summary of results 159

7.2 Structural interpretation of drug binding by ABCG2 161

7.3 Structural interpretation of drug transport by ABCG2 166

7.4 Deciphering the molecular mechanism of ABCG2 using purified protein 169

7.5 Conclusion 173

References 174

Appendices 207

List of Tables

Table 1.1: ABC transporter subtypes and their roles 5

Table 1.2: ABCG2 substrate repertoire 28

Table 1.3: ABCG2 inhibitors 28

Table 1.4: Site directed mutagenesis for key ABCG2 residues 38

Table 5.1: Potential fluorescent substrates used for drug efflux assays 117

Table 5.2: Relative efflux data- Ko143 inhibited transport of fluorescent drugs by TM3 mutant isoforms 123

Table 6.1: NBD interface Mutants 134

Table 6.2: Ko143 inhibited transport of fluorescent drugs by NBD interface mutant isoforms 150

List of Figures

Figure 1.1: Schematic representation of the fluid mosaic model 2
Figure 1.2: Schematic representation of core domain organisations of ABC transporters. 6
Figure 1.3: Structure of the MJ0796-E171Q ATP Sandwich Dimer interface……..……...8
Figure 1.4: Dimeric P-gp NBD showing conserved residues involved in ATP-binding..... 10
Figure 1.5: TM helical arrangement in ABC transporters..... 14
Figure 1.6: Schematic representation of an ATP switch model for an ABC exporter..... 15
Figure 1.7: Drug resistance in human cancer 18
Figure 1.8: The structure of recombinant human P-gp..... 19
Figure 1.9: Molecular architecture of bovine ABCC1 21
Figure 1.10: ABCG2 predicted and experimental membrane topology 32
Figure 1.11: ABCG2 structure resembles type II transporter fold 42
Figure 1.12: Structure of ABCG2 44
Figure 1.13: Cryo-EM structure of ABCG2 homodimer 46
Figure 1.14: Structural mapping of the highly conserved residues at the NBD: NBD interface..... 47
Figure 2.1: Analysis workflow for drug transport assays..... 65
Figure 2.2 : Flow cytometric analysis workflow for surface expression..... 67
Figure 2.3: Cryo-EM structure with the assigned brox for molecular drug docking studies..... 69
Figure 3.1: ABCG2 expression in mammalian and insect cell (Sf9) lines 71
Figure 3.2: Maximising the expression of ABCG2 in Sf9 cells by increased viral load..... 73
Figure 3.3: ABCG2 transport function monitored in intact crude membrane vesicles 76
Figure 3.4: Time course to monitor the impact of ABCG2 expression on cell viability..... 79
Figure 3.5: Functional analysis of Sf9 cells/Sf9 cells expressing ABCG2 to transport mitoxantrone: ABCG2- non functional 81
Figure 3.6: Addition of cholesterol does not restore ABCG2 transport 84
Figure 3.7: Effect of cholesterol doping on ABCG2 transporter functionality 85
Figure 3.8: Functional analysis of mammalian cells (HEK293T) expressing wild type protein ABCG2 88
Figure 4.1: TM3 helix residues mapped on ABCG2 structure……..90
Figure 4.2: pcDNA3.1Zeo_sfGFP_ABCG2 schematic plasmid map ..... .91
Figure 4.3: PvuII restriction digest profile of ABCG2 mutant isoforms..... 93
Figure 4.4: Confirmation of presence of R482A mutant isoform 95
Figure 4.5: Case study- M496A mutant isoform generation..... 96
Figure 4.6: Confirmation of the desired mutation using Sanger Sequencing..... 97

Figure 4.7: : Expression analysis for p3.1Zeo_sfGFP_ABCG2 transfected stable cell lines 99

Figure 4.8: Immunoblot analysis for ABCG2 expressed in HEK293T cells (wild type and mutant isoforms) 101

Figure 4.9: Cell surface localization of the ABCG2 isoforms..... 103

Figure 4.10: GFP expression as a reliable indicator of sfGFP_ABCG2 for cell surface expression.. 105

Figure 4.11: Cell surface expression for TM3 mutant isoforms using a two channel flow cytometry107

Figure 5.1: Schematic representation of the primary components of a flow cytometer 111

Figure 5.2: Flow cytometry gating parameters demonstrated for HEK293T cells expressing wild type ABCG2..... 112

Figure 5.3: GFP_ABCG2 expression levels vary across the mutant isoforms 114

Figure 5.4: Functional phenotypic effects observed by HEK293T cells expressing the mutant isoforms. 115

Figure 5.5: Functional analysis of ABCG2 variants-role in altered drug export capacity..... 120

Figure 5.6: TM3 helix mutant isoforms show altered phenotypic effects in drug transport..... 122

Figure 5.7: Phenotypic effects for altered function observed by the ABCG2 variant isoforms 125

Figure 5.8: Putative drug binding site identified in close proximity to TM3 helix 128

Figure 5.9: Cryo-EM structure of ABCG2 homodimer depicting M496 localisation within TM3 helix 131

Figure 6.1: Sequence alignment of the ABCG family..... 134

Figure 6.2: Structural intricacies of the NBD: NBD interface 136

Figure 6.3: Confirmation of the NBD interface mutants in the mammalian expression vector. 137

Figure 6.4: Generation of stable cell lines for NBD interface mutant isoforms 138

Figure 6.5: Expression of NBD interface mutant isoforms in HEK293T cells, probed using BXP-21 139

Figure 6.6: Cell surface localisation of NBD interface mutants..... 140

Figure 6.7: Cell surface expression for NBD interface mutant isoforms using a two-channel flow cytometry 142

Figure 6.8: Structural insight to N288D mutation……..……143

Figure 6.9: Trafficking defect observed for N288D mutant isoform compared to the wild type 146

Figure 6.10: Altered transport function in NBD interface mutants 147

Figure 6.11: NBD interface mutants show altered phenotypic effects in drug translocation 149

Figure 6.12: ABCG2 specific ATPase activity 152

Figure 6.13: ATPase activity for key NBD interface mutants with altered transport capacity 153

Figure 6.14: NBD close contact residue E285 and its potential intra and inter molecular interactions……...157

Figure 7.1: *In silico* docking studies reveal the potential substrate binding sites..... 163

Figure 7.2: Cryo-EM structure of ABCG2 with bound compounds in the central cavity (cavity 1).. 164

Figure 7.3: TM3 helix as a putative gatekeeper for hydrophobic drugs..... 165

Figure 7.4: ABCG2 catalytic cycle for drug translocation..... 168

Figure 7.5: ABCG2 SMA solubilisation and purification 170

Chapter 1: Introduction

1.1 Cell membrane

The plasma membrane forms a selectively permeable barrier between the cell membrane and extracellular environment (Watson, 2015). The current view on the structure and dynamics of bio-membranes is based on the fluid mosaic membrane model proposed by Singer and Nicolson in 1972 (Singer and Nicolson, 1972). It is based on thermodynamic principles of organization of membrane lipids and proteins and available evidence of asymmetry and lateral mobility within the membrane matrix. It comprises of mobile globular integral membrane proteins and glycoproteins intercalated into the fluid lipid bilayer of phospholipids arranged in a lamellar fashion (figure 1.1). The lipids are arranged with hydrophobic tails in the centre and hydrophilic head groups facing either the intracellular or extracellular space. Importantly, there is an asymmetry of lipid distribution with lipid composition known to influence the physical properties of the membranes (Nicolson, 2014). For example, the inner layer of the human red blood cell membranes is rich in phosphatidylserine, whilst conversely, phosphatidylcholine mostly occurs in the outer monolayer (Goñi, 2014). Every cell contains a myriad of membrane types, each with unique properties bestowed by the mix of proteins and lipids. The nature of a particular cell membrane is highly variable depending on species, cell type and cellular activation state (Goñi, 2014). The asymmetry in the lipid bilayer has structural (example, curvature of the membrane) and functional (example, phosphatidylserine exposure on the outer leaflet as an apoptotic signal due to lipid scrambling) importance. It also helps ensure the correct orientation of membrane associated proteins (Goñi, 2014).

These membrane proteins can be surface, peripheral or integral (figure 1.1) (Lee, 2004). Membrane proteins play a vital role in biological membranes, as they help to maintain the structural integrity, organization and flow of material through membranes. The positions and movements of the proteins and lipids can be guided by interactions with each other but also by interactions with cytoskeletal components (Szymanski et al., 2015).

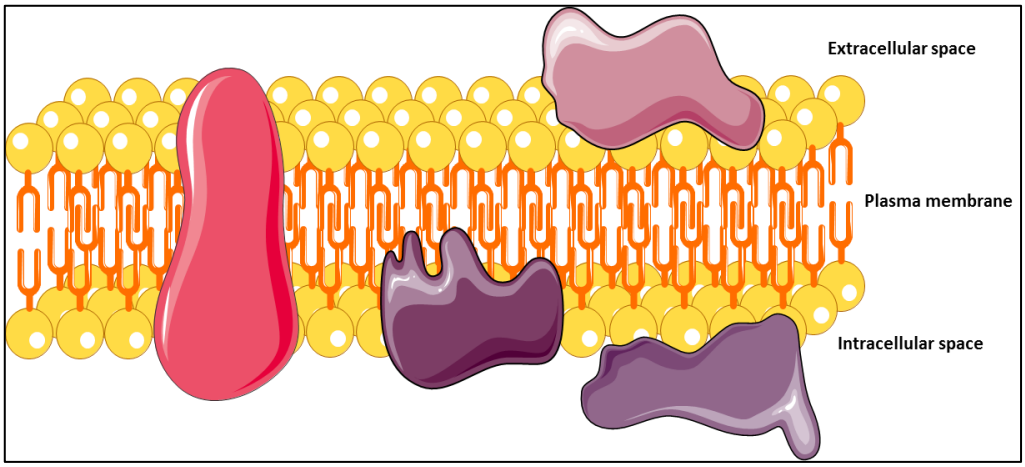


Figure 1.1: Schematic representation of the fluid mosaic model

The lipids (orange/yellow) are arranged in a lamellar fashion with the hydrophobic tails facing inward and the polar head groups at the periphery. This bilayer helps ensure the correct orientation of membrane associated proteins (surface, peripheral or integral). The figure is generated using smart servier medical art, licenced under a creative common attribution 3.0 generic licence. http://smart.servier.com.

Lateral heterogeneity in the lipid bilayer is also achieved due to protein–protein contacts, protein–lipid interactions, protein crowding and lipid packing parameters. Lateral heterogeneity gives rise to membrane microdomains (including lipid rafts; enriched in sphingolipids and cholesterol) which may have specific lipids and/ or proteins conferring specific cellular functions (Simons and Ikonen, 1997). Therefore, the biological membrane forms a very dynamic environment which is crucial for several cellular processes.

1.2 Transport across the membrane barrier

The uptake and efflux of compounds across the membranes of cells and organelles is facilitated by transporters. Gaseous molecules (e.g. CO_2 and O_2) readily pass through the membrane by simple diffusion (Yang and Hinner, 2015). Membrane protein transporters facilitate the movement of all other substances across the membranes (Hediger et al., 2004). Transporters act as gatekeepers of small molecules and can be divided into two categories depending on the mode of action: passive, where the substrate is transported down its concentration gradient and active, where energy is required to transport the substrates. Passive diffusion is facilitated by channels or carriers (example, propagation of action potentials such as voltage-gated sodium channels). Carrier proteins have a much slower rate of membrane transport than

channels (Brooker et al., 2010). Energy associated with the movement of substances by channels or carriers is provided by the potential energy associated with the concentration gradient maintained across the membrane. Active transporters can be classified as primary or secondary. Primary active, ATP dependent transporters include members of the ATP binding cassette (ABC) transporter family and ion pumps (ATPases). P-type ATPases consist of α-helical bundles and are mainly involved in cation uptake or efflux (Palmgren and Nissen, 2011). Ion pumps hydrolyse ATP to actively pump ions (Na^+, K^+, H^+, Ca^{+2}, Cu^{+2}) out of the cells or into the organelles (Cox and Moore, 2002; Dunbar, 2000). These pumps generate and maintain electrochemical gradients across the membranes. These gradients are in turn used by the secondary active transporters (ion-coupled) to drive uphill transport of nutrients across biological membranes. Secondary active transport is either unidirectional or bidirectional; symport or antiport (with the example of sodium-calcium exchanger being an antiporter) (Brooker et al., 2010).

The ATP-binding cassette (ABC) and solute carrier (SLC) transporters are the two main super families considered through perspective of drug transportation. In addition to the transport of metabolites into and out of cells/ organelles, a number of transporters are involved in the uptake and efflux of xenobiotics. There is considerable interest in transporters from both families, particularly those with broad substrate specificities, such as multidrug resistance protein 1 (MDR1; also known as P-glycoprotein (P-gp) or ABCB1) and organic anion transporter 1 (OAT1; also known as SLC22A6) and those that serve in the absorption, distribution and elimination (ADE) of structurally and pharmacologically diverse drugs. Such transporters may be sites for drug–drug interactions that underlie drug toxicities (Hediger et al., 2004, 2013).

The OATP (organic anion transporter polypeptide) family has many different identified substrates including bile acids and hormones (Mikkaichi et al., 2004a). The OAT (organic anion transporter family) family is a subset of the solute carrier subfamily 22 that are responsible for transporting a number of common drug types (including antivirals, antibiotics and diuretics) (Nigam et al., 2015). The OCT (organic cation transporter) family also has a broad range of transport substrates that includes a number of drugs such as metformin (antidiabetic) and oxaliplatin (chemotherapy agent) (Nies et al., 2011; Roth et al., 2012). There is also the MATE (multidrug and toxic compound extrusion) family which is associated with antibiotic resistance in

bacteria but is also found in humans where, for example, MATE1 is found in the liver and kidney where it transports toxic cations into the bile or urine (Kuroda and Tsuchiya, 2009; Otsuka et al., 2005)(Otsuka *et al.*, 2005). Pharmacologically relevant agents such as statins, anti-diabetic, anti- rheumatic and anti- neoplastic are extruded into the blood or bile *via* the OATPs as metabolites or parental compounds to be exported by ABC transporters ABCC4, ABCC2, ABCB1 and ABCG2 (Russel, 2010). Understanding the role of one of these drug pumping ABCs, namely ABCG2, is the focus of this study.

1.3 ABC transporters

ATP binding cassette (ABC) transporters are one of the largest families of polytopic membrane proteins that use energy derived from ATP hydrolysis to actively transport substrates across the membrane. The ABC transporter field emerged in the 1970's with studies on nutrient uptake in bacteria by substrate binding protein dependent transport systems and by the 1990's the term ABC transporters had been coined (Theodoulou and Kerr, 2015). ABC transporters are found in all domains of life, ranging from archaebacteria, fungi, plants and mammals. The human genome encodes nearly 50 ABC transporters (Kerr et al., 2011). Eight major subfamilies (table 1.1) of eukaryotic ABC transporters, which have arisen by divergent evolution, have been identified based on domain organization and phylogenetic analysis (Annilo et al., 2006). Many human ABC transporters have biomedical relevance, for example the transporter of antigenic peptides (TAP), a heterodimer of ABCB2 and ABCB3, has a role in adaptive immune response (Eggensperger and Tampé, 2015; Locher, 2016). ABC proteins are also responsible for a fraction of multidrug resistance of cancer cells (ABCB1, ABCG2, ABCC1 transporters). Mutations in a number of ABC genes are the cause of inherited diseases (cystic fibrosis; ABCC7, Stargardt disease; ABCA4) and disorders related to cholesterol metabolism (sitosterolemia; ABCG5/G8) (Annilo et al., 2006; Vasiliou et al., 2008). The focus of this research is human ABCG2, sometimes also known as BCRP (breast cancer resistant protein). It confers multidrug resistance to tumour cells due to its overexpression. ABCG2 assists in the transport of a wide variety of anti- cancer drugs and is overexpressed in some forms of drug resistant cancers. Hence, a better understanding of its molecular mechanism can lead to the development

of therapeutic approaches towards treating cancer by overcoming multidrug resistance of ABCG2.

Transporter sub-families	Number of members in humans	Significant examples and their roles
ABCA	A1-13	Lipid trafficking (ABCA1, ABCA4), cholesterol efflux (ABCA7)
ABCB	B1-11	Multi drug resistance (ABCB1), peptide presentation (ABCB2/B3), PC transport (ABCB4), iron transport (ABCB6).
ABCC	C1-12	Ion channel (ABCC2/ ABCC7), receptors on cell surface (sulfonylurea receptor; ABCC6), MDR (ABCC1, ABCC3), drug resistance in breast cancer (ABCC11)
ABCD	D1-4	VLCFA transport regulation (ABCD1), involved in import of fatty acids and/or fatty acyl-coenzyme A into the peroxisome (ABCD3)
*ABCE	E1	Oligo-adenylate binding protein (ABCE1)
*ABCF	F1-3	Susceptibility to autoimmune pancreatitis (ABCF1), tumour suppression at metastatic sites and in endocrine pathway for breast cancer/ drug resistance (ABCF2)
ABCG	G1-8	Cholesterol efflux in macrophages, may regulate cellular lipid homeostasis (ABCG1), MDR, urate and haem transport (ABCG2), transport specific peptides and hydrophobic compounds from lymphocytes (ABCG3), biliary excretion of steroids (ABCG5/ G8)

Table 1.1: ABC transporter subtypes and their roles

Depicting seven major subfamilies of eukaryotic ABC transporters and their characteristic roles. Each of the G subfamily types have been described for their specific roles (Kerr et al., 2011; Vasiliou et al., 2009). * ABCE and ABCF do not possess the transmembrane domain (TMD), hence do not play a role in the transport processes but rather are involved in other cellular processes. The eighth subfamily ABCH has also been identified which shares homology with prokaryotic transporters and is also associated with drug resistance but does not appear in humans (Verrier et al., 2008).

1.4 ABC transporter domain organisation

The basic functional unit of an ABC transporter comprises four domains: two cytoplasmic nucleotide binding domains (NBD1, NBD2) and two hydrophobic transmembrane domains (TMD1, TMD2) (figure 1.2) (Higgins and Gottesman, 1992;

Linton, 2007). ABC transporters may form a complex from four separate single-domain polypeptides to a single four domain polypeptide (Higgins and Gottesman, 1992). ABC transporters can further be classified based on the topological organisation of the NBDs and TMDs as full transporters (usually comprising of a single polypeptide chain with two TMDs and two NBDs; example P-gp; figure 1.2 A), half transporters (single TMD and NBD or reverse; example TAP; figure 1.2E, Sav1866 or ABCG2; figure 1.2 B) or a variation thereof (example ribose transporter). ABCG2, a multidrug transporter, the protein under investigation in this study, is a reverse half transporter and requires a homodimer to function. In order to form a functional transporter, half transporters need to interact with identical (homo) or closely related subfamily members (hetero, for example, ABCG5/G8; figure 1.2 C) to form a dimer or higher order oligomer (figure 1.2) (Wong et al., 2014).

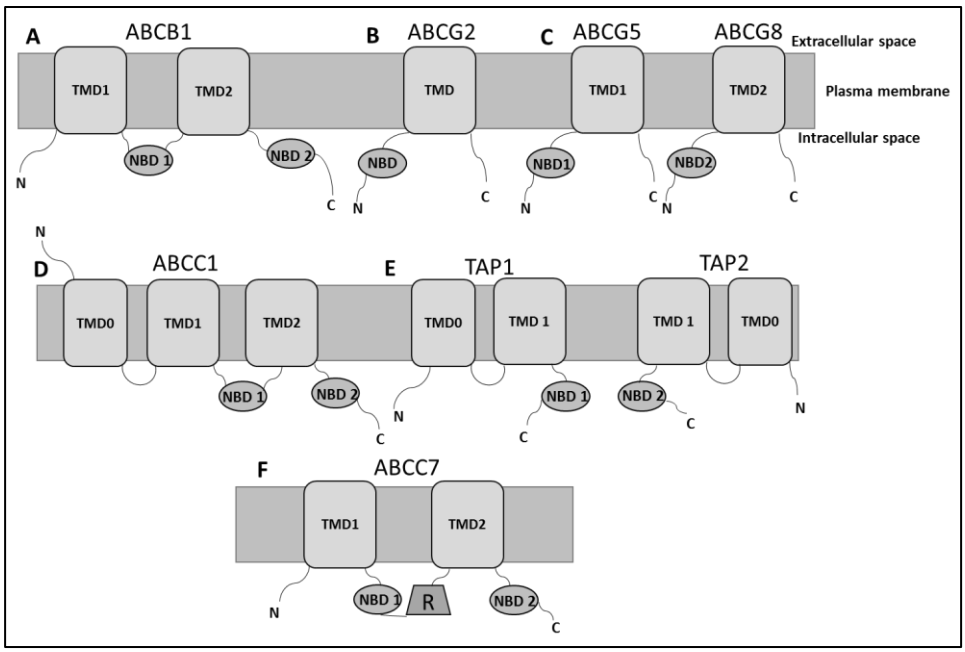


Figure 1.2: Schematic representation of core domain organisations of ABC transporters

A typical ABC transporter consists of two intracellular nucleotide binding domains (NBDs) and two membrane spanning domains (TMDs). In humans, the majority of these proteins are encoded by a single polypeptide as is the case for ABCB1 (A) (Aller et al., 2009). They can also be 'half-transporters' that form dimers to function, for example the ABCG2 homodimer (B) and ABCG5/G8 heterodimer (C) (Lee et al., 2016). More complex arrangements are also seen, such as in ABCC1 (D; Johnson and Chen, 2017) which requires a lasso motif (a linker between TMD0 and TMD1) for folding and function along with the presence of TMD0 or in TAP1/ TAP2 the presence of N terminal TMD_0 that interacts with tapasin (E) (Oldham et al., 2016). ABCC7 (F) requires the presence of an additional regulatory domain for its function (Zhang and Chen, 2016).

Many ABC transporters have additional domains to the existing core domain architecture. Prokaryotic ABC importers require solute binding proteins (SBPs) to bind the substrate with high affinity and deliver it to the transporter complex (Rice et al., 2014). The human CFTR (cystic fibrosis transmembrane conductance regulator (ABCC7; figure 1.2 F) also contains an additional regulatory domain that separates the two halves of the transporter. Phosphorylation of the regulatory domain regulates the chloride channel activity (Cheng et al., 1991; Zhang and Chen, 2016). Other ABC transporters of ABCC subfamily such as MRP1 (ABCC1; figure 1.2 D) and SUR (sulfonylurea receptor; ABCC8/9) have an additional N terminal TMD (TMD0) which is known to modulate the activity of the transporter (Babenko and Bryan, 2003; Bakos et al., 1998).

1.5 Nucleotide Binding Domains (NBDs)

The NBDs share sequence identity across all ABC transporters irrespective of function or species origin (Holland and A. Blight, 1999). All ABC transporter NBDs possess common inter-domain communications (Jones, 1999). The NBD sequence is most highly conserved in seven distinct motifs. Two of these motifs, namely the Walker-A and -B motifs are common to other ATP-binding proteins (Walker et al., 1982). The remaining five motifs; the signature motif, A-, H-, Q- and D-loop are thought to be exclusive to the ABC transporter NBDs (Kerr, 2002; Lawson et al., 2008; Linton and Higgins, 2007a; Smith et al., 2002). The conserved motifs, NBD structure and dimerization have been explained in detail in the subsequent sections.

1.6 NBD crystal structure, dimer formation and ATP binding

The first high resolution crystal structure (1.5 Å) for an NBD was of histidine permease (HisP) from *Salmonella typhimurium*, published in 1998 by Hung et al. The structure revealed an L- shaped topology of the NBD monomer, consisting of two subdomains; firstly an α/ β sub- domain which shows some structural homology to the F1- ATPase and RecA structures and four of the conserved motifs (Walker-A, Walker-B, H- loop and A- loop) present in all ABC transporters. It is also termed as a core domain. The

second sub- domain is an α- helical sub-domain, which contains the characteristic signature motif (C- loop) (Hung et al., 1998).

A structural and thermodynamic model for ABC transporters has been based on experiments with Rad50, a mechanoenzyme involved in DNA repair. Rad50 NBD dimer structure from *Pyrococcus furiosusis* displays the two L-shaped domains in an interlocking arrangement with two ATP (or AMP-PNP) molecules sandwiched between the two monomers, interacting with the classical Walker-A and –B motifs of one NBD, and signature motif of the opposite NBD. This model hypothesizes that ATP-driven dimerization of ABC's represents the force-transducing "power stroke" of ABC transporter pumps. The nucleotide-mediated inter subunit interactions in this structure are similar to those predicted by Jones and George (1999) based on analysis of the structure of an ABC monomer (Jones, 1999; Kerr, 2002).

HisP represented a significant advancement in understanding the NBD structure but did not reveal how two NBDs interact in a dimer. Structural studies on the MJ0796 ABC transporter were pivotal to understand whether an NBD: NBD interaction observed in a distantly related cytosolic protein, Rad50, was conserved in ABC transporters (figure 1.3).

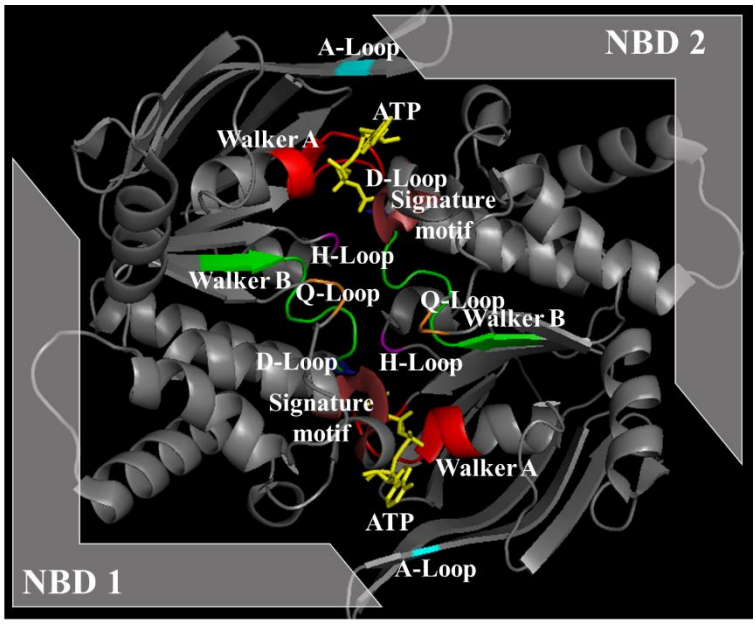


Figure 1.3: Structure of the MJ0796-E171Q ATP Sandwich Dimer interface

The MJ0796-E171Q structure shows head to tail arrangement of the NBD monomers (L- shaped) with ATP molecules sandwiched between the Walker-A (red) and -B (green) motifs of one NBD monomer and signature motif (raspberry) of the other opposing monomer. Potential interaction of the nucleotides with the NBD conserved motifs (A- loop; cyan, H-loop; purple, Q- loop; orange and D-loop; blue) have been highlighted. Figure created with PyMol (PDB ID: 1L2T).

A dimer of the MJ0796 ABC from *Methanococcus jannaschii* was obtained with a mutation of glutamate to glutamine in the Walker-B motifs that resulted in formation of a stable dimer upon binding ATP (Moody et al., 2002; Yuan et al., 2001). The crystal structure of the stable ATP-bound MJ0796 dimer showed a symmetrical ATP sandwich complex similar to that observed in Rad50 (figure 1.3). The two LSGGQ signature motifs complete the ATPase active sites in the ABC dimer by capping the nucleotide triphosphates bound to the Walker-A (P-loop) sequences in the symmetry-related subunits (Smith et al., 2002).

Although the above study explains in detail the possibility of NBD dimerization and ATP hydrolysis, there is still a lack of information with regards to the vectorial transport of substrates. There are still questions pertaining to substrate transportation based on ATP binding or hydrolysis and the necessity of the two/ one active ATPase site for substrate transportation that need further understanding.

1.7 Conserved NBD motifs

The highly conserved motifs Walker-A and Walker-B, first identified by Walker et al. are common to many nucleotide binding proteins and interact with the bound nucleotide by hydrogen bond (Walker et al., 1982). The phosphate-binding loop (P-loop) also known as Walker-A motif is a glycine-rich loop (G-X-S/T-G-X-GK-S/T-S/T). It facilitates interactions with the phosphate groups (of the nucleotide) and the magnesium ion of the bound Mg^{2+} and nucleotide complex (Jones, 1999). Multiple studies have reinforced that the conserved lysine residues in both NBDs are required for cycles of ATP binding and hydrolysis (for example, K433 and K1076 within the Walker-A motif of both the P-glycoprotein (P-gp) NBDs (figure 1.4) and K86 in the Walker-A motif of the ABCG2 NBD (Azzaria et al., 1989; Henriksen, 2005; Müller et al., 1996). Studies have also shown the importance of serine within the Walker-A motif and the importance of symmetrical function of the two catalytic sites within P-gp. Ser-OH is crucial to coordinate Mg^{2+} in MgATP, Mg-ATPase activity and assisting in attaining the transition state (Urbatsch et al., 2000a).

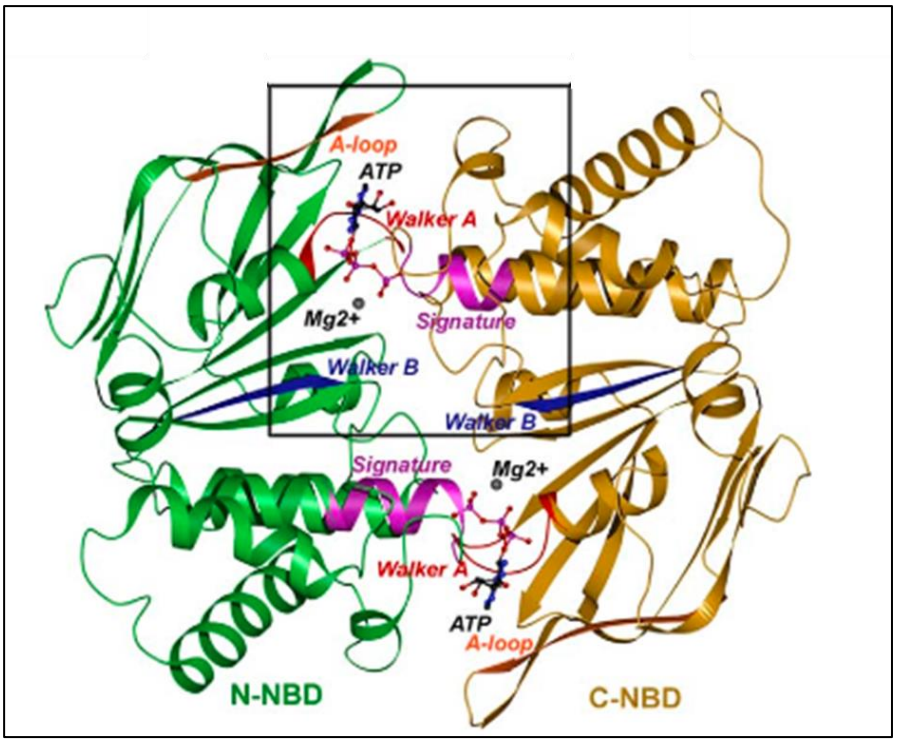


Figure 1.4: Dimeric P-gp NBD showing conserved residues involved in ATP-binding

The atomic model structure of the dimeric P-gp NBDs based on the coordinates from the crystal structure of the MJ0796 E171Q dimer (PDB code: 1L2T) by mapping the N- and C-terminal NBD sequence to either subunit. The N-terminal NBD is depicted in green; and the C-terminal NBD is represented in gold. Functionally important sequence motifs are highlighted in different colours. The Walker-A motif appears in red, the Walker-B motif blue, the signature motif magenta and the A-loop brown. The modelled ATP is shown as a ball-and-stick model with carbon atoms in black, oxygen red, nitrogen blue and phosphorous magenta. The Mg^{2+} ion is shown as a metallic ball. The tyrosine residue of the conserved A-loop (shown in brown) stacks against the adenine ring of ATP. Figure adapted from (Ambudkar et al., 2006).

The Walker-B motif (h-h-h-h-D, where 'h' is a hydrophobic residue) is crucial to form contacts with the nucleotide. This motif constitutes a buried β-strand within the core of the nucleotide-binding fold. The highly conserved aspartate residue is involved in the coordination of the catalytic Mg^{2+} ion. The glutamate residue, also referred to as catalytic carboxylate is thought to activate water molecules for the hydrolysis reaction and mutation of this glutamate residue blocks nucleotide hydrolysis but not binding (Hanson and Whiteheart, 2005).

The ABC signature motif; LSGGQ, (erroneously referred to in some publications as Walker-C) is proposed to form a part of the dimer interface within the ATP binding pocket. Mutation studies have shown the importance of this motif (Bakos et al., 1998). Mutating the conserved serine residues in both the N and C terminal NBDs of P-gp

showed an effect on ATPase activity. Single mutants showed mildly impaired ATPase activity with effects on the function. Based on vanadate- ADP and beryllium fluoride-ADP trapping experiments, serine to alanine mutations reduced the strength of Mg.ATP/ ADP binding and transition state formation. Double mutations (S528A and S1173A) resulted in a synergistic effect showing strong catalytic impairment. This was supported by structural data from NBD-NBD dimers that indicate "head-to-tail" arrangement with the ABC signature motif that forms an ATP binding interface with the Walker-A motif of the opposite NBD (figure 1.4) (Tombline et al., 2004). The consecutive glycine residues are crucial to provide the flexibility to maintain the initial α- helical turn post the signature motif. Mutations of the glycine residues to aspartic acid, serine or valine abrogate the ATPase activity and protein expression (Bakos et al., 1998; SZAKÁCS et al., 2001).

The conserved aromatic amino acid of the A-loop (located 25± 2 residues upstream of the Walker-A motif) stacks in a π–π fashion with the adenine ring of the bound nucleotide. Site-directed mutagenesis studies demonstrate that this residue is critical for nucleotide binding and hydrolysis. In P-gp, Y397 and Y1040 (residues of the A loop; figure 1.4), in NBD1 and NBD2, respectively, seem to play an important role by positioning and maintaining of the nucleotide in the active site (Carrier et al., 2007). In bacterial histidine permease, Y16S mutation in the HisP subunit was found to abolish the binding of ATP and its transport function (Shyamala et al., 1991). The importance of the conserved aromatic residues may also be related to the role of the NBDs in which they are located.

The Histidine-loop (βθβμH; where β is a branched aliphatic residue, θ is any hydrophobic residue and μ is a hydrophilic residue) is situated 30-40 amino acids C-terminal to the Walker-B motif and is thought to coordinate the ATP dependant switch region (Kerr, 2002; Lawson et al., 2008; Smith et al., 2002). In *E. coli* HlyB (Haemolysin B), the conserved H- loop residue H662 can act as a chemical linchpin (as a general acid and then as a general base) to shuttle proton transfer during ATP hydrolysis (Zhou et al., 2013). In Histidine permease (HisP), the conserved histidine residue of the His loop (H211) also makes a contact with the γ-phosphate of ATP through a bound water molecule (Hung et al., 1998; Kerr, 2002).

The D-loop (SALD), located in the subdomain interface is proposed to aid in the formation of cross-dimer interactions. It is known to interact via the His residue with

the opposing ATP binding site, thus acting as a "linchpin" for the hydrolysis cycle (Lawson et al., 2008; Zaitseva et al., 2005).

The final conserved motif, Q- loop is located between the Walker-A motif and the signature motif. The highly conserved glutamine residue located within the Q loop may be involved in inter-domain communications (NBD: TMD) (Lawson et al., 2008). Point mutations of P-gp glutamines (Q475 and Q1118) to glutamate or alanine affected the ATPase activity. The mutant isoforms displayed normal binding capacity for the substrates and the nucleotide but reflected reduced ATPase activity, thereby suggesting disruption in the NBD: TMD communications (Urbatsch et al., 2000b). The Q- loop is also known to directly interact with the nucleotide. The recent cryo-EM structure of P-gp in ATP bound outward facing conformation (catalytic glutamates E556Q and E1201Q, located in the Walker-B motif), revealed the importance of the Q- loop in coordinating the Mg^{2+} ion for ATP hydrolysis (Q475 and Q1118 coordinate the Mg^{+2} ion and γ- phosphate of ATP making Van der Waals contacts with the ABC signature motif of the opposite NBD), to communicate the chemistry at the ATPase site to the conformational changes in the TMDs and to facilitate NBD closed dimer formation. In both the NBDs, the Q- loop is a part of the NBD and TMD interface, interacting with the coupling helixes IH2 and IH4. Mutations of the Q- Loop may disturb the geometry of the ATPase site and destabilise the NBD dimer (Kim and Chen, 2018).

The highly conserved NBD motifs lay the foundation for the NBD features common across the ABC transporter family, even though substantial variations exist that are outside the scope of this thesis.

1.8 TMD topology of an ABC transporter

The TMDs constitute a translocation pathway that generally display no significant sequence conservation due to the diverse nature of the transport substrate but share a similar topology within a transporter class. For example, sequence conservation between TMD1 and TMD2 in P-glycoprotein is approximately 30 %, suggesting that the two TMDs in these transporters are a result of gene duplication originating from homodimeric ancestors (Wilkens, 2015). In eukaryotes, the majority of ABC transporters comprise a single polypeptide that contains all four functional units, with some members assembled from "half" transporters with either homodimeric or

heterodimeric halves (Wilkens, 2015). The structural and sequence comparisons of ABC transporters from prokaryotes and eukaryotes have led to identification of some common TMD architectures, namely type I and type II folds and an exporter type fold. The divergence in ABC transporters can be explained based on helix topology and the mechanism of transport adopted by the ABC importers, type I and type II respectively (figure 1.5). ABC exporters show a common structural fold consisting of six TM α-helices per TMD (Dean et al., 2001).

Type I importers constitute either a homodimer or structurally similar TMDs (for example the maltose transporter Mal<u>FG</u>K_2, where the underlined domains are the TMDs) (figure 1.5 A) (Oldham et al., 2007; ter Beek et al., 2014). There is an additional N-terminal helix that wraps around the helices of the other TMDs and intertwines the TMDs, making a total of 12 TM helices. In type II fold importers, the TMDs are lined up next to each other and do not have helices that cross over to the other TMD (figure 1.5 B). In each TMD, there is a pseudo two-fold symmetry between the segments containing TM helices 2–5 and TM helices 7–10. Intriguingly this 2-3 TM helix with inverted topology is also seen in other membrane proteins, for example aquaporins, perhaps hinting at the genetic emergence of transporter proteins (Gonen et al., 2004). These two subdomains have a similar helical packing but with opposite orientation with respect to the membrane. The helices of a single TMD are tightly packed together, and the two TMDs line a translocation pore at the interface (for example vitamin B_{12} importer $BtuC_2D_2F$) (Locher et al., 2002; ter Beek et al., 2014). Both type I and type II importers contain the coupling helices to couple substrate translocation along with ATP hydrolysis as has been identified in the TMDs of ABC exporters (Dawson et al., 2007). Type I exporters also show domain swapping where TMHs from each half of the protein cross over to the opposing TMD, with an intracellular loop extending into the opposing NBD also thought to couple transport (Dawson and Locher, 2007; Zolnerciks et al., 2007).

NBDs contain sequences that allow ATP binding and subsequent hydrolysis to ADP (Hyde et al., 1990; Linton and Higgins, 2007b). The energy is used in a ‘power stroke’ through which a protein undergoes conformational changes that result in the translocation of the respective transport substrate and/or the resetting of the transporter to a conformation ready for another transport cycle (Chen et al., 2003).

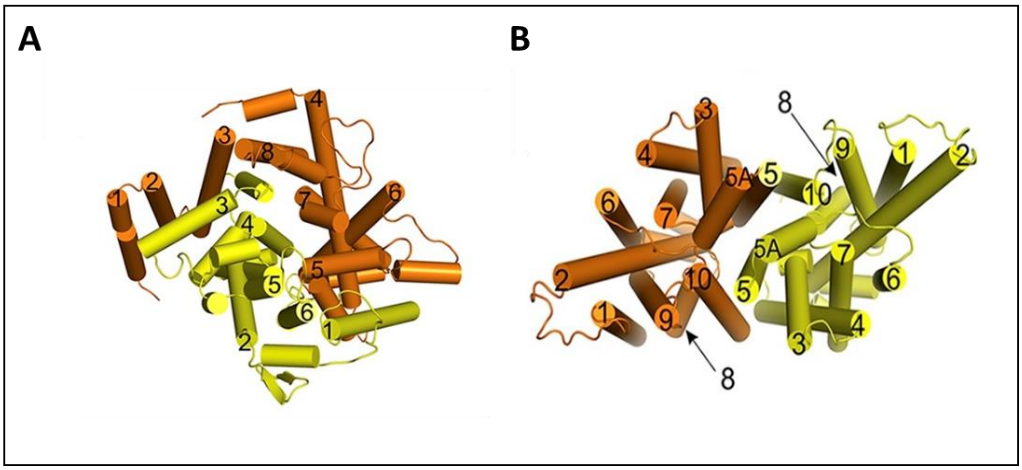


Figure 1.5: TM helical arrangement in ABC transporters

A trans-side top down view (along an axis perpendicular to the membrane plane) for the helical arrangement in the type I importer; crossover of helix bundle of the maltose transporter MalEFGK2 (PDB ID: 3RLF) (A), compared to the distinct bundle arrangement of the type II importer; the BtuC dimer of the vitamin B12 transporter $BtuC_2D_2F$ (PDB ID: 1L7V) (B). Figure adapted from Ter Beek et al., 2014.

Type I importers tend to be capable of higher capacity, lower affinity transport than Type II importers due to association of a greater number of substrate binding proteins (SBPs) which are an integral part of bacterial ABC importer function (ter Beek et al., 2014). SBPs are not a part of human ABC transporters and the functional importance of the different SBP sub classes is not yet clear. The next section covers the mechanism of transport based on the two models of ABC exporters.

1.9 ABC transporter mechanism

Even though advancements in the structural studies have been made, many fundamental questions regarding substrate recognition, translocation and coupling of ATP binding and hydrolysis to conformational changes in the transmembrane domains have not yet been deciphered in detail. Several models have been presented to understand the transport mechanism of these transporters based on the data obtained for bacterial transporters (MBP and HisP) and P-gp (Nikaido and Ames, 1999; Sauna and Ambudkar, 2000; van Veen, 2000). The gold standard is the Sav1866 crystal structure, resolved at 3Å, which represents the outward facing conformation (orientation of transport) with the two nucleotide-binding domains in close contact. The closed conformation (apposition of the NBDs) was crystallised in presence of

ADP and represented the ATP bound conformation (Dawson and Locher, 2006). Later, an open outward conformation of Sav1866 was also resolved with ATP bound structure (AMP: PNP) (Dawson and Locher, 2007). The two well accepted models to explain the coupled mechanism for drug translocation are the 'ATP- switch' and 'constant contact' models that are described in this section.

One of the most favoured paradigms to explain the transport cycle of an exporter is an ATP switch model, also known as the tweezers like or processive clamp models (figure 1.6) (Chen et al., 2003; Van Der Does and Tampé, 2004). This model involves changes between two principal conformations, i.e. a closed dimer upon binding of two ATP molecules to an open dimer upon ATP hydrolysis and release of Pi and ADP. This facilitates a conformational change across the TMDs leading to vectorial transport of the potential substrates (Higgins and Linton, 2004; Linton and Higgins, 2007a).

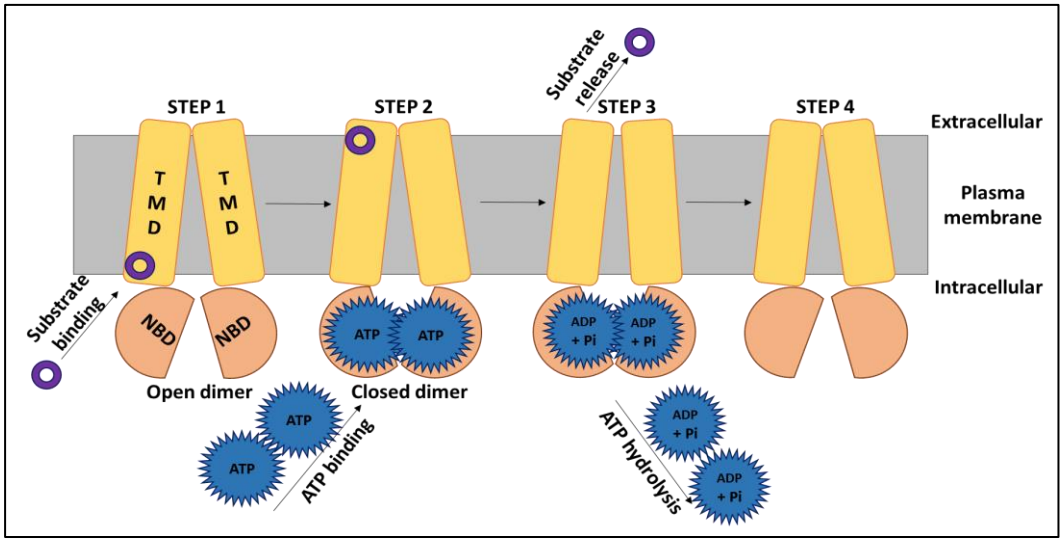


Figure 1.6: Schematic representation of an ATP switch model for an ABC exporter

Step 1, the substrate binds to the drug binding pocket in the TMDs in the high-affinity open NBD conformation, inducing increased affinity for ATP. Step 2, ATP binding facilitates the closed NBD dimer formation, which in turn stimulates a large conformational change in the TMDs which is sufficient to translocate the substrate. ATPs bind cooperatively to the NBDs. Step 3, ATP hydrolysis initiates separation of the closed NBD dimer, facilitating the formation of the transition state. Step 4, transporter reset to the basal state; Pi and ADP are released and the protein is restored to a high affinity state for another cycle of substrate binding (Linton, 2007). The stoichiometry implied in this figure (i.e. 2ATP/ 1 substrate) may not be true for all ABCs.

The transport cycle is initiated by binding of substrate to high affinity sites on the TMDs (figure 1.6 step 1). Substrate binding lowers the activation energy for the ATP dependent NBD dimerization and induces conformational changes in the NBDs, thereby facilitating ATP binding (figure 1.6 step 2). ATP binding induces closed dimer formation, thereby aligning the ABC signature motif of one NBD with the Walker-A and -B motifs of the other NBD, forming 2- ATP binding pockets (Higgins and Linton, 2004). In presence of ATP binding, the NBDs form a complete interface and sandwich the ATP molecules (figure 1.6 step 2) (Beis, 2015). ATP binding acts as a switch, thereby facilitating a closed dimer formation (Smith et al., 2002).

Interactions of the γ phosphate of ATP with the conserved glutamine in the ABC signature motif (LSGGQ) of the other NBD and the interaction of the conserved glutamine in the Q- loop with bound nucleotide and hydrolytic water provide the necessary energy for the conformational changes, i.e. the power stroke for the substrate transport (Smith et al., 2002). The Q- loop and the coupling helix at the NBD: TMD interface couple the conformational changes between NBDs and TMDs (Beis, 2015). This facilitates a conversion of high affinity substrate binding state to a low affinity state and the transporter adopts an outward facing conformation releasing the substrate (figure 1.6 step 3) (Smith et al., 2002). Evidence has been accrued to support the hypothesis that ATP binding provides the power stroke and alters the substrate binding properties via substantial conformational changes in the TMD's. Medium resolution 2- D crystallographic studies showed significant conformational changes in P-gp following ATP binding and subsequent limited changes upon ATP hydrolysis substantiating the power stroke (Rosenberg, 2001; Rosenberg et al., 2003). Recent studies on the ABCG2 and ABCC1 transporters have shown that binding of non-hydrolysable ATP analogue (AMP- PNP) results in reduced affinity for daunomycin and oestrone sulphate respectively (McDevitt et al., 2008; Rothnie et al., 2006).

ATP hydrolysis initiates the basal, open dimer conformation by destabilizing NBD closed dimer (figure 1.6 step 3 and 4). Studies on transporters ABCG2 and ABCC1 subjected to vanadate in post hydrolytic state have shown to have low substrate binding affinity (McDevitt et al., 2008; Rothnie et al., 2006). This is followed by sequential release of ADP and inorganic phosphate, restoring the protein to its basal state. The electrostatic repulsion caused due to the coordination interaction between ADP and Walker-A motif of one NBD and the inorganic phosphate and signature motif of the other NBD. This leads to restoration of the open dimer conformation due to the rigid

body rotation of the subdomains of each NBD (Smith et al., 2002). A high resolution structure of the maltose transporter in pre- hydrolysis and transition state configurations showed that glutamate residue at the end of Walker-B motif and the residues in other conserved motifs (Q, D and H loops) polarizes the water molecule for an attack on the γ-phosphate and ATP hydrolysis (Oldham and Chen, 2011).

Several mechanisms within the catalytic cycle of ABC transporters are yet to be fully characterised. One of the major factors for further debate in the ATP switch model is the NBD's separation in the nucleotide free-state, with an approximate separation of 20- 30Å (George and Jones, 2012). This significant separation of the NBDs could be an artefact of detergent solubilisation (Wright *et al.*, 2018).

The constant contact model proposed by George and Jones, derived from the 'alternating sites' model, proposed in 1995 by Senior et al. reflects on the asymmetric functioning of the NBDs suggesting reciprocating function in the TMDs (Senior et al., 1995). The nucleotide binding domains do not fully dissociate, and ATP hydrolysis occurs alternately at each of the two active sites. One of the sites remains closed and always contains an occluded nucleotide. The cassettes remain in contact, and the active sites swing opens in an alternately seesawing motion (George and Jones, 2012).

Despite the advancement in structural resolution, we are still far from fully understanding translocation by ABC transporters. The mechanism underpinning substrate translocation remains elusive and requires further investigation to understand the pathophysiological roles of the transporters.

1.10 Multidrug resistance and ABC transporters

Tumours evolve resistance to traditional therapies leading to drug resistance, which necessitates further research and treatment development (figure 1.7). Various mechanisms circumvent drug cytotoxicity. These include drug inactivation (or decreased drug activation) through altered metabolism by cytochrome P_{450} and UDP-glucuronosyltransferase, alterations to signal transduction pathways, for example, changes in expression of growth factor receptors can cause altered efficacy of Herceptin (trastuzumab) (Mikkaichi et al., 2004b). Drug resistance can also be achieved by metabolic pathway adaptation, for example, reduced conversion of cyclophosphamide, increased repair of the damage caused by the drug (O-6-methylguanine- DNA methyltransferase (MGMT) - mediated temozolomide

resistance) and direct drug extrusion from the cells by multidrug pumps (figure 1.7) (Hinds et al., 1991; Maier et al., 2010; Palmberg et al., 1997; Wong et al., 2014).

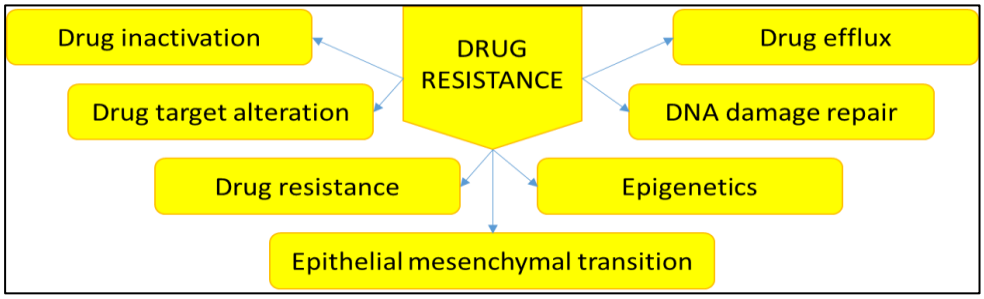


Figure 1.7: Drug resistance in human cancer

Categories of mechanisms that can facilitate direct or indirect drug resistance, independently or in combination with various signal transduction pathways adapted from Housman et al., 2014.

Multidrug transporters catalyse drug export from the cells, thereby conferring cellular resistance to chemotherapeutic drugs. The primary phenotype for cancer resistance is based on the reduction of anti-tumour drug concentrations within the cells. Many tumour cells display multidrug resistance, thereby causing failure of chemotherapy and facilitating tumour growth. An insurmountable obstacle in treating cancers arises from their ability to become resistant to a variety of chemical compounds. It is a defence mechanism adopted by tumour cells to combat the cytotoxic effects of drugs by reducing the accumulation to a sub- efficacious concentration level. Hence, understanding drug recognition and transport *via* the multidrug pumps is crucial to circumvent drug resistance.

Three human ABC transporters, namely P-glycoprotein (ABCB1), multidrug resistance protein 1 (ABCC1) and breast cancer resistance protein (ABCG2) have been associated with multidrug resistance in cancer cells. Most of the knowledge of multidrug resistance proteins is associated with ABCB1 and ABCC1 (Callaghan, 2015; Cole, 2014). Less information is available regarding the molecular mechanisms of ABCG2. Understanding the role of ABCG2 in MDR will be a key step towards a therapeutic approach and forms the basis for research. Structural comparisons with ABCB1 and ABCC1 will advance our knowledge of the similar and unique features and properties in multidrug resistance to chemotherapy.

ABCB1 encodes a 170kDa protein that comprises an N-terminal transmembrane domain and a C-terminal nucleotide binding domain in tandem repeat (i.e. TMD1-

NBD1-TMD2-NBD2). The protein was identified in colchicine resistant Chinese hamster ovary cell line. The pleiotropic drug resistant cells displayed certain surface glycoproteins that controlled drug permeation by modulating the hydrophobic membrane regions. These were referred to as P- glycoprotein (P stands for permeability factor) (Juliano and Ling, 1976). It is expressed at the apical surface of renal tubular cells, bile canaliculi, and intestinal epithelium as well as at the luminal surface of capillary endothelial cells in the blood-testes and blood-brain barriers, thereby protecting the sensitive tissues and the foetus from endogenous and exogenous toxicity (Cascorbi, 2011).

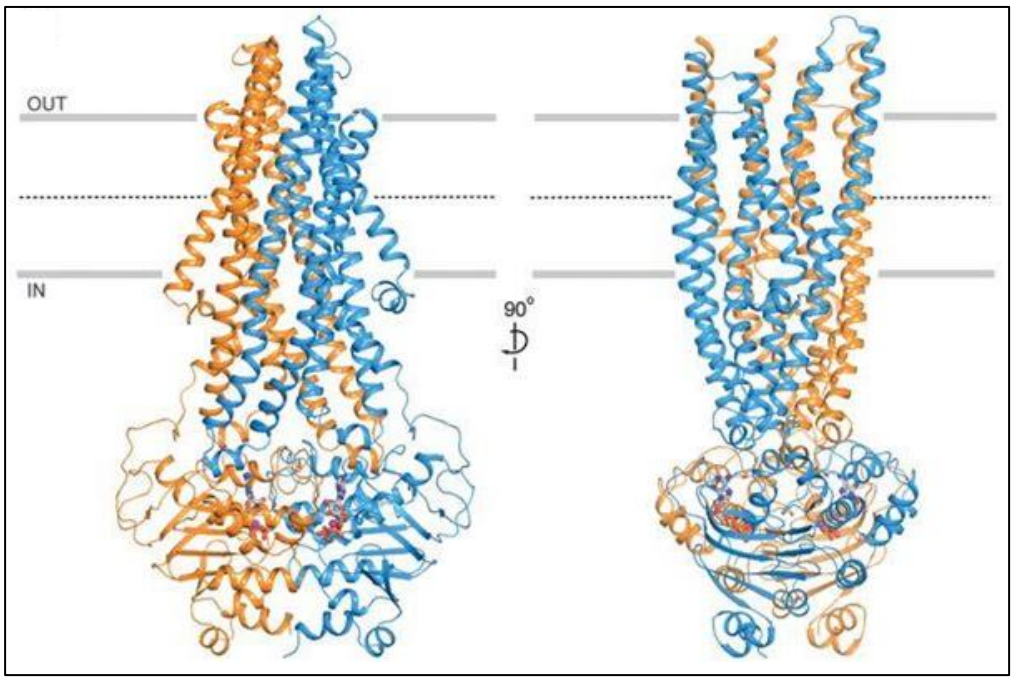


Figure 1.8: The structure of recombinant human P-gp

The E556Q/E1201Q double mutant human ABCB1 is displayed in an outward facing conformation. The N and C terminal halves (TMD1-NBD1 and TMD2-NBD2) are displayed in orange and blue respectively. ATP is represented in a ball and stick format with the Mg^{2+} shown as a sphere. Figure adapted from Kim and Chen, 2018 (PDB ID:6C0V).

P-gp substrates are generally lipid-soluble, and partition into the membrane before the transporter expels them into the aqueous phase, much like a 'hydrophobic vacuum cleaner'. The transporter may also act as a 'flippase', moving its substrates from the inner to the outer membrane leaflet (Higgins and Gottesman, 1992). The substrates include anticancer agents, immunosuppressants, steroid hormones, calcium channel

blockers, beta-adrenoreceptor blockers and cardiac glycosides etc. (Frances J. Sharom, 2011).

The overexpression of P-gp (ABCB1) has been linked to clinical resistance to chemotherapy and a poor clinical outcome in adult patients with acute leukaemia's (Marie et al., 1991). It has also been shown to be overexpressed in soft tissue sarcomas, ependymomas (malignant brain tumour in children) and certain breast cancers (Abolhoda et al., 1999; Sabnis et al., 2019; Trock et al., 1997).

P-gp expression and stability can regulate tumour cell progression. Kinases, oestrogens, MAPK signalling proteins (HRas, c- Raf, MEK1/2, ERK1/2), growth factors (EGF, FGF) and HSP90 are known to regulate P-gp expression (Housman et al., 2014; Imai et al., 2005; Katayama et al., 2007; Mutoh et al., 2006). Targeting these may be useful in reducing P-gp expression and tumour cell sensitisation.

Researchers have been focusing to combat MDR conferred by P-gp, to achieve improved drug bioavailability, uptake of drug in the target organs and more efficacious chemotherapy (Mlejnek et al., 2017). Development of modulators that can enhance cellular uptake, transport, half-lives of drugs, target specific organs/ tissues and predict the pharmacokinetics accurately will shorten the treatment time with optimal drug delivery and facilitate a revolution in the field of drug delivery (Amin, 2013). The nebulous question of whether P-gp can be considered a pharma target, even after failed attempts is based on the available structural information with drug binding sites, understanding the pharmacokinetics of drug substrates, identifying modulators and modulating its expression.

The recent cryo-EM structure of human P-gp revealed an outward facing conformation at 3.4 Å, in presence of ATP, precluding the substrate binding site, suggesting ATP release (figure 1.8). The collapse of the drug binding site and absence of the substrate suggests substrate release prior to ATP hydrolysis. This has facilitated the development of a hypothetical model of unidirectional transport of a wide range of substrates (Kim and Chen, 2018).

Another contributor towards MDR is the Human MRP1 (ABCC1), a 190kDa protein transporter with a topological arrangement (TMD0-TMD1-NBD1-TMD2-NBD2). It is amplified at least 100-fold in the multidrug-resistant lung cancer cell line from which the mRNA was first isolated. ABCC1 was first identified from doxorubicin-selected lung cancer cell line H69AR (Cole et al., 1992).

ABCC1 is known to transport a variety of antitumor drugs (vincristine, etoposide, anthracyclines and methotrexate) and drugs used in non-malignant disease treatments (opiates, antidepressants, statins and antibiotics) (Deeley et al., 2006). It is also known to transport physiologically important molecules such as pro-inflammatory molecules (leukotriene C4), hormones (oestrogens and prostaglandins) and antioxidants (oxidised and reduced glutathione) (Leier et al., 1994). The substrates are predominantly amphipathic organic acids with large hydrophobic groups.

MRP1 is widely expressed in the lung, testis, kidney, skeletal and cardiac muscles, and the placenta. It is highly detectable in proliferating hepatocytes and liver cancer cell lines, such as HepG2. MRP1 is also expressed in a cell specific manner in the brain, as well as the blood-brain barrier and cerebrospinal fluid barrier (Leslie et al., 2005; Slot et al., 2011). There is clear evidence to show elevated expression of MRP1 in a variety of solid tumours (Deeley et al., 2006).

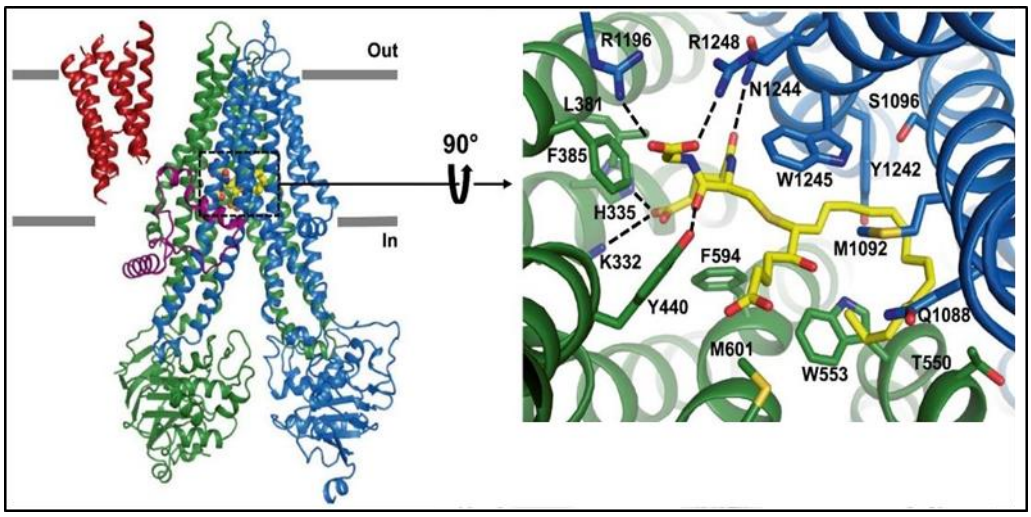


Figure 1.9: Molecular architecture of bovine ABCC1

The left-hand panel shows TMD0 (red) attached via the Lasso region (purple) to subunit 1 (green). Leukotriene C4 (yellow) is found in the drug binding region between TMD1 (green) and TMD2 (blue). This binding region is highlighted (right) with key residues indicated (adapted from: Johnson and Chen, 2017, PDB ID: 5UJ9).

The unique feature for MRP1 is the presence of an additional N- terminal transmembrane domain (TMD0) (Leslie et al., 2005). The recent cryo-EM structure of bovine MRP1 in presence of its physiological substrate leukotriene C_4 sheds light on how substrate binding primes ATP hydrolysis (figure 1.9). The translocation pathway of MRP1 is highly basic and is shielded from both the membrane leaflets. The binding

site is divided into two parts, a positively charged region that coordinates with the glutathione (GSH) moiety (P- pocket) and a large hydrophobic area with the lipid tail (H- pocket). Binding of the substrate facilitates NBD proximity (bringing the two halves close to each other), achieved by rotation of two rigid bodies comprising of a lasso motif, TM1 bundle and NBD1 and the other consisting of TM2 and NBD2 (figure 1.8). This is similar to what is seen for bacterial maltose transporter (Johnson and Chen, 2017). It most likely recruits its substrates directly from the cytoplasm based on the bipartite nature (the ability to recognize large, amphipathic substrates) and plasticity (that allows for adaptability to a variety of substrates) of the single substrate binding site.

This has provided new insights into the functional diversity of the multidrug transporter. There is limited information available regarding molecular mechanism of ABCG2 and hence is the focus for this thesis.

1.11 Discovery of a multidrug resistance transporter: ABCG2

ABCG2, also referred to as a breast cancer resistance protein (BCRP) was first identified by Doyle et al. in a breast cancer subline; MCF-7/AdrVp. The cell line displayed an ATP-dependent reduction in the intracellular accumulation of anthracycline anticancer drugs (mitoxantrone, doxorubicin and daunorubicin) with basal expression of known multidrug resistance transporters ABCB1 and ABCC1. RNA fingerprinting identified a 2.4 kb mRNA, overexpressed in MCF-7/AdrVp cells, encoding a 663 amino acid member of the ATP-binding cassette superfamily of transporters, known as BCRP (Doyle et al., 1998b).

Allikmets et al. around the same time also characterised a new human ATP-binding cassette (ABC) transporter, highly expressed in the placenta. The ABCP gene, encoded a 655 amino acid protein that could play a role in the placental barrier, either by protecting the foetus from toxic compounds or by transporting some important substrates, thereby maintaining placental homeostasis (Allikmets et al., 1998).

A third group demonstrated homology of cDNAs identified from the mitoxantrone-resistant S1-M1-80 human colon carcinoma cells to ABC transport genes. They identified two cDNAs, overexpressed in several mitoxantrone-resistant cell lines.

These cDNAs showed high degree of homology to ABCP. This ATP dependent mitoxantrone resistance was linked to an ABC transporter and referred to as MXR (Miyake et al., 1999).

The ABCP protein was renamed ABCG2 as the wild type sequence whereas the other two sequences contained single point mutations, presumably as a result of significant drug selection.

1.12 Molecular ABCG2 gene expression regulation

The human ABCG2 gene is located on chromosome 4q22 and spans over 66 kb. It comprises of 16 exons and 15 introns. Bailey et al. characterized ABCG2 promotor activity by luciferase reporter assay in cell lines with high endogenous ABCG2 expression such as human choriocarcinoma cell lines (JAR, JEG-3, BeWo cells) and breast cancer cells (MCF- 7). The exons range from 60 to 532 bp, with the translational start site found in the second exon. The first exon mostly comprises of 5' UTR (untranslated regions). The ABCG2 gene is characterized by TATA less promoter with the basal promoter activity conferred by a sequence approximately 312 bases upstream of the transcription start site. It contains a CCAAT box at about 274 bases upstream of the transcription start site; its removal is known to regulate the transcriptional activity. There are 5 putative Sp1 sites downstream of the putative CpG island (Bailey-Dell et al., 2001; Nakanishi and Ross, 2012).

There are numerous mechanisms by which ABCG2 gene expression can be regulated with influences on transcription, m-RNA suppression and modulation of protein expression, some of which have been described below. Consistent with studies indicating a role for ABCG2 in the protection of haematopoietic stem cells against hypoxia, the proximal promoter region of ABCG2 contains a hypoxia response element. ABCG2 regulation under hypoxia conditions is a potential protection mechanism adopted by cells/ tissues to limit damage from protoporphyrin accumulation (Krishnamurthy et al., 2004; Nakanishi and Ross, 2012).

In human myeloid dendritic cells, ABCG2 expression is found to be upregulated based on the activation of a nuclear receptor; peroxisome proliferator- activated receptor (Nakanishi and Ross, 2012). Upregulation of ABCG2 expression has also been observed by the interaction of aryl hydrocarbon agonists (polycyclic aromatics and

phytochemicals) with aryl hydrocarbon receptor (AHR) (Nakanishi and Ross, 2012; Tan et al., 2010). A nuclear factor erythroid 2 related transcription factor; Nrf- 2 is found to assist in the rescue of cells from oxidative and electrophilic stress mediated by xenobiotics as an external stimuli. Nrf- 2 functions as a transcription factor for ABCG2 gene expression in hepatocytes. A known Nrf- 2 inducer, tert-butylhydroquinone silenced the Nrf- 2 gene expression, thereby leading to abolished ABCG2 m-RNA expression. This process provides the rationale behind up regulation of ABCG2 in protective roles against xenobiotics (Adachi et al., 2005; Dhakshinamoorthy et al., 2001; Nakanishi and Ross, 2012).

Post translational modifications are also known to regulate ABCG2 translocation. Threonine 362 is crucial for ABCG2 phosphorylation by serine/ threonine kinase Pim-1, essential for plasma membrane translocation, as observed in human prostate cancer LNCaP cells. Pim-1L knockdown studies in the drug-resistant prostate cancer cells abolished higher order oligomer of endogenous ABCG2 and resensitized the resistant cells to chemotherapeutic drugs (docotexal and mitoxantrone), reinstating the importance of BCRP phosphorylation for functionality induced by Pim-1L. This could be a potential therapeutic area to investigate by disrupting Pim-1 signaling to reverse ABCG2-mediated multidrug resistance (Xie et al., 2008). Role of ABCG2 in preventing chorionic low-grade associated obesity was established in humans and mice through knockdown studies *ex vivo* (human intestinal epithelial cells) and *in vivo* (knockout mouse models) experiments respectively. Studies related to human obesity induced reduced intestinal JAK3 expression, JAK3 knockout in mouse or siRNA-mediated β- catenin knockdown in human intestinal epithelial cells result in significant loss of intestinal ABCG2 expression and compromised colonic drug efflux and barrier functions. During obesity there is loss of Janus kinase 3 (JAK3)-mediated tyrosine phosphorylation of ABCG2 which is crucial to promote its interactions with membrane-localized β-catenin essential for ABCG2 expression, surface localization and maintenance of ABCG2 mediated intestinal drug efflux and barrier functions (Mishra et al., 2019).

Post transcriptional regulation of ABCG2 mediated by microRNAs (miR) has been reported in some cancer cells. MiRs are small non-coding RNA molecules. miR- 328, through mRNA cleavage is known to decrease ABCG2 protein levels. In hematopoietic stem cells obtained from umbilical cord blood, hsa-miR-520h has shown to down regulate ABCG2 expression, leading to inhibition of pancreatic cancer

cell's migration and invasion. The proximal miRNA response element (MRE) of ABCG2, located in the 3'- UTR of ABCG2 mRNA in various cancer cell lines, is lost in drug resistant cell lines, therefore leading to evasion of mRNA degradation facilitating ABCG2 overexpression. It is proposed that some drug selected cell lines are devoid of both 5' and 3' UTR putative binding sites leading to an increase in ABCG2 expression (To et al., 2008). Understanding the multiple levels of regulation of ABCG2 transporter proteins can assist in modulating cancer cells to overcome MDR.

1.13 ABCG2 tissue distribution, sub-cellular localization and physiological role

The localization of ABCG2 transporter in tissues sheds light on its physiological function. ABCG2 plays a crucial role in self-defence systems, as an efflux transporter for xenobiotics and unwanted toxic compounds. The strategic tissue distribution of ABCG2 reflects its role in limiting absorption (small intestine), mediating distribution (blood-brain and blood-placental barriers) and facilitating elimination (biliary and renal) of xenobiotics/ drugs that are ABCG2 substrates. The high expression of the BCRP gene in some tumour conditions has been shown to be related to multidrug resistance to chemotherapeutic drugs.

Several studies have shown the ABCG2 protein and mRNA are located in cells at the blood: brain barrier, specifically the protein being localised at the luminal surface of brain microvessel endothelial tissue and brain cortex (Cisternino et al., 2004; Cooray et al., 2002). This is consistent with a role in preventing brain penetration of drugs; indeed, functional studies have confirmed this by mitoxantrone and prazosin *in situ* brain transport studies, suggestive of the fact that ABCG2 tends to be concentrated in brain microvessel cells (Aronica et al., 2005). The expression of ABCG2 in brain endothelial cells limits the permeability of brain to the drugs and is a potential source of drug-drug interaction (Cisternino et al., 2004). ABCG2 in concert with ABCG4 has been shown to be involved in efflux of amyloid-β peptide (Aβ) from the brain, and thus a potential role for ABCG2 in Alzheimer's disease (Do et al., 2012).

ABCG2 expression has been observed in the proximal tubule brush border of the apical membrane of the human kidney, thereby suggesting a key role in renal drug extrusion

in addition to its role in mediating renal urate secretion (see section 1.18) (Huls et al., 2008). ABCG2 is present on the luminal membrane of intestinal epithelial cells. ABCG2 mRNA expression is maximal in the duodenum and subsequently decreases through the digestive tract (Gutmann et al., 2005). The presence of ABCG2 in the apical membrane of the small intestine and canicular suggests a role in xenobiotic and endogenous substrate export and substrate absorption in the GI tract (Adachi et al., 2005). ABCG2 mediated intestinal drug efflux and barrier functions regulates the role in preventing chronic low-grade inflammation associated obesity. Study has indicated a role in limiting the uptake of dietary carcinogens (e.g. 2-amino-1-methyl-6-phenylimidazo (4,5-b) pyridine (PhIP) - found in cooked meats) (van Herwaarden et al., 2003).

The highest expression levels of ABCG2 are observed in placental syncytiotrophoblast, the apical surface of chorionic villi (Jonker, 2000). Multiple studies above have confirmed that the expression of ABCG2 in the syncytiotrophoblast leads to protection of the foetus by returning ABCG2 substrates into maternal circulation (Jonker, 2000; Zhang et al., 2007).

ABCG2 has also been observed in the ducts and lobules of the breast (Maliepaard et al., 2001a). ABCG2 has shown to transport not only toxic compounds (topotecan, 2-amino-1- methyl-6- phenylimidazo [4, 5- b] pyridine) but vitamins (riboflavin) into breast milk (Jonker et al., 2005; van Herwaarden et al., 2007). This also extends to the dairy industry, where in bovines a common SNP has been shown to influence milk composition, with an effect on milk disposition and quality (Jonker et al., 2005).

ABCG2 is also known to be expressed in a variety of stem cells, especially hematopoietic stem cells as demonstrated in their ability to form a drug exporting sub-population in flow cytometry assays (Goodell et al., 1996). ABCG2 expression is known to vary during haematopoiesis, with the highest level in the primitive bone marrow stem cells followed by sharp decline upon stem cell differentiation (Scharenberg et al., 2002; Zhou et al., 2001). Together with knockout mouse studies indicating greater sensitivity of HSCs to mitoxantrone, this indicates that ABCG2 has a key role in protecting stem cells (Zhou et al., 2002). ABCG2's endogenous expression in healthy tissues has a significant role in drug distribution and pharmacology. Due to its wide tissue distribution, ABCG2 is known to play a key role in maintaining the drug homeostasis, thereby contributing towards tissue and cellular protection.

1.14 ABCG2 pharmacology: substrates and inhibitors

ABCG2 is a poly-specific drug transporter with a vast array of substrates (Mao and Unadkat, 2015). The identified spectrum has increased over the years to include cytotoxic compounds, antibiotics, sterols, dietary xenobiotics, photosensitizers, antibiotics, antiretrovirals, TKI's and carcinogens. ABCG2 is also known to export endogenous compounds such as conjugated organic anions, porphyrin heme, folates, urate and amyloid- β- peptides. The substrates identified in literature are summarised in table 1.2.

ABCG2 wild substrates- chemotherapeutic and non- chemotherapeutic	
Antibiotics	**References**
Erythromycin	(JANVILISRI et al., 2005)
Fluoroquinolone antibiotics (e.g. ciprofloxacin, ofloxacin, norfloxacin)	(Ando et al., 2007; Merino et al., 2006; PULIDO et al., 2006)
Nitrofurantoin	(Merino et al., 2005)
Moxidectin	(Perez et al., 2009)
Anthracenes	
Mitoxantrone	(Litman et al., 2000; Robey et al., 2003)
Bisantrene	(Litman et al., 2000)
Antivirals	
Ganciclovir	(Hu and Liu, 2010)
Zidovudine	(Wang et al., 2013)
Lamivudine	(Kim et al., 2007)
Abacavir	(Pan et al., 2007)
Anti-inflammatories	
Sulfasalazine	(van der Heijden, 2004)
Diclofenac	(Lagas et al., 2009)
Camptothecin derivatives	
Topotecan	(Litman et al., 2000)
SN-38	(Nakatomi et al., 2001)
Irinotecan	(Maliepaard et al., 2001b; Rabindran et al., 1998)
Diflomotecan	(Sparreboom et al., 2004)
Polyglutamates	
Methotrexate	(Z.-S. Chen et al., 2003)
Methotrexate - Glu_2/ Glu_3	(Z.-S. Chen et al., 2003; Volk and Schneider, 2003)
Nucleoside analogues	
AZT	(Wang et al., 2003)
Lamivudine (3TC)	(Wang et al., 2003)
Other drugs	
Prazosin (alpha-1-adrenergic receptor antagonist)	(Litman et al., 2000)
Flavopiridol (flavonoid alkaloid CDK9 kinase inhibitor)	(Robey et al., 2001b)
Gefitinib (tyrosine kinase inhibitor)	(Elkind et al., 2005)
Imatinib (kinase inhibitor)	(Burger et al., 2004)
Nilotinib (tyrosine kinase inhibitor)	(Brendel et al., 2007)
Glyburide (hypoglycaemic agent)	(Zhou et al., 2008)
Cimetidine (histamine H2-receptor antagonist)	(Pavek et al., 2005)
Rosuvastatin (HMG-CoA reductase inhibitor)	(Kitamura et al., 2008)

Table 1.2: ABCG2 substrate repertoire
For each class of transported substrates some examples have been provided. Data based on Mao and Unadkat, 2015.

Efforts have been made to therapeutically target ABCG2 with a range of inhibitors having varied chemical structures have been identified (table 1.3). Inhibiting ABCG2 is useful to counteract multidrug resistance, thereby facilitating the action of cancer drugs. Rabindran et al. reported the first ABCG2 specific inhibitor, fumitremorgin C (FTC). FTC analogues (Ko 132, 134, 143) with lower *in vivo* neurotoxicity and higher potency have also been developed but these have not yet advanced beyond *in vitro* studies (Rabindran et al., 1998).

ABCG2 Inhibitors	
Tyrosine kinase inhibitors	**References**
Gefitinib	(Elkind et al., 2005)
Imatinib	(Burger et al., 2004)
Nilotinib	(Dohse et al., 2010; C Hegedűs et al., 2009)
Lapatinib	(Dai et al., 2008)
HIV protease inhibitor	
Ritonavir	(Gupta et al., 2004)
Nelfinavir	(Gupta et al., 2004)
Lopinavir	(Gupta et al., 2004; Weiss et al., 2006)
HCV protease inhibitor	
Boceprevir	(Christian et al., 1997a)
Telaprevir	(Fujita et al., 2013)
Calcium channel blockers	
Dipyridamole	(Zhang et al., 2005)
Nicardipine	(Zhang et al., 2005)
Nimodipine	(Zhang et al., 2005)
Nitrendipine	(Zhang et al., 2005)
Antifungal zones	
Ketoconazole	(Gupta et al., 2007)
Itraconazole	(Gupta et al., 2007)
Fluconazole	(Gupta et al., 2007)
Fumitremorgin C (FTC)	(Rabindran et al., 1998)
Immunosuppressants	
Cyclosporin A	(Gupta et al., 2007)
Tacrolimus	(Gupta et al., 2007)
Sirolimus	(Gupta et al., 2007)
Other drugs	
Omeprazole	(Breedveld et al., 2004)
Pantoprazole	(Breedveld et al., 2004)
Reserpine	(Zhou et al., 2001)
Ko143 (synthetic derivative of FTC)	(Allen et al., 2002)

Table 1.3: ABCG2 inhibitors
Representation of each class of ABCG2 inhibitor with a few examples mentioned above. Table adapted from Mao and Unadkat, 2015.

The molecular mechanism of ABCG2 inhibition is not yet fully understood. This is partly due to inconsistencies in definition; some reports suggest competitive inhibition, i.e. the inhibitor is also transported and so inhibits the transport of the drug under investigation. Other inhibitors are likely to bind but not be transported by ABCG2. Having experimental systems that can distinguish these are necessary to fully understand the structure activity relationships (SAR) and molecular mechanism of inhibition of ABCG2. Some inhibitors allosterically affect the binding sites. Giri et al. and Clark et al. provided evidence for multiple binding sites for ABCG2 substrates. Nelfinavir, an HIV protease inhibitor, showed inhibition effect on zidovudine and abacavir efflux but showed no effect on prazosin and imatinib efflux, thereby confirming the presence of multiple binding sites (Giri et al., 2009).

The only available SAR study is based on camptothecin (CPT) analogues. One of the few SAR studies have been performed on a series of camptothecin analogues. These agents are topoisomerase 2 inhibitors exemplified irinotecan and its intracellular active metabolite SN- 38 (7- ethyl- 10- hydroxycamptothecin). Yoshikawa et al. in their study synthesised a range of analogues with varying polarities and identified that increasing polarity was associated with ABCG2 inhibition and lower polarity analogues being good ABCG2 substrates (Yoshikawa et al., 2004). Based on quantitative SAR methods, certain properties have been associated with the potential ABCG2 inhibitors; lipophilicity a potential determinant for inhibition (flavonoids and FTC analogues), planar structure, amine bonded to carbon of heterocyclic ring and hydrogen bonding potential (Basseville et al., 2016a; Mao and Unadkat, 2015).

The SAR study fits with theoretical considerations of ABCG2 substrates which concluded that ABCG2 transports compounds with higher amphipathicity than P-gp, whose substrates tend to be more hydrophobic (Egido et al., 2015). Pan et al. developed Bayesian classification method to predict the ABCG2 inhibitors based on virtual screening methods with an overall prediction accuracy of 70% (Basseville et al., 2016a; Mao and Unadkat, 2015).

Hazai et al. developed a support vector machine to predict wild type ABCG2 substrates with prediction accuracy of 76%. It is a free web server used to predict whether a query compound is the substrate for ABCG2 and hence determine its physiochemical properties. This model has proven to be valuable in screening the potential ABCG2 substrates (Basseville et al., 2016a; Hazai et al., 2013). Prediction of whether a

compound is an ABCG2 substrate or inhibitor is still subject to low success rates due to limited SAR, thus all new drugs are routinely tested for ABCG2 transport.

To further knowledge on the pharmacology and mode of action against tumour cells, the molecular mechanism behind the promiscuous drug binding sites need to be revealed. A better understanding of ABCG2 pharmacology is required for the development of better methods to probe ABCG2: substrate interactions in wild type and mutant protein variants.

1.15 Role of ABCG2 in multidrug resistance (MDR)

Overexpression of ABCG2 in several cancer tissues is associated with multidrug resistance (Ross and Nakanishi, 2010). Several clinical studies on ABCG2 have shown it confers multidrug resistance in acute myeloid leukaemia (AML) and a correlation has been observed between high levels of ABCG2 expression and its poor outcome (Natarajan et al., 2012). ABCG2 expression is correlated to resistance to flavopiridol (in blast cells; Ross et al., 2000) or complete failure to cytosine arabinoside (Steinbach et al., 2002). Studies have also indicated the association of higher ABCG2 with lower overall survival rates but not always lower frequencies of complete remission (Benderra, 2005). ABCG2 overexpression has also been detected in a variety of solid tumours such as retinoblastoma, lung, liver and pancreatic cancers (Diestra et al., 2002). High levels of ABCG2 mRNA expression and poor response to anthracycline based chemotherapy was observed with a borderline significance in one study (Burger et al., 2003). A study on resected pancreatic ductal adenocarcinoma ABCG2 expression has been reported as a prognostic factor for early tumour recurrence and poor survival (Nakanishi and Ross, 2012).

ABCG2 overexpression has also been observed in various cancer cell lines such as gastric carcinoma, fibrosarcoma, NSCLC, glioblastoma, prostate cancer and myeloma (Nakanishi and Ross, 2012; Volk et al., 2002; Xie et al., 2008). Flow cytometry and a tetrazolium dye assay revealed topotecan accumulation and drug sensitivity in lung cancer cells. The results declared significant correlation of ABCG2 mRNA expression and function with sensitivity to SN-38 and topotecan (International Transporter Consortium et al., 2010).

1.16 ABCG2 overall topology

ABCG2 is a 72kDa integral membrane protein of 655 amino acids. It is a polytopic transmembrane protein comprising 6 transmembrane helices and an amino terminal nucleotide binding domain (Allikmets et al., 1998). It has a reverse organization with the NBD- N-terminal to TMD. It is referred to as a half transporter with one NBD and one TMD, in lieu of the typical canonical structure of ABC transporters comprising of two TMDs and two NBDs (Mao and Unadkat, 2015; McDevitt et al., 2008). Wang et al. confirmed the predicted membrane topology of ABCG2 using epitope insertion and immunofluorescence. A single, N- glycosylation site at Asparagine 596 is present in the extracellular loop between transmembrane 5 and 6. The predicted transmembrane helices 1, 3, 4 and 6 fall in agreement with the experimental topology, with TM2 and TM5 slightly shifted between the experimental and predicted data (figure 1.10 A) (Mao and Unadkat, 2015; Wang et al., 2008). More recent structural observations have seen a refinement of this topological model as indicated in figure 1.10 B.

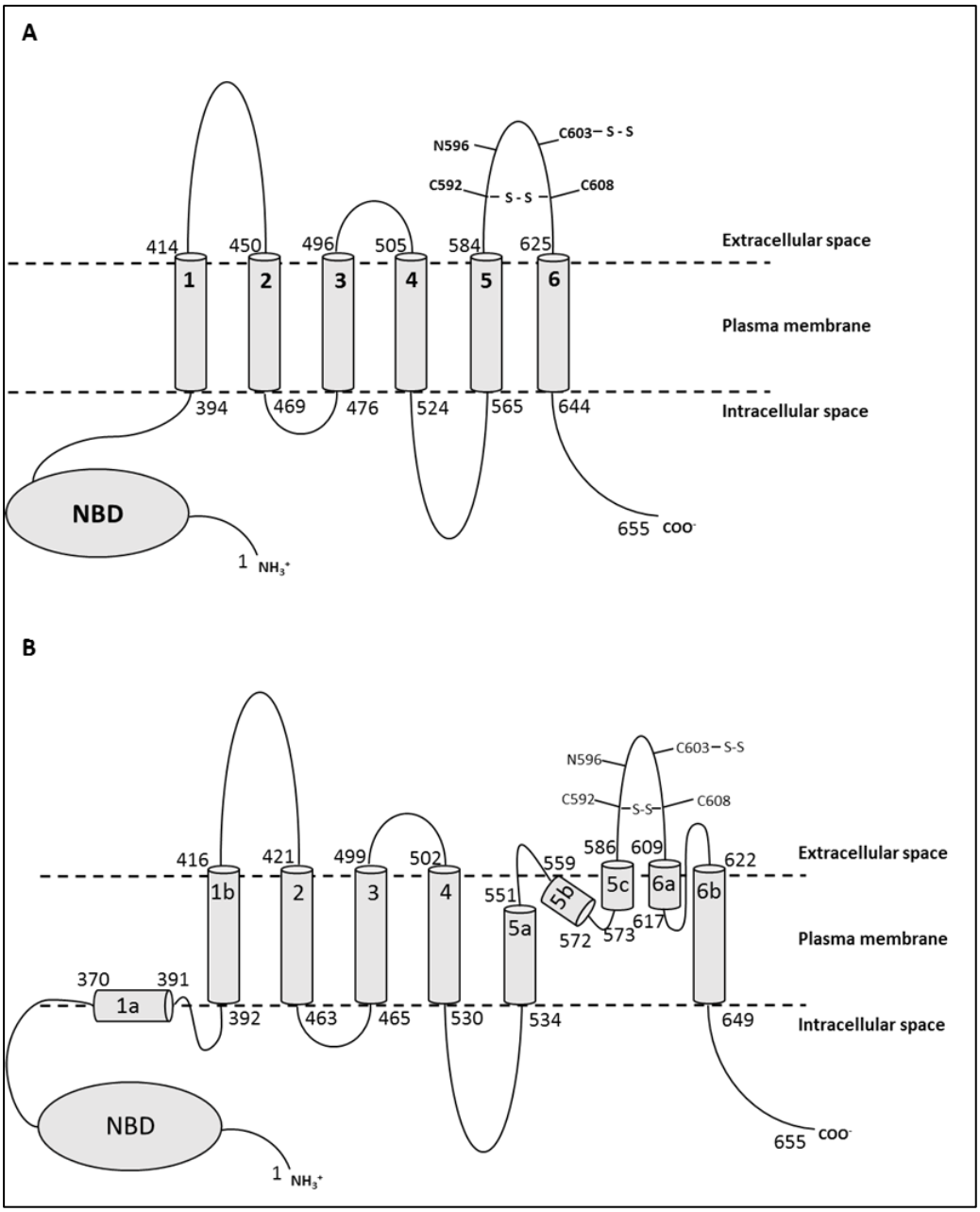


Figure 1.10: ABCG2 predicted and experimental membrane topology

A monomer of ABCG2 transporter comprising of 6 α helical TMD and NBD in a reverse organization, i.e. with the NBD N- terminal to the TMD. A) The boundary of trans-membrane domain α helices is an approximate determination based on computation predictions, epitope insertion and immunofluorescence (Wang *et al.*, 2008). B) The structure of ABCG2 by cryo-EM results in a different assignment of TM regions (Taylor et al., 2017). N- glycosylation site Asn596 and the three cysteine residues Cys 592, 603 and 608 mentioned in the text as being involved in disulphide bond formation are also shown.

1.17 Oligomerization state for a functional ABCG2 transporter

Understanding the oligomerization state of ABCG2 is a critical step to understand the function of the transporter. Various studies have outlined the necessity of having two membrane spanning and two nucleotide binding domains to form a translocation pathway for an ABC transporter. ABCG2, being a half transporter, could simply function as a homodimer.

Cysteine-scanning mutagenesis of ABCG2 by Kage et al. suggested the occurrence of a homodimer bridged by disulphide bonds between residues C603 in the extracellular loops (Kage et al., 2005). The Hrycyna group demonstrated that ABCG2 dimers were present even in the absence of C603 disulfide bond indicating that the intermolecular disulphide bond was not a requirement for dimerization but perhaps a consequence of dimerization (Bhatia et al., 2005).The oligomeric state of ABCG2 was also characterised using chimeric fusion proteins of two ABCG2 proteins joined either a peptide linkers. Biotinylation and cell surface antibody labelling experiments proved plasma membrane localisation of chimeric ABCG2 dimers and fluorescent drug accumulation assays confirmed drug transport activity. Mutation of the conserved Asp210 residue in the Walker-B motif rendered the dimer non-functional. The study demonstrated the importance of two ATP sites for activity and that the basic functional unit of ABCG2 is a dimer. Photoaffinity and chemical cross-linking experiments indicated that ABCG2 can form dimers under reducing conditions and that the interface between monomers include interactions between the NBDs as well as disulphide linkages between cysteines in the third extracellular loop of each monomer. The study also demonstrated a lack of importance of the extracellular disulphide bridges in function, rendering them not critical for dimerization (Bhatia et al., 2005).

Xu et al., have shown higher order oligomeric states for ABCG2. They provided evidence for occurrence of a homotetramer based on detergent solubilisation of ABCG2 (McDevitt et al., 2009; Ni et al., 2010). FRET analysis has been performed to determine the higher order oligomeric state of ABCG2, using GFP/ YFP tagged protein. The FRET efficiencies for tagged ABCG2 were higher than in the GFP/ YFP pair control, thereby suggesting homooligomer formation (Ni et al., 2010). Structural data by McDevitt et al. based on, low resolution EM, illustrated the formation of higher

order oligomeric complex in detergent solutions with as many as 8 ABCG2 monomeric units in the electron density (McDevitt et al., 2006). Rosenberg et al. improved the structural resolution of ABCG2 expressed in *Pichia pastoris* by cryo-EM. The structure was determined at 5Å resolution with 4 ABCG2 monomers (tetrameric state) in one-unit cell of the crystal (Ni et al., 2010; Rosenberg et al., 2010). Analysis of R482G mutant ABCG2 by blue native gel and EM provided evidence of large oligomeric complex (octameric state- tetramer of dimers). This higher order oligomeric state was stable in the presence of a reducing agent, thereby confirming the presence of non-covalent protein-protein interactions, shielding the disulphide bridges (McDevitt et al., 2006).

Recently, Wong et al., characterized the oligomeric organization of ABCG2 transporter in live mammalian cells using single particle imaging techniques. This revealed the presence of dimers and tetramers with the suggestion that tetrameric organisation of ABCG2 may indicate transient complexes (Wong et al., 2016). Recent cryo-EM structures demonstrate the protein to form dimeric complexes. This has been explained in detail in section 1.22.

1.18 Molecular mechanism of ABCG2: do naturally occurring SNPs help?

Single nucleotide polymorphisms (SNPs) lead to generation of natural variants in the coding region of ABCG2 that may have a significant effect on physiological and pharmacological relevance. More than 80 SNPs have been identified for ABCG2 that incorporate the promoter, intronic and protein coding changes (Heyes et al., 2018).

These SNPs are located throughout ABCG2 but only a very small number of these have been studied well enough to recognize its effect on the protein's structure and mechanism. A complete overview of SNPs is given in Heyes et al. 2018.

The most well characterised SNP is Q141K (421C>A, rss2231142), where glutamine is replaced by lysine. This substitution is found between the Walker-A motif and the signature region of the NBD (figure 1.10 B) (Owen M. Woodward et al., 2009).

One of the key outcomes of Q141K has been its with high serum urate levels (Dehghan et al., 2008; O. M. Woodward et al., 2009; Woodward, 2015; Woodward et al., 2013). This observation was supported by *in vitro* studies demonstrating that ABCG2 could

transport radiolabelled urate whereas the Q141K variant had reduced expression and function (O. M. Woodward et al., 2009).

This can be rationalised using the cryo-EM structural data (see section 1.22), where the positively charged lysine residue leads to electrostatic repulsion with transmembrane helix 1a leading to a folding defect and degradation by endoplasmic reticulum based protein degradation system (Heyes et al., 2018; Lászloá et al., 2016; Taylor et al., 2017; Wakabayashi-Nakao et al., 2009). Clinically, this SNP was shown to be associated with variations in the pharmacokinetic response to several drugs presumably as a result of the effects on expression and function (Cleophas et al., 2017; Higashino et al., 2017). An *in vitro* study with camptothecin analogues has shown Q141K cells to be more susceptible to diflomotecan treatment with IC_{50} values 1.2 to 2.3 fold lower compared to the wild type (Morisaki et al., 2005; Sparreboom et al., 2004). Q141K has shown to have no significant influence on irinotecan and its metabolite (SN-38) disposition (Han et al., 2007; Sai et al., 2010). *In vitro* studies based on irinotecan pharmacokinetics support cellular resistance to SN-38 (Jandu et al., 2016; Tamura et al., 2007). 421C>A genotypes have shown 1.5-fold increased steady state gefitinib accumulation compared with the wild type (Cusatis et al., 2006). The SNP has also been associated with increased drug induced diarrhoea in Korean patients being treated with Gefitinib therapy or receiving rituximab and cyclophosphamide/ doxorubicin/ prednisone (Basseville et al., 2016b; Kim et al., 2008).

Q141K has been linked to poorer outcomes in prostate cancer with reduced efflux of folate from the tumour cells facilitating cancer proliferation. It is also known to reduce the efflux of docetaxel, resulting in improved drug efficacy (Sobek et al., 2017).

The Q141K SNP is one of the strongest predictors of serum hyperuricemia and so attempts have been made to rescue the mis-trafficked Q141K mutant. Given the location of this mutation being structurally identical to the D508F mutation in CFTR, several CFTR correctors (including VRT- 325) as well as other known small molecule effectors (4- phenylbutyrate and romidepsin) have been investigated and shown to restore expression and function etc. with efficacy in gout treatment (Basseville et al., 2012; Woodward et al., 2013).

There are mutations in the TMD that might impact protein stability and drug specificity (figure 1.10 B). Some of the key SNPs have been discussed below. F431L, located in the TM2 segment leads to loss of function, resulting in impaired porphyrin transport,

decreased resistance to SN-38 and mitoxantrone (Tamura et al., 2007; Yoshioka et al., 2007). This may result in increased risk for hypersensitivity to anticancer agents such as methotrexate, where the transport is completely abolished (Yoshioka et al., 2007). S441N, located in TM2 causes protein instability, facilitating enhanced proteasomal degradation and reduced protein expression levels at the plasma membrane (Wakabayashi-Nakao et al., 2009). Cell based assays have reported reduction and abolition of urate, porphyrins, SN-38 and mitoxantrone transport (Sjöstedt et al., 2017; Tamura et al., 2007, 2006). F489L, located in the TM3 helix, which is a crucial part of this study, is known to impair protein function (unable to transport methotrexate) (Tamura et al., 2006). F489A variant, expressed in this study is also known to reduce pheophorbide-a transportation, with no effect on protein expression (Cox et al., 2018). Intriguingly, ABCG2 has been identified as the genetic basis for the Junior (Jr) blood group system, where the null alleles of ABCG2 cause the Jr (a-) blood type, which leads to insertion of a premature stop codon (Saison et al., 2012; Zelinski et al., 2012). Alleles associated with Jr blood group include Q126X (376 C>T) (Honjo et al., 2002). R246X (706 C>T) (Kasza et al., 2012), R236X, R113X, G262X, Q531X and delS340 (Zelinski et al., 2012). However, studies need to be undertaken to understand the role of Jr (a-) blood group type on the drug pharmacokinetics, disposition and treatment outcome.

The above-mentioned polymorphisms though reflect on ABCG2 expression, but limited research is available to shed light on their effects on drug therapy. *In vivo* research is needed to understand the effects on ABCG2 expression and drug pharmacokinetics before any definitive conclusions can be drawn.

1.19 Site directed mutagenesis

Site directed mutagenesis has been employed to determine the structure and function of ABCG2 transporter. It is key to determine critical residues for substrate selectivity and transport. The mutations may or may not affect the protein expression and alter the substrate specificity or activity. A list of mutagenesis analysis studies that affected expression and function have been documented in table 1.4.

The most relevant mutations for this study are at two sites in the 3rd TM helix (TM3). Certain drug selected cell lines used in the cloning of ABCG2 contained mutations of

position 482, where typically the wild type arginine was replaced by a glycine or threonine (R482G/T) and it became clear that these mutations confer increased substrate repertoire upon ABCG2 (Robey et al., 2003). The R482G (or T) mutant transports daunorubicin, rhodamine 123 and lyso tracker green, none of which are substrates of the wild type ABCG2 (Honjo et al., 2001). Site directed mutagenesis of proline 485 to alanine which is located one helical turn apart from R482 has also shown to reduce the efflux of BODIPY- prazosin (up to 70%) and pheophorbide A (porphyrin derivative) compared to the wild type ABCG2 protein (Haider et al., 2015; Mao and Unadkat, 2015).

The location of two proximal residues in TM3 helix that alter drug transport provides the foundation for one aspect of this thesis which postulates a general role for TM3 in drug transport.

Residue	Mutation	Effects	References
K86 (NBD Walker-A motif)	K86M, K86I	Alter transporter activity, complete loss of ATPase activity and transport, altered sub cellular localisation and cell surface targeting	(Henriksen, 2005; Özvegy et al., 2002)
E211 (NBD Walker-B motif)	E211Q	Complete loss of ATPase activity and ATP dependant transport of methotrexate.	(Hou et al., 2009)
R482 (TM3 helix)	R482G/T/A	Altered substrate repertoire, gain of function mutation for daunorubicin and rhodamine 123 but complete loss of transport activity for methotrexate.	(MITOMO et al., 2003; Miwa et al., 2003; Özvegy-Laczka et al., 2005; Robey et al., 2003)
P485 (TM3 helix)	P485A	Altered substrate repertoire (for Mx, pheo-A and prazosin)	(Cox et al., 2018; Haider et al., 2015)
I573 (TM5 helix)	I573A	Disrupted glycosylation, reduced expression and trafficking kinetics	(Haider et al., 2015)
N596 (ECL3)	N596Q	Post translational modification- loss of glycosylation, enhanced ubiquitin mediated degradation, altered protein expression	(Diop and Hrycyna, 2005; Mohrmann et al., 2005)
C603 (ECL3)	C603A	No effect on membrane expression and function; disulphide bridge. No expression on membrane expression, function and dimerization *in vivo*. Triple mutation (C592A, C603A and C608A) leads to decreased expression with no measurable transporter activity. C603A and C608A double mutation is involved in ABCG2 dimerization. Triple mutation of C592, C603 and C608 to serine shows impaired expression and sub cellular localisation but retained activity with altered substrate specificity.	(Henriksen et al., 2005; Kage et al., 2005; Ni et al., 2010; Shigeta et al., 2010)

Table 1.4: Site directed mutagenesis for key ABCG2 residues

Site directed mutagenesis of residues of interest to study expression, stability, selectivity and transporter activity of ABCG2.

1.20 Multiple drug binding sites

There is clear evidence that ABCG2 (like P-gp) possesses multiple drug binding sites. Crude membranes generated from the insect cells expressing ABCG2 were used to quantify binding of [^{3}H] daunomycin. The study revealed that doxorubicin, prazosin and daunomycin completely displaced the bound [^{3}H] daunomycin, whereas mitoxantrone and Hoechst 33342 partially displaced the bound [^{3}H] daunomycin, thereby suggesting multiple drug binding sites (non-allosteric, pharmacologically distinct drug binding sites) on the transporter (Clark et al., 2006). An *in vitro* study involving MDCKII cells transfected with murine ABCG2 also confirmed multiple binding regions in the protein. The nucleoside substrates zidovudine and abacavir seem to bind to a region that may have minimum or no overlap with the binding regions of both prazosin and imatinib (Giri et al., 2009). The possibility of multiple drug binding sites on ABCG2 cannot be refuted and hence further investigations need to be performed to understand the drug selectivity and translocation by the multidrug transporter.

1.21 Conformational change associated with ATP hydrolysis, drug binding and translocation by ABCG2

Drug translocation requires drug binding events in the TMD to be coupled to catalytic cycles within the NBDs. The translocation process involves alteration of the drug binding sites from high affinity (inward facing conformation) to low affinity (outward facing conformation). The energy produced by ATP hydrolysis is harnessed to set the transporter in the inward facing conformation. Nucleotide binding provides the power stroke needed to translocate the substrates. The evidence to support communication between ABCG2 NBD and TMD is shown by the substitution of the catalytic carboxylate E211 (Walker-B motif) to a non-charged glutamine residue. This substitution completely abolished the ATP dependent methotrexate transport, thus demonstrating the importance of ATP hydrolysis in drug translocation (Hou et al., 2009). Thus, ATP binding plays a crucial role in the formation of the NBD- ATP dimer sandwich structure and ATP dependent solute transport.

In a study by McDevitt et al. the binding of daunomycin was abrogated by the presence of ATP analogues (ATP-γ- S and TNP-ATP), transitioning to a low affinity conformation prior to ATP hydrolysis. This sequence of events indicate that the binding of ATP provides the power stroke for drug translocation, suggesting cross talk between the NBDs and the TMDs during substrate transportation (McDevitt et al., 2008).

The recent cryo-EM structure of ABCG2 bound to the Ko143 derivative MZ29 sheds light on the conformational coupling between the NBDs and the TMDs. Jackson et al. identified MZ29 as the most potent synthetic inhibitor for the ATPase activity as it fully abolished the estrone-1-sulfate transport. The plausible explanation for this is dependent on the relative affinities of the potential substrates and inhibitors. The inhibitors tightly bind to the central cavity and lock the inward facing state. MZ29 was identified to be bound at 2:1 molar ratio of the inhibitor to ABCG2 homodimer. Binding of inhibitor in the central cavity indicates cross talk between the NBDs and TMDs due to conformational coupling. Closure of central cavity and subsequent development of the inward facing conformation and concomitant NBD dimer closure is a prerequisite for outward facing conformation, ATP hydrolysis and substrate translocation (Jackson et al., 2018).

1.22 ABCG2 structure advances from past to current with the cryo-EM revolution

To unravel the molecular mechanism behind the structure activity relationship between ABCG2 substrates, inhibitors and modulators, high resolution structural studies are a must. Prior to high resolution structural information being available on ABCG2 there were a plethora of models based on templates such as MalK, Sav1866, murine P-gp and MsbA to interpret low resolution electron microscopy data (McDevitt et al., 2009; Rosenberg et al., 2015). However, these were unable to serve as a basis to make any rational interpretation of the mechanism of protein function, primarily as these structures did not make for suitable homology modelling templates (Kerr et al., 2010).

Early EM studies, either using single particle imaging (McDevitt et al., 2006) or projection structures from 2D crystals (Rosenberg et al., 2015, 2010) were at too low

a resolution to define much more than the molecular envelope of ABCG2 and confirm that conformational changes of the protein occurred upon drug binding. The first 3D structure of human full length ABCG2 by electron crystallography revealed an inward facing apo conformation with the NBDs well separated, a refinement to the homology model (Rosenberg et al., 2015, 2010). The model identified the NBDs and TMDs along with their organisation in the homodimer, but due to a lack of high-resolution data, the structure did not reveal molecular details at the NBD-TMD interface (intracellular loops and the linker region) (Rosenberg et al., 2015). Murine ABCB1 structure was chosen to interpret 3D map due to its inward facing state with the V shape constituting the angle, which appeared to be compatible with the 3D map (figure 1.11 A). The model represents crossing over of the intracellular loops (ICL2) to directly contact the NBD of the opposing monomer and likely to function as a coupling helix. This is reminiscent of type 1 exporters, where the TMDs interact with the NBDs of the opposite monomer *via* intracellular loops and facilitate substrate transportation coupled with ATP hydrolysis (Dawson et al., 2007; Zolnerciks et al., 2007).

The past decade has seen tremendous growth in membrane protein biology research, attributed to technical progress made in the cryo-EM field. Rapid advancement has been seen in the field based that have led to better structural reconstitutions. Firstly, the new generation of electron detectors provide movie mode functionality by integrating signals from the individual movies. Another factor is the development in image processing tools that have synergised better reconstructions from heterogeneous samples and facilitated electron beam irradiation, inducing sample movement. These new processing tools facilitate image classifications based on different structural states. These advancements yield density maps with sufficient data to deduce atomic resolution structures. This makes cryo-EM a resolution rival to X-ray crystallography (Bai et al., 2015).

This revolution has seen huge progress in terms of availability of structural data for the multidrug transporter ABCG2 based on cryo EM studies performed by Kasper Locher's group. The first 3.8 Å resolution 3- D structure for human ABCG2 in complex with two antigen binding fragments of the inhibitory antibody; 5D3 (5D3-Fab) was determined using single particle cryo EM. The structure was broadly in agreement with a landmark crystal structure of the related heterodimeric ABCG5/ G8 protein obtained earlier the same year (Lee et al., 2016), which demonstrated a novel G- family ABC transporter fold. Despite similarities there were a plethora of

differences that were difficult to interpret initially due to lack of higher resolution structural data (Taylor et al., 2017). The structure reveals a compact conformation of ABCG2 when compared to the B subfamily ABC transporters (figure 1.11 A and C). The compact fold observed is more reminiscent of bacterial ABC importers (figure 1.10 C). The fold also resembles type II exporters as the TM helices do not cross over to contact the opposite NBDs. Instead the TMDs only form contacts with the NBDs through the ICLs between TMH2 and TMH3. This contact is further stabilised by the preceding helix (TMH1a), that acts as a membrane anchor, also called the connecting helix. The connecting helix is known to form contacts with ICL1 (intracellular loop 1, between TM2 and TM3 helices) and an α- helix within the NBD containing Q141, which could potentially shed light on destabilisation incurred by the Q141K mutation (Lászloá et al., 2016; Lee et al., 2016; Taylor et al., 2017).

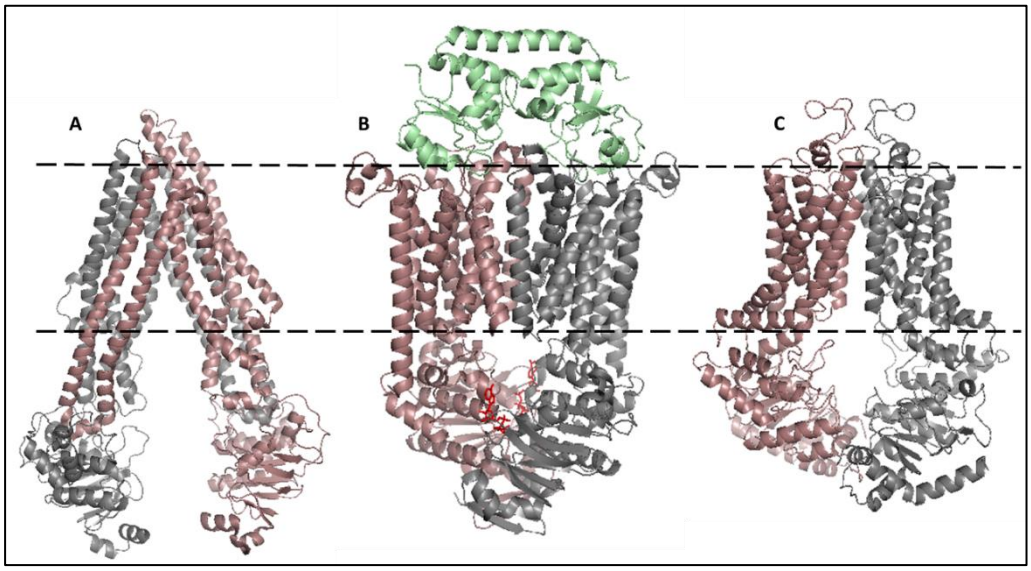


Figure 1.11: ABCG2 structure resembles type II transporter fold

(A) Type 1 exporter structural topology of human ABCB1 in the post hydrolytic open inward conformation represent domain swapping (PDB: 6GDI). (B) A type II importer fold exemplified by the ButCD-F transporter in the nucleotide bound state with SBP (green). The TMD organisation does not reflect any domain swapping (PDB: 4FI3). (C) ABCG2 structure adopts a compact conformation with no domain swapping, reminiscent of type II importer (PDB: 6ETI). One half of each structure has been highlighted as dull violet for ease of visualisation.

The structure reveals an inward open conformation with a large hydrophobic slit like cavity (cavity 1, multidrug binding pocket) enveloped by the transmembrane helices (TM5 and TM2a of the opposite monomers) (figure 1.12). The cavity also revealed the

presence of 2 cholesterol molecules bound, thereby suggesting the possibility of substrates with similar properties such as estrone-3-sulphate (E_1S) to bind. This large cavity is separated from a smaller, more extracellular cavity by a "leucine plug" formed by the residues L554- L555 of the opposing monomers (figure 1.12) (Taylor et al., 2017). Despite the availability of this structure, the caveat in the study is the presence of inhibitory antibody that locks the conformation of the transporter in an inactive state (Cox et al., 2018).

The novel G- family fold reveals contact between the NBDs even in the absence of the bound nucleotide (Taylor et al., 2017). Similar contacts were observed in the crystal structure of ABCG5/ G8, in the absence of the bound nucleotide, at the cytoplasmic interface to form a closed conformation through a pair of NPXDF motifs (Lee et al., 2016). These motifs are highly conserved amongst the ABCG subfamily and hence form a subset for this study to be investigated in detail in chapter 6. Another notable characteristic of the ABCG structures is the presence of short helices (TM 5b, 5c and 6a) which appear to form a structural cap at the extracellular interface of the NBDs (figure 1.12) (Lászloá et al., 2016; Lee et al., 2016; Taylor et al., 2017).

More recently, cryo-EM structures of human ABCG2 bound to distinct inhibitors (synthetic derivative of Fumitremorgin C; Ko143 or multidrug resistance modulator tariquidar) in the central cavity (cavity 1), in the presence of Fab- 5D3 were published (figure 1.12). This cavity can potentially bind one or more inhibitors symmetrically or asymmetrically depending on the size of the inhibitor. The binding pocket (central cavity/ cavity 1) forms a 2-fold symmetry axis, completely occupied by the inhibitors. The study proposes competitive binding of the inhibitors in cavity 1, thereby locking the transporter in the inward facing orientation, which disrupts the NBD closure and ATP hydrolysis. The study also highlights allosteric effects associated with cholesterol binding, thereby suggesting the importance of cholesterol in ABCG2 structure and function and the presence of an ordered cholesterol molecule in the binding cavity 1 consistent with earlier experimental observations (Jackson et al., 2018; Manolaridis et al., 2018; Storch et al., 2007a; Taylor et al., 2017).

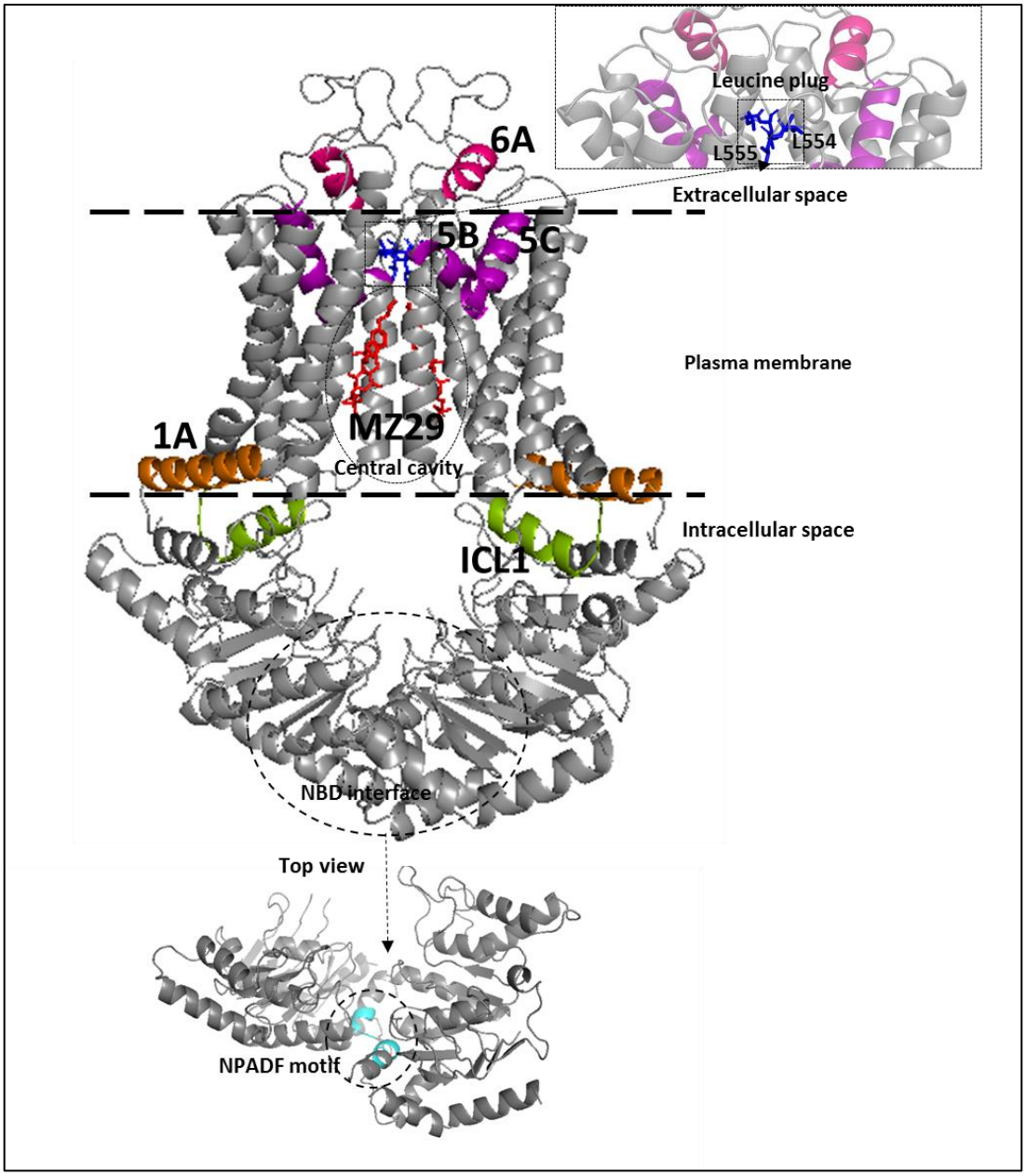


Figure 1.12: Structure of ABCG2

ABCG2 homodimer cryo-EM structure with key structural elements highlighted. The central cavity (cavity 1) of the cryo-EM structure shown here is occupied by an inhibitory Ko143 derivative, MZ29 (red stick representation). This large central cavity is separated from a smaller, more extracellular cavity by a "leucine plug" (enlarged view) formed by the residues L554- L555 of the opposing monomers (blue stick representation). The key folds of the structure reveal contact between the NBDs (top view, enlarged) despite the absence of bound nucleotide at the cytoplasmic interface to form a closed conformation through a pair of NPXDF motifs (cyan) that are highly conserved amongst the ABCG subfamily. This fold also consists of the elbow helix (1a; orange), the intracellular loop 1 (lime green). Another notable characteristic of the ABCG2 structure is the presence of short helices (TM 5b, 5c; purple and 6a; pink) which appear to form a structural cap at the extracellular interface. Figure generated in PyMOL software (PDB: 6ETI; (Jackson et al., 2018)).

1.23 Project Objectives and outlines

The structures of ABCG2 show a novel ABCG family fold that means that any previous homology model-based interpretation of transport mechanism of this family will be inaccurate. The structures are powerful advances in research, but they leave several questions unanswered.

- How does the structure help understand the role of TM3 helix in drug selectivity?
- How do drugs access cavity 1 prior to being transported?
- What is the role of the novel ABCG family NBD interface?
- What distinguishes inhibitors from substrates?
- Is the leucine plug model for transport correct?

Previous studies have shown the TM3 helix is involved in drug selectivity. Although, the structure of ABCG2 suggests that this is due to allosteric effects there is data indicating a wider role of TM3 helix in drug selectivity. Transmembrane 3 (TM3) helix of ABCG2 has been shown to play a role in determining substrate specificity. Previous research indicated that R482 and P485 within the TM3 are crucial to drug binding and/ or translocation (figure 1.13). The two residues are one helical turn apart, where the nature of the residue at position 482 has shown to alter the substrate repertoire whereas P485 substitution has shown to reduce the substrate transportation. The ABCG2 mutants (R482T and R482G) transport daunorubicin, rhodamine 123, lyso tracker green (non-wild type substrates). The wild type and the mutant isoforms are also known to transport mitoxantrone, prazosin and Hoechst 33342, whereas the wild type transports methotrexate. Site directed mutagenesis of proline 485 to alanine in TM3 has shown to reduce the efflux of BODIPY- prazosin and pheophorbide-a (porphyrin derivative) compared to wild type ABCG2 protein (Haider et al., 2015; Mao and Unadkat, 2015).

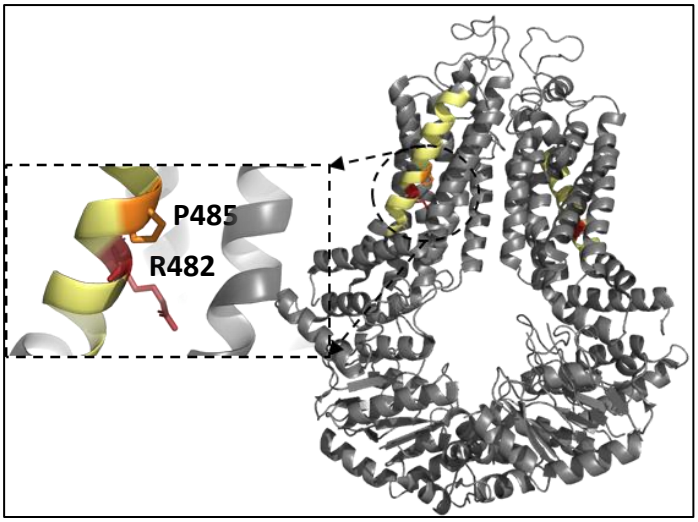


Figure 1.13: Cryo-EM structure of ABCG2 homodimer

The ABCG2 homodimer structure with TM3 helix highlighted in pale yellow and the key residues that altered substrate specificity highlighted (stick representation), i.e. R482 (red) and P485 (orange), one helical turn apart (enlarged). Figure generated in PyMOL (PDB: 6ETI; (Jackson et al., 2018))

As described earlier, the study of ABCG2 TM 3 helix is crucial to understanding its role in drug binding, interaction and transport selectivity (Clark et al., 2006; Haider et al., 2015; Robey et al., 2003). The research hypothesis emerged from studies of R482 and P485. Point mutations were generated along the length of the TM3 helix (D477-L497) in order to understand the role of these residues in drug interactions and transport selectivity and made us consider whether TM3 helix would harbour further residues of interest that would influence the substrate specificity.

The study also focuses on understanding the role of novel ABCG specific NBD: NBD interface region. An unusual feature of the ABCG subfamily structures is the presence of two NBD: NBD interaction interfaces (figure 1.14). The classical interface between the Walker-A and -B motifs of one NBD with the signature motif of the opposing NBD. The second is the presence of unique NPXDF motif, located C-terminal to the His-switch motif (figure 1.14).

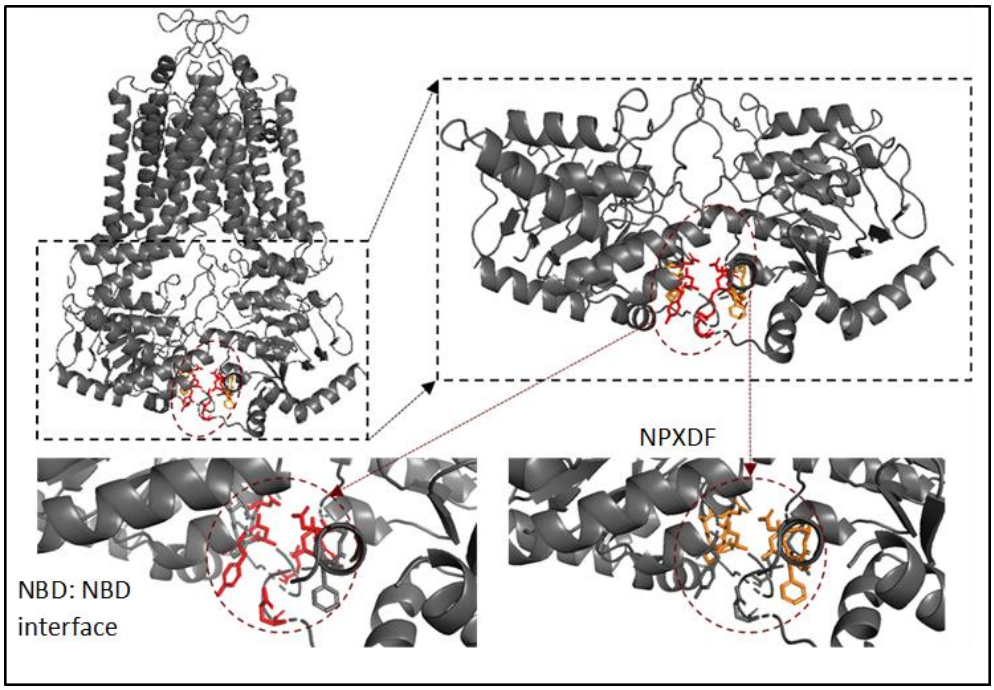


Figure 1.14: Structural mapping of the highly conserved residues at the NBD: NBD interface
The ABCG2 homodimer cryo-EM structure with the enlarged view of the NBD, *de novo* built based the side chain density. The structure depicts the NBD: NBD interface. The structural mapping of the highly conserved motif, unique to the G subfamily; NPXDF motif in orange stick representation and the NBD interface residues (Y247, E285, N289 and D292) are in red stick representation. Figure generated in PyMOL (PDB: 6ETI; (Jackson et al., 2018)).

We investigate the significance of this unique NBD: NBD interface by point mutation of residues contributing to this interaction surface. The combined information from the two studies will hopefully enable a better understanding of the molecular mechanism of translocation adopted by the multidrug transporter.

The aims of this project are three-fold-

i) Understand the contribution of residues in transmembrane helix 3 to drug binding and translocation.

ii) Address how drugs access cavity 1 from the membrane.

iii) Understand the role of the unique NBD interface.

The transporter functionality understanding would facilitate future studies of the mechanisms of ABCG2 substrate recognition and provide an improved toolset for assessing substrate/inhibitor interactions.

Chapter 2: Experimental design: methods

All molecular biology reagents were purchased from New England Biolabs (NEB, Hitchin, UK) and Promega (Southampton, UK), unless stated otherwise. The primers for site directed mutagenesis were ordered from Sigma-Aldrich (Poole, UK). All the molecular biology reagents were purchased from New England Biolabs. All chemicals were obtained from Sigma and Thermo-Fisher and were of laboratory reagent grade or higher available unless otherwise mentioned.

2.1 Molecular biology

2.1.1 Primer designing for site directed mutagenesis

Oligonucleotide primer pairs (forward and reverse) were designed for the plasmid pcDNA3.1Zeo_sfGFP_ABCG2, which encodes wild type (WT) ABCG2 with an N-terminal superfolder (sf) green fluorescent protein (GFP) tag. The primers were designed to insert the desired mutation into the amplified sequence from the template DNA. Primer sequences were designed to be 25- 45 bases in length with 40- 60 % GC (guanine and cytosine) content and were analysed using NetPrimer (PREMIER Biosoft; http://www.premierbiosoft.com/netprimer/). Reverse complement was performed using the RevSeq (EMBOSS: revseq- Bioinformatics; www.bioinformatics.nl/cgi-bin/emboss/**revseq**) in order to generate the reverse primer. The list of primer pairs generated are depicted in table 2.1.

Mutation	Forward (F') primer	T_M (°C)
Transmembrane helix 3 mutant isoforms		
D477A	5′ ggaaaactgttatct**GCC**ttattacccatgagg 3′	71.3
L478A	5′ ctgttatctgat**GCC**ttacccatgaggatg 3′	72.5
L479A	5′ ctgttatctgattta**GC**acccatgaggatg 3′	68.6
P480A	5′ gttatctgatttatta**GCG**atgaggatgttacc 3′	67.1

M481A	5′ ctgatttattaccc**GCC**aggatgttacc 3′	68.4
R482A	5′ gatttattacccatg**GC**gatgttacc 3′	64.5
M483A	5′ gatttattacccatg**C**g**AGCG**ttaccaagtattatatttacc 3′	74.7
L484A	5′ cccatgaggatg**GCA**ccaagtattatatttacc 3′	71.6
S486A	5′ gaggatgttacca**GCC**attatatttacctg 3′	65.6
I487A	5′ gttaccaagt**GCG**atatttacctg 3′	58.3
I488A	5′ gttaccaagtatt**GCC**tttacctgtatagtg 3′	65.1
F489A	5′ ccaagtattata**GCG**acctgtatagtgtac 3′	60.9
T490A	5′ ccaagtattatatt**CG**cctgtatagtgtacttcatg 3′	67.9
C491A	5′ caagtattatatttaccGCCatCgtgtacttcatgttagg 3′	73.7
I492A	5′ gtattatatttacctgt**GCC**gtgtacttcatg 3′	65.7
V493A	5′ cctgtata**GCG**tacttcatgttaggattg 3′	63.8
Y494A	5′ cctgtatagtg**GCG**ttcatgttaggattg 3′	67.6
F495A	5′ cctctatagtgtac**GCT**atgttaggattg 3′	65.4
M496A	5′ gtatagtgtacttc**GCC**ttaggattg 3′	58.7
L497A	5′ gtgtacttcatg**GCG**ggattgaagcc 3′	70.8
NBD interface residues mutant isoforms		
Y247A	5′ CatcagcctcgaGCttccatcttc 3′	66
E285A	5′ gctggttatcactgtgCTgcctataataac 3′	67
E285K	5′ gctggttatcactgtAAAgcctataataac 3′	62
N288A	5′ ctgtgaggcctatGCtaaccctgcagac 3′	71
N288D	5′ ctgtgaggcctatGataaccctgcagac 3′	70
D292A	5′ cctataataaccctgcTgCcttcttcttgg 3′	70
D292K	5′ cctataataaccctgcTAaGttcttcttgg 3′	65

Table 2.1: List of oligonucleotide primer pairs for site directed mutagenesis

The table depicts the primers generated as explained in section 2.1.1 to introduce the desired mutations into transmembrane helix 3 and NBD interface of ABCG2. The mutational sites are depicted as bold upper cases. The characteristic property related to TM (melting temperature) of the primer pairs is also given. Mutation of R482A, M496A and Y247A introduces a restriction site for NcoI, Bsu36I and XhoI respectively (highlighted), thereby facilitating mutation screening through restriction digest profile.

2.1.2 Site directed mutagenesis

The mutant isoforms of pcDNA3.1Zeo_sfGFP_ABCG2 vector were generated using a Quikchange- style- site directed mutagenesis protocol. Polymerase chain reaction (Sensoquest Labcycler, Gottingen, Germany) was performed in order to incorporate the desired mutation of interest in the template strand. Typically, reaction volumes of 50 µL contained the *Pfu* polymerase reaction buffer diluted from the manufacturer's supplied 10X stock, 200 µM dNTPs, 50- 100 ng template DNA, 100 µM stock forward and reverse primers and 5 units of *pfu* polymerase enzyme. The reaction conditions were typically an initial denaturation (95 ˚C, 60s), followed by 17 cycles of amplification (template denaturation 95 ˚C, 60s; primer annealing 55 ˚C, 60s; extension 72 ˚C, 17min) with a final extension at 72 ˚C, 600s and cooling overnight (hold) at 15 ˚C. These cycle conditions were followed for the site directed mutagenesis for all the mutant positions except for position 496, where the annealing and extension temperatures were lowered to 51 ˚C and 68 ˚C respectively. In order to avoid undesired mutations, lower number of PCR cycles were employed.

2.1.3 DpnI digestion

The PCR product was DpnI digested in order to degrade the methylated template DNA. Completed PCR reactions were supplemented with 5- 10 units of DpnI and incubated at 37 ˚C for 1 hour 30 minutes.

2.1.4 Transformation

$DH_5\alpha$ cells are employed as the competent cells for transformation purposes. Aliquots (100 µL) of *E. coli* competent cells (prepared in-house by Deborah Briggs) were thawed on ice in pre-chilled sterile eppendorf tubes and 5 µL of the DpnI digested PCR product was added with gentle mixing. The cells were incubated on ice for 30 minutes and then subjected to heat shock at 42 ˚C for 90 seconds and subsequently returned to ice for 2- 3 minutes. LB- broth (10.0 g/L NaCl, 10.0g/L tryptone, 5.0g/L yeast extract) was added to the heat shocked DNA- cell mixture to make up the total volume of the mixture 1 mL. The mixture was incubated in a shaker incubator at 37 ˚C for 1 hour. A fraction (10%) of the transformation mixture was plated on LB (Luria Bertani) - agar- Ampicillin plates (LB components, 15g/L agar and 100µg/mL

Ampicillin). The remaining 90% of the transformation was centrifuged at 13,000 rpm for 1 minute and the bacterial cell pellets then re-suspended in 100 µL of LB and plated onto selective LB- agar plates. The plates were incubated at 37 ˚C overnight for growth of healthy isolated colonies.

2.1.5 Plasmid mini preparations and long-term storage of bacterial stocks

Isolated DH5α bacterial colonies from LB- agar plates were inoculated in a 30 mL Sterilin^{TM} tube containing 5mL LB broth and 100 µg/mL ampicillin. The bacterial cultures were incubated in an orbital shaker at 200 rpm (Jencons scientific limited, Bedfordshire, UK), 37 ˚C for overnight growth. Glycerol stocks were made with the overnight grown bacterial cultures (500µL) with 30% (v/v) glycerol (500 µL) and stored at -80 ˚C. The bacterial cultures were centrifuged at 4000 rpm (Eppendorf centrifuge 5810) for 5minutes and plasmid DNA was extracted based on the manufacturer's protocol Nucleospin plasmid kit (Macharey-Nagel). The miniprep method is based on the alkaline lysis method. Briefly, the plasmid DNA is liberated from *E. coli* by the SDS/ alkaline lysis and neutralized to bind to a silica membrane. Pure DNA is isolated in low ionic strength slightly alkaline buffer (5mM Tris/ HCl, pH 8.5).

The concentration and the purity of DNA samples were determined and assessed using a Nanodrop 2000 (Thermo Scientific, Labtech International). The purity of the DNA was measured based on the A_{260}/ A_{280} ratio. The DNA samples with A_{260}/ A_{280} ratio of 1.7- 2.0 were considered pure (ideal range) and subjected to further experimentation.

2.1.6 Restriction digestion, agarose gel electrophoresis and visualization of DNA

Plasmid DNA (200- 500 ng) was digested in 15 µL reaction volume containing the appropriate reaction buffer (identified by consulting product datasheets) and 5- 20 units of enzyme. Reactions proceeded at the optimum reaction temperature (typically 37˚C) for 1 hour 30 minutes. 6X loading dye (0.25% bromophenol blue, 40% w/v sucrose) was added to the reaction mixture and the final mixture was loaded on 0.7- 1.0% w/v agarose gels containing 1µg/µL ethidium bromide. The PCR product was

confirmed for the presence of pcDNA3.1Zeo_sfGFP_ABCG2 vector by analysing the restriction digest profile using the restriction enzyme PvuII.

Gel electrophoresis was performed in 1X TBE buffer (90 mM Tris, 90 mM boric acid and 2 mM EDTA pH 8.0). Digested DNA bands were analysed under the transilluminator (Syngene GENE bioimaging system) and compared against 1kb DNA ladder loaded alongside the DNA samples.

2.1.7 DNA Sequencing

The sfGFP_ABCG2 constructs were fully sequenced using three forward primers SeqF0, SeqF2, Seq482 and two reverse primers; SeqR1 and SeqGFP-rev (table 2.2). The GFP construct was sequenced with the help of a reverse primer, SeqGFP-rev. DNA samples (100 ng μL^{-1}) and primer samples (at least 3.2 pmoles μL^{-1}) were supplied for external sequencing reactions (Source Bioscience; Nottingham, UK). The chromatograms were analysed in the Chromas program, version 2.4.4 (Technelysium pvt Ltd.).

Primers	Sequence
SeqR1	339- ATAAATGGAGCACCACGA- 322
SeqF0	147- GAGTGGCTTTCTACCTTGTC- 166
SeqF2	699- GCAGGGACGAACAATCATCT- 718
Seq482	1337- AACTCTTTGTGGTAGA- 1352
SeqGFP-rev	477- GCTGTTGTAGTTGTATCCAG- 427

Table 2.2: List of primers employed for sequencing the ABCG2 construct

The table depicts the list of primers used to sequence the p3.1Zeo_sfGFP_ABCG2 vector. The position where the primers anneal to the plasmid constructs are listed below.

2.2 ABCG2 expression in mammalian cells

2.2.1 Human embryonic Kidney cells maintenance (HEK293T cells)

HEK293T cells (ATCC® CRL-3216™) used in this study, originally referred as 293tsA1609neo, derived from human embryonic kidney 293 cells, contain the SV40

T-antigen. This allows transfections with high copy number of plasmids containing an SV40 origin of replication.

Normal growth for HEK293T cells was maintained in DMEM (Dulbecco's modified eagle's medium, comprising 4.5 g/L D-glucose, 0.11 g/L sodium pyruvate and sodium bicarbonate and 0.58 g/L L-glutamine) supplemented with 10% v/v FCS (foetal calf serum) and 100 units/mL penicillin and 100 µg/mL streptomycin in a T-25 or T- 75 flask and placed in the humidified incubator set at 37˚C and 5% CO_2. The cells were routinely monitored for their morphology and confluency under the light microscope (10X objective). On reaching 90% confluency, the cells were passaged. The cells were washed in PBS (phosphate buffered saline; 1.44 g/L KH_2PO_4, 90.0 g/L NaCl and 7.95 g/L Na_2HPO_4, pH set at 7.3- 7.5) and trypsinised (trypsin/EDTA diluted in PBS; 0.3 mL T-25 or 1.0 mL T- 75), placed in the incubator at 37 ˚C for up till 1 minute to avoid any damage caused to the cell surface proteins. The detached cells were re-suspended in fresh DMEM media and subsequently centrifuged at 500×g (Biofuge primo Heraeus) for 5 minutes. The media containing trypsin was aspirated and the cell pellet was re-suspended in fresh DMEM media. The cells were passaged in typically a 1:10 ratio into a new T-25 or T- 75 flask.

2.2.2 Cell seeding

A haemocytometer was used to count the number of cells present per unit volume of suspension obtained from the T- 25/ 75 flasks. Upon trypsinisation and re-suspension in DMEM media as described in section 2.2.1, 10 µL of the cell suspension was pipetted on the haemocytometer chamber (depth 0.01 mm^2), placed under the light microscope and the cells were counted in the desired grid to obtain the cell density (cells/mL).

2.2.3 Polyethyleneimine (PEI) mediated transfection

The cells were seeded 24 hours prior to transfection in a 6 well dish (2.5×10^5 cells per well). Three hours prior to transfection, the DMEM (10% v/v FCS, 1% Pen/ Strep) media was replaced with reduced FCS (5% v/v) DMEM media. Cells were transfected using the linear PEI. PEI stock solutions were prepared at 23mM in PBS and neutralized with 1M HCl and filter sterilized. Prior to use, PEI was diluted to 2.3mM

working solution. The ratio of N (PEI): P (DNA) molecules was maintained at 15:1 for successful transfection (Boussif et al., 1995). DNA was typically added at 2 μg. The PEI (9 μL) was added to the DNA in order to prepare the transfection mixture. The transfection mixture was added dropwise to the seeded cells and the cells were placed in the humidified incubator set at 37˚C, 5% CO_2. Cells were observed using an inverted epifluorescence microscope (Mercury lamp, Carl Zeiss, Birmingham, UK) to confirm successful transfection, 24 hours post transfection. DMEM media was replaced with 10% FCS DMEM media 24 hours post transfection. The cells were harvested 48 hours post transfection and transferred to a T- 25 flask. To obtain stable cell lines 200μg/mL Zeocin™ (Invitrogen, USA) was added. The growth of cells was observed over a period of 3-4 weeks in order to obtain Zeocin™ selected stable cell lines. The cells were observed for protein expression at each stage (GFP tagged) using the epifluorescence microscope connected to an inbuilt camera (AxioCam MRm, Zeiss) and analysed using the software Axio Vision release 4.8.2 SP3.

2.2.4 Generation and maintenance of stable cell lines

Stable cell lines were generated for HEK293T cells expressing the plasmid construct based on the Zeocin™ sensitivity in the media. All the cell lines were grown as adherent monolayers. The cells, harvested in a T-25 flask on becoming confluent, were trypsinised and transferred to a T- 75 flask and maintained in the selection media (containing Zeocin™) for a period of 3- 4 weeks. The cells were observed on a regular basis and the media was replaced every 3-4 days. Once healthy colonies were obtained, Zeocin™ concentration was reduced to 40 μg mL^{-1} to maintain selection of the cells. The cells were frozen for long term storage.

2.2.5 Freezing cells for long term storage

The cells were frozen in freezing media (90% v/v FCS and 10% v/v tissue culture grade Dimethyl sulfoxide (DMSO)). The cells were pipetted in 1 mL aliquots (typically 1- 2 x 10^6 cells) into cryo-vials and placed in a controlled freezing vessel and stored in -80˚C. The freezing vessel would facilitate gradual decrease in the temperature (1˚C per minute) and reduce the chances of damaging cells from the

formation of ice crystals. The cells were transferred to liquid nitrogen subsequently for long term storage.

2.2.6 Cell culture for membrane preparation, generation of crude membranes

Cells were seeded at a cell density of 8- 10×10^6 cells in 450cm^2 culture plates. For ABCG2 expressing cell lines the growth medium (DMEM, 10% FCS and 1% pen/strep) was supplemented with 40µg/ml Zeocin^{TM}. The culture plates were incubated at 37°C, 5% CO_2 for 36 hours. 10 mM sodium butyrate (transcriptional activator) was added 24 hours prior to harvesting. The cells were harvested *via* scraping into sterile 1 × PBS. The cell suspension was washed by centrifugation (350xg, 5 minutes, 4°C) with sterile PBS and the cell pellet stored at -80°C for the membrane preparation as explained in section 2.6.1.

2.3 ABCG2 protein expression: Sf9 cells

2.3.1 Generation and maintenance of insect cells

Insect expression cell line (Sf9), a clonal isolate from the IPLBSF-21 cell line, derived from the pupal ovarian tissue of the fall army worm, *Spodoptera frugiperda* was used to express ABCG2 (Ryan, 1993).

Insect cells were seeded in suspension cultures (50 mL) in glass flasks (200 mL) cultured at 27°C with orbital shaking (120- 130 rpm) at a cell density of 1×10^6 cells/mL. Cells were maintained until the cell density reached 6-8 × 10^6 cells/mL; typically, 3 days as the doubling time of Sf9 cells is 18- 24 hours. Sf9 cells were grown in Insect-Xpress (protein-free insect cell medium with L-glutamine) supplemented with 10% (v/v) FCS and 2% (v/v) Pen-Strep (100 units/mL penicillin and 100 µg/mL streptomycin), in either tissue culture flasks (T-25 flasks) or borosilicate round bottom flasks incubated at 27°C in air.

2.3.2 Insect cell infection

Insect cells were seeded at 1 x 10^6 cells/mL infected with baculovirus infected insect cell (BIIC) stocks (viral load (µL): culture volume (mL) ratio- 1:1000, 1:5000) 24 hours post seeding. The ratios were obtained by diluting the BIIC stocks into the

expression culture. The infection was monitored over the course of 72 hours from the time of BIIC stock infection. The cell size and density were monitored (normal cell size- 15-16 µm). Non-infected cells were used as a control. The cells were harvested, centrifuged (1500g, 15 minutes) and stored in -80°C for subsequent cell lysis and membrane preparation.

2.3.3 Preparation of BIIC stocks

Cryo preserved BIIC were prepared as described by Wasilko et al. (Wasilko and Lee, 2006). Sf9 cells were seeded at 1 x 10^6 cells mL^{-1} (500 mL culture). The cells were infected with titered liquid stocks based on multiplicity of infection (MOI) 24 hours post seeding. Cells were monitored for cell size (normal cell size- 15-16 µm) and density post infection using the cell counter (Moxi^Z mini automated cell counter; ORFLO, USA). When the average diameter of the cells increased by 2-3 µm and while the cell viability was still high (> 90%), the BIIC cultures were cryopreserved. Cells were harvested at 750 *g* for 5 mins and then re-suspended in 2.5 mL of Xpress media supplemented with 10 % (v/v) DMSO and 2 % (v/v) Pen/Strep. Aliquots of 100-200 µL in cryo-vials were frozen slowly to -80 °C. These BIIC stock aliquots in cryo-vials were stored in liquid nitrogen for long term storage and used for subsequent infections.

2.3.4 Cell Viability

Insect cells were seeded at 1 x 10^6 cells mL^{-1} infected with BIIC stocks and harvested over a course of set time intervals. The count and viability of the cells was monitored using the Muse cell analyser (Millipore). The Muse^{TM} delivers rapid measurements of cell concentration, viability, apoptotic status and cell cycle distribution. The concentration of the Sf9 cells was maintained at 1×10^6 cells mL^{-1}. The count and viability cell dispersal reagent (comprised of propidium iodide solution) was added at a dilution factor of 10 with respect to the cell suspension volume.

2.3.5 Cholesterol hemisuccinate doping

A reproducible method was used to manipulate the cellular cholesterol content by modifying the cyclodextrin: cholesterol molar ratios (Christian et al., 1997b). The experimental set up was designed to prepare 50 mL of 25 mM methylβcyclodextrin

(MβCD): cholesterol hemisuccinate solution with a molar ratio of 12.5:1. A stock solution of cholesterol hemisuccinate (50 mg mL^{-1}) was prepared in chloroform: methanol (1:1, v/v) ratio in a round bottom glass flask. The solvent was evaporated in a gentle stream of liquid nitrogen. Mass of 1.67g of MβCD, dissolved in 50 mL serum free insect Xpress medium was added to the glass round bottom flask containing dried cholesterol hemisuccinate. The flask was vortexed to bring the dried cholesterol hemisuccinate off the flask wall and subsequently sonicated for 1-3 minutes. This generated 100% saturated MβCD: cholesterol hemisuccinate solution, which was incubated at 37°C overnight on an orbital shaker set at 140 rpm. The solution was subsequently filtered in the tissue culture hood using a 0.45 µm syringe filter to remove excess cholesterol hemisuccinate crystals.

The insect cells were seeded in 4 flasks with a culture volume of 225 mL each as explained above (2.2.6 and 2.2.7). Cells seeded in two round bottom flasks were infected with 225 µL BIIC stock (His_Strep_ABCG2) each. A flask of cells infected with BIIC stock and a flask of cells devoid of infection were subjected to 25 mL MβCD: cholesterol hemisuccinate solution (12.5:1 molar ratio). The cells were harvested 72 hours post infection. The cells were centrifuged at 350g for 15 minutes to collect the cell pellets and subsequently stored at -80°C until needed for membrane preparation.

2.4 Protein expression: SDS PAGE and Western Blot

HEK293T Cells expressing the wild type ABCG2 and mutant isoforms (TM3 helix residues and NBD interface residues) were centrifuged (1500 g, for 5min at 4 ˚C) in order to collect the cell pellets for protein quantification. The supernatant was removed, and the cell pellets were resuspended in ice cold PBS containing 10% (v/v) glycerol and EDTA free protease inhibitor cocktail set V (Calbiochem). Cells were sonicated (Jencons Scientific LTD- Sonics and materials INC, USA) thrice at 40% power output for 10 seconds. Protein concentration was determined by a commercial, modified Lowry protein assay (Bio- Rad DC; (Lowry *et al.*, 1951)).

A standard curve was set with 0-10 µg bovine serum albumin (BSA) constructed in parallel. All samples were analysed in duplicate.

SDS PAGE was performed based on Laemmli's method (Quandt et al., 1993) (LAEMMLI, 1970). Protein samples were mixed with protein sample loading buffer

(0.25 M Tris- HCl, pH 6.8, 5% (w/v) SDS, 20 % (v/v) glycerol and bromophenol blue) containing 5% (v/v) 2-mercaptoethanol. The samples were incubated at 99˚C for 15 minutes. Equal amounts of the protein samples (20 µg - 50 µg) alongside molecular weight markers (See Blue Plus 2 pre-stained, Novex) were loaded and resolved on 10% (w/v) polyacrylamide gels. The gel was electrophoresed at 30 mA/ gel for 1 hour 30 minutes in a protein running buffer (250 mM Tris base, 192 mM glycine, 35 mM SDS). The gels were stained with Instant Blue (Expedeon), a Coomassie based staining solution for protein gels.

After SDS PAGE, the gels were subjected to wet transfer (transfer buffer- 25 mM Tris, 192 mM glycine and 20% v/v methanol) in order to transfer the proteins onto the nitrocellulose membrane (Amersham) by electroblotting (200 mA, 1 hour 30 minutes). The nitrocellulose membrane was cut into 2 halves for quantification of ABCG2 and GAPDH (control) proteins respectively. The nitrocellulose membranes were washed with PBS-Tween 20 (0.1% v/v) (PBS-T) and incubated with a blocking solution (5% w/v skimmed milk powder in PBS-T for 1 hour at room temperature to prevent any non-specific binding. Nitrocellulose membranes were incubated with primary monoclonal mouse antibody (Bxp21; Calbiochem or BXP-53; Santa Cruz Biotechnology) at 1:1000 dilution and goat anti- GAPDH antibody (SICGEN) at 1:5000 dilution in blocking solution (overnight at 4˚C). The membranes were subsequently washed 4 times with PBS-T and subsequently incubated with fluorescent secondary antibodies (anti- mouse IR680 and anti- goat IR800, Life technologies) respectively at 1:10,000 dilution in blocking solution for 1 hour at room temperature. The nitrocellulose membranes were washed with PBS-T. Finally, the specific proteins were detected using the LI-COR scanner (Odyssey, Bioscience UK, Ltd.). Alternatively, the membranes were incubated with a secondary antibody, rabbit anti-mouse horseradish peroxidase (DAKO), at 1:2000 (in PBS-T) for 1 hour at room temperature. The membranes were then washed several times in PBS-T to remove unbound secondary antibody. The membranes were incubated with enhanced chemiluminescence reagent, ECL (Supersignal West Pico, Thermo Scientific) and developed using light sensitive film.

2.5 Live cell Imaging

2.5.1 Confocal plate reader-ImageXpress

Live cell imaging of HEK293T cells stably transfected with sfGFP_ABCG2 wild type and mutant isoforms was performed using an ImageXpress (IX) Ultra confocal plate reader (Molecular devices using a plan-apochromat 40X objective, with excitation wavelength of 488 nm and emission bandpass filter of 520/50 nm). Greiner plates (96 well black walled, clear bottom) were Poly-L-lysine coated 30 minutes prior to being seeded. Cells were seeded at a cell density of 30,000- 40,000 cells per well in DMEM, 24 hours prior to imaging. Cells were washed twice with pre warmed phenol red free HBSS (Hank's balanced salt solution, Sigma Aldrich) half an hour prior to imaging. The cell images were analysed on MetaXpress software.

2.5.2 Immunostaining and fixing mammalian cells

HEK293T cells stably transfected with sfGFP_ABCG2 wild type and mutant isoforms were seeded in a 24 well dish, 24 hours prior to fixing. Prior to addition of cells in the wells, coverslips (no. 1.5 category coverslips with a diameter of 13mm, VWR) were gently placed inside each well. Appropriate dilution (1:10) of cells was added to each well (500 µL per well). The plate was incubated at 37°C, 5% CO_2 for 24 hours. Cells were washed with 1 × PBS, fixed with 4% paraformaldehyde (w/v) in 1 × PBS for 15 minutes and then subsequently washed (twice) with 1 × PBS. The coverslips were immersed in 50 mM NH_4Cl for 10 minutes. The cells were incubated in a blocking and permeabilization buffer (0.05% (w/v) saponin, 0.5% (w/v) BSA in 1 × PBS) for 15 minutes. Cover slips were removed from their respective wells and placed on a drop (50 µL, on a parafilm) containing the primary antibody (monoclonal antibody anti-BCRP1, clone 5D3 (1:500; Millipore)) in blocking buffer. The cover slips were incubated in a humid environment for 30 minutes. The cover slips were placed back in the respective wells and washed with 1 × PBS (5 times). A similar procedure was applied to incubate the coverslips with secondary antibody (AF647 (Highly cross adsorbed; 1:500 Thermofisher Scientific). The cover slips were washed inside the respective wells with 1 × PBS (5 times). The coverslips were mounted on the slide

using a small drop of the mounting medium (6 µL, Fluorogel Mounting Medium, MP Biomedicals).

Visualisation of cells was performed on an LSM710 confocal laser scanning microscope (Zeiss, Jena, Germany) equipped with a Plan-Apochromat 63x/1.40 Oil Ph3 DIC M27 objective and argon laser.

A 2% argon laser power was used with the pinhole set to 2 AU (area unit). The excitation was set at 488 nm and emission collected between 500-530 nm (FITC channel) to monitor GFP fluorescence and for AF647 signal, the excitation and emission wavelengths were set at 650 nm and 668 nm respectively. Corresponding phase contrast images were acquired in at least three different viewing positions for any given culture dish.

2.6 Membrane based assays

2.6.1 Preparation of crude membrane fractions

Cell pellets were washed with ice cold 1 × PBS (three times), centrifuged (500-1000 g for 5 minutes) and re-suspended in at least 5-10 X (wet membrane weight) membrane isolation buffer 1 (MIB 1- 0.01 M Tris pH 7.4, 0.25 M sucrose, 0.2 mM $CaCl_2$) supplemented with protease inhibitor cocktail set III (Calbiochem; diluted 1:100). Nitrogen cavitation was used for membrane preparations. The nitrogen cavitation vessel (Parr Instrument Company) was pre-cooled on ice. The cell suspension was poured in the vessel, which was sealed, attached to the nitrogen cylinder and the system was left to equilibrate at a pressure of 1000 psi on ice for 10 minutes. The cavitation vessel outlet was opened to release the sample to atmospheric pressure. The process was repeated. The cell lysate was collected in a 50 mL tube and centrifuged at 1500g for 15 minutes at 4°C. The supernatant was collected and the remaining pellet comprising of cell debris was removed. The supernatant was subjected to ultracentrifugation (100,000g for 1 hour at 4°C). The supernatant was removed, the pellet obtained comprised of the crude membranes. The crude membranes were re-suspended in MIB-IV (50 mM Tris, 250 mM sucrose, pH8) supplemented with protease inhibitor (1:100), sheared 10-15 times using a 25G needle. Crude membranes prepared from mammalian cell lines to be used for downstream activity assays were re-suspended in TSN buffer (50 mM Tris, 250 mM Sucrose, 150 mM NaCl, pH8)

supplemented with protease inhibitor (1:100) and subsequently sheared. Cell membranes were either used immediately or stored at -80°C in 50- 100 µL aliquots. The protein concentration was measured by Lowry assay.

2.6.2 Vesicular transport assays

The membrane-based assay was used to detect the translocation of drug molecules across the inside out generated ABCG2 membrane vesicles (normal or cholesterol doped) in an ATP dependant manner. Crude membranes re-suspended in MIB-IV were sheared 6-10 times with 25G needle before use. Crude membrane vesicles (20 µg membrane protein) were combined with either DMSO (solvent control, 0.01% v/v), substrate- Lucifer yellow (50 µM or 100 µM) or mitoxantrone (10 µM), in the presence or absence of the ABCG2 inhibitor, Ko143 (1 µM). The total reaction volume was made up to 50 µL with MIB-IV buffer. Each reaction was supplemented with 10 mM $MgCl_2$, with subsequent addition of either ATP (5 mM) or AMP (5 mM). The reactions were incubated at 37°C for 10 minutes in a water bath. The reaction was immediately transferred to ultracentrifuge tubes containing 950 µL of ice cold MIB-IV to stop the reaction. The tubes were centrifuged at 60,000g for 5 minutes at 4°C to rapidly separate the membrane vesicles from the free excess drug and nucleotides in the reaction volume. The supernatant was discarded, and the membrane pellets were re-suspended in 1 mL of MIB-IV and transferred to a quartz cuvette prior to analysis by fluorescence spectroscopy. Lucifer yellow excitation wavelength was set at 430 nm and emission wavelength was set at 538 nm, whereas the excitation and emission wavelengths for mitoxantrone were set at 607 nm and 684 nm respectively using a SpectraMax® M2 microplate reader (Molecular Devices).

The data was analysed using Prism 7 (GraphPad). The data is reported as a relative drug uptake by inside out vesicles, determined by the ratio of ATP: AMP dependent drug uptake in presence or absence of Ko143, corrected for the vehicle only fluorescence.

2.6.3 ATPase assay

Basal and drug stimulated ATPase activities of ABCG2 were measured using a colorimetric assay to monitor the release of inorganic phosphate, based on the method described by Chifflet *et al.*, 1988.

The assay was performed in a 96 well clear bottom plate. ABCG2 (wild type and isoforms) crude membranes (100 µg) were incubated in a final assay buffer (50 mM KCl, 2.5 mM EGTA; pH 8.0, 1.3 mM ouabain, 2 mM DTT) combined with 5 mM $MgSO_4$ and either solvent control (DMSO (1% v/v)) or substrate (lucifer yellow (100 µM)) in the presence or absence of 1 µM Ko143. The final reaction volume (50 µL) was made up with the TSN buffer. The reaction was equilibrated at 37°C for 5 minutes (96 well plate covered with a clean film and a lid). Each reaction condition was supplemented with either ATP or AMP (5 mM), added to the reaction volume at a regular time interval (30 seconds) and incubated at 37°C for 15 minutes. The reaction was stopped with SDS (2.5% final concentration) at a regular interval of 30 seconds. To the reaction mixture, 50 µL of distilled water was added, followed with 40 µL of phosphate detection reagent (1% (w/v) ammonium molybdate, 0.014% (w/v) antimony potassium tartrate, 2.5 N sulphuric acid) and 1% w/v (20 µL) ascorbic acid. The plate was incubated at room temperature for 12 minutes and the absorbance intensity from the formation of phosphomolybdate was measured at 880 nm using a SpectraMax® M2 microplate reader (Molecular Devices).

The data was analysed using Prism 7 (GraphPad). The data is reported as ATP-dependent inorganic phosphate release in presence or absence of Ko143.

2.7 Live cell assays

2.7.1 Flow cytometry, Drug efflux assays

To evaluate the functionality of ABCG2 in mutant HEK293T cell lines, drug accumulation assays were performed by flow cytometry. Cells were seeded in FACS tubes (1 mL seeding volume) at a cell density of 1×10^6 cells/ mL in phenol red free DMEM (Sigma) and incubated with either DMSO (control vehicle), mitoxantrone (10 µM, Mx), Pheophorbide A (10 µM) or daunorubicin (10 µM) in presence or absence of ABCG2 specific inhibitor Ko143 (1 µM) at 37˚C with occasional agitation for 30

minutes (Table 2.3). Subsequently, the cells were centrifuged at 350 g for 5 minutes at 4˚C to remove excess drug from the solution. Samples were resuspended in fresh media (excluding the drug but including Ko143 for tubes with drug plus inhibitor). The vehicle control tubes were incubated on ice, whereas reactions with drug only or drug and Ko143 were incubated in a water bath set at 37˚C for 1 hour with occasional agitation. The cells were centrifuged at 350 g for 5 minutes at 4˚C and resuspended in phenol red free DMEM. GFP fluorescence was determined using excitation wavelength 488 nm and emission at 526 nm, mitoxantrone fluorescence was measured using excitation at 635 nm and emission at 670 nm using FC500 flow cytometer, channel FL4- 633/75 (Beckman Coulter, UK) (Table 2.1). Pheophorbide A fluorescence was measured using excitation at 400 nm and emission at 710 nm (channel 355-692/75) and daunorubicin fluorescence was measured using excitation at 490 nm and emission at 610 nm (channel 488-710/45) respectively using Moflo Astrios flow cytometer system (Beckman Coulter) (Table 2.3).

Drugs	**Stock Conc (mM)**	**Working Conc (µM)**	**Fluorescence spectrum**		**Flow cytometry channel**
			Excitation wavelength (nm)	**Emission wavelength (nm)**	
Mitoxantrone (Mx)	20	10	635	670	FL4- 633/75 FC500
Pheophorbide A (Pheo A)	10	10	400	710	355-692/75 Astrios
Daunorubicin (DNR)	10	10	490	610	488-710/45 Astrios
Ko143 (inhibitor)	1	1	N.A.	N.A.	N.A.

Table 2.3: Potential fluorescent substrates for drug efflux assays

Summary of the potential fluorescent substrates and the ABCG2 specific inhibitor employed to test the functionality of ABCG2 transporter using flow cytometry

2.7.2 Flow cytometry data analysis (Kaluza analysis version 1.5)

Cells were gated for monodispersity based on the forward and side scatter indices to exclude cellular debris from the analyses (figure 2.1 A). Forward scatter (FSC) height versus area gating was applied to separate monodispersed cells from aggregated cells (figure 2.1 B). Subsequently, a final gating parameter was defined based on the GFP histogram profile, demonstrating a clear split population for GFP expression/ fluorescence as high and low, so that low expressing cells could be gated out (Figure 2.1 C). These gating parameters were established for WT_sfGFP_ABCG2 and were applied to all the other files. An overlay histogram was generated for the vehicle control, drug alone and drug plus inhibitor with regards to GFP expression and drug fluorescence (Figure 2.1 E, F and G). The median values generated were analysed using GraphPad Prism and Excel. The vehicle control was used for baseline correction from the values of drug alone and drug plus inhibitor. The efflux capability of the protein was determined based on the fractional difference calculated between the sample with drug plus inhibitor and drug alone and normalised for GFP expression.
The drug accumulation normalised for GFP expression was determined as stated below-

$$F_{L\ \text{Drug alone}} - F_{L\ \text{DMSO}} = \alpha$$

$$F_{L\ \text{Drug + Ko143}} - F_{L\ \text{DMSO}} = \beta$$

$$\text{Fractional difference in accumulation} = (\beta - \alpha)/\ \alpha$$

Wild Type GFP Fluorescence (average of DMSO, Drug alone and Drug plus inhibitor) = C

Mutant GFP Fluorescence (average of DMSO, Drug alone and Drug plus inhibitor) = D

$$\text{Fold change in expression (GFP fluorescence)} = C/D$$

$$\text{Drug accumulation, normalised for expression} = (C/D) * [(\beta - \alpha)/\ \alpha]$$

To determine whether mutants differed in their ability to efflux drugs, the data for high expressing population was subjected to one-way ANOVA and post statistical tests (Dunnett's multiple comparison test) against the wild type. Low expressing population was excluded from further analysis due to non-significant impact on efflux capabilities.

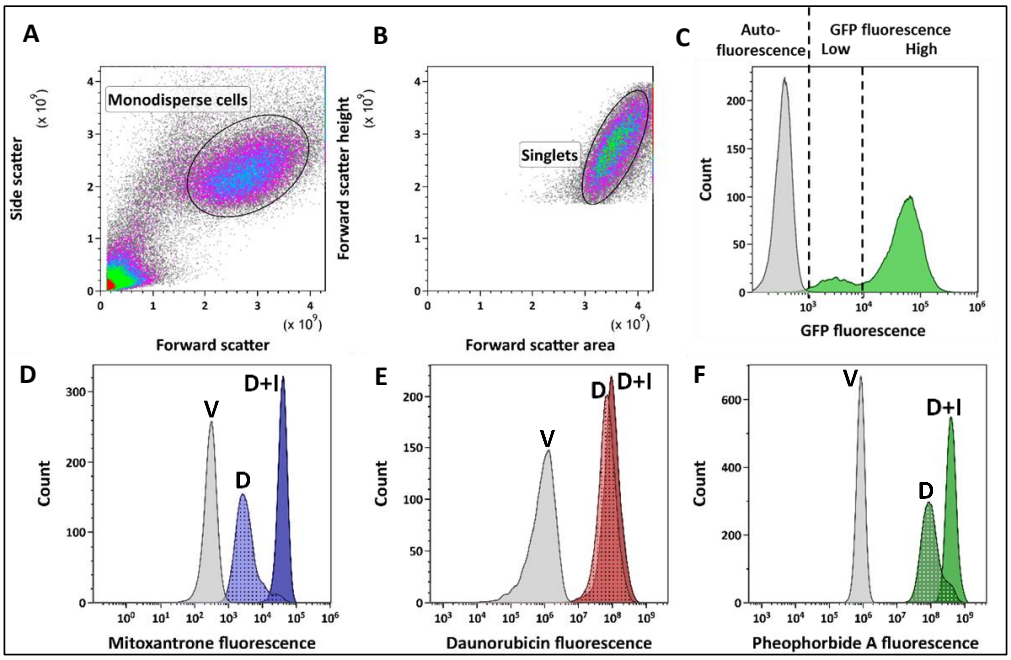


Figure 2.1: Analysis workflow for drug transport assays

HEK293T cells expressing ABCG2 protein (wild type and mutant) were subjected to a two-channel flow cytometry to monitor the expression and function. Histograms represent the GFP expression profile (C) showing a low and high expressing population, mitoxantrone expression profile (D), daunorubicin profile (E) and pheophorbide-A profile (F). An overlay histogram was generated for the 3 conditions (vehicle control (V), drug alone (D) and drug plus inhibitor (D+I)) for each drug (E, F, G). An increased accumulation of drug is seen in the overlay histograms in presence of ABCG2 specific inhibitor. The drug efflux capabilities were determined from these parameters as explained in section 2.7.2.

2.7.3 Data analysis

Numerical data analyses were performed using Microsoft Excel and statistical analyses were performed using GraphPad Prism7. All the statistical tests were analysed with P- values less than 0.05, considered significant for a given set of data.

2.7.4 Cell surface expression

To determine the cell surface localization of ABCG2 protein, cell surface expression was performed for the mutant cell lines. Cells were seeded (1 mL seeding volume) at a cell density of 1×10^6 cells per mL in FACS buffer (1X PBS and 1% w/v BSA) and incubated with either primary monoclonal antibody anti- BCRP1, clone 5D3 (1:200; Millipore), control monoclonal antibody TRP1 (Tyrosinase type 1 membrane protein,

TA99; 1:200; Santa cruz Biotechnology, Inc) or devoid of any antibody respectively. The cells were incubated on ice for 30 minutes, subsequently centrifuged at 350 g for 5 minutes at 4˚C and resuspended in FACS buffer. The wash steps were repeated twice, and cells were finally resuspended in FACS buffer. Secondary antibody AF647 (goat anti-mouse; 1:200 Thermofisher Scientific) was added to the tubes and incubated on ice for one hour followed by repetition of the wash steps. Finally, the cells were resuspended in FACS buffer and analysed for GFP and AF647 fluorescence using Astrios (Beckman Coulter). The GFP fluorescence was determined using excitation wavelength at 488 nm and emission at 526 nm. AF647 fluorescence was measured using excitation at 650 nm and emission at 670 nm (channel 640-671/30).

2.7.5 Data analysis using Kaluza

The mutant cell lines were analysed for cell surface expression using Kaluza analysis version 1.5. Cells were gated for monodispersity. Final gating parameters were set based on GFP and AF647 histogram profiles. Cells were gated for GFP fluorescence as a measure of total ABCG2 expression using a single channel histogram. GFP fluorescence was corrected for autofluorescence by gating for non expressing cells. Immunodetection of the surface exposed epitope by anti-ABCG2 (5D3) antibody treated with secondary goat anti-mouse Alexa fluor 647 antibody, enabled quantification of the cell membrane localisation of ABCG2, depicted by the single channel histogram. Subsequent quadrant analysis (figure 2.2) demonstrated the 1% of cells positive for both total GFP_ABCG2 expression and surface localised ABCG2 expression.

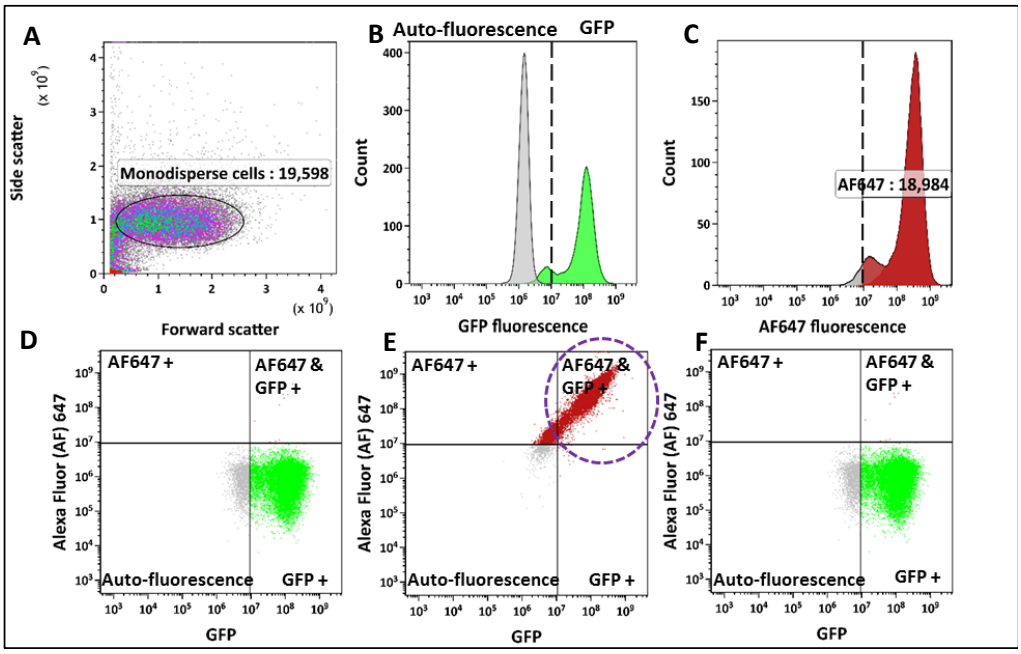


Figure 2.2 : Flow cytometric analysis workflow for surface expression

HEK293T cells expressing stable mutants of ABCG2 protein were subjected to a two-channel flow cytometry. The cells were gated for monodispersity (A). Final gating parameters were set based on GFP fluorescence (B), as a measure of total ABCG2 expression and AF647 fluorescence (C), as a measure of cell surface ABCG2. Quadrant analysis based on the two gates (B and C) for cells expressing sfGFP_ABCG2 incubated with no antibody (D), incubated with primary antibody 5D3 and secondary antibody AF647 (E) and cells incubated with control primary antibody TRP1 and secondary antibody AF647 (F) respectively. Quadrant E clearly depicts that wild type cells expressing sfGFP_ABCG2 show >90% cell surface localisation based on GFP fluorescence (GFP +) and AF647 fluorescence (ABCG2 +).

2.7.6 Mitoxantrone efflux assay in intact Sf9 cells

Sf9 cells were infected with ABCG2 expressing baculovirus and were harvested 40 hours post infection. They were washed once and resuspended in HPMI (120 mM NaCl, 5 mM KCl, 400 µM $MgCl_2$, 40 µM $CaCl_2$, 10 mM Hepes (Melford), 10 mM $NaHCO_3$, 10 mM α-D-glucose (Acros) and 5 mM NaH_2PO_4, pH 7.4), MPMI-I (pH 6.2) and MPMI-II (pH 6.6) or insect Xpress media (pH 6.2) respectively. Cells were seeded at cell density of 2×10^6 cells mL^{-1} in FACS tubes (1 mL seeding volume) and incubated with either DMSO (vehicle) and Ko143 (1 µM, Sigma) respectively at 37˚C with occasional agitation for 5 minutes. Reactions were initiated by addition of 10 µM mitoxantrone. The cells were incubated at 37˚C for 30 minutes and then centrifuged at

350 g for 5 minutes at 4˚C to remove excess drug from the solution. The cells were then washed with the respective buffers and resuspended in ice cold medium, containing 30 µg mL^{-1} propidium iodide to stain for the dead cells. Cells were stored on ice until the measurements using the flow cytometer (FC500, Beckman Coulter). Mitoxantrone fluorescence was measured using excitation at 635 nm and emission at 670 nm using FC500 flow cytometer. Propidium iodide fluorescence was measured using excitation at 488nm and emission 620nm.

2.8 Molecular drug docking and visualisation

Molecular drug docking studies were performed on the cryo-EM structure of ABCG2 bound to Ko143 derivative MZ29 and Fab fragments of 5D3 antibody (PDB: 6ETI, Jackson et al., 2018). Prior to docking studies, the bound MZ29 molecule and Fab fragments were deleted in PyMOL. The coordinates and parameters for the fluorescent substrates mitoxantrone, pheophorbide A and daunorubicin were obtained from ChemSpider (http://www.chemspider.com/). The protein and the drug files were converted to Vina executable PDBQT files *via* AutoDockTools (v1.5.6; http://vina.scripps.edu/). A grid box (dimensions 40x30x30 Å) was generated at an approximate geometric midpoint of the TMD (residues 517/ 518) of an ABCG2 monomer as a search region for AutoDock Vina molecular docking software (Trott and Olson, 2010). The exhaustiveness (8) and all other parameters were set to default to find the most energetically favourable poise. The PDBQT output files were visualised using PyMOL© (Schrodinger, LLC).

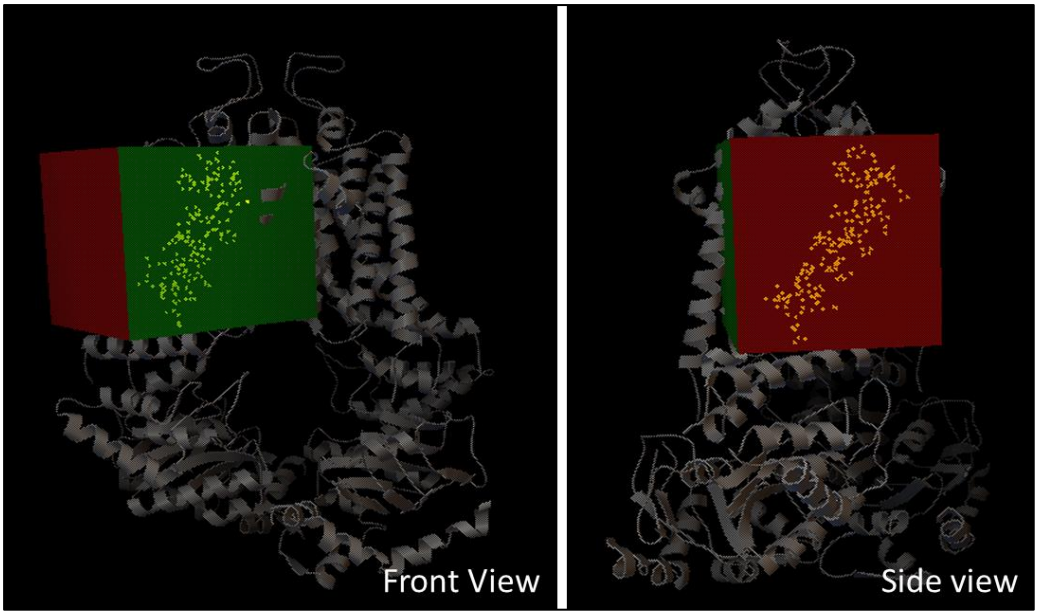


Figure 2.3: Cryo-EM structure with the assigned box for molecular drug docking studies

Molecular docking studies performed on the cryo-EM structure of ABCG2 (cartoon, grey). The grid box (40 x30x30 Å) centred at the approximate geometric midpoint of the TMD of ABCG2 was assigned using python molecular viewer. TM3 helix residues are highlighted in yellow spheres within the grid box.

Chapter 3: Insect expression system as a model for heterologous production of ABCG2

3.1 Introduction

The aim of the present study is to establish large scale expression for membrane protein, ABCG2 and provide quantitative characterisation for the substrate transportation and ATP hydrolysis activity. The Sf9 baculovirus system has previously been established as a suitable expression system for expressing ABC transporters such as MRP1, MRP2 and ABCG2 (Bakos et al., 2000; Sarkadi et al., 1992). They have been used in membrane-based assays due to higher yields of protein expression compared to the mammalian expression system (for example HEK293T). Insect cells offer high levels of protein expression with ease of scale-up, and simplified cell growth that can be readily adapted to high-density suspension culture for large-scale expression. The potential caveats of the insect expression system are whether post translational modifications such as N- linked glycosylation and the lipid bilayer composition mirror those in mammalian cells. The native mammalian glycoproteins are complex type N-glycans with terminal sialic acids compared to insect cell derived recombinant glycoproteins with simpler side chains such as paucimannosidic N-glycans. In addition, insect-derived N-glycans may contain core α-1,3-linked fucose residues, which are known to be allergenic (März et al., 1995; Shi and Jarvis, 2007). Sf9 cells are known to be rich in phospholipids (phosphatidylcholine and phosphatidylethanolamine), monounsaturated fatty acids (oleic acid and palmitoleic acid) and saturated fatty acid, mainly stearic acid. The cholesterol to phospholipid ratio was demonstrated to be lower than in mammalian cell lines (Marheineke et al., 1998). They are also not well characterised with regards to the endogenous transporters expressed within Sf9 cells as compared to their mammalian counterparts.

An immunoblot from the Kerr lab (Sunehera Sarwat; MRes thesis), compared ABCG2 protein expression in insect and mammalian expression system (figure 3.1). Crude

membrane samples (P_2 samples (20 µg of total protein)) were resolved on 8 % (w/v) polyacrylamide gel. ABCG2 expression was detected using ABCG2 specific monoclonal antibody BXP-21 (m-AB BXP-21), which recognizes an intracellular epitope within the nucleotide binding domain of ABCG2 (residues 271- 396) (Maliepaard et al., 2001a). The immunoblot clearly represented large quantities of ABCG2 expressed in insect cell lines compared to the mammalian expression system. The ABCG2-Sf9 exhibited a single immune-reactive band at around 65 kDa whereas the mammalian cells (which were expressing sfGFP_ABCG2) showed two clear bands at around 100 kDa (GFP tagged, glycosylated) and the other approximately 80 kDa (non-glycosylated) representing the two subpopulations (figure 3.1).

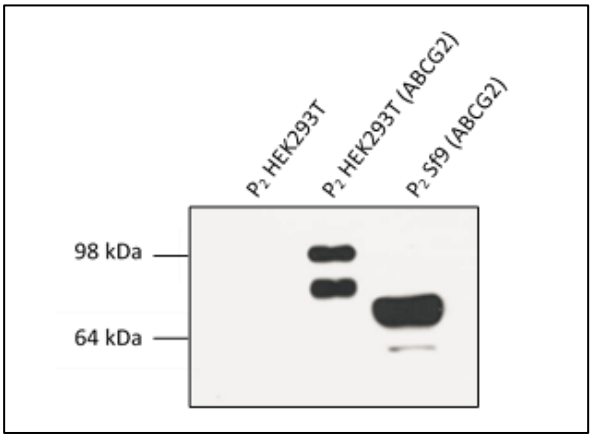


Figure 3.1: ABCG2 expression in mammalian and insect cell (Sf9) lines

20 µg of crude membranes for HEK293T cells expressing ABCG2 (N- terminally fused to His and GFP tag) and Sf9 cells expressing ABCG2 were resolved on 8% w/v polyacrylamide gel. HEK293T cells not expressing ABCG2 were used as a negative control. The immunoblot shows large scale ABCG2 expression in Sf9 cells compared to the HEK293T cells. Immunoblot obtained from Sunehera Sarwat (MRes student, Dr. Ian Kerr's Lab).

The study documents the applicability of the Sf9 expression system in direct, quantitative investigations of the ABCG2 expression and function. The project delves into optimisation of protein expression, membrane and live cell-based drug transport assays. The research also focuses on the importance of cholesterol hemisuccinate doping in the ABCG2 transporter functionality. The regulatory effects of cholesterol on ABCG2 transporter functionality have been reported previously (Pál et al., 2007; Telbisz et al., 2007; Velamakanni et al., 2008). ABCG2 shows complex interactions with a variety of lipid molecules and the transporters function is significantly modulated by cholesterol and cholesterol derivatives at the posttranslational level.

Multidrug transporter localisation has been reported in the lipid rafts (caveolar regions) (Bacso et al., 2004; Tietz et al., 2005). ABCG2 is also located in membrane rafts and cholesterol has known to have an impact on its efflux activity based on cholesterol depletion and repletion experiments using methyl-β- cyclodextrins (Storch et al., 2007b). Studies using placental microvillus membranes and BeWo cells suggested that cholesterol may play a role in the post translational regulation of ABCG2 in placental lipid rafts (Szilagyi et al., 2017). Coimmunoprecipitation and western blot experiments have also indicated a physical interaction between ABCG2 and caveolin-1. Is cholesterol sensitivity of the ABCG2 protein linked to lipid raft/ caveolar localisation? This requires further analysis (Storch et al., 2007b).

3.2 Optimising the heterologous expression system

The study investigates large scale expression for ABCG2 protein using a heterologous system for protein production using Sf9 (*Spodoptera fugiperda*) cells. Sf9 cells, originated from the IPLBSF-21 cell line, derived from the pupal ovarian tissue of the fall army worm, are suitable for expression of recombinant proteins. The Bac to Bac expression system was used to generate recombinant baculoviruses, based on site-specific transposition of an expression cassette into a baculovirus shuttle vector (bacmid) propagated in *E. coli* (Ciccarone et al., 2003; Luckow et al., 1993).

The baculovirus expression system facilitates high level gene expression leading to recombinant protein production driven by a strong AcMNPV polyhedrin (PH) promoter, in virus infected Sf9 cells (Luckow et al., 1993). Sf9 cells were transfected with recombinant baculoviruses carrying the human ABCG2 cDNAs (His_{12}_Strep_ABCG2).

Test screens were performed to determine the optimal expression conditions. The Sf9 cells were subjected to different viral loads in order to establish a suitable culture volume and viral load needed to express ABCG2 in large quantities (figure 3.2 A and B). ABCG2 expression in Sf9 cells was investigated by altering the baculovirus to culture volume ratio (1:1000 or 1:5000). Cells were harvested 72 hours post infection. Membrane fractionation was performed to generate the crude membranes.

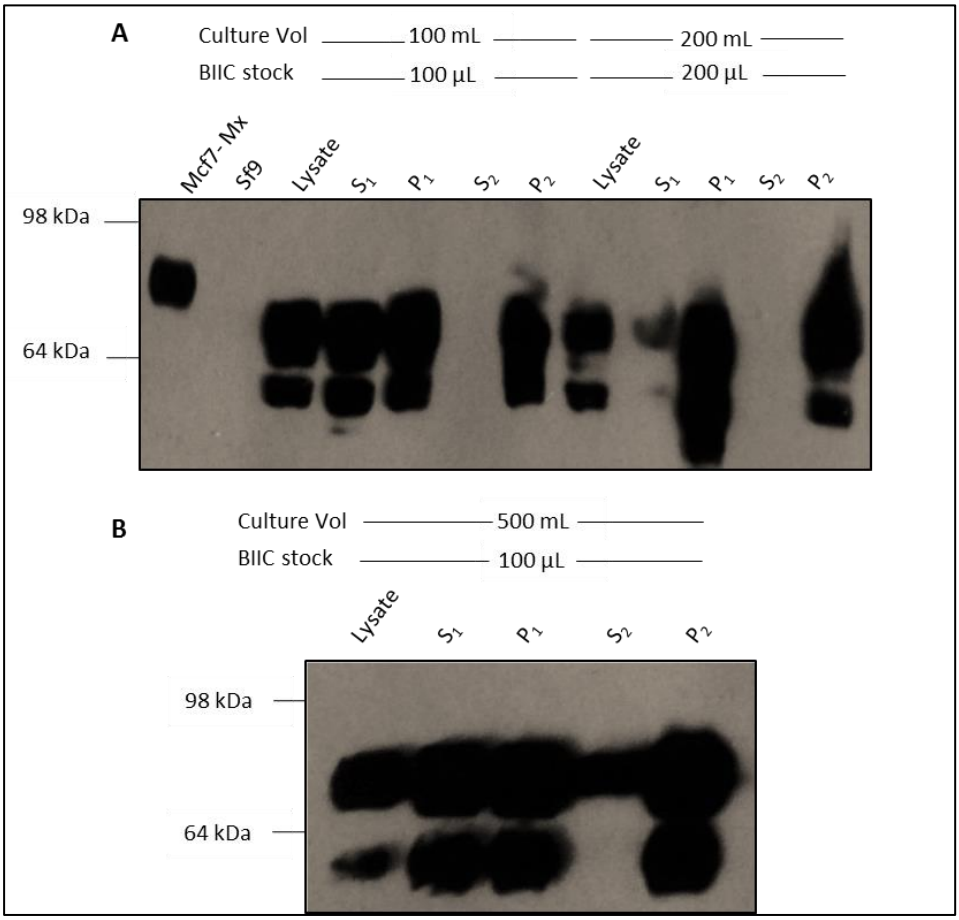


Figure 3.2: Maximising the expression of ABCG2 in Sf9 cells by increased viral load

Large scale expression for ABCG2 was monitored in Sf9 cells. Varying culture volumes and altered viral load were used to test for expression. Sf9 cells were cultured in a 100 mL, 200 mL and 500 mL culture volume and infected with a viral load (BIIC stock) of 100 µL, 200 µL and 100 µL respectively. The cells were harvested 72 hours post infection. Membrane preparation samples (Lysate, S1, P1, S2 and P2; 10µg) were resolved on 8 % (w/v) polyacrylamide gels, transferred to nitrocellulose membrane and probed with mouse BXP-21 antibody (1:1000) and a peroxidase-conjugated rabbit anti-mouse secondary antibody (1:2000). MCF7-Mx (adrenocarcinoma) was used as a positive control and uninfected Sf9 cells as a negative control. The immunoblot clearly shows large scale ABCG2 expression is still obtained in a 500 mL culture even with a 100 µL BIIC stock infection.

ABCG2 expression was detected using ABCG2 specific m-AB BXP-21. Figure 3.2 clearly depicts ABCG2 expression detected in the cell lysate and the crude membranes (P2) at approximately 65 kDa. Some protein is lost in the cellular debris (depicted by pellet 1, figure 3.2 A). The molecular weight of ABCG2 was smaller than in a mammalian positive control due to improper glycosylation. ABCG2 is normally glycosylated at position 596, located in the third extracellular loop. This is not glycosylated in insect cell expression but studies suggest that N-glycosylation at N596 is not essential for the expression, trafficking to the plasma membrane, or the overall function of ABCG2 (Diop and Hrycyna, 2005).

The immunoblot clearly depicted that large scale ABCG2 expression can sufficiently be obtained in 500 mL Sf9 cells infected with a viral load of 100 µL (figure 3.2 B).

3.3 Monitoring ABCG2 function in intact membrane vesicles

After optimisation of ABCG2 expression in insect membranes, the next step was to monitor the biological activity of the ABC transporter *in vitro*. This could be achieved by vesicular transport assays. Research studies based on direct vesicular transport measurements have allowed detailed kinetic analysis of the biochemical parameters of the transport for MRP2 transporter. Vesicular transport studies using glucuronide substrates identified two co-operative binding sites on MRP2, a substrate site and a modulator site (Zelcer et al., 2003) (Bodó et al., 2003).

We adapted a vesicular transport assay to investigate drug transport by ABCG2. Crude membranes contain a mixture of right-side vesicles and inside out vesicles (IOVs). Only IOVs, in which the NBDs are accessible to ATP, would display ATP dependent drug accumulation (figure 3.3 A). Rapid separation of vesicles from the reaction buffer is essential and was achieved by ultracentrifugation. Rapid filtration using glass fiber filters or nitrocellulose membranes can also be used to separate the vesicles from the incubation solution and the test compound trapped inside the vesicles is retained on the filter (Bakos et al., 1998). For the ease of experimentation, rapid separation of the membrane vesicles comprising of the transported substrates was achieved using the high-speed spin (100,000 g, 5minutes) of the crude membranes using the airfuge and ultracentrifuge. Comparison of two ultracentrifuges revealed that 100,000 g for 5 minutes achieved more than 80% pelleting (figure 3.3 B).

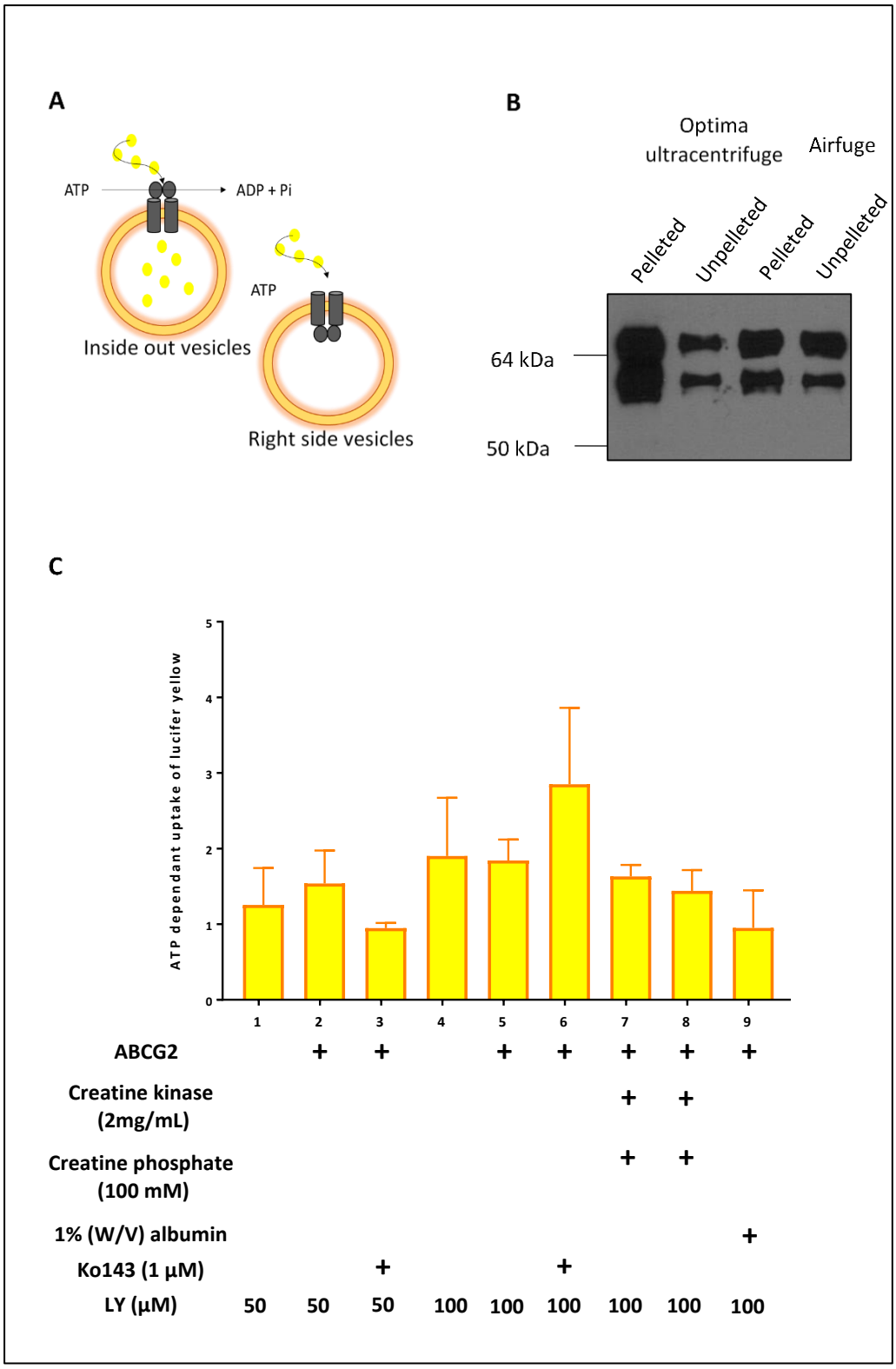

A
ATP
ADP + Pi
ATP
Inside out vesicles
Right side vesicles
B
Optima ultracentrifuge
Airfuge
Pelleted
Unpelleted
Pelleted
Unpelleted
64 kDa
50 kDa
C
ATP dependant uptake of lucifer yellow
0
1
2
3
4
5
1 2 3 4 5 6 7 8 9
ABCG2 + + + + + + + +
Creatine kinase (2mg/mL) + +
Creatine phosphate (100 mM) + +
1% (W/V) albumin +
Ko143 (1 µM) + +
LY (µM) 50 50 50 100 100 100 100 100 100

Figure 3.3: ABCG2 transport function monitored in intact crude membrane vesicles

A) Schematic diagram depicting the transport assay. Vesicles with inside out orientation will accumulate the potential substrates (Lucifer yellow; yellow circles) in presence of ATP and be inhibited by ABCG2 specific inhibitor; Ko143 (1 µM). Right side out vesicles will not be able to transport the substrate due to lack of interaction of ATP with the NBD's. B) Immunoblot to monitor the reproducibility in pelleting crude membranes at high speed (100,000g) using airfuge (Dr. Claire Friel's lab, University of Nottingham) or Optima ultracentrifuge. The crude membranes were centrifuged at 100,000g for 5 minutes and the supernatant (unpelleted) and pellets were analysed by western blot. C) The bar graph depicts the ratio of ATP dependent uptake of Lucifer yellow by 20 µg of crude membranes expressing ABCG2. The transport ratio was calculated as the transport in the presence of ATP divided by transport in the presence of AMP. ABCG2 specific uptake was monitored in presence of 1 µM Ko143 (3 and 6). Regeneration system for ATP availability (2 mg/mL creatine kinase and 100 mM creatine phosphate; 7 and 8) and 1% w/v fatty acid free albumin (9) were added to the reaction volume in order to see an effect of the required additives on ATP dependent relative uptake of Lucifer yellow by crude membranes. The data represents at least 3 or more independent repeats with error bars depicting SEM.

The membrane-based assays are important compared to the whole cell assays as they can be prepared in large batches and cryopreserved for later usage. One of the major disadvantages of the direct transport of substrates is that compounds with medium-to-high passive permeability are not retained inside the vesicles making measurements difficult to be obtained. The vast majority of ABCG2 substrates are hydrophobic and hence non-specific vesicular accumulation can occur resulting in a decreased signal to noise ratio. Monitoring transport of hydrophobic compounds that bear medium or high passive membrane permeability may result in false negative results as they cannot be trapped inside the membrane vesicles (Csilla Hegedűs et al., 2009).

In order to avoid any issues with vesicles being permeable to hydrophobic ABCG2 substrates we employed a water soluble ABCG2 specific drug substrate, Lucifer yellow (Csilla Hegedűs et al., 2009). Its low passive permeability makes it an ideal test compound for studying transporter: substrate interactions. Lucifer yellow is a fluorescent drug substrate with an excitation/ emission wavelength of 430 nm and 538 nm respectively. The fluorescent spectra of Lucifer yellow significantly overlaps with the fluorescent spectra of the GFP tag, hence an altered construct of ABCG2 (His-strep-ABCG2) was used in the study.

The experimental set up involved incubating 20 µg of crude membranes expressing ABCG2 protein, with 50 µM or 100 µM Lucifer yellow in the presence and absence of the ABCG2 specific inhibitor; Ko143 (1 µM), to monitor ABCG2 specific

transportation (Weidner et al., 2015). ATP dependent transportation was monitored by measuring Lucifer yellow fluorescence using a microplate reader (figure 3.3 C). Sf9 cells expressing ABCG2 treated with AMP (100 µM) were used as negative controls. Figure 3.3 C depicts ATP dependent uptake of Lucifer yellow by ABCG2 crude membranes (figure 3.3 C, bar graphs 2,3,5-9). The expected observation was that ABCG2 expressing vesicles would accumulate more Lucifer yellow than controls, with marked inhibition by Ko143. The considerable variability of the data in 3.3 C did not inspire confidence in this vesicular system. ABCG2 crude membranes show ATP dependent and ABCG2 specific uptake of Lucifer yellow (100 µM), compared to the membranes treated with 50 µM Lucifer yellow. Bar graphs 1 and 4 (figure 3.3 C) show baseline accumulation of Lucifer yellow by Sf9 crude membranes (negative controls).

As previously described, the ATP concentration was maintained at constant levels for a period sufficient for measurement (at least 20 min) with the creatine phosphate and creatine kinase reaction system. Accumulation of Lucifer yellow in presence of the regeneration system was comparable to non-expressing and ABCG2 expressing Sf9 membranes (figure 3.3 C, bar graph 4 and 5). Addition of an ATP regeneration system did not increase Lucifer yellow accumulation.

Attempts were made to understand the role of albumin in the kinetic parameters of the efflux transport. BSA (bovine serum albumin) was used as a solubiliser to monitor its role in drug transportation (figure 3.3 C, bar graph 9). Research has shown that 0.1% (w/v) BSA produced a small (28%), statistically significant increase in LY uptake by ABCG2 crude membranes (Deng et al., 2016). The study also revealed a reduction in the magnitude of BSA's effect as the protein concentration increased. Attempts were also made to understand the albumin concentration effect on LY transport, with 0.1% BSA showing a larger effect on LY transport (lower concentrations, 20 µM). This facilitated the use of BSA (1% w/v) in the VTA to facilitate the uptake of LY by the crude membranes. Accumulation of Lucifer yellow in the presence of 1% BSA was comparable to non-expressing and ABCG2 expressing Sf9 membranes (figure 3.3 C, bar graphs 9, 4 and 5). The data shown in figure 3.3 represents at least 3 or more independent repeats with error bars representing the internal SEM. The data are highly variable across the tested conditions and do not reflect active ABCG2 transporter overexpressed in Sf9 cells.

Even though ABCG2 expressed in our hands in Sf9 cells is inactive, various previous studies have shown an active ABCG2 transporter in crude membranes. ABCG2 ATPase activity was first reported using Sf9 crude membranes expressing the variant R482G isoform. This membrane preparation showed a very high baseline vanadate sensitive ATPase activity, which could be stimulated by a variety of ABCG2 substrates (Özvegy et al., 2001). In one of the studies a VTA was also performed using estrone-3-sulfate as a substrate. Estrone-3-sulfate showed a K_M of 7.8 µM and also showed competitive inhibition by Ko143 (Glavinas et al., 2007). In another study, 50 µg of crude membranes from Sf9 cells overexpressing ABCG2 were subjected to 50 µM Lucifer yellow and 4 mM ATP and rapidly filtered. The wild type ABCG2 showed a K_M of 45.1 µM. Although studies above show a functional ABCG2 transporter expressed in Sf9 membranes, in house generated crude membranes seem to be non-functional.

3.4 Monitoring ABCG2 function in Sf9 cells expressing ABCG2

To facilitate investigation of ABCG2 transport characteristics in Sf9 cells, appropriate assay conditions needed to be developed. As an alternative to a vesicle-based assay, we attempted to establish a whole cell Sf9 ABCG2 transport assay. Initial attempts were made to monitor cell viability during Sf9 cell infection (figure 3.4 A). A 100 mL Sf9 cell culture was infected with the BIIC stock, cells were harvested at different time points and checked for viability and ABCG2 expression using a MUSE cell analyser and an immunoblot respectively. Cells were stained with propidium iodide to gate for the dead cells. Sf9 cells not infected with the BIIC stock were used as a negative control and treated in the same manner. Cells were harvested at 22, 40, 47, 63 and 70 hours. A time course of cell viability established 40-hour infection as suitable for intact cell assays. The cells maintained a viability of $\geq$ 82%, compared to the uninfected Sf9 cells harvested at the same time point (figure 3.4 A). Immunodetection of ABCG2 expression using m-AB BXP-21 at the harvesting time points also confirmed ABCG2 expression (figure 3.4 B).

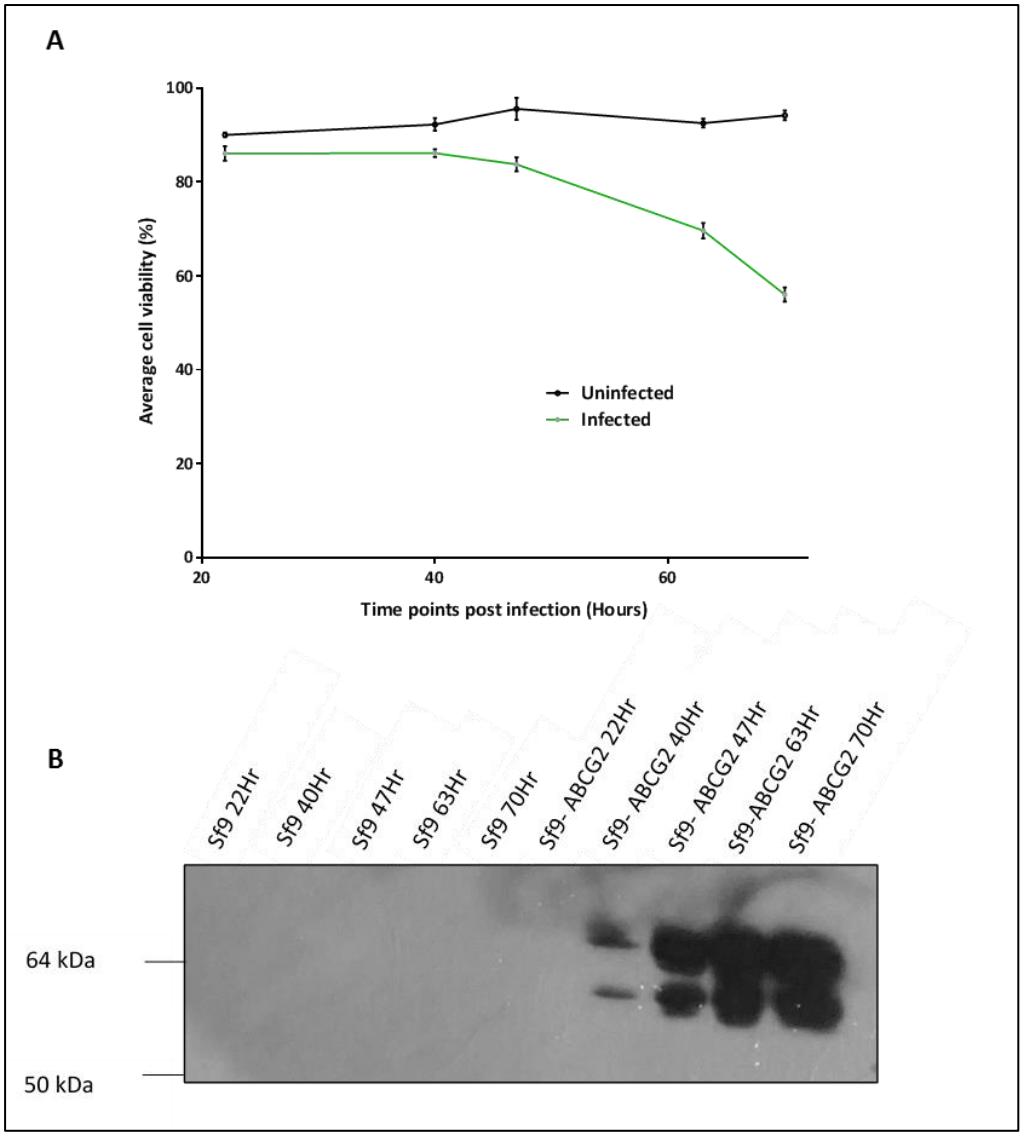


Figure 3.4: Time course to monitor the impact of ABCG2 expression on cell viability

A) Sf9 cells were infected with BIIC stocks expressing ABCG2. Cells were harvested at varying time points post infection. Cells not infected with BIIC stock were used as a negative control. The cell viability was monitored by addition of propidium iodide to the cells using the Muse count and viability kit. The viability was monitored using a Muse cell analyser (Dr. Sally Wheatley, University of Nottingham). Each time point is representative of technical triplicates. B) Immunoblot to monitor ABCG2 expression at each harvesting time point (shown in A). Cell lysates (10 µg) obtained through sonication were resolved on 8 % (w/v) polyacrylamide gels. Immunodetection using mouse BXP-21 showed protein expression between 40Hr- 70Hr time points.

The above conditions were used to monitor drug extrusion of a fluorescent ABCG2 substrate (mitoxantrone) by flow cytometry. The 40-hour time point showed ideal amounts of ABCG2 expression and minimum cell destruction upon infection with the baculovirus to less than 20 % (figure 3.4 A and B). Different buffer conditions (Insect

Xpress media- pH 6.2, MPMI- pH 6.2 and 6.6 and HPMI- pH 7.4) were examined to identify the optimal buffer condition to monitor live cell drug efflux in the assays. Cells were incubated with mitoxantrone for 30 minutes at 37°C in the presence or absence of Ko143 in their respective buffers. Özvegy et al. have previously suggested pH 7.4 as optimal for ABCG2 transport in insect cells (Özvegy et al., 2001). Insect express media is pH 6.2. So the experiment was repeated with cells resuspended in varying pH buffers (figure 3.5 C- H). Cells were gated for the dead cells using propidium iodide staining, enabling to monitor the cell viability and also drug transport simultaneously. Figure 3.5 A and B demonstrate mitoxantrone accumulation in uninfected cells (A) versus infected cells (B) in insect Xpress media (pH 6.2). There was no Ko143 inhibitable transport of mitoxantrone. There is no Ko143 inhibitable mitoxantrone accumulation observed for uninfected and infected Sf9 cells incubated in MPMI buffer at pH 6.2 (figure 3.5 C and D).

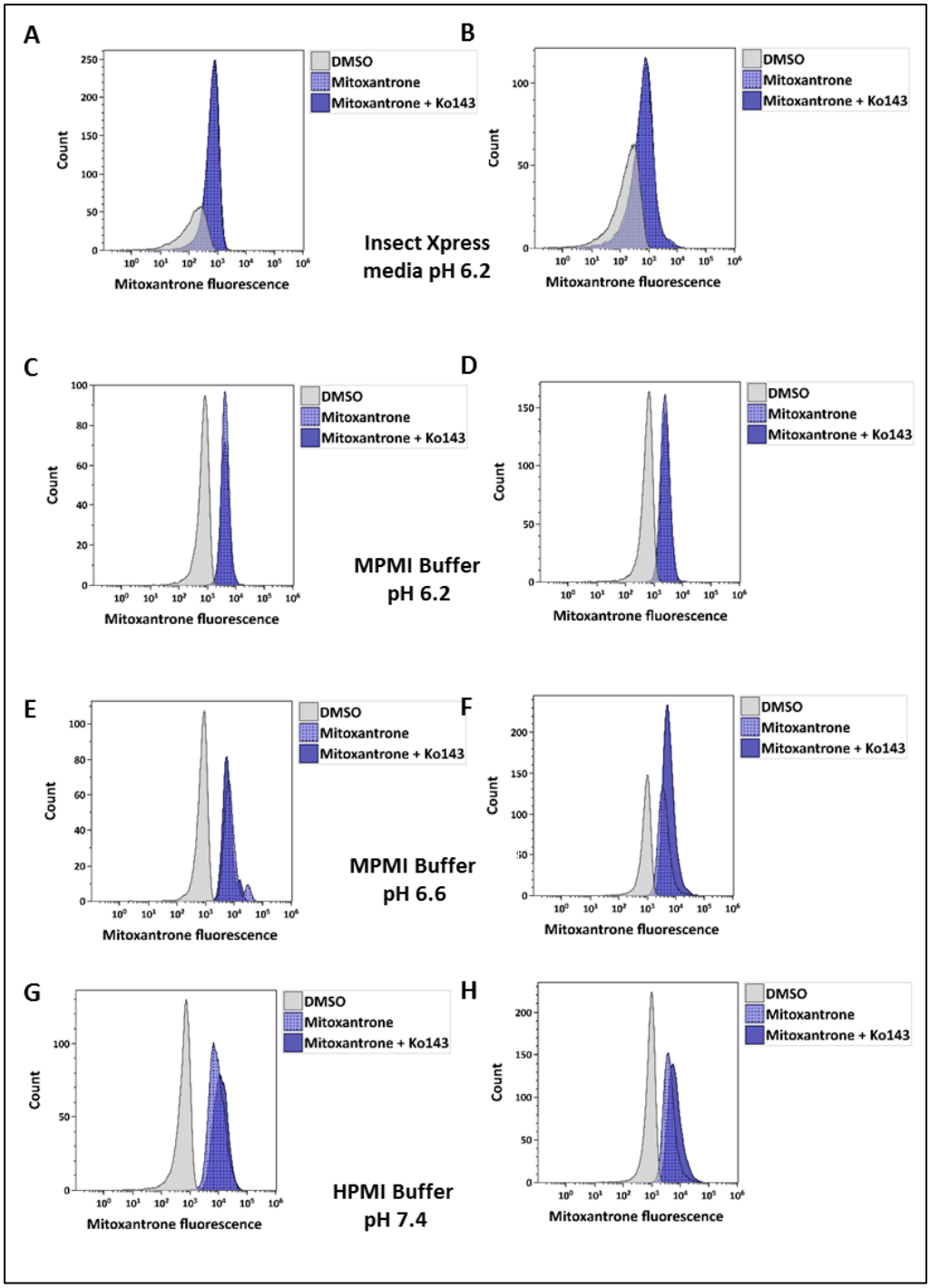

A
B
C
D
E
F
G
H
DMSO
Mitoxantrone
Mitoxantrone + Ko143
Count
Mitoxantrone fluorescence
Insect Xpress media pH 6.2
MPMI Buffer pH 6.2
MPMI Buffer pH 6.6
HPMI Buffer pH 7.4

Figure 3.5: Functional analysis of Sf9 cells/Sf9 cells expressing ABCG2 to transport mitoxantrone: ABCG2- non functional

Sf9 cells expressing ABCG2 and Sf9 cells (negative control) were harvested at 48-hour time point post the BIIC infection for the drug efflux assays. The cells were seeded at 1×10^6 cells mL^{-1} in varying buffers (insect Xpress media pH 6.2 (A and B), MPMI-1 pH 6.2 (C and D), MPMI-2 pH 6.6 (E and F) and HPMI pH 7.4(G and H) in FACS tubes. Cells were treated with 10 µM mitoxantrone (dotted blue histogram) in absence and presence of 1 µM Ko143 (dark blue histogram). Cell population were analysed for their drug efflux capabilities using flow cytometry, with excitation and emission wavelength for mitoxantrone 635/670nm. Insect cells expressing ABCG2 do not show mitoxantrone efflux in buffers insect Xpress media, MPMI-1 and 2 and HPMI.

Sf9 cells show minimal uptake of Mx in buffers MPMI, pH 6.6 (figure 3.5 E and F) and HPMI, pH 7.4 (figure 3.5 G and H) as is seen by a marginal rightward shift in the histogram upon addition of Ko143. Marginal activity at pH 7.4 or 6.6 unlikely to be sensitive enough to distinguish changes in activity due to point mutations in putative drug binding sites.

3.5 Cholesterol and its role in potentiating activity in heterologous system

The activity of the membrane transporters can be affected by the lipid composition and the physical state of the plasma membrane. Membrane micro-domains are known to partly house ABC transporters ABCB1, MRP1 and MRP2 (Demeule et al., 2000; Hinrichs et al., 2004). Micro-domains may even play an integral part in the development of multidrug resistance, due to the up regulation of caveolae and caveolar constituents in MDR tumour cells (Liscovitch and Lavie, 2000). Variation in cell membrane cholesterol content is known to modulate P-gp activity *in vitro* and *ex vivo* (Rothnie et al., 2001; Troost et al., 2004a, 2004b).

Previous studies have shown that cholesterol content may affect the ABCG2 ATPase activity in isolated insect membranes expressing ABCG2 (Pál et al., 2007). Studies suggest that the drug stimulated ATPase activity is profoundly affected by the low cholesterol content of the insect membranes, which is at least 10 fold lower than the human plasma membrane (Gimpl et al., 1995; Marheineke et al., 1998; Pál et al., 2007). It has been shown that destroying membrane rafts by cholesterol depletion causes about a 40% decrease in ABCG2 activity (Pál et al., 2007).

The mechanism by which cholesterol influences ABCG2 activity is not yet fully understood. There are various possibilities that can be suggested to substantiate the explanation behind the influence of cholesterol on ABCG2 function. Cholesterol is an integral component and contributor of lipid rafts/caveolae, which might be crucial for optimal ABCG2 activity through interaction of ABCG2 with caveolin-1 (Storch et al., 2007a). Alternatively, ABCG2 function may be modulated by cholesterol through the interactions with the transmembrane regions of the transporter and/ or altering the nucleotide-binding domains as suggested for P-gp. The binding of hydrophobic/ lipophilic substrates might be influenced by cholesterol as depicted for P-gp (Romsicki and Sharom, 1999).

As membranes prepared from the insect cells have a low level of cholesterol, this might lead to discrepancies in studying ABCG2 function. To overcome this, the cholesterol content of the transporter expressing Sf9 membranes may be increased. The most widespread tool for cholesterol loading is the cholesterol-cyclodextrin (CD) complex, where CD traps the hydrophobic compound within its cavity. The cholesterol-CD complex can be applied directly to Sf9 membrane-based assays in a 1-5 mM concentration (Christian et al., 1997b).

Cellular cholesterol content for Sf9 cells was altered using cyclodextrins as cholesterol delivery vehicles in cell culture systems. A 25 mM MβCD: cholesterol hemisuccinate with a molar ratio of 12.5:1 was prepared as explained in section 2. A 100 % saturated cyclodextrin: cholesterol hemisuccinate solution was added to the Sf9 cells infected with BIIC stock and non-infected cells, 12 hours prior to cells being harvested (section 2.3.5). Cells were harvested 72 hours post infection and subjected to membrane fractionation to generate cholesterol hemisuccinate doped and ABCG2 enriched crude membranes. A cholesterol assay was performed to quantify the amount of cholesterol doped in the Sf9 cells suggesting that the cholesterol content had been doubled by this treatment (to 22 µg).

The next step was to monitor ABCG2 expression and activity in cholesterol doped Sf9 cells. The immunoblot (using m-AB BXP-21) clearly depicts ABCG2 expression in cholesterol enriched crude membranes (figure 3.6 A). A VTA was performed to monitor ABCG2 activity in presence of ABCG2 substrate Lucifer yellow (figure 3.6 B).

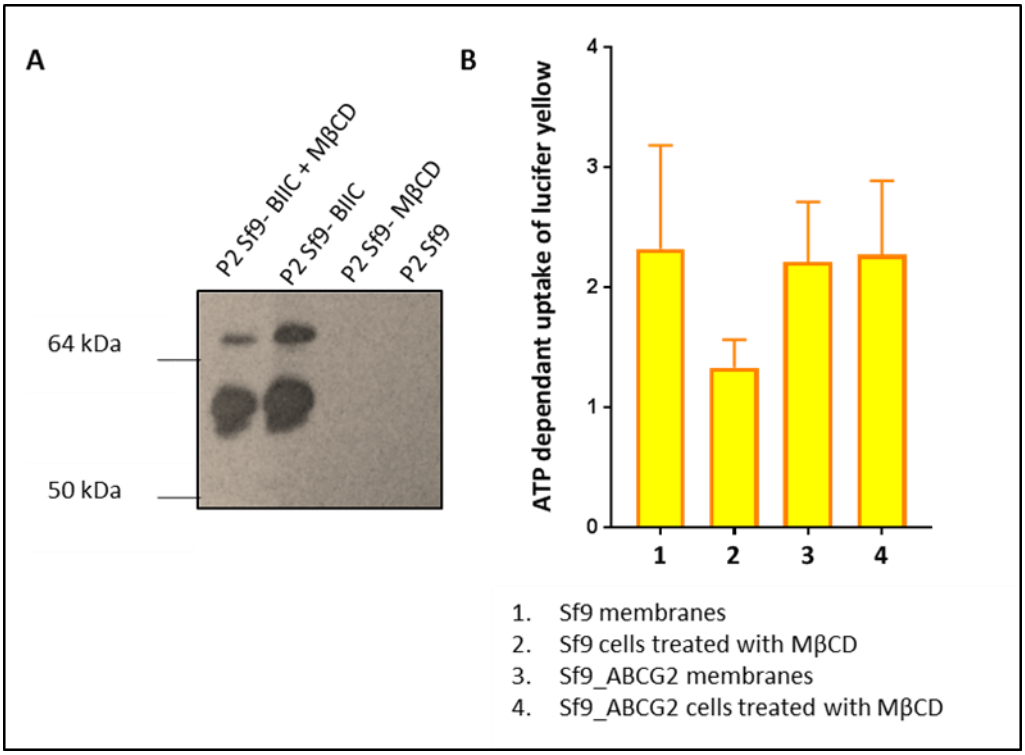


Figure 3.6: Addition of cholesterol hemisuccinate does not restore ABCG2 transport

A) Sf9 cells and Sf9 cells infected with BIIC stock were subjected to cholesterol hemisuccinate: methyl-β-cyclodextrin to enrich the Sf9 cells with cholesterol. Cholesterol hemissuccinate: methyl-β-cyclodextrin (12.5:1 molar ratio) was added to cells 12 hours prior to harvesting. Immunodetection with m-AB BXP-21 revealed ABCG2 expression at considerable levels in cells enriched with cholesterol and devoid of excess cholesterol. B) VTAs to check the functionality of ABCG2 in cells doped with cholesterol and devoid of excess cholesterol. The bar graph depicts the ratio of ATP dependent uptake of Lucifer yellow by 20 µg of crude membranes. There is no significant difference in Lucifer yellow uptake by Sf9 cells and Sf9 cells infected with BIIC or Sf9 cells infected with BIIC and doped for cholesterol. The VTA represents at least 4 independent repeats with error bars showing the SEM.

Figure 3.6 B depicts ATP dependent uptake of Lucifer yellow by cholesterol hemisuccinate doped, ABCG2 expressing crude membranes. Crude membranes show ATP dependent uptake of Lucifer yellow (100 µM), but there is no clear difference between membranes not-expressing/ expressing ABCG2 or cholesterol hemisuccinate doped/ devoid of cholesterol hemisuccinate doping and ABCG2 expressing/ non-expressing membranes. The data represents 4 independent repeats. The data suggests a non-active ABCG2 transporter (figure 3.6 B).

As these observations were contradictory to literature reports (Morisaki et al., 2005; Özvegy et al., 2002), we obtained cholesterol hemisuccinate doped, ABCG2

expressing crude membranes from Dr. Csilla Ozvegy (Hungarian Academy of Sciences, National Blood Center). The crude membranes were confirmed for expression using immunodetection with m-AB, BXP-21 (figure 3.7 A). Cholesterol hemisuccinate doped ABCG2 overexpressing crude membranes from above were assessed in parallel. VTA was performed as mentioned above (figure 3.7 B). ABCG2 substrate mitoxantrone was used in the assay (Robey et al., 2001a). For mitoxantrone, there was a Ko143 inhibitable transport of drug in the vesicles obtained from Hungary, but the variability of this transport assay was significant as is visible from the error bars. In contrast, our in-house membranes did not show Ko143 inhibitable transport. The variability can be attributed to the hydrophobic nature of the substrate, leading to permeability of the drug from the vesicles.

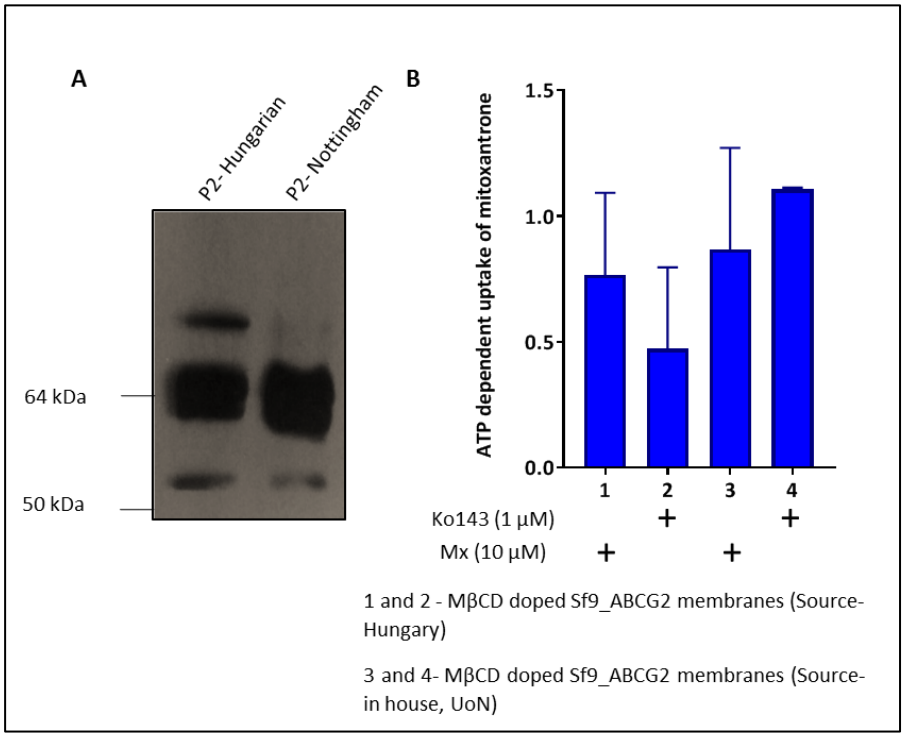


Figure 3.7: Effect of cholesterol hemisuccinate doping on ABCG2 transporter functionality

A) Immunoblot to detect ABCG2 expression in cholesterol hemisuccinate doped Sf9 cells (Hungary) and Sf9 cells expressing ABCG2 (in house, Nottingham). Crude membranes (10 µg) were resolved on 8% w/v polyacrylamide gel and immunodetected using m-AB BXP-21. B) VTAs to check the functionality of ABCG2 in cells doped with cholesterol hemisuccinate and devoid of excess cholesterol hemisuccinate. The bar graph depicts the ratio of ATP dependent uptake of mitoxantrone by 20 µg of crude membranes. The VTA represents at least 3 independent repeats with error bars showing SEM.

Studies indicate cholesterol loading significantly enhances ABCG2 mediated transport. MXR- Sf9 crude membranes clearly depict cholesterol loading has an impact on the maximal velocity of the methotrexate transport but does not affect the K_m. Significant transport for Prazosin was also observed by the MXR- Sf9 membrane vesicles. Cholesterol loaded ABCG2 overexpressing insect cells therefore act as suitable models to investigate substrate transportation in the non-cell based environment (Pál et al., 2007)

Effect of cholesterol on transporter activity has been well investigated for ABCB1 (Garrigues et al., 2002; Pál et al., 2007). Another finding suggests the presence of endogenous ABC drug transporters within Sf9 cells that have not yet been well characterized. Cholesterol doping has shown to activate the transport of substrates by the endogenous transporters. Several of these probe substrates have been used to study the drug transport by human ABC transporters. E_1S (estrone sulphate), a substrate for ABCG2, did not show significant ATP dependent uptake in cholesterol doped Sf9 vesicles (S C Hyde et al., 1990).

The exact mechanism of how cholesterol stimulates the activity is still unanswered.

Cholesterol loading and depletion experiments at the membrane phase stage (membrane vesicles generated from Sf9 cells expressing ABCG2) can help ascertain the role of cholesterol in ABCG2 function. Methyl-β cyclodextrin or digitonin can be used to extract/ chelate cholesterol from lipid phase of the native membranes expressing ABCG2 to monitor ABCG2 function (Garrigues et al., 2002; Nishikawa et al., 1984; Pal et al., 2007). Uptake experiments using radiolabelled cholesterol can be used to monitor cholesterol as a substrate for ABCG2. Photon counting histogram analysis can be employed to undertsand the role of ABCG2 substrates in dissociating the fluorescent labelled cholesterol analogue (Frances J Sharom, 2011). Investigations could ascertain residues involved in direct cholesterol binding.

Cholesterol loading is known to activate ABCC2 dependent transport of some substrates. Cholesterol might bind directly to the transporter, due to structural similarities with the steroid substrates as is seen in the cryo-EM based structure of ABCG2 (Taylor et al., 2017). It might contribute towards the rigid membrane environment needed for the proper transporter conformation (Shi and Jarvis, 2007). Cholesterol is known to play a role in partitioning ABCB1 substrates in the lipid bilayer, thereby facilitating their access to the substrate binding site (Eckford and Sharom, 2008).

The stimulating effect of cholesterol on ABCG2 function might indicate the potential of cholesterol to be a substrate, but no studies have shown any signs of cholesterol mediated ABCG2 transport inhibition. Cholesterol may act as an allosteric regulator for ABCG2 mediated function, but further studies are needed to substantiate the potential role of cholesterol as a mediator, regulator or a bona fide substrate.

3.6 Summary and conclusion

Attempts have been made in this chapter to explore a heterologous expression system using Sf9 cells to overexpress ABCG2 and monitor its substrate transportation activity in crude membranes. This chapter was integral to the development of high throughput methods to evaluate ABCG2 expression and function, but the data suggests ABCG2 expressed in this system is non-functional.

Sf9 cells are a very good system to overexpress recombinant ABCG2 using the Bac to Bac system. The studies involved monitoring ABCG2 function in crude membranes and live cells using VTA and flow cytometry respectively. The data is highly variable across the tested conditions for the VTA and does not reflect an active ABCG2 transporter over expressed in Sf9 cells.

Since, the activity of membrane transporters is known to be affected by the lipid composition and the physical state of the plasma membrane, Sf9 cells were cholesterol hemisuccinate doped and tested for ABCG2 expression and function. Crude membranes provided by a collaborator were also obtained; in all cases we failed to observe a reliable, reproducible ABCG2 functional assay.

Attempts were made to monitor ABCG2 transporter function in live cells using flow cytometry in different buffer conditions. Sf9 cells expressing ABCG2 showed > 82% cell viability at 40-hour time point for monitoring transporter functionality using flow cytometry. The data reiterated the fact that ABCG2 is not functional in insect cells and no Ko143 dependent transport is observed in Sf9 cells overexpressing ABCG2.

In brief, in our hands, we can overexpress ABCG2 in Sf9 cells but are not able to demonstrate ABCG2 function, in either activity-based assays in live cells or crude membranes. Since Sf9 cells have varied lipid bilayer composition, treating cells with different sterols and lipids during expression stage could help revive ABCG2

transporter functionality, which was beyond the scope of this PhD thesis (Telbisz et al., 2013).

This made us consider a mammalian expression system to investigate ABCG2. Indeed, a single experiment using HEK293T cells expressing WT ABCG2 was performed at this stage to investigate the suitability of the HEK cells as a platform for studying ABCG2 mutant isoforms. These data (figure 3.8) prompted all subsequent studies to be performed in a mammalian cell system.

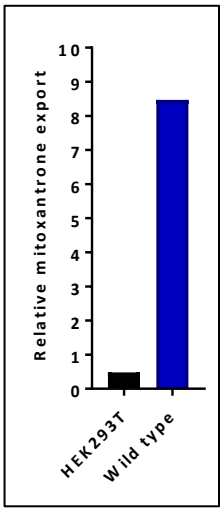


Figure 3.8: Functional analysis of mammalian cells (HEK293T) expressing wild type protein ABCG2

Transport studies were performed for wild type ABCG2 protein expressed in mammalian expression system (HEK293T cells) using the wild type substrate mitoxantrone (10 µM) in absence/ presence of ABCG2 specific inhibitor Ko143 (1µM). Cell population was analysed by flow cytometry, with the excitation and emission wavelength pairs for GFP- 488/526nm and mitoxantrone- 635/670 nm. The wild type isoform displays a fold change of 8.47 in mitoxantrone accumulation in presence of Ko143. The negative control (HEK293T) is non-functional in mitoxantrone transport.

Chapter 4 and 5 dive deep into the world of mammalian expression to generate TM3 helix mutant isoforms and understand the role of the TM3 helix residues in drug binding and/ or translocation.

Chapter 4: Generation, expression and localisation of transmembrane (TM) helix 3 mutant isoforms

4.1 Introduction

ABCG2, due to its expression in liver, intestines, kidneys, brain and placenta, assumes a protective role by limiting the bioavailability and absorption of xenobiotics and toxic compounds (Cooray et al., 2002; Huls et al., 2008; Maliepaard et al., 2001a). ABCG2 is also known to transport endogenous metabolites such as estrogen metabolites and uric acid, and many antineoplastic and anticancer compounds (Imai et al., 2003; O. M. Woodward et al., 2009). Despite the important role of ABCG2 in protecting the vital organs against xenobiotics and drugs, the molecular mechanism behind how it interacts, binds and translocates a vast array of structurally unrelated compounds remains enigmatic. Several mutational studies have been performed in order to understand crucial residues involved in drug binding and translocation pathways.

Arginine 482 is the most well-known residue of TM3 helix to influence substrate transport (figure 4.1). Its role in function emerged at the same time as the gene was cloned. ABCG2 was cloned by Doyle et al., in 1998 from doxorubicin resistant MCF 7 breast cancer cell lines (MCF- 7/ AdrVp) (Doyle et al., 1998b). During the same period ABCG2 was also cloned from placental tissues and mitoxantrone resistant cell lines by two other groups and were designated as ABCP or MXR, suggesting that ABCP, MXR and BCRP differed at position 482 (Allikmets et al., 1998; Miyake et al., 1999). Overexpression of ABCG2 in doxorubicin resistant mouse fibroblast cells, reflected R482M or R482S mutation. Another ABCG2 variant was identified to harbour R482M mutation in a doxorubicin resistant $CD4^+$ T- cell line. ABCG2 mutants from the drug selected cell lines showed a broader substrate transport phenotype than the wild type protein. The R482 mutations markedly changed the spectrum of the transported substrates. The ABCG2 mutants R482T and R482G transport daunorubicin, rhodamine 123 and lyso tracker green (non-wild type substrates). The wild type and the mutant isoforms are also known to transport mitoxantrone, prazosin

and Hoechst 33342, whereas the wild type transports methotrexate (Allen et al., 1999; Mao and Unadkat, 2015; Robey et al., 2001a).

Site directed mutagenesis of proline 485 (within the adjacent turn of R482 of the presumed α helix) to alanine in TM3 has also been shown to reduce the efflux of BODIPY- prazosin and pheophorbide A (porphyrin derivative) compared to the wild type ABCG2 protein (figure 4.1) (Haider et al., 2015). This made us consider whether the highly conserved TM3 helix (appendix 3) would harbour further residues of interest that would influence the substrate specificity.

In this study, point mutations to alanine have been made along the entirety across of TM3 helix (D477- L497), in order to understand the role of TM3 helix in drug binding and translocation (figure 4.1). A mammalian expression system (HEK293T cells) has been used to generate stable cell lines expressing ABCG2 variants. These mutant isoforms have been investigated for their expression and membrane localisation in this chapter. Their role in function has been investigated and explained in detail in chapter 5.

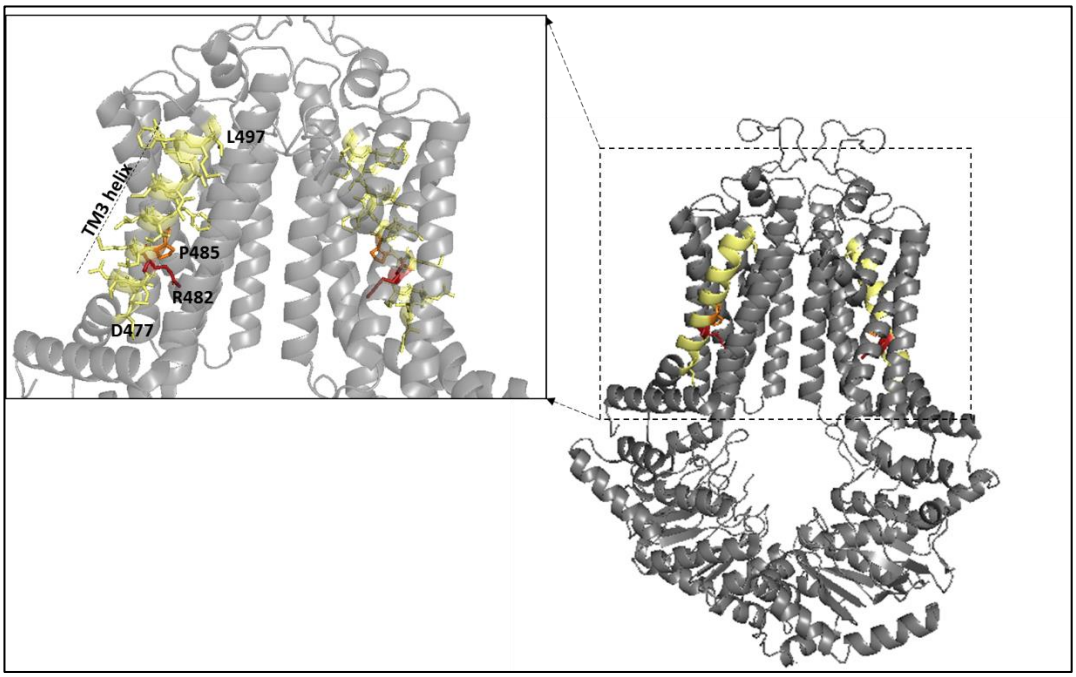


Figure 4.1: TM3 helix residues mapped on ABCG2 structure

The ABCG2 homodimer structure with the TM3 helix residues (D477- L497), highlighted in pale yellow (stick representation). The key residues with altered substrate specificity (R482 and P485) have also been highlighted. Figure generated in PyMOL software (PDB ID: 6ETI).

4.2 Plasmid construct

The ABCG2 mutant isoforms were generated using the mammalian expression vector pcDNA^{TM}3.1 Zeocin^{TM} (+) (figure 4.2). This vector is designed to have high levels of constitutive protein expression. It contains a strong promoter system, i.e. CMV enhancer promoter regulatory region for high levels of expression of the gene of interest, a forward orientation multiple cloning site. The plasmid also contains an antibiotic resistance cassette (ampicillin) for the purpose of genetic engineering (bacterial selection) and a selectable marker, Zeocin^{TM} resistance gene for generation of stable mammalian cell lines (figure 4.2).

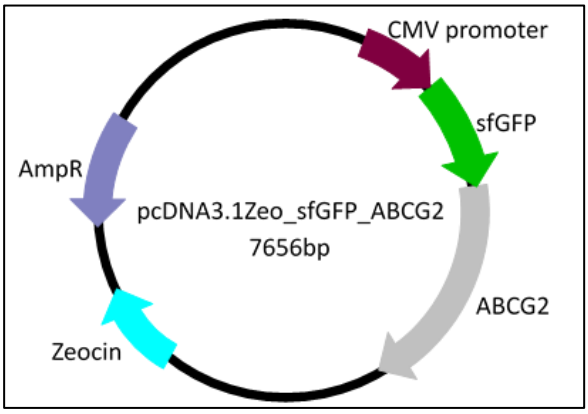


Figure 4.2: pcDNA3.1Zeo_sfGFP_ABCG2 schematic plasmid map

The vector backbone encodes for the multidrug transporter ABCG2, N-terminally fused to sfGFP tag for visualization of protein. The vector comprises of a strong CMV promoter regulatory region for enhanced expression, the bacterial ampicillin resistance gene for genetic engineering and a selectable marker, i.e., Zeocin^{TM} resistance gene for generation of stable protein expression in mammalian cell lines.

The plasmid encodes a super folder green fluorescent protein (sfGFP), fused N-terminally for fluorescent studies (figure 4.2). A robust folded version of GFP; known as superfolder GFP, characterised and generated by Pédelacqe and co-workers was employed in the study (Pédelacq et al., 2006). GFP has the tendency to dimerize at higher concentrations (von Stetten et al., 2012), through a hydrophobic patch identified by Zacharias and co-workers (Zacharias, 2002). As ABCG2 is a dimer and can form higher order structures, we wanted to ensure the tag (sfGFP) could not interfere with this, therefore, for this study, GFP with A206K mutant isoform was employed, in order

to maintain the monomeric states (von Stetten et al., 2012; Wong et al., 2016). Previous studies also indicate that N- terminal sfGFP tag does not alter the expression and function of ABCG2 (Haider et al., 2015; Wong et al., 2016).

4.3 Generation of TM3 helix mutant isoforms

A simple and widely used technique in the determination of the catalytic or functional role of protein residues involves alanine- scanning mutagenesis. Substitution of the residues of interest to alanine eliminates the side chain beyond the β- carbon, does not tend to alter the main chain conformation, nor does it impose strong electrostatic or steric clashes. It is structurally neutral and has high propensity to form α- helices and thus is unlikely to cause any significant perturbations to the overall protein folding (Lefevre, 1997). Oligonucleotide primer pairs were designed for plasmid pcDNA3.1Zeo_sfGFP_ABCG2 vector (chapter 2, section 2.1.1). The primers were designed to insert the desired mutation for the 20 residues in TM3 helix. Mutant isoforms were generated using site directed mutagenesis based on the *in vitro* amplification of DNA by PCR, using the pcDNA3.1Zeo_sfGFP_ABCG2 template. Target DNA amplification was confirmed by agarose gel electrophoresis (data not shown). Trouble shooting was performed in order to successfully generate the M496A mutant isoform by reducing the extension temperature to 68 ˚C from 72˚C in the PCR cycle.

Following the temperature cycling process, the PCR products were subjected to DpnI digestion. DpnI endonuclease acts on methylated and hemimethylated parental DNA template and therefore provides the basis for selection of mutation- containing synthesized DNA (chapter 2, section 2.1.3). The DpnI digested mutant DNA were transformed using the competent cells $DH_{5\alpha}$ (chapter 2, section 2.1.4). Plasmid DNA was extracted based on the manufacturer's protocol for the nucleospin plasmid kit (chapter 2, section 2.1.5) and the recovery of plasmid constructs containing sfGFP_ABCG2 were confirmed by a restriction digestion screen using the enzyme PvuII. PvuII cuts in a site-specific manner thereby producing bands at 4486 bp, 1749 bp and 1421 bp (figure 4.3 A and B and appendix 1).

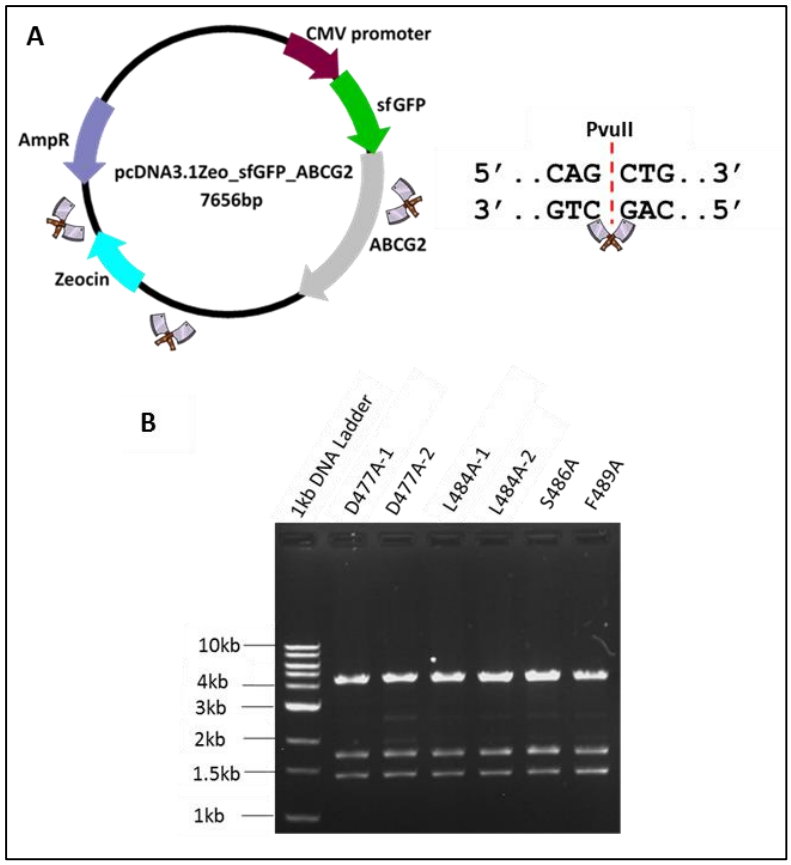


Figure 4.3: PvuII restriction digest profile of ABCG2 mutant isoforms

A) Restriction digestion profile with PvuII enzyme confirms the presence of p3.1zeo_sfGFP_ABCG2 vector in the variant forms. It cuts the vector at 3 positions (two in the plasmid backbone and one in the ABCG2 gene sequence (indicated with a pair of cleavers) with a recognition sequence of CAGCTG. The plasmid DNA for each mutant isoform was subjected to restriction digestion profile using the PvuII enzyme and analysed on 0.7% w/v agarose gel to confirm the presence of p3.1Zeo_sfGFP_ABCG2 vector in each isoform. B) Depicts the agarose gel loaded with isoforms of p3.1Zeo_sfGFP_ABCG2 vector (D477A, L484A, S486A and F489A). 1kb DNA ladder is used as the marker. Vector presence in all the isoforms is confirmed by the 3 bands of the expected sizes. Screening of the remaining mutant isoforms has been documented in appendix 1.

4.4 R482 and M496 case study- incorporation revealed by restriction enzyme digestion

Two of the mutant isoforms (R482A and M496A) could be screened for the incorporation of the mutation as the primers also included novel/ additional sites for the restriction enzymes NcoI (R482A) and Bsu36I (M496A). Restriction digest analysis was performed using the specific restriction endonuclease for each mutant

482 and 496 isoforms. The mutation R482A could be distinguished by the presence of additional NcoI, with this enzyme resulting in bands of 3.4 kb, 2.5 kb, 1.4 kb, 0.22 kb and 0.13 kb rather than 4 bands with the wild type ABCG2, as depicted in figure 4.4 A and B. The mutation R482A results in the 2.6 kb band being cut into a 2.5 kb and 0.13 kb band (figure 4.4 B, red box).

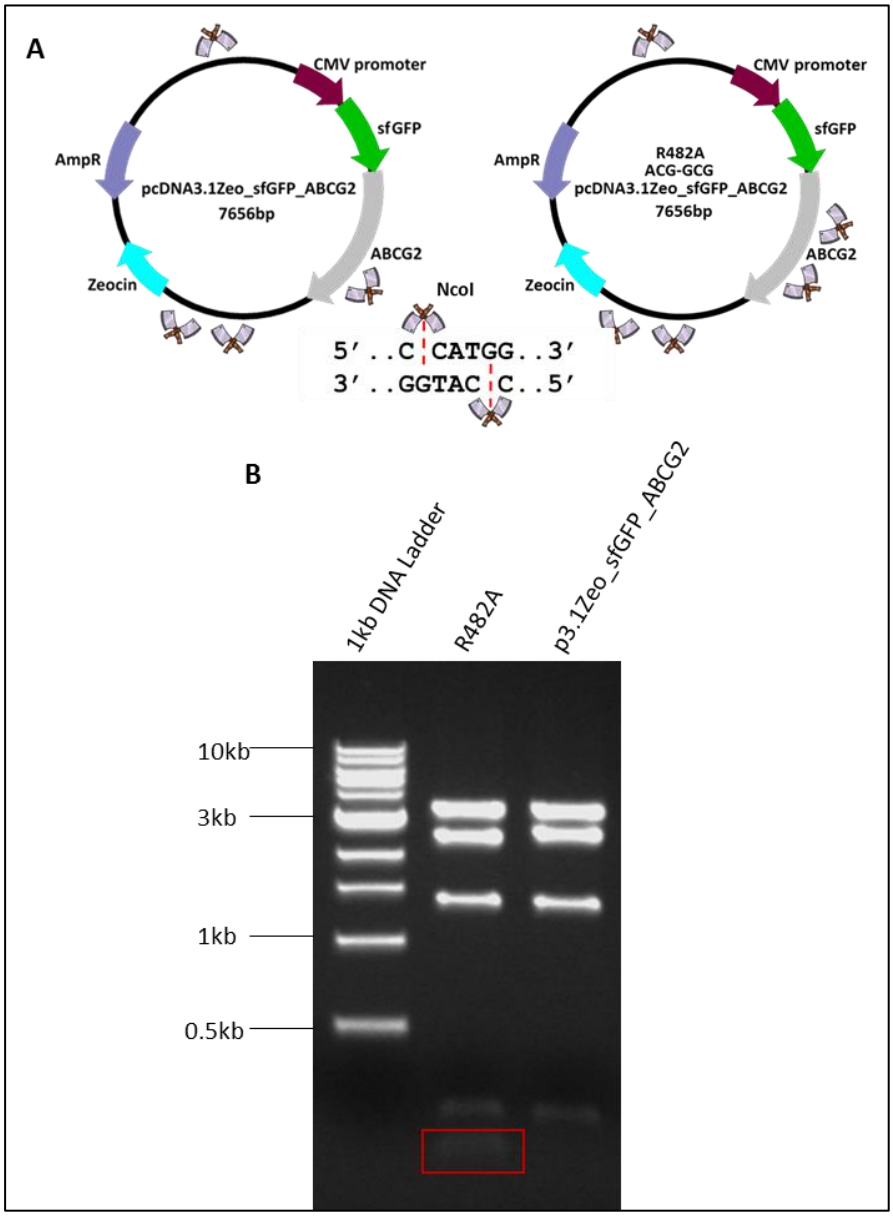


Figure 4.4: Confirmation of presence of R482A mutant isoform

The presence of R482A variant isoform was confirmed with restriction digest profile using NcoI restriction endonuclease. A) Schematic representation of the putative cut sites (depicted by a pair of cleavers) associated with NcoI restriction endonuclease in wild type and R482A mutant isoform. The wild type DNA has 4 cut sites for NcoI enzyme, thereby producing 4 bands (3.4kb, 2.6kb, 1.4kb and 220bp). Site directed mutagenesis for R482A mutant isoform introduces another cut site for NcoI restriction endonuclease thereby producing 5 bands upon digestion (3.4kb, 2.5kb, 1.4kb, 220bp and 126bp (red grid box) respectively). B) Agarose gel electrophoresis (0.7% w/v) analysis for screening the presence of R482A mutant isoform. The construct depicts the accurate banding pattern associated with R482A mutant isoform as explained above in A.

The restriction digest screen profile for R482A clearly depicts the development of the desired mutations. The R482A contains the diagnostic fifth band, thereby confirming successful mutation (figure 4.4 B, red grid box).

The M496A mutant was screened for mutation using the restriction double digest profile for Bsu36I and NdeI. The double digest profile for the wild type DNA produced 2 bands of 5.7 kb and 1.9 kb as depicted in figure 4.5 A. The M496A isoform DNA has an extra site for Bsu36I enzyme. Therefore, the double digest profile of mutant M496A produced 3 bands of 4.9 kb, 1.9 kb and 0.7 kb, as depicted in figure 4.5 A. The mutation M496A results in the 5.7 kb band being digested into a 4.9 kb and a 0.7 kb band (figure 4.5 A and B).The digest profile for the wild type and mutant M496A isoform can easily be differentiated based on an extra recognition site for Bsu36I, as depicted in figure 4.4 B red grid box. The M496A isoform was confirmed for the desired mutation based on the double digest restriction digest profile (figure 4.5 A and B). The restriction enzyme digestion of the isoforms R482A and M496A confirmed the presence of desired mutation.

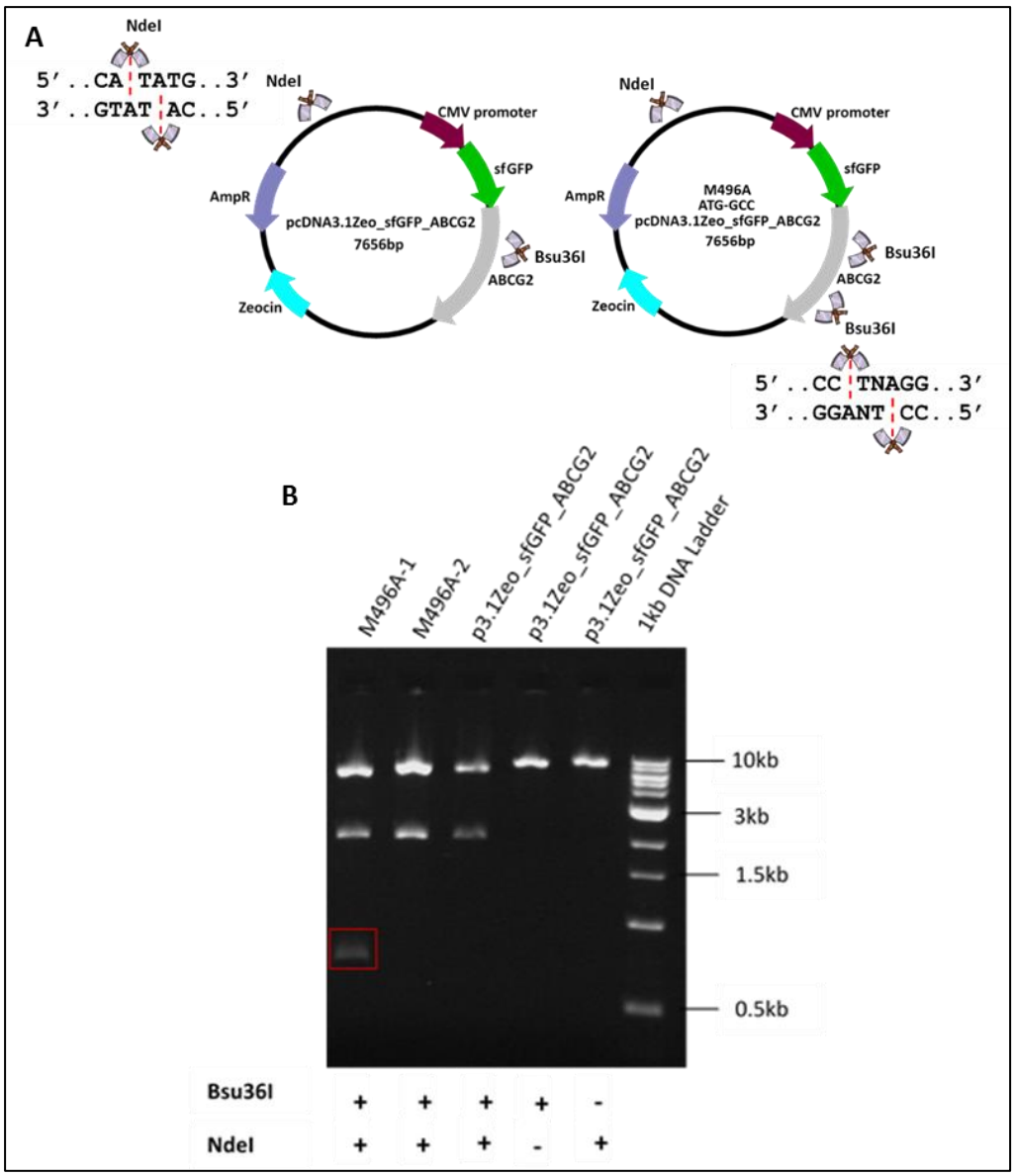


Figure 4.5: Case study- M496A mutant isoform generation

A) Schematic representation of the putative cut sites (depicted by a pair of cleavers) associated with Bsu36I and NdeI restriction endonucleases in wild type (left) and M496A mutant isoform (right). The wild type DNA has 1 cut site for each enzyme respectively, thereby producing 2 bands (5.7kb and 2kb). Site directed mutagenesis for M496A mutant isoform introduces another cut site for Bsu36I restriction endonuclease thereby producing 3 bands upon double digestion (5kb, 2kb and 708bp respectively). B) The restriction digest profile for the wild type (P3.1Zeo_sfGFP_ABCG2) and the mutant 496 isoforms (M496- 1-2) analysed on 0.7% w/v agarose gel. 1 Kb DNA ladder is used as the marker. The M496A-1 mutant DNA contains the diagnostic band (red grid box) for the double digest profile, thereby confirming the presence of the desired mutation.

4.5 Sequence analysis confirms all mutations

To confirm the presence of successful mutants in the p3.1Zeo_sfGFP_ABCG2 constructs, the DNA samples were sent for Sanger sequencing (Source Bioscience). Analysis of data from the primer Seq482 sequenced the transmembrane 3 of the ABCG2, thereby confirming the presence of desired mutation. To ensure no secondary mutations were incorporated in the p3.1Zeo_sfGFP_ABCG2 constructs, samples were sequenced using the primers Seq F0, Seq F2, Seq R1, GFP rev. These primers sequenced the entire sfGFP_ABCG2 construct. A schematic representation of the primers used to sequence sfGFP_ABCG2 construct is depicted in figure 4.6 A.

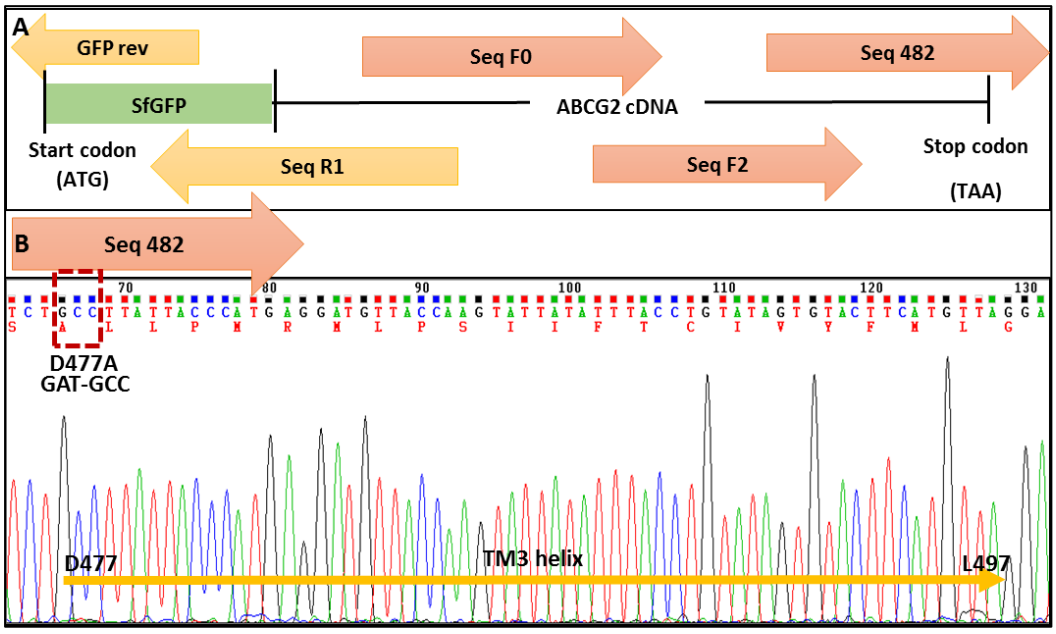


Figure 4.6: Confirmation of the desired mutation using Sanger Sequencing

A) Loci for the primers of interest that anneal to the p3.1Zeo_sfGFP_ABCG2 cDNA and sequence the desired region of interest (sfGFP_ABCG2). The 5 primers (GFP- rev, Seq F0, Seq R1, Seq F2 and Seq 482) depicted cover the entire region of interest with an overlap of 100- 200 bp between adjacent sequence reads. B) Sequence analysis performed using the Chromas software. Seq 482 primer data successfully demonstrates the incorporation of the point mutation to Alanine for the amino acid D477 (GAT>GCC), present in the TM3 helix. The mutation depicted above has been indicated by a red box. The analysis performed for the other TM3 helix residues has been documented in appendix 2.

The sequencing data retrieved from Source Bioscience were analysed on Chromas (sequencing chromatograms) for the desired mutation site (figure 4.6 B, appendix 2). Analysis was further made with NCBI: BLAST to align the predicted and observed

sequence data. All the primers showed 100% sequence similarity with the wild type p3.1Zeo_sfGFP_ABCG2 with an overlap of 100- 200 bp between adjacent sequence reeds. This comparison confirmed that each of the 20 mutations had been made without the presence of secondary mutations.

4.6 Generation of stable cell lines

A mammalian expression system derived from human embryonic kidney cells (HEK293T) was used in this study to generate stable cell lines and for further localisation and functional analyses. The normal HEK cells were transformed by being exposed to the sheared fragments of adenovirus type 5 DNA. These transformed cells were designated as 293 cells (Russell et al., 1977). HEK293T cells express a mutant version of temperature sensitive SV40 large T antigen (simian vacuolating virus 40 T antigen). The SV40 shuttle system is used by the cells to their advantage (DuBridge et al., 1987). Plasmids containing SV40 origin of replication were used to transfect the HEK293T cells. In HEK293T cells, SV40 T antigen acts as a transcriptional activator, resulting in increased production of constitutive recombinant proteins. It helps maintain a high copy number of the plasmid, thereby increasing the recombinant protein production (DuBridge et al., 1987; Russell et al., 1977).

HEK293T cells were transiently transfected with sfGFP_ABCG2 plasmids (chapter 2, section 2.2.3). PEI mediated transfection was conducted (Boussif et al., 1995). The mutant constructs were transiently transfected into HEK293T cells using PEI mediated transfections with N (PEI): P (DNA) molecules ratio 15:1 (Haider et al., 2015; Wong et al., 2016). PEI fulfils the goal of being a synthetic gene delivery vehicle that assembles the DNA/ vector complex, being inert and efficient to be successfully transfected to the host cells. PEI, due to high cationic charge density potential and substantial buffering capacity at physiological pH, acts as an efficient vector for delivery of oligonucleotides and plasmids (Boussif et al., 1995).

Stable cell lines were generated based on the Zeocin^{TM} (200 µg mL^{-1}) mediated selection process. Zeocin^{TM} resistant colonies developed over a period of 10- 14 days. These eventually reached confluency over a period of 14- 20 days. The expression of ABCG2 was confirmed by observation of GFP fluorescence under an epifluorescent microscope (figure 4.7). The expression and cellular localization of sfGFP_ABCG2

was imaged for all mutant isoforms in phase contrast and fluorescent modes. This resulted in the generation of mixed population (high and low GFP fluorescence) stable cell lines for wild type ABCG2 and TM3 helix mutant isoforms (figure 4.7 and appendix 4).

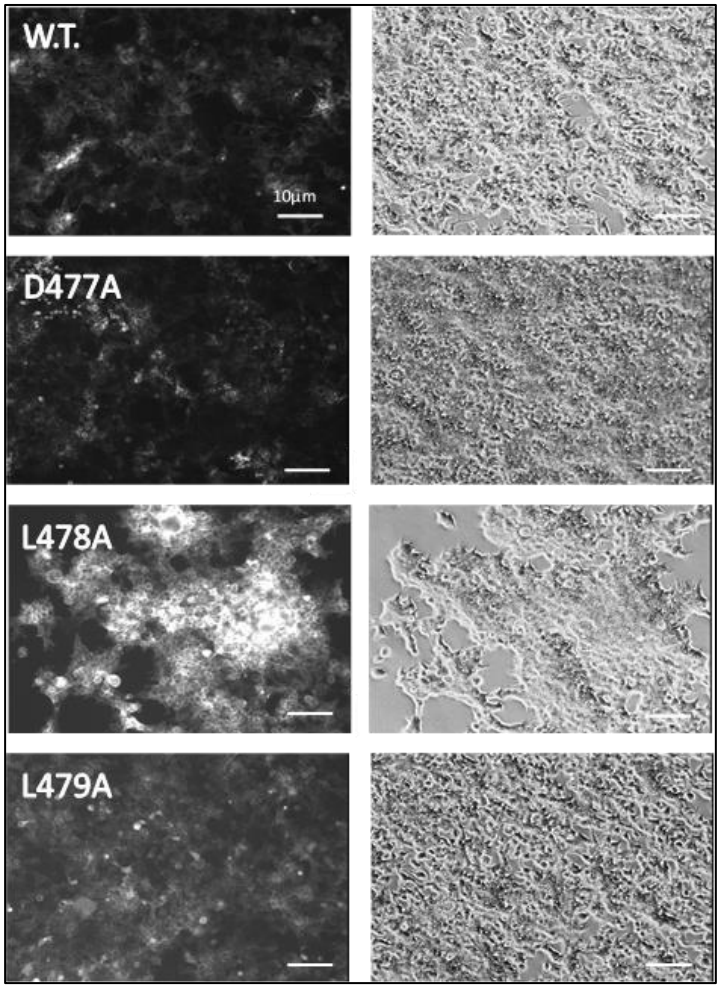


Figure 4.7: Expression analysis for p3.1Zeo_sfGFP_ABCG2 transfected stable cell lines

HEK293T cells were transiently transfected with sfGFP_ABCG2 plasmids (wild type and mutant isoforms). Stable cell lines were generated based on the zeocin™ (200 µg mL^{-1}) mediated selection process. Zeocin™ resistant colonies developed over a period of 10- 14 days. GFP fluorescence was observed using an epifluorescent microscope (phase 1, 10 X objective; Carl Zeiss, Birmingham, UK) connected to an inbuilt camera (AxioCam MRm, Zeiss) and analysed using the software Axio Vision release 4.8.2 SP3. Phase contrast images are on the right-hand panel whereas fluorescence images are on the left-hand side. Scale bars represent 10 µm.

4.7 Expression characterisation of TM3 helix mutant isoforms

To confirm the expression of the wild type ABCG2 and the mutant isoforms along with a negative control (E211Q, catalytically inactive Walker-B mutant) immunoblotting was performed. Western blots for the whole cell lysates (20 μg) were performed using 10% (w/v) polyacrylamide gels. ABCG2 expression was detected by immunoblotting with BXP-21 antibody which recognizes an intracellular epitope within the nucleotide binding domain of ABCG2 (residues 271-396) (Maliepaard et al., 2001a). An immuno-reactive sfGFP_ABCG2 band was detected at approximately 100 kDa (72 kDa ABCG2 and 27 kDa sfGFP) for the wild type and the mutant isoforms (for example, D477A, L478A, L479A, M481A, I487A, C491A, V493A, L497A; figure 4.7 A and B). Some of the mutant isoforms displayed a second immune-reactive band at approximately 80kDa (for example, L479A, M481A, L484A, I487A, C491A, I492A; figure 4.8 A and B). This second band could be indicative of breakdown during cell lysis, which was minimised by utilising freshly obtained cell pellets, rather than frozen ones. This could also be due to reduced maturation (incomplete glycosylation).

Most of the mutant isoforms showed similar ABCG2 expression compared to the wild type, consistent with maturation and protein trafficking, except E211Q, R482A, I488A and Y494A (figure 4.8 A and B). The lower expression of these mutant isoforms suggests stability issues associated with reduced stability or reduced rate of translation. GAPDH was chosen as a loading control. A clear band is visible for all the mutant isoforms and the wild type at approximately 37 kDa (figure 4.8 A and B).

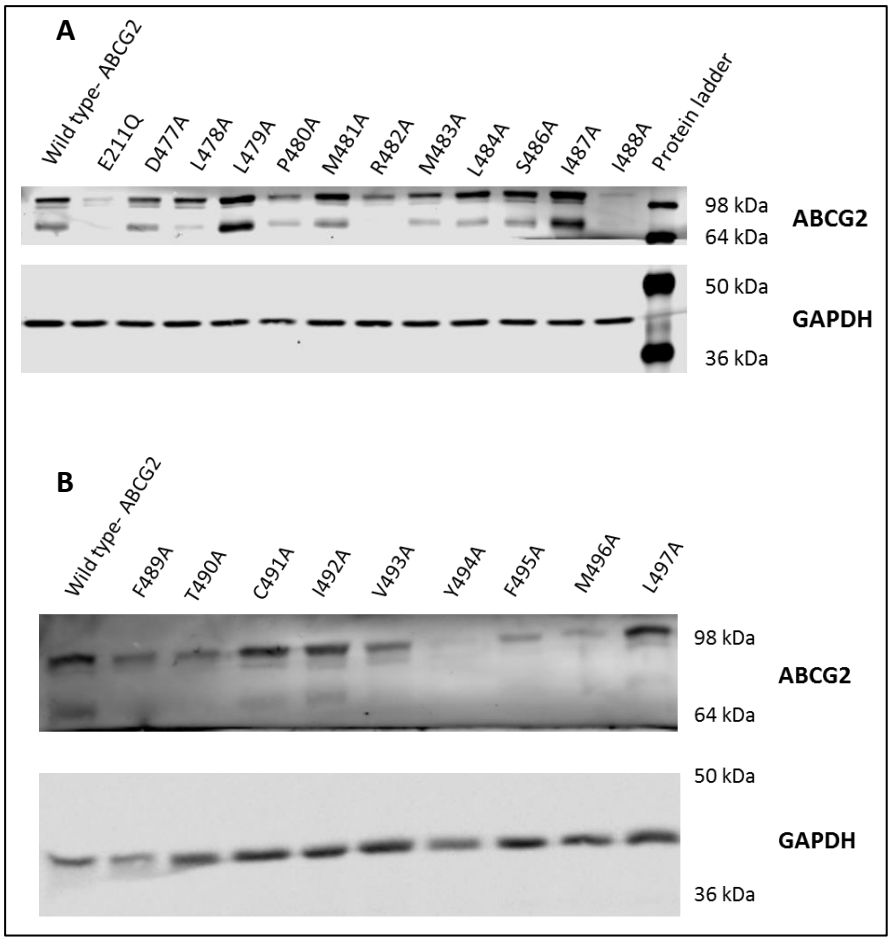


Figure 4.8: Immunoblot analysis for ABCG2 expressed in HEK293T cells (wild type and mutant isoforms)

Cell pellets were harvested from HEK293T mutant stable cell lines and subjected to lysis. The cell lysates (20 µg) were resolved on 10% w/v polyacrylamide gels. PEI transfected HEK 293T cells served as a negative control. Western blot analysis was performed to confirm the expression of ABCG2 isoforms by probing with primary monoclonal antibody Bxp-21. A clear band is visible at approximately 100 kDa for sfGFP_ABCG2 protein. GAPDH (37 kDa) served as a loading control, probed with goat anti- GAPDH antibody.

4.8 Cell surface localisation and expression

ABCG2, a membrane transporter protein, localises to the cell surface in order to function as a drug efflux transporter. After generation of TM3 helix mutant isoforms, the next step was to confirm whether substitution of the TM3 helix residues to alanine perturbed protein folding and translocation to the plasma membrane. Membrane proteins produced from the endoplasmic reticulum must fold and assemble correctly (following proper biogenesis), which is crucial for cellular and organismal function

(Ellgaard et al., 2016). The ABCG2 protein is fused with an N-terminal sfGFP tag for the fluorescent studies. It provides an opportunity to directly monitor dynamics (subcellular trafficking or change in localisation) in a living cell. The presence of this tag does not alter the wild type ABCG2 localisation to the plasma membrane (Haider et al., 2011; Orbán et al., 2008; Wong et al., 2016). In this study, monitoring GFP fluorescence on the cell surface indicated total ABCG2 expression, which has been further confirmed using immune detection of a surface exposed epitope (extracellular loop 3 of the TMD) using flow cytometry (explained in section 4.9) to confirm plasma membrane expression of ABCG2. Stable HEK293T cell lines expressing the wild type sfGFP_ABCG2 and the TM3 helix mutant isoforms were generated and confirmed for expression and localisation using confocal microscopy. To screen the 21 mutant isoforms, a confocal plate reader was considered for its ease of use. Cells were seeded in a 96 well clear bottom black out Greiner plates, grown overnight and subsequently observed 24 hours post seeding. Most of the mutant isoforms showed clear cell membrane localisation with varying levels of protein expression (GFP signal intensity) comparable to the wild type (figure 4.9). This suggests that point mutations are not deleterious to protein folding and translocation. Yet there were some mutant isoforms such as R482A, I488A, Y494A and M496A that showed reduced number of GFP fluorescent cells (figure 4.9). This may indicate reduced stability or reduced translation or lower plasmid copy number in the stable cells, in agreement with the western blot.

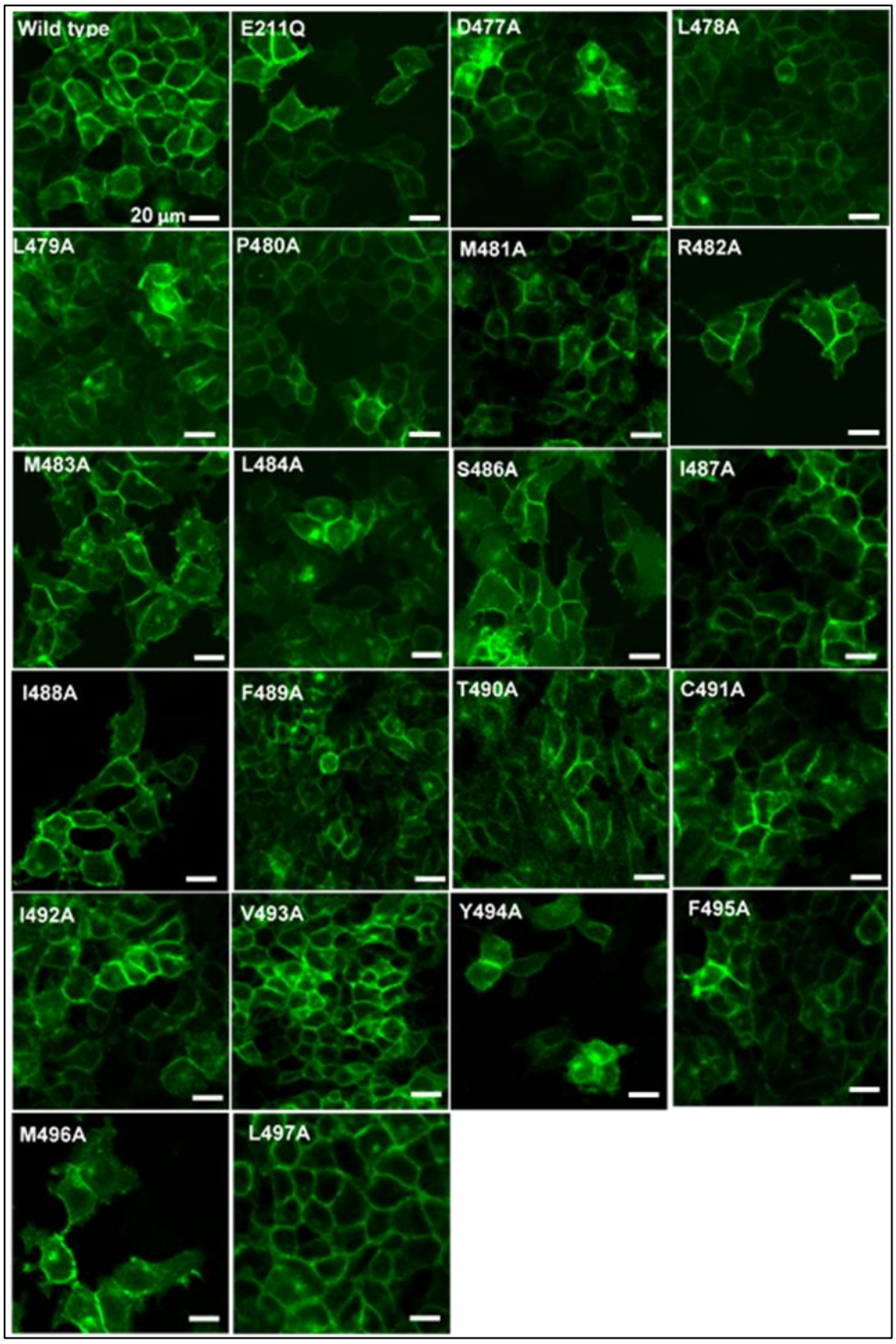


Figure 4.9: Cell surface localization of the ABCG2 isoforms

Confocal microscopy was performed to visualize cell surface localization of ABCG2 isoforms in stable cell lines. All the mutant isoforms were N- terminally sfGFP tagged. Most of the mutant isoforms showed clear cell membrane localization with varying levels of protein expression comparable to the wild type. Some mutant isoforms such as R482A, I488A and Y494A showed a reduced number of GFP fluorescent cells. Live cells were imaged using an ImageXpress (IX) Ultra confocal plate reader (plan-apochromat 40X objective, with excitation wavelength of 488 nm and emission bandpass filter of 520/50 nm). Scale bars represent 20 µm.

4.9 Cell surface expression and localisation of ABCG2 mutant isoforms

Two channel flow cytometry was employed to monitor heterogenous expression levels of ABCG2 on the cell surface. HEK293T cells expressing stable TM3 mutant isoforms were labeled with the conformation sensitive monoclonal antibody 5D3 that recognizes a cell surface epitope within extracellular loop 3 of ABCG2 (Özvegy-Laczka et al., 2008)

Quantitative analysis of the percentage of cells expressing ABCG2 at the cell surface was acquired based on the principle of gating (explained in more detail in chapter 5, section 5.2). Monodisperse cells (figure 4.10 A) were gated for GFP fluorescence as a measure of total ABCG2 expression using a single channel histogram (figure 4.10 B). GFP fluorescence was corrected for autofluorescence by gating for non expressing cells. Immunodetection of the surface exposed epitope by anti-ABCG2 (5D3) antibody treated with secondary goat anti-mouse Alexa fluor 647 antibody enabled quantification of the cell membrane localisation of ABCG2, depicted by the single channel histogram (figure 4.10 C).

A quadrant drawn on a cytogram facilitates quantification of the percentage of cells in a subpopulation (figure 4.10 D-F). The x-axis represents GFP fluorescence and the Y-axis represents AF647 fluorescence. The top right quadrant thus depicts cells positive for GFP fluorescence and AF647 fluorescence, thereby suggesting the percentage of cells with cell surface localisation of sfGFP_ABCG2. The bottom right quadrant depicts the percentage of cells positive for GFP fluorescence. The top left quadrant depicts the percentage of cells positive for AF647 fluorescence, indicative of a population of cells expressing ABCG2, devoid of GFP fluorescence. The bottom left quadrant depicts percentage of cells not expressing sfGFP_ABCG2 (figure 4.10 D-F). The specificity of labelling was validated using the appropriate controls. Quadrant D depicts HEK293T cells expressing WT ABCG2, treated with no antibody. The bottom right clearly shows >90% cells positive for GFP fluorescence, as ABCG2 is N-terminally fused with sfGFP (figure 4.10 D). Quadrant F depicts HEK293T cells expressing WT ABCG2, treated with a non specific primary antibody (TRP1) and secondary antibody (AF647). Again, >90% of cells are positve for GFP fluorescence (figure 4.10 F). Quadrant E depicts cells treated with primary antibody 5D3 and

secondary antibody AF647. This clearly represents >90% of cells are positive for GFP fluorescence, reassuring cell membrane localisation of ABCG2 (figure 4.10 E).

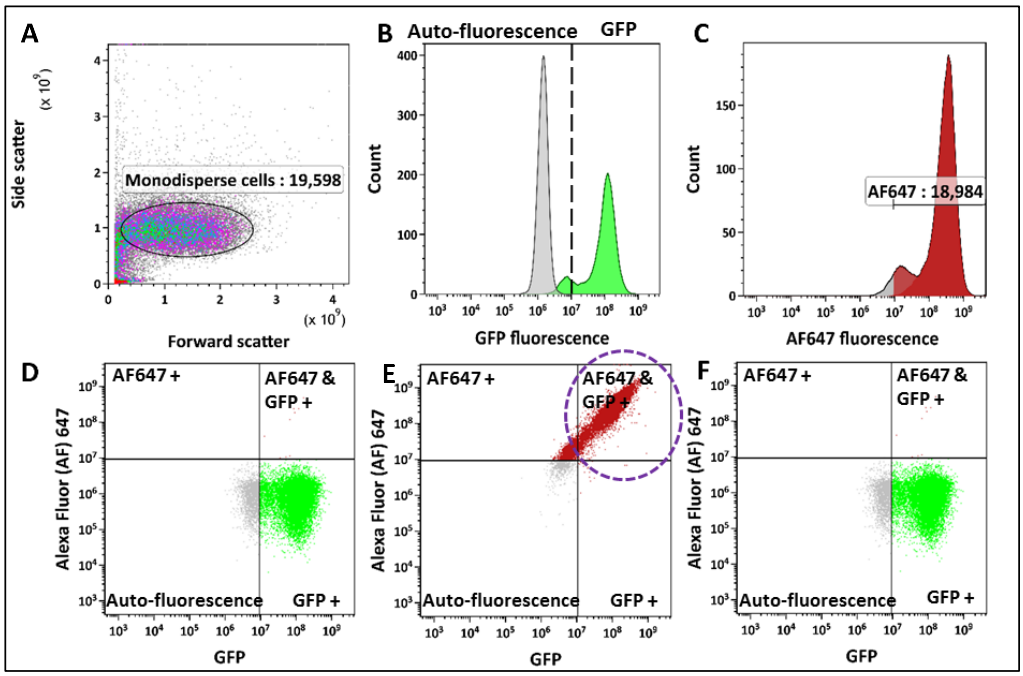


Figure 4.10: GFP expression as a reliable indicator of sfGFP_ABCG2 for cell surface expression

HEK293T cells expressing stable mutant isoforms of TM3 ABCG2 protein were subjected to a two-channel flow cytometry. The cells were incubated with primary monoclonal antibody anti ABCG2, clone 5D3 (1:200), negative control primary monoclonal antibody TRP1 (mouse anti-tyrosinase; 1:200) and devoid of any antibody respectively. The cells were analysed for GFP and AlexaFluor 647 (AF647) expression to monitor total protein expression at the cell surface using Astrios (Beckman Coulter). The cells were gated for monodispersity (A). Final gating parameters were set based on GFP fluorescence (B), as a measure of total ABCG2 expression and AF647 fluorescence (C), as a measure of cell surface ABCG2. B) A single histogram depicts GFP fluorescence from cells expressing sfGFP_ABCG2 separate from the low fluorescence (auto-fluorescence) obtained from the un-transfected HEK293T cells. Quadrant analysis based on the two gates explained in B and C for GFP and ABCG2 expression respectively. Cells expressing sfGFP_ABCG2 were incubated with no antibody (D), cells expressing sfGFP_ABCG2 were incubated with primary antibody 5D3 and secondary antibody AF647 (E) and cells expressing sfGFP_ABCG2 were incubated with primary antibody TRP1 and secondary antibody AF647 (F) respectively. The percentage of cells expressing GFP and AF647 fluorescence (upper right corner) were quantified for cell surface expression. Quadrant E clearly depicts that wild type cells expressing sfGFP_ABCG2 show >90% cell surface localisation based on GFP fluorescence (GFP +) and AF647 fluorescence (ABCG2 +). Non-specific primary antibody (TRP1) and no antibody controls validated the specificity of this labelling. The GFP fluorescence (green) was determined using excitation wavelength at 488nm and emission at 526nm. AF647 fluorescence (red) was measured using excitation at 650 nm and emission at 670 nm (channel 640-671/30). The data were analysed using Kaluza software (analysis software version 1.5, Beckman Coulter).

Several of the mutant isoforms, particularly where a decline in total expression was evident, were investigated for cell surface expression. The percentage of cells positive for GFP and AF647 fluorescence (quadrants) is more than 70% in all except one case, with wild type depicting nearly 91% cell surface localisation and expression of ABCG2 (figure 4.11). This clearly depicts that ABCG2 is correctly localised to the plasma membrane in the mutant isoforms. R482A isoform shows nearly 12 % cells surface localisation and expression (figure 4.11). This clearly suggests that generation of TM3 helix mutant isoforms are not deleterious to ABCG2 expression and localisation.

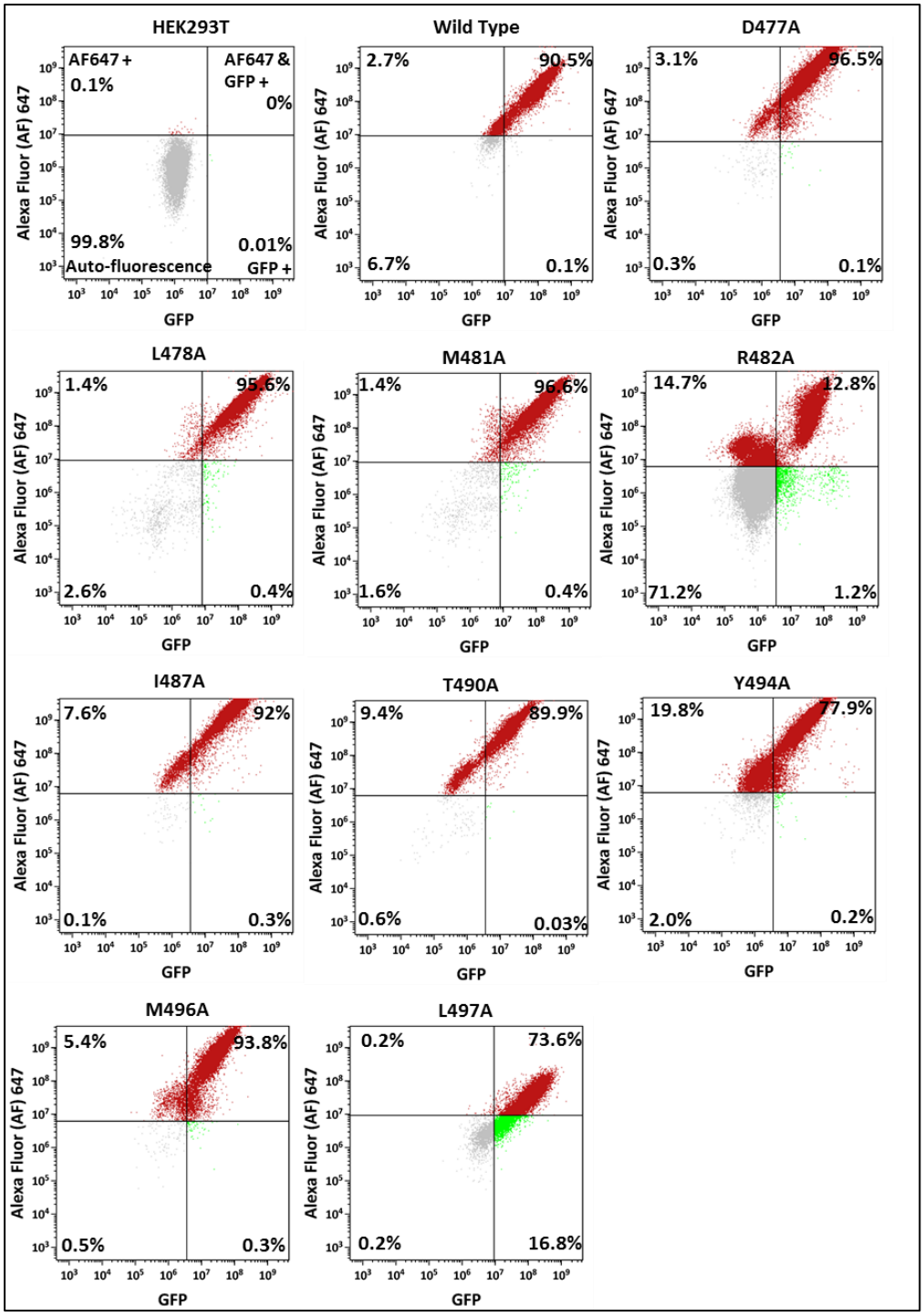


Figure 4.11: Cell surface expression for TM3 mutant isoforms using a two-channel flow cytometry

The cells were labelled with 5D3 antibody and a secondary antibody conjugated to AF647 enabling individual cells to be quantified for cell surface ABCG2 expression (y-axis) and total GFP expression (x-axis). The cells were analysed for GFP and AF647 expression using Astrios (Beckman Coulter). The cells in the upper right corner of the quadrant represent the cells with ABCG2 surface expression. The percentage of cell surface expression for HEK293T, wild type and TM3 mutant isoforms have been documented in the quadrant.

4.10 Conclusion and summary

In this study, 20 TM3 mutant isoforms were generated, with N-terminal sfGFP tag and investigated for their cell surface expression and localisation using the 3 complementary approaches of western blot, confocal microscopy and flow cytometry. Earlier studies have shown the presence of N terminal tag to not have an effect on the expression, localisation and function of ABCG2 (Wong et al., 2016) (Haider et al., 2015) . Site directed mutagenesis was used to generate point mutations for all the TM3 helix residues to alanine. Stable cell lines were generated for all the 20 mutants. Western blot analysis using BXP-21 antibody was performed to confirm the expression of the mutant isoforms. All the mutant isoforms were confirmed to express the fully glycosylated band of ABCG2. Variation in expression was observed across the mutant isoforms. Some of the mutant isoforms showed a second immunoreactive band, attributed to reduced glycosylation levels or breakdown of ABCG2. Three mutant isoforms showed reduced ABCG2 expression (R482A, I488A and Y494A). Confocal microscopy was used to monitor GFP fluorescence as a measure of cell membrane localisation of ABCG2 across the mutant isoforms. All the mutant isoforms depicted membrane localisation of ABCG2, thereby suggesting no associated trafficking defects or structural effects. To further screen the mutant isoforms for being associated with trafficking defects, protein expression and localisation was quantified using flow cytometry. A 2-channel flow cytometry was performed to monitor GFP fluorescence as a measure total ABCG2 expression and immunodetection of ABCG2 using 5D3 antibody conjugated to AF647 as a measure of plasma membrane localisation of ABCG2. All the mutant isoforms showed >70% membrane localisation as opposed to wild type ABCG2 with >90% cells depicting surface localisation. R482A mutant showed 13% of cells with cell surface localisation due to stability issues or translation issues.

The study clearly represents that TM3 point mutations have not been deleterious to the folding and trafficking of ABCG2 protein as shown through western blot, confocal microscopy and flow cytometry. After documenting that the mutants do not impair trafficking of ABCG2, the next step is to screen the mutant isoforms for their role in drug transport. The next chapter dwells into this aspect in detail.

Chapter 5: Functional characterisation of ABCG2 mutant isoforms- role of transmembrane helix 3 in drug binding and/ or translocation

5.1 Introduction

As described earlier, the study of ABCG2 TM 3 helix is crucial to understanding its role in drug binding, interaction and transport selectivity (Clark et al., 2006; Haider et al., 2015; Robey et al., 2003). The research hypothesis arose from studies of R482 and P485, therefore as detailed in chapter 4, point mutations were generated along the length of the TM3 helix (D477- L497) in order to understand the role of TM3 in drug interaction and transport selectivity. This made us consider whether TM3 helix would harbour further residues of interest that would influence the substrate specificity.

There are several *in vitro* based assays to monitor the function of the transporter using membrane preparations or intact cells. Cell based assays include fluorescent dye transport assays, cytotoxicity assays, monolayer transport assays and flow cytometry, whereas crude membrane-based assays include vesicular transport assays, ATPase assays and photoaffinity labeling/nucleotide trapping/drug binding.

Earlier set ups involved cell-based assays in a 96 well plate, but these assays came with their share of drawbacks. Quantification of ABCG2 in a mixed cell line on a cell to cell basis and monitoring function and their correlation to obtain a quantifiable data set was difficult (Csilla Hegedűs et al., 2009). In this study, a sensitive, robust, reliable and reproducible cell based assay has been used to monitor ABCG2 specific extrusion of several fluorescent compounds whilst simultaneously measuring the protein expression levels using flow cytometry (Hegedus et al., 2009; Robey et al., 2001a; Weidner et al., 2015).

5.2 Introduction to flow cytometry

Flow cytometry is a popular and highly sensitive laser-based technology used to analyse the characteristics of cells and particles. The experimental paradigm of flow cytometry has been used in this research to monitor drug retention and efflux, a key step towards understanding drug resistance. Robey et al., measured the function of ABCG2 (R482G) in drug selected cell lines, by monitoring FTC- inhibitable mitoxantrone or prazosin efflux and demonstrated the sensitivity, reliability and specificity of flow cytometry based drug efflux assays (Robey et al., 2001a).

A fluidics system enables the flow cytometer to stream the cells in a single file, thereby facilitating the detection of individual particles by the detection system. Cell suspension is passed through the nozzle, forming a tiny stream of fluid facilitated by the hydrodynamic focus generated by the sheath fluid surrounding the sample fluid. Bernoulli's effect enables the sample to focus in the centre. This generates a stream of particles in a single file, called hydrodynamic focussing. The cells pass through the laser one at a time and the scattered light is detected using several detectors positioned to measure the forward scatter (FS) and side scatter (SS). Subsequently, fluorescence detectors, measure the fluorescence emitted from the cells or particles. Filter sets enable the FS, SS and the fluorescent light to be split into defined wavelengths, detected by sensors, i.e. photomultiplier tubes (PMT's). The pulse of emission over time, detected by the PMT's are converted to a voltage pulse. The voltage pulse area correlates to the intensity of fluorescence (figure 5.1) (Jaroszeski and Radcliff, 1999).

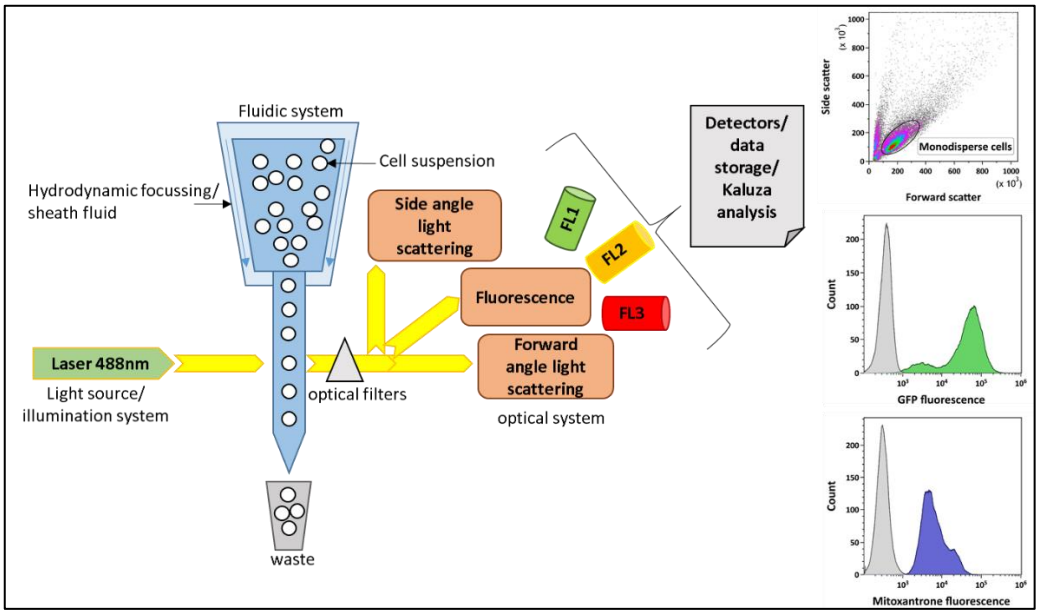


Figure 5.1: Schematic representation of the primary components of a flow cytometer

Cell suspension is passed through the fluidic system into the flow chamber in a narrow stream, subsequently being subjected to an illumination system using a focused laser beam. Particle interrogation takes place in the flow chamber. The resulting forward and side scattered beam provide information on the size/ granularity of the sample. Fluorescent probes (used in any given set of an experiment) define the fluorescent intensities for each cell. Retrospective data analysis is performed using the software Kaluza analysis 1.5.

Multiparametric flow analysis enables us to monitor drug fluorescence (drug accumulation) and correlate that to protein expression simultaneously on a cell to cell basis. Flow cytometry based assays are advantageous as they provide functional, quantitative information about the multidrug resistance protein. The analysis is performed using the flow software, i.e. Kaluza analysis 1.5.

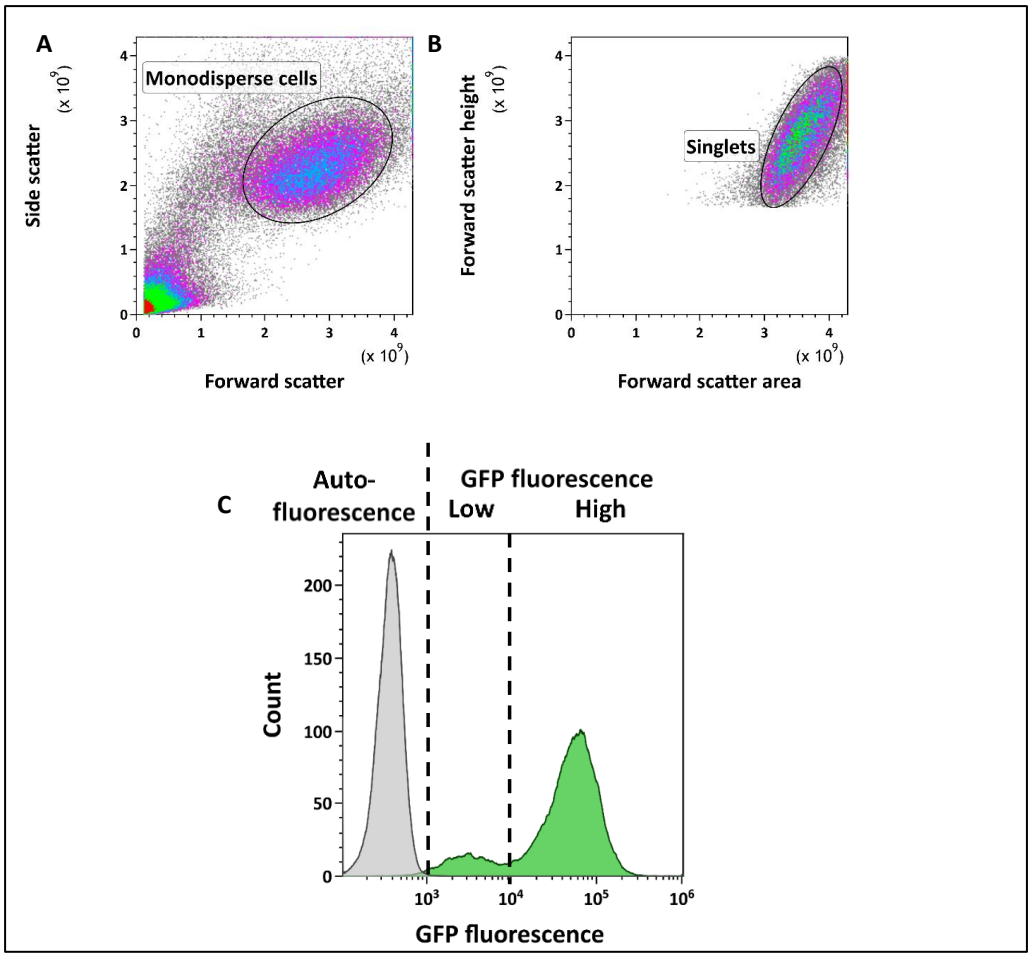


Figure 5.2: Flow cytometry gating parameters demonstrated for HEK293T cells expressing wild type ABCG2

A) The forward and side scatter plot gate for monodisperse cells separating them from the cellular debris. B) The forward scatter area versus height plot gates for singlets, thereby segregating any aggregates. C) The single channel histogram obtained from HEK293T cells expressing the wild type ABCG2 protein quantifies GFP fluorescence as a measure of total ABCG2 protein expression. It depicts a mixed population gated for low and high GFP expression. The shoulder region depicts the population of cells with low GFP fluorescence compared to the large peak for population of cells with high GFP fluorescence. The grey region represents the level of background fluorescence (auto-fluorescence) generated from the untransfected HEK293T cells. Flow cytometry analysis performed on Kaluza.

Flow cytometry data analysis is based on the principle of gating (figure 5.2). Gates and regions are assigned to population of cells based on common characteristics (forward scatter, side scatter and marker expression) in order to investigate and quantify these population of interests. The analysis involves distinguishing cells based on their forward and side scatter properties, which provides an estimation of the size and granularity of the cells respectively (figure 5.2 A). The density scatter plot provides the basis to distinguish between the viable cells and cell debris. The density

plot for forward scatter height versus area enables the user to distinguish between the singlets and doublets (aggregated population of cells, figure 5.2 B). The above mentioned 2 parameter dot plot displays data as dots from a population of individual particles, with one dot representing one acquired event. The position of the dot represents the relative intensities of the 2 measured parameters for that event (Jaroszeski and Radcliff, 1999; Lugli et al., 2010).

Single parameter histograms are set to identify population of cells based on a single acquired parameter (example, protein expression) for further investigations. Gating is employed to distinguish cells expressing the protein (GFP_ABCG2 fluorescence) from non-fluorescing cells (figure 5.2 C). This gating also assists in distinguishing the mixed population, thereby generating sub gates (low and high expressers respectively, figure 5.2 C). This gating is then further utilised to monitor drug fluorescence, to determine the function.

5.3 Single cell ABCG2 expression profile using flow cytometry

Three complementary approaches were used in chapter 4 to confirm expression and trafficking defects associated with the ABCG2 TM3 helix mutant isoforms. To further confirm ABCG2 expression profile across the mutant isoforms, a single channel flow cytometry analysis was performed, where GFP fluorescence was used as a quantitative measure of the total ABCG2 expression. The gating parameters were applied as explained before (figure 5.2 C). The arithmetic mean fluorescence of the whole population (mixed), normalised against wild type expression to formulate the relative expression for the whole population.

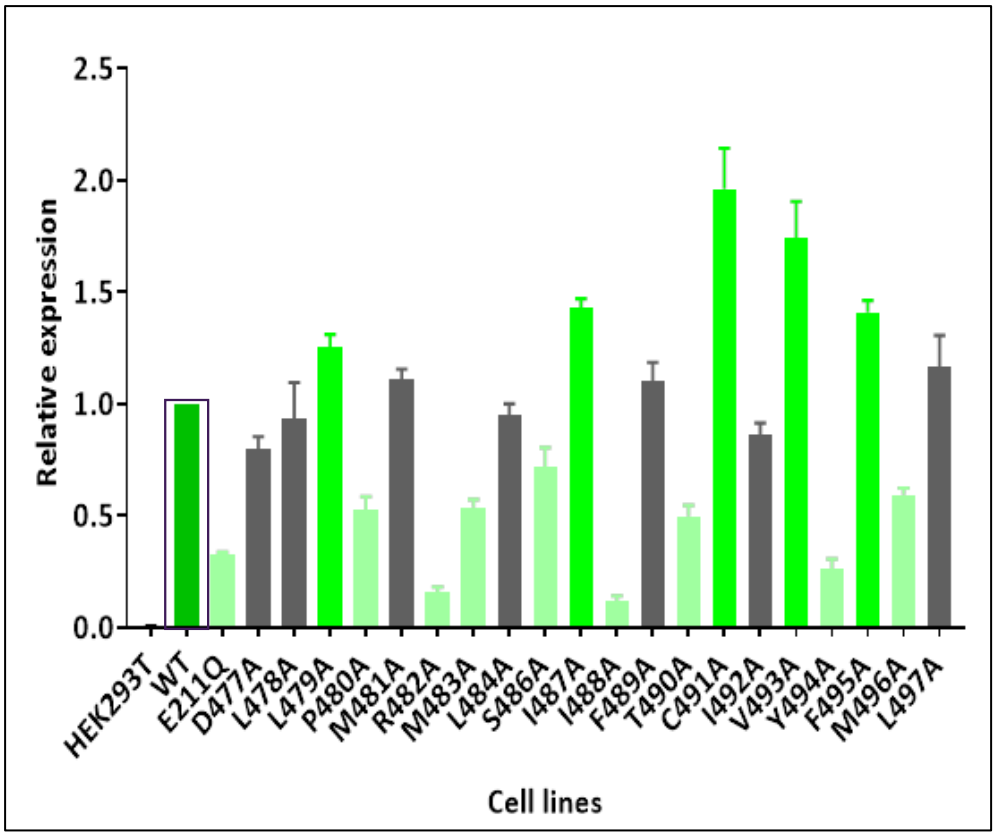


Figure 5.3: GFP_ABCG2 expression levels vary across the mutant isoforms

The relative expression of the whole population as measure of GFP fluorescence to quantify total ABCG2 expression. The arithmetic mean of GFP channel (protein expression) was normalised with respect to wild type GFP fluorescence (green bar encased with a purple box). Several mutant isoforms show low (mint green bars) or high levels (bright green bars) of GFP fluorescence. Significance was based on one-way ANOVA ($P < 0.05$, $n > 3$) and post statistical test (Dunnett's multiple comparison test).

The results of this data suggest that E211Q, P480A, R482A, M483A, S486A, I488A, T490A, Y494A and M496A show statistically significant ($P < 0.05$) low GFP expression compared to wild type, whereas L479A, I487A, C491A, V493A and F495A show statistically significant ($P < 0.05$) high GFP expression compared to the wild type (figure 5.3). Quantifying the variation in protein expression is crucial and taken into consideration while monitoring the function. A final gating of a split population (low and high expressers) will enable monitoring the accumulation of substrates within the cells expressing homogeneous levels of protein (figure 5.2) and will ensure that any altered phenotypic effects observed are not due to differences in the protein expression.

5.4 Functional analysis of ABCG2 TM3 helix mutant isoforms- drug accumulation assays

There are 3 possible scenarios to depict the relative drug export by the cells (figure 5.4). The mutant isoforms could function as a wild type phenotype (figure 5.4 A), show reduced/ impaired efflux for wild type substrate (as P485A, figure 5.4 B) or show enhanced efflux capacity for native substrates (figure 5.4 C). The mutant isoforms could also show gain in function phenotype, where they show export of non-native substrate, such as R482G/T/A mutant isoform (gain of function for daunorubicin transport, figure 5.4 C). Any variability in expression, if not taken into consideration, could then result in false data output; e.g. a mutant isoform with low ABCG2 expression could be erroneously interpreted as having low functionality.

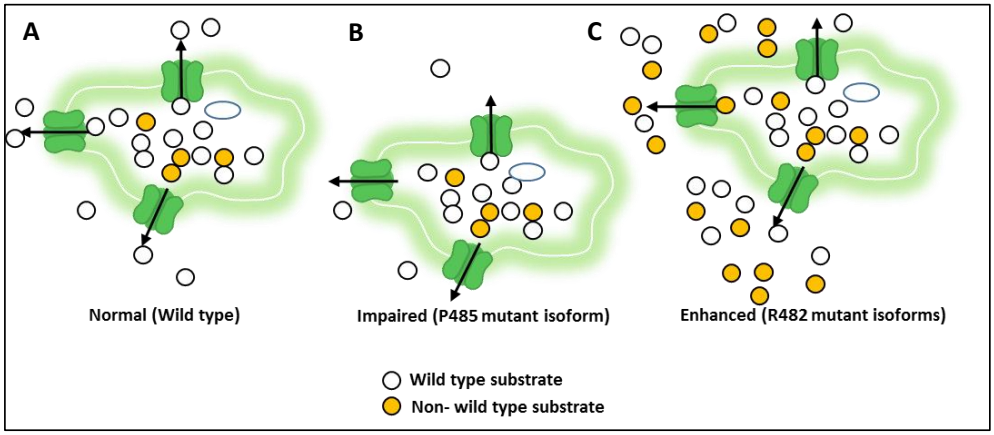


Figure 5.4: Functional phenotypic effects observed by HEK293T cells expressing the mutant isoforms.

There are three possible scenarios observed when monitoring the drug efflux capacity of the cells. The cells can function as a wild type (A), i.e. export ABCG2 substrates (mitoxantrone, pheophorbide A, to name a few), or show reduced/ impaired efflux capacity, such as P485 mutants (B, reduced efflux for ABCG2 substrates such pheophorbide A), or show enhanced export of wild type substrates or non-wild type substrates (C, gain in function mutation for daunorubicin transport by R482 mutants).

Flow cytometry based drug transport assays were performed using the three fluorescent substrates mitoxantrone (anthracenedione, a topoisomerase II inhibitor) pheophorbide A (chlorophyll metabolite) and daunorubicin (topoisomerase II

inhibitor) (table 5.1) (Doyle et al., 1998; Jonker et al., 2002; Robey et al., 2003). Mitoxantrone and pheophorbide A are well known wild type substrates whereas daunorubicin is a well-studied substrate of the mutant isoform R482G/T but not of the wild type ABCG2 (Ejendal et al., 2006; Honjo et al., 2001; Robey et al., 2004, 2003). Daunorubicin was used to screen any gain in function (broader specificity) mutation.

Stable cell lines expressing ABCG2 TM3 mutant isoforms were investigated in this study for drug accumulation using a 2-channel flow cytometry to quantify ABCG2 expression (GFP fluorescence) and function (drug fluorescence) simultaneously. The cells expressing mutant isoforms and the respective fluorescent substrates were incubated in presence/ absence of ABCG2 specific inhibitor Ko143 (Weidner et al., 2015).

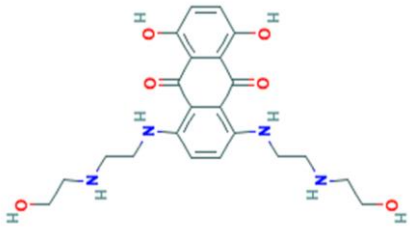
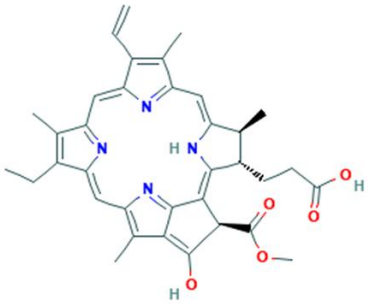
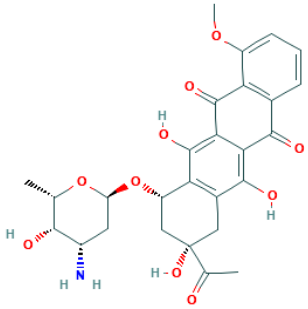
Substrates	Fluorescence spectrum		Flow cytometry channel
	Excitation wavelength (nm)	Emission wavelength (nm)	
Mitoxantrone (Mx) 	635	670	FL4- 633/75 FC500
Pheophorbide A (PheoA) 	400	710	355-692/75 Astrios
Daunorubicin (DNR) 	490	610	488-710/45 Astrios

Table 5.1: Potential fluorescent substrates used for drug efflux assays

Summary of the potential fluorescent substrates (structures and spectral properties) employed to test the functionality of ABCG2 transporter using flow cytometry. The chemical structures have been obtained from PubChem.

Incubation of cells in the presence of a fluorescent substrate resulted in a population of cells representing an equilibrium level of substrate accumulation Figure 5.5, speckled blue, green and red), which is well separated from the auto-fluorescing cells (figure 5.5, grey). This represents a measure of an isoform's drug efflux in absence of ABCG2 specific inhibitor; Ko143.

The addition of Ko143 inhibits ABCG2 and results in an increased accumulation of mitoxantrone (figure 5.5 B, blue solid colour plot and speckled plot) and pheophorbide A (figure 5.5 B, green solid colour plot and speckled plot). This increased accumulation is seen as a rightward shift in the cell population. By contrast there is no shift observed for daunorubicin (figure 5.5 B, red solid colour plot compared to speckled distribution). As is clearly visible from figure 5.5, there is no rightward shift in substrate fluorescence upon addition of Ko143 for HEK293T (figure 5.5 A, solid colour plot and speckled distribution) or cells expressing E211Q mutant isoform (figure 5.5 C, solid colour plot and speckled distribution), as expected for these two negative controls. The rightward shift is a measure of the isoforms ability to display Ko143 inhibitable transport of a drug. Assuming that the mutant does not interfere with Ko143 binding this shift is a quantitative measure of drug efflux.

Experimental analysis was carried out on wild type, negative controls (HEK29T and E211Q) and 20 TM3 mutants with the three fluorescent drugs mentioned before. D477A showed rightward shift in Mx transport (figure 5.5 D, blue) as opposed to pheophorbide A and daunorubicin transport (figure 5.5 D, green and red). The gain of function mutation R482A shows Ko143 dependent rightward shift in Mx, pheophorbide A and daunorubicin transport (figure 5.5 E). M496A shows a significant rightward shift in Mx accumulation (figure 5.5 E blue). The single channel (drug fluorescence) histogram plots for the entire series of TM3 mutant isoforms have been displayed in appendix 5.

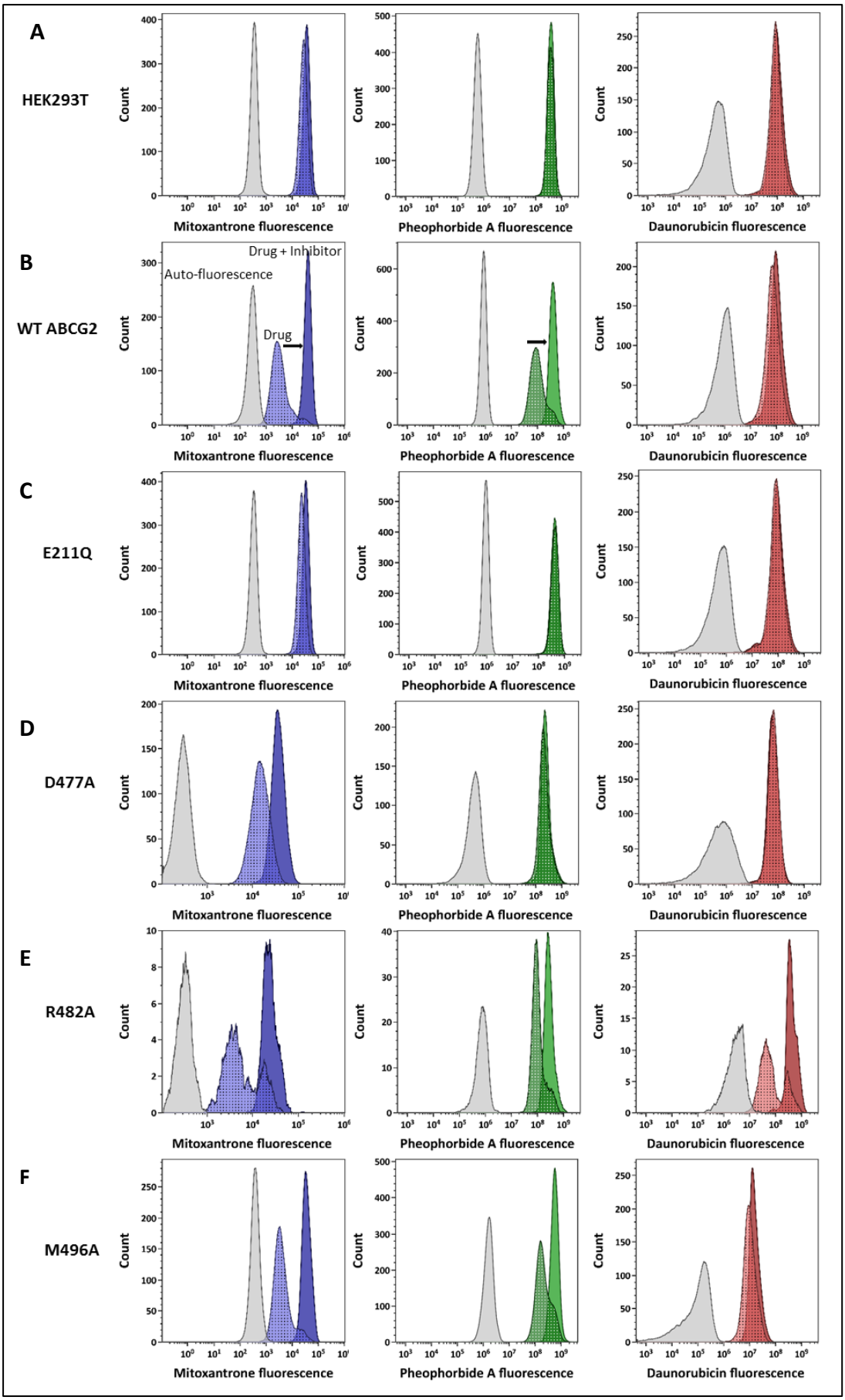

A
HEK293T
B
WT ABCG2
Drug + Inhibitor
Auto-fluorescence
Drug
C
E211Q
D
D477A
E
R482A
F
M496A
Count
Mitoxantrone fluorescence
Pheophorbide A fluorescence
Daunorubicin fluorescence

Figure 5.5: Functional analysis of ABCG2 variants-role in altered drug export capacity

Single channel overlay histogram plots to monitor mitoxantrone, daunorubicin and pheophorbide A fluorescence based on the drug efflux capacity of the HEK293T cells expressing wild type ABCG2 (B), catalytically inactive mutant (E211Q, C), non-expressing cells (A) and TM3 mutants with altered drug efflux capacity (D477A (D), R482A (E) and M496A (F)). Grey histograms represent the autofluorescence of HEK293T cells. The dotted blue, green and red histograms depict equilibrium level of substrate accumulation (mitoxantrone, pheophorbide A and daunorubicin respectively). Quantitative analysis of the rightward shift of substrate accumulation seen by HEK293T cells expressing wild type ABCG2 (increased fluorescence for mitoxantrone and pheophorbide A) in presence of ABCG2 specific inhibitor Ko143 (black arrow), denote inhibition of efflux.

Median fluorescence values (GFP fluorescence and drug fluorescence values) from each data set were quantified to interpret the altered phenotypic effects observed. The vehicle control (0.2% v/v DMSO) established the baseline fluorescence and was used for baseline correction (subtracted) from the samples of drug alone and drug plus inhibitor. Fractional difference was then calculated between the samples with drug plus inhibitor and drug alone. The raw measure for drug efflux calculated from the fractional difference was normalised for expression of the ABCG2 mutant isoforms relative to the wild type (as explained in methods section 2.7.2). This resulted in relative drug accumulation by the mutant isoform, comparable to and normalised to the wild type for ABCG2 expression level (figure 5.6, table 5.2 and summarised in the Venn diagram (figure 5.7).

The data obtained were subjected to one-way ANOVA and post statistical tests (Dunnett's multiple comparison test) against the wild type, thereby suggesting altered phenotypic effects observed for drug accumulation by the TM3 ABCG2 mutant isoforms. The data represents the mutant isoforms (TM3 helix ABCG2) with normal, impaired or enhanced relative drug efflux compared to the wild type (figure 5.6).

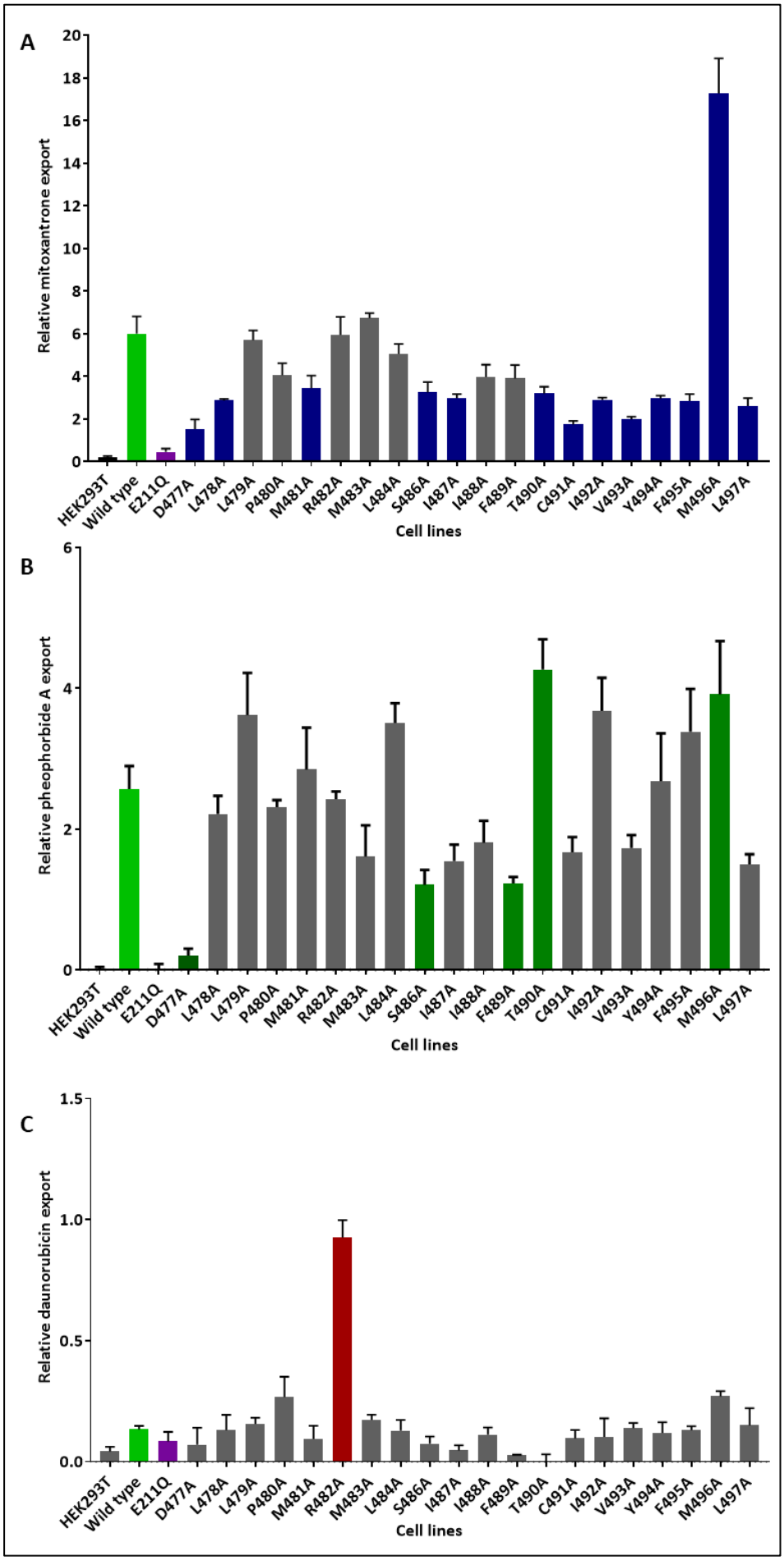

A
Relative mitoxantrone export
20
18
16
14
12
10
8
6
4
2
0
HEK293T
Wild type
E211Q
D477A
L478A
L479A
P480A
M481A
R482A
M483A
L484A
S486A
I487A
I488A
F489A
T490A
C491A
I492A
V493A
Y494A
F495A
M496A
L497A
Cell lines
B
Relative pheophorbide A export
6
4
2
0
HEK293T
Wild type
E211Q
D477A
L478A
L479A
P480A
M481A
R482A
M483A
L484A
S486A
I487A
I488A
F489A
T490A
C491A
I492A
V493A
Y494A
F495A
M496A
L497A
Cell lines
C
Relative daunorubicin export
1.5
1.0
0.5
0.0
HEK293T
Wild type
E211Q
D477A
L478A
L479A
P480A
M481A
R482A
M483A
L484A
S486A
I487A
I488A
F489A
T490A
C491A
I492A
V493A
Y494A
F495A
M496A
L497A
Cell lines

Figure 5.6: TM3 helix mutant isoforms show altered phenotypic effects in drug transport

The bar graphs represent the average fold difference in substrate accumulation in presence of Ko143, normalised for GFP expression compared to the wild type (green bar). Data represents median fluorescence values for substrate (mitoxantrone (A), pheophorbide A (B) and daunorubicin (C)) accumulation (+/-SEM) for $n \geq 3$ independent repeats. In all the bar graphs, the relative efflux by HEK293T cells is represented by the grey bar and the efflux by catalytically inactive mutant isoform, E211Q is represented by the purple bar. A) Bar graph represents the relative efflux of mitoxantrone by the mutant isoforms, with statistically significant (p values < 0.05) ones represented by the blue bar. B) Pheophorbide A efflux capacity by the mutant isoforms, with altered phenotypic effects (reduced efflux- D477A, S486A and F489A, enhanced efflux- T490A and M496A), green bar representing the statistically significant isoforms (p values < 0.05). c) Daunorubicin efflux by the mutant isoforms with the gain of function mutation, R482A highlighted in red.

The wild type ABCG2 displayed a relative efflux of Mx of 6.01(± 0.81; bright green, figure 5.9A and table 5.2) whereas the catalytically inactive mutant, E211Q (charge neutralising mutation in the Walker-B motif of the NBD; purple, figure 5.6 A) displayed a relative drug efflux of 0.46 (± 0.16) (figure 5.6 A and table 5.2). Screening of mutant isoforms identifies thirteen isoforms (D477A, L478A, M481A, S486A, I487A, T490A, C491A, I492A, V493A, Y494A, F495A and L497A) that showed statistically significant (ANOVA and Dunnett's post-test, P< 0.05) reduced relative Mx efflux capacity (blue bars, figure 5.6 A and table 5.2) compared to the wild type. M496A isoform showed enhanced (17.28 ± 1.63) relative Mx efflux capacity compared to the wild type (blue bar; figure 5.6 A and table 5.2). The remaining mutant isoforms (L479A, P480A, M481A, R482A, M483A, L484A, I488A and F489A) showed Mx efflux capacity similar to the wild type (grey bar; figure 5.6 A).

Cell lines	MITOXANTRONE		PHEOPHORBIDE A		DAUNORUBICIN	
	Mean	SEM	Mean	SEM	Mean	SEM
HEK293T	0.21	0.05	0.01	0.03	0.11	0.05
Wild Type	6.01	0.81	2.57	0.33	0.37	0.05
E211Q	0.46**	0.16	0.01**	0.08	0.28	0.14
D477A	1.52**	0.46	0.20**	0.10	0.21	0.20
L478A	2.86**	0.08	2.21	0.26	0.38	0.21
L479A	5.70	0.45	3.62	0.60	0.44	0.08
P480A	4.05	0.57	2.31	0.10	0.92	0.39
M481A	3.45*	0.59	2.85	0.59	0.26	0.16
R482A	5.95	0.85	2.42	0.11	8.11**	1.79
M483A	6.74	0.23	1.61	0.44	0.49	0.08
L484A	5.06	0.46	3.51	0.28	0.36	0.14
S486A	3.25*	0.49	1.21*	0.21	0.19	0.08
I487A	2.98**	0.18	1.55	0.23	0.12	0.05
I488A	3.98	0.57	1.80	0.32	0.30	0.09
F489A	3.90	0.63	1.23**	0.09	0.06	0.01
T490A	3.19*	0.32	4.27**	0.43	0.01	0.07
C491A	1.74**	0.17	1.67	0.21	0.26	0.10
I492A	2.90**	0.10	3.68	0.47	0.30	0.21
V493A	1.98**	0.13	1.73	0.18	0.38	0.07
Y494A	2.97**	0.13	2.68	0.68	0.33	0.14
F495A	2.85**	0.32	3.38	0.61	0.35	0.05
M496A	17.28**	1.63	3.92*	0.76	0.87	0.09
L497A	2.61**	0.37	1.50	0.14	0.45	0.25

Table 5.2: Relative efflux data- Ko143 inhibited transport of fluorescent drugs by TM3 mutant isoforms

The data depicts the mean (with standard error of the mean) of the fractional difference in Ko143 inhibited drug efflux compared to the wild type. The raw data for mitoxantrone and pheophorbide A were processed using one-way ANOVA and post statistical test (Dunnett's multiple comparison) against the wild type. The data for daunorubicin efflux was subjected to log transformation due to positive skewed data for R482A mutant isoform, prior to analysis of significance. The data are representative of $n \geq 3$ independent repeats. Asterisks indicate the level of significance with $p \leq 0.05$ for * and $p \leq 0.01$ for **.

The relative drug efflux capabilities for pheophorbide A of the wild type and the mutant isoforms were also tested (ABCG2 TM3 helix residues, figure 5.6 B and table

5.2). The pattern of pheophorbide A transport observed by TM3 mutants was different to that for Mx transport. The wild type displayed a relative efflux of 2.57 (± 0.28) (figure 5.6 B and table 5.2). Mutant isoform D477A again displayed statistically significant reduction (0.20 ± 0.10) in pheophorbide A efflux capacity compared to the wild type (green bar; figure 5.6 B and table 5.2). S486A and F489A also showed reduction in pheophorbide A export compared to the wild type (green bar; figure 5.6 B and table 5.2). T490 and M496A showed higher relative efflux for pheophorbide A transport (green bar; figure 5.6 B and table 5.2).

For daunorubicin, which is not a substrate for wild type ABCG2, only the R482A mutant displayed the ability to efflux the substrate, thereby suggesting gain of function mutation, in accordance with the published literature (figure 5.6 C and table 5.2). The data set for R482A displayed variability in the mean fold change as a result of asymmetric distribution of the data sets, hence in order to obtain normal distribution of the data sets, log transformation was employed to the statistics (Clarke, 2003).

The relative drug efflux assays using flow cytometry have enabled us to screen the mutant isoforms and helped determine at least 16 isoforms of ABCG2 protein associated with altered transport of the one of the three tested compounds. Only one residue showed altered daunorubicin transport suggesting at substrate specificity. Only three residues altered both Mx and pheophorbide A transport, suggesting overlapping sites for substrate interaction. Most predominantly the effects observed were residue specific. The results are summarised in the Venn diagram (figure 5.7). The homology model for ABCG2 based on the ABCG5/ G8 crystal structure by Lászloá et al. describe the four potential binding sites, of which binding site 2 (a more defined binding pocket) comprises of several of the TM3 helix residues (D477, L478, M481, R482, P485 and S486) that have shown altered phenotypic effects for drug translocation as explained above (Lászloá et al., 2016).

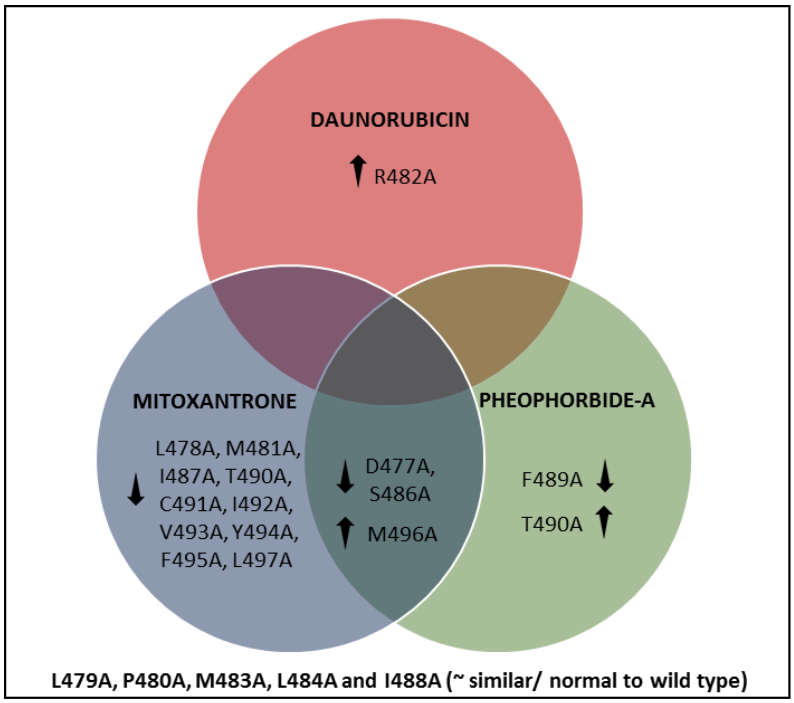


Figure 5.7: Phenotypic effects for altered function observed by the ABCG2 variant isoforms

ABCG2 mutant isoforms were screened for drug efflux capacity as shown in figure 5.9 and table 5.2. The data has been summarised in the Venn diagram which represents the relative efflux (reduced, enhanced or similar to wild type) of the fluorescent substrates (blue- mitoxantrone, green- pheophorbide A and red- daunorubicin), normalised for GFP expression compared to the wild type. The results are based on the post statistical tests with the p value < 0.05, considered significant for the given data set ($n \geq 3$ independent repeats).

To better understand the phenotypic effects observed in ABCG2 substrate translocation by the TM3 helix mutant isoforms, the data can be rationalised against the structure, to shed light on the molecular mechanism behind drug recognition/ binding and translocation. Screening of mutant isoforms for the drug efflux assays facilitated the establishment of key residues associated with the functional importance. Can we suggest that TM3 helix acts as a putative gatekeeper for translocation of the substrates through the leucine plug model as described by Jackson et al. (Taylor et al., 2017). The fundamental concept of "sequence implies structure and structure implies function" underpins the importance of mapping key residues of functional interests to provide a molecular explanation of the transporter functionality phenotypes observed. This has been achieved and well explained using molecular docking studies on the cryo-EM structure for ABCG2 in the next section 5.5 (Jackson et al., 2018). This structural and functional interpretation has helped us propose a drug translocation mechanism for hydrophobic substrates, detailed in chapter 7 (section 7.3).

5.5 Structural interpretation of the potential drug binding sites

With the advancement in cryo-EM detection systems and image processing algorithms, the cryo-EM structural revolution led to the development of ABCG2 structures in presence of cholesterol, Ko143 derivatives and a bonafide substrate estrone-1 sulphate (Jackson et al., 2018; Manolaridis et al., 2018). Molecular docking was used as a tool to build a picture of drug binding in ABCG2, in particular to understand the role of TM3 helix in drug binding, emphasising the role of TM3 as a putative gatekeeper for hydrophobic substrates. Autodock Vina was used to dock ABCG2 substrates (Mx, pheophorbide A and R482G substrate; daunorubicin) on to the protein (figure 5.8). A grid box was assigned to the structure enclosing majority of the TMD (monomer), centred at its geometric mid-point. Docking was performed with the exhaustiveness set at an automated value (8) to find a global minimum for the relative drug affinities. Docking revealed the putative drug binding sites in TM3 helix, thereby reinstating the importance of the key residues identified in TM3 helix in selectivity and specificity. A putative binding site was identified for the three compounds under investigation between the groove defined by TM helices 1b, 2 and 3 (referred to as a groove site), facing towards the central cavity (as proposed by the cryo-EM structures) (figure 5.8) (Taylor et al., 2017). The TM3 helix residues show potential interactions (based on proximity, ≤5Å) with the three compounds. Based on the functional studies for drug transport in section 5.4, 15 TM3 helix residues have shown perturbed drug efflux capacity that reside in close proximity to the identified binding site for the three compounds. Based on the docking studies, Mx shows close contacts with R482, P485 and F489 (figure 5.8 A), whereas pheophorbide A shows close contacts with only F489 (figure 5.8 B), in accordance with the functional data. Daunorubicin, a substrate for R482G mutant, shows potential contacts with R482, P485 and F489 (figure 5.8 C).

The groove site demonstrates partial similarities with other ABCG2 drug docking studies and could indicate that TM3 helix could possibly form the entry point for hydrophobic substrates, thereby acting as a gatekeeper (Cox et al., 2018; Jackson et al., 2018; Lászloá et al., 2016; Manolaridis et al., 2018; Taylor et al., 2017). Lászloá et al identified a more defined pocket (consisting of the residues from the groove site

R482 and P485) based on *in silico* docking studies on ABCG2 homology model (Lászloá et al., 2016, discussion section 7.2). Cox et al proposed a buried site with significant contribution from TM3 helix which overlaps with residues identified in the groove site (Cox et al., 2018, discussion section 7.2). The putative binding sites demonstrate partial similarities with other ABCG2 drug docking studies and could indicate that the identified sites are distinct drug access sites or form part of a translocation pathway (see discussion for further details, section 7.2). The partial overlap of the putative binding sites for Mx and pheophorbide A are in accordance with the mutagenesis study, where residues mutated to alanine show perturbed function compared to daunorubicin transport. The groove site could possibly form the part of a translocation pathway thereby facilitating the substrates to enter the central cavity as described by the cryo-EM structures. The study enabled us to formulate a translocation mechanism which has been described in chapter 7 (section 7.3, see discussion for further details).

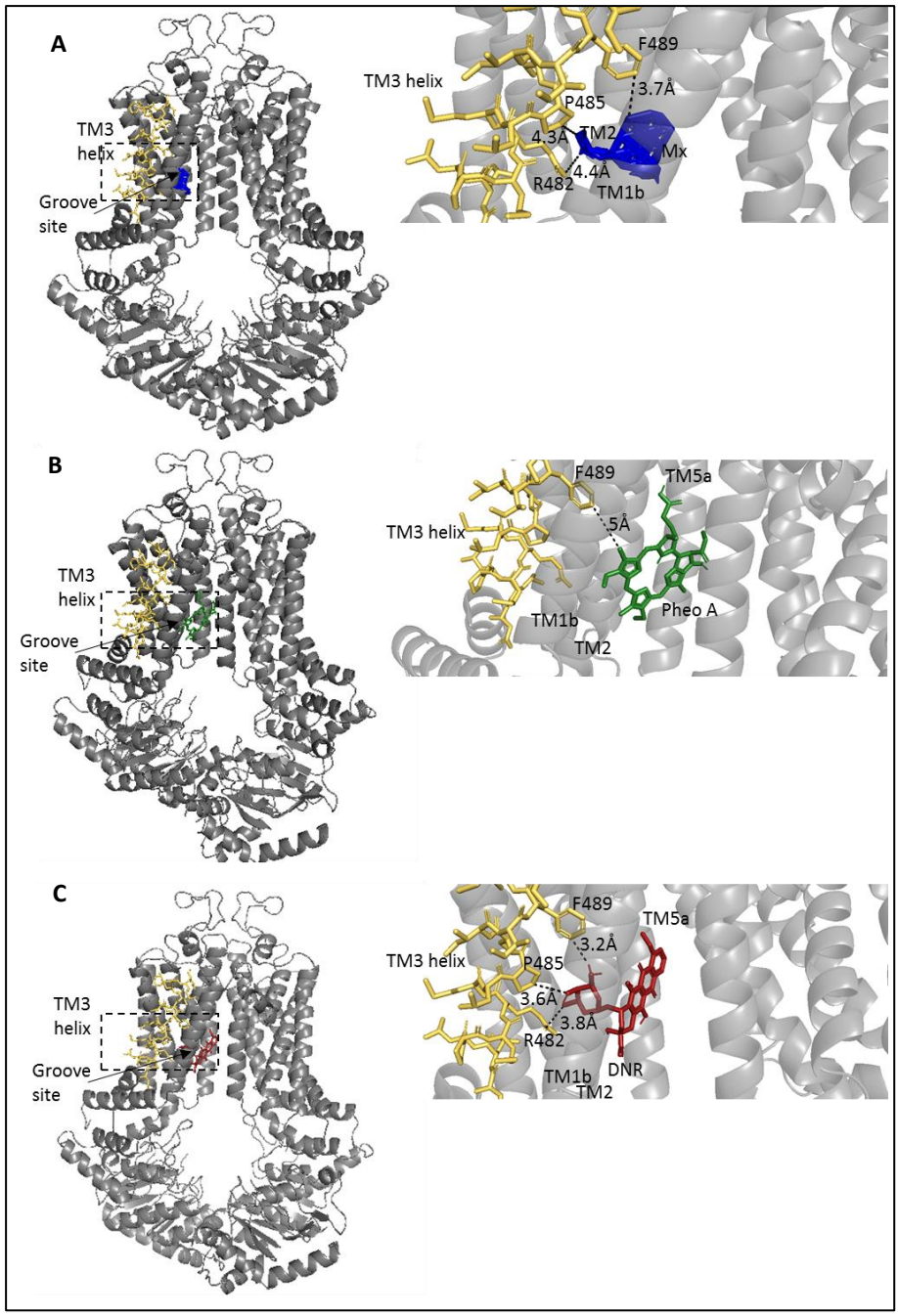


Figure 5.8: Putative drug binding site identified in close proximity to TM3 helix

PyMOL image of ABCG2 cryo-EM structure (PDB: 6ETI) with the TM3 helix shown in yellow stick representation. The left panel shows the whole view of ABCG2 with the docked molecules (within the dotted box) and the right panel shows enhanced view of the binding site. A putative binding site (groove site) has been identified aligned by helices TM1b, 2 and 3. A) Mitoxantrone docked to a site lined by residues from TMH 1b, 2 and 3. Mx is shown in blue sticks (clustered poise) with potential interactions from residues R482, P485 and F489 (shown in dotted black line). B) Pheophorbide A (shown in green stick representation) docked to a site lined by residues from TMH 1b, 2 and 3 with the potential contact with residue F489 (dotted black line). C) Daunorubicin (shown in red stick representation) with potential interactions from residues R482, P485 and F489 (shown in dotted black line). Potential contacts shown with TM3 helix residues at equal to or less than 5Å to the docked substrate.

5.6 Discussion and summary

The molecular basis for substrate recognition and translocation for the prototypic multidrug transporter ABCG2 is still not well understood. One step towards understanding this process was to illustrate the role of TM3 helix in the above said events. The aim of this chapter was to understand the importance of TM3 helix in drug translocation and whether it would harbour residues of interest that could influence substrate transport. Point mutations made across the N and C termini of the TM3 helix were not deleterious to the folding and trafficking of ABCG2 protein (chapter 4). This enabled us to monitor drug binding/ interaction with the multidrug transporter ABCG2 using flow cytometry. The relative drug efflux gave a measure of relative drug fluorescence (mitoxantrone, pheophorbide A and daunorubicin) in the presence and absence of the ABCG2 specific inhibitor Ko143, normalised for ABCG2 expression (sfGFP fluorescence) compared to the wild type. Some of the key residues identified have been discussed below with regards to functional and structural interpretation.

The vast majority of the TM3 mutant isoforms (13) showed reduction in mitoxantrone drug efflux compared to the wild type. Mutant D477A showed significant reduction in Mx and pheophorbide A transport. Indeed, D477A was comparable to E211Q (catalytically inactive mutant). Khunweeraphong et al., in their study suggest critical importance of D477 in shaping the inner central cavity. D477 is just one helical turn below R482. The biochemical and modelling data from Karl Kuchler's laboratory proposed a series of charged and polar residues at the TMD:NBD interface (which includes the ICL1, intracellular loop 1, between TM2 and TM3 helices) that act as an allosteric conduit ('polar relay') between the NBDs and TMDs, with ICL1 acting as a molecular spring to couple the two domains. The side chain of D477 is known to contribute towards the polar relay (Khunweeraphong et al., 2017).

As is published in the literature, R482A mutant showed gain in function for a non-native substrate transportation (daunorubicin) (McDevitt et al., 2008; Robey et al., 2003, 2001a). R482 has also shown potential contacts with Mx and daunorubicin, leading to identification of the putative drug binding site (groove site, docking studies and figure 5.8 C). A study by McDevitt et al. on the R482G isoform has enabled characterisation of three pharmacologically distinct binding sites, two of which display allosteric communications. Binding of daunomycin showed negative cooperativity,

unique to ABCG2 multidrug transporter. Stabilisation of daunomycin binding site *via* positive heterotrophic allostery in presence of different compounds, such as rhodamine 123 and partial displacement in presence of Mx and Hoeschst 33342 suggest multiple binding sites in the isoform (Clark et al., 2006; McDevitt et al., 2008). Homotropic allostery for multiple binding sites seen in the mutant isoform is unique to the bacterial transporter LmrA (Clark et al., 2006; van Veen, 2000). R482G mutant isoform has also shown abolished pheophorbide A transport in presence of telmisartin (Deppe et al., 2014).

S486A and F489A showed decrease in pheophorbide A transport. Data for F489, a common site for polymorphisms is in accordance with the published literature (Tamura et al., 2006). Based on the docking studies (section 5.5) F489 is a key residue that shows potential contacts with Mx, pheophorbide A and daunorubicn (figure 5.8 A, B and C). The aromatic ring at position 489 could potentially play a key role in transporting porphyrin compounds. F489L variant has been shown to have substrate dependent changes in transport activity, despite showing membrane localisation, i.e. methotrexate activity was not observed whereas, the mutant isoform showed reduced resistance to Mx and SN-38 transport compared to the wild type (Tamura et al., 2006). F489L variant expressed in HEK293-Tet-On cells was used to monitor pheophorbide A efflux capacity. The variant showed reduced expression level of ABCG2 protein and impaired basal pheophorbide A efflux. The variant also showed increased inhibition of pheophorbide A efflux by telmisartan (AT1 receptor antagonist). The studies above suggest the increased risk of patients harbouring F489L variant isoforms in developing adverse drug reactions (Deppe et al., 2014).

C491A shows reduced efflux for Mx transport. In one study cysteine mutation to serine resulted in irinotecan sensitivity indicating mild effect on drug transport (Liu et al., 2008). T490A showed altered phenotypic effects for mitoxantrone (reduced) and pheophorbide A (enhanced) transportation, suggesting drug specific interactions.

M496A mutant isoform showed significant increase for mitoxantrone transport and marginal increase in pheophorbide A transport. This suggests a lack of drug specificity associated with the phenotypic effects observed and M496 may contribute towards drug recognition and play a crucial role in drug binding. M496 faces the lipid surface at the lipid protein interface and probably conformational changes may contribute towards the allosteric effects, thereby facilitating hydrophobic drug translocation (figure 5.9).

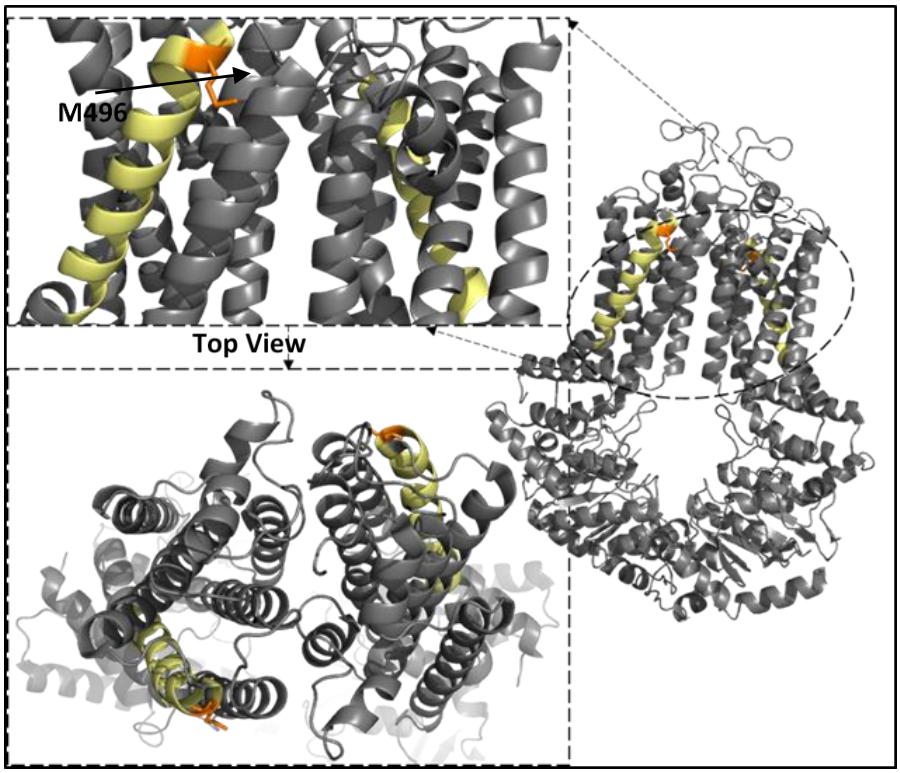


Figure 5.9: Cryo-EM structure of ABCG2 homodimer depicting M496 localisation within TM3 helix

The ABCG2 homodimer structure with the TM3 helix highlighted in pale yellow and the key residue M496 with altered substrate specificity highlighted (orange, stick representation). The top view, the enlarged view and the entire ABCG2 homodimer are presented. Figure generated in PyMOL software (PDB ID: 6ETI).

For mitoxantrone, pheophorbide A and daunorubicin, although the docking site was consistent, the orientation of the molecules showed variation. Docking of substrates was performed with high exhaustiveness (to find a global minimum based on Gibbs free energy) and revealed the global minimum within the groove site. This provides a partial structural explanation for the experimental data observed. The phenotypic effects observed for the TM3 mutant isoforms suggest the importance of TM3 in drug translocation. Data suggests that recognition and transport for mitoxantrone and pheophorbide A may share some structural features as opposed to daunorubicin transport. The data is consistent with previous studies on R482 (summarised by Mao and Unadkat), thereby reassuring the importance of R482 in ABCG2 function, in accordance with the interpretation by Hegedus and colleagues on the residue 482 and its effects on local conformation and dynamics as changes in selectivity (R482A) (Ejendal et al., 2006; Lászloá et al., 2016; Mao and Unadkat, 2015). Loss of the basic

arginine at amino-acid 482 may be critical to substrate specificity, mechanistic studies are needed to understand the changes (Allen et al., 1999). Since the wild-type arginine is a bulky, positively charged amino acid, it could impede binding or transport of positively charged compounds. This could explain the poor transport of doxorubicin and daunorubicin (or gain of function R482A mutation), both of which possess aliphatic amino groups that are positively charged at a physiological pH (7.6) (Robey et al., 2003).

During the course of this study ABCG2 homology models and the cryo-EM structures (presence of cholesterol, presence of inhibitor and substrate or bound nucleotide) have been published (Jackson et al., 2018; Manolaridis et al., 2018; Taylor et al., 2017). These structures shed light on the domain organisation and the helical arrangement. The study has enabled us to deduce key residues crucial in drug transportation and map the available cryo-EM structure, to rationalise the functional effects observed against the structural data and identify the putative drug binding site. I would like to call the TM3 helix as the putative gatekeeper for substrate translocation. Why and how has been discussed in chapter 7. We still need to garner better understanding of the structural basis for drug interactions and the influence of the surrounding lipid environment on drug uptake, in short, to understand the dynamic nature of drug interactions and translocation pathways.

Chapter 6: Importance of the highly conserved, unique NBD: NBD interface region in ABCG2

6.1 Introduction

NBDs are the motor domains of ABC transporters with RecA like subdomains (catalytic core domain) and α helical subdomains. NBD dimerization, a critical step for the mechanistic diversity was first elucidated by studies of the DNA repair enzyme Rad50 (Hopfner et al., 2001). The key element behind the head to tail dimer arrangement is the presence of conserved motifs of the two NBDs at the shared interface, these are either involved in ATP binding and hydrolysis or facilitate crucial interfaces in the assembled transporter. This arrangement facilitates the formation of two ATP binding sites between the P-loop of one NBD and the signature motif (LSGGQ) of the other NBD (Oswald et al., 2006).

The 3.9 Å crystal structure of human ABCG5/G8, reconstituted into DMPC bicelles, shows a nucleotide free state, with a spatial separation of the opposing Walker-A and signature motifs (Hopfner, 2003; Kerr, 2002; Lee et al., 2016; Smith et al., 2002). A novel interface which appears to be unique to the G subfamily, where the C-terminal extensions (C- terminal to the conserved His-switch motif) of the two NBDs interact has been observed (Jackson et al., 2018; Manolaridis et al., 2018; Taylor et al., 2017; Zaitseva et al., 2005). This interface contains the highly conserved NPXDF motif (figure 6.1).

The sequence is located between the NBD and TMD and contains five amino acid residues. Asn, Pro, Asp, and Phe are conserved among all the five G subfamily members (figure 6.1). The middle amino acid residue is an Ala in all subfamily members except for ABCG5, where it is a Phe.



Figure 6.1: Sequence alignment of the ABCG family

Partial display of sequence alignment across the G subfamily that includes the conserved NPXDF motif and the NBD interface residues (Y247, E285 and N288) have been highlighted here. Sequence alignment has been performed using Omega.

The recent cryo-EM structures have confirmed this interface in ABCG2, and sequence analysis of the ABCG family demonstrates conservation not just of the central NPXDF motif but also some residues N-terminal to this. The presence of the unique NBD: NBD interaction led us to hypothesize that this constant contact unique interface could be detrimental to ABCG2 function. The key residues in the study are located in the G-family specific sequence motif NPXDF that have been identified to be functionally significant in ABCG1. Studies on ABCG1 indicated that this motif plays a role in cholesterol efflux and point mutations (either single or multiple) lead to significant effects on the transporter including; failure of membrane trafficking (N316Q and F320I) and reduced cholesterol transfer to apoA1 (N316A/D/Q and F320A/I) simultaneously or individually (Wang et al., 2013). Point mutations were made at these conserved positions to alter the charge, size of the amino acid that could potentially disrupt interactions (table 6.1).

Residues	Mutations
Y247A	Polar- Nonpolar
E285A/ K	Acidic (-) –Nonpolar/ Basic (+)
N288A/ D	Polar- Nonpolar/ acidic (-)
D292A/ K	Acidic (-) – Nonpolar/ Basic (+)

Table 6.1: NBD interface Mutants

The table depicts the point mutations made in the NBD interface residues and the type of mutations designed to understand their role in the catalytic cycle.

Asp-292 forms inter-molecular interactions with the equivalent residue on the opposite NBD and was mutated to either neutralize the charge (D292A) or reverse it (D292K)

(figure 6.2 D). Y247, N288, and E285 were shown to be involved in a network of short-range (3.9–4.8Å) electrostatic interactions across the interface (figure 6.2 C and E). To disrupt these interactions, Y247 was mutated to alanine (Y247A), N288 was mutated to alanine to remove any polar interaction (N288A), or to aspartate to investigate the effect of introducing a charged residue at this position (N288D), and E285 was mutated either to remove the charge (E285A) or to reverse the charge (E285K). Analysis of the multiple sequence alignment of ABCG family members in humans (Figure 6.1) shows that Y247 is a Ser/Ala in ABCG5/G8/G1 and ABCG4, E285 is a Pro in ABCG5/G8/G1 and ABCG4 and N288 is Ser in ABCG5/G8 and His in ABCG1/G4 respectively. These residues are highly conserved across the animal kingdom (appendix 8).

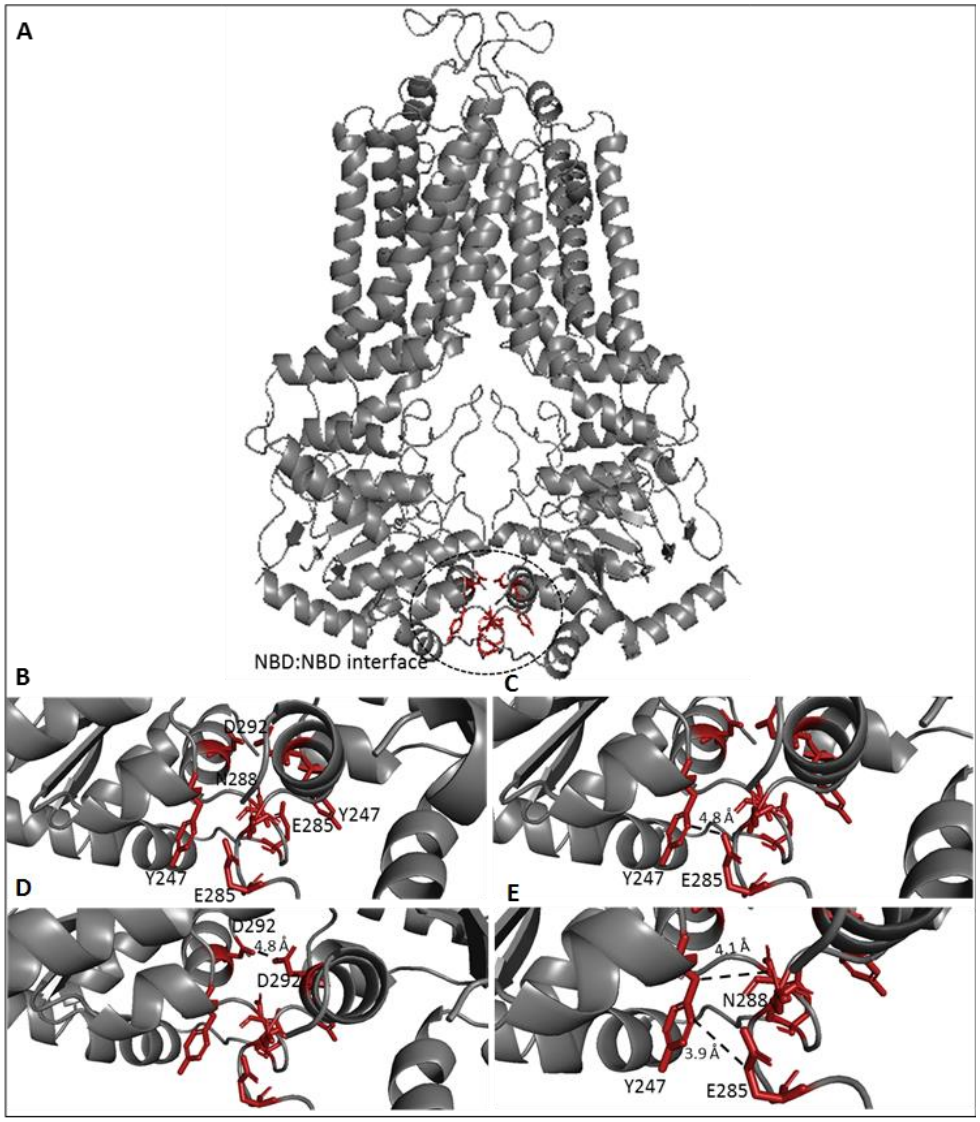


Figure 6.2: Structural intricacies of the NBD: NBD interface

The ABCG2 homodimer cryo-EM structure (A, whole view) with the enlarged view of the NBDs showing the novel constant contact interface (red, B). Structural mapping of the mutated NBD interface residues: Y247, E285, N288 and D292 (red, C-E) including the relative positions of the interacting residues (<5 Å). Figure generated in PyMOL software using PDB: 6ETI; (Jackson et al., 2018); adapted from Kapoor *et al*., 2020 (Kapoor et al., 2020).

Here we investigate the importance of the NBD: NBD interface residues that tentatively disrupt the interactions, thereby destabilizing the ABCG2 dimer. We also probe the contribution of these residues in drug binding, translocation and ATP hydrolysis.

6.2 Construct generation

Mutants were generated using site directed mutagenesis (methods section 2.1.2) using the mammalian expression vector pcDNA^{TM}3.1 Zeocin^{TM} (+). Successful mutants were confirmed using Sanger sequencing (figure 6.3 and appendix 7).

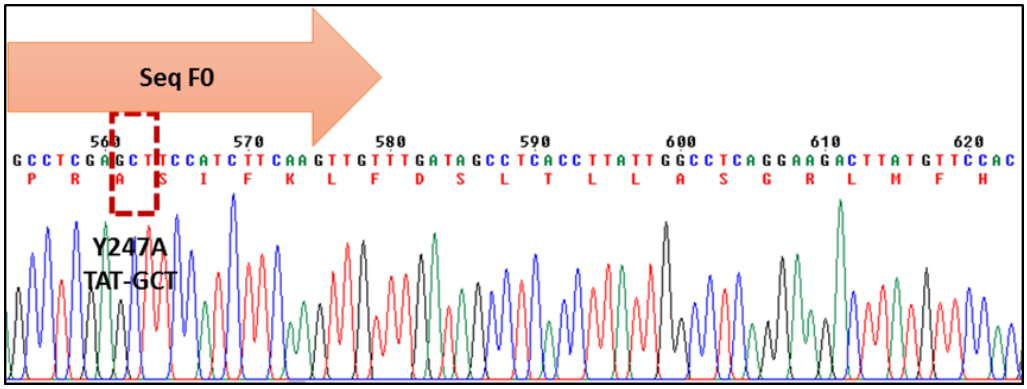


Figure 6.3: Confirmation of the NBD interface mutants in the mammalian expression vector. A chromatogram sequence, depicting point mutation for Y247A; TAT—>GCT (red box), confirmed by Sanger sequencing trace using Seq F0 primer (Figure 4.5 A). Sequence data for all mutants attached in appendix 2.

6.3 Generation of stable cell lines for NBD interface mutants

HEK293T cells were transfected with sfGFP_ABCG2 plasmids (section 2.2.3 and 2.2.4). Stable cell lines were generated based on the zeocin^{TM} mediated selection process. The expression of ABCG2 was confirmed by observation of GFP fluorescence under an epifluorescent microscope (figure 6.4). The expression and cellular localization of sfGFP_ABCG2 was imaged for all mutant isoforms in phase contrast and fluorescent microscope. This resulted in generation of mixed population stable cell lines for wild type ABCG2 and NBD interface mutant isoforms.

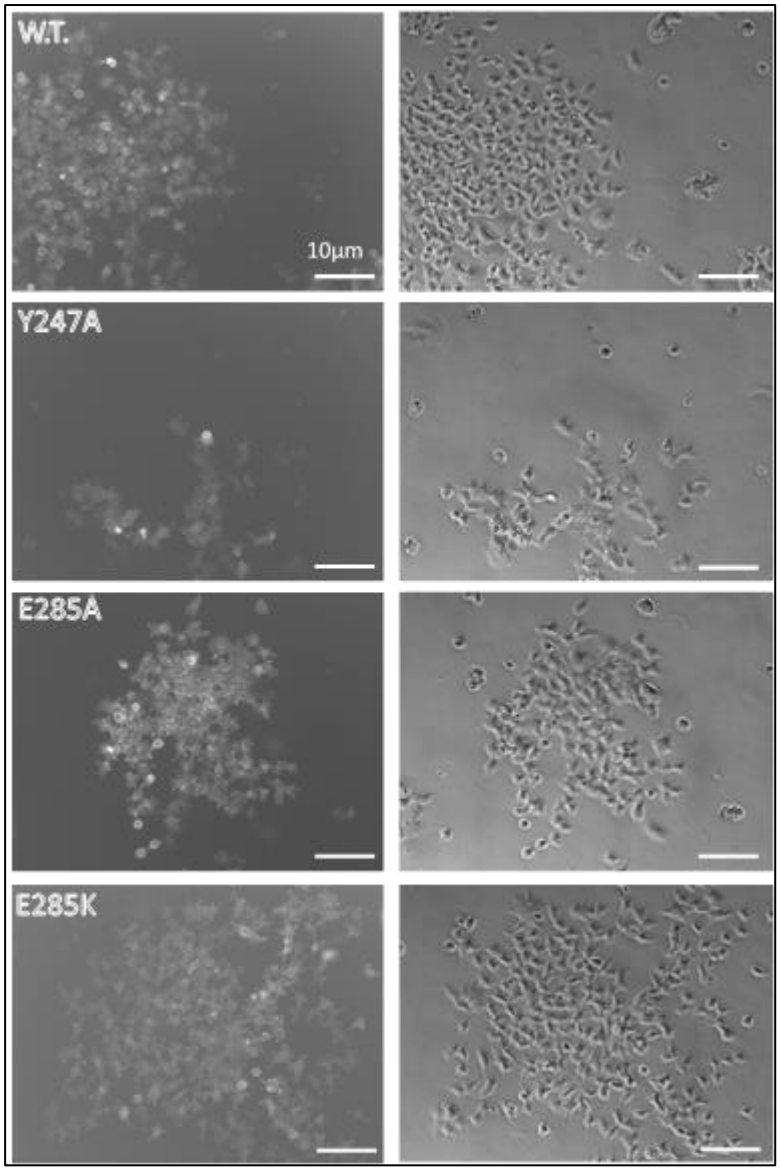


Figure 6.4: Generation of stable cell lines for NBD interface mutant isoforms

HEK293T cells were transfected with sfGFP_ABCG2 plasmids (wild type and mutant isoforms). Stable cell lines were generated based on the zeocin^{TM} (200 µg mL^{-1}) mediated selection process. GFP fluorescence was observed using an epifluorescent microscope (phase 1, 10 X objective; Carl Zeiss, Birmingham, UK) connected to an inbuilt camera (AxioCam MRm, Zeiss) and analysed using the software Axio Vision release 4.8.2 SP3. Phase contrast images are on the right panel whereas fluorescence images are on the left panel. Scale bars represent 10 µm. Images for all the remaining mutants included in appendix 7.

6.4 Cell surface expression and localisation

Cell surface expression was confirmed using a western blot and localisation using confocal microscopy. Expression of the wild type ABCG2 and mutants (Table 6.1)

was tested using immunoblotting using a catalytically inactive mutant (E211Q) as negative control. Western blots for the whole cell lysates (20µg) from stable cell lines were performed using 10% (w/v) polyacrylamide gels. ABCG2 expression was detected by immunoblotting with BXP-21 antibody (figure 6.5).

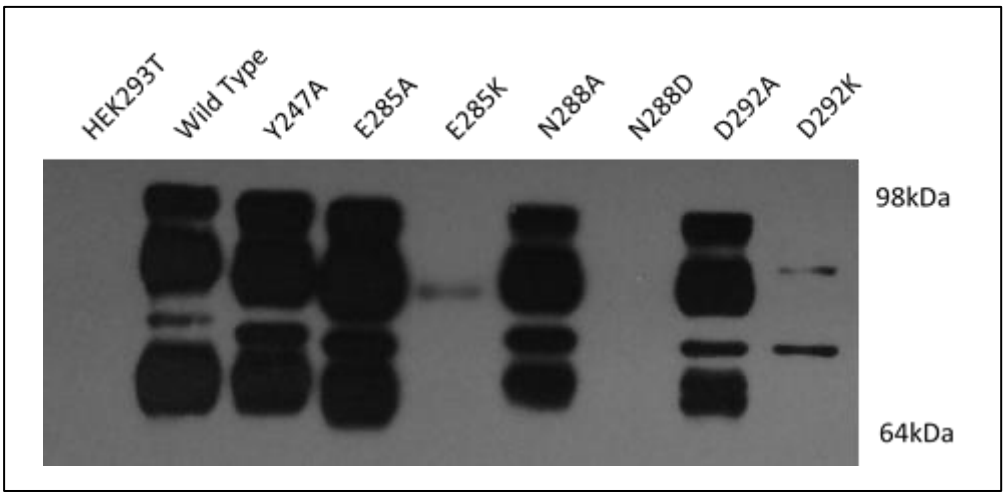


Figure 6.5: Expression of NBD interface mutant isoforms in HEK293T cells, probed using BXP-21

Cell pellets were harvested from HEK293T mutant stable cell lines and subjected to lysis. The cell lysates (20µg) were resolved on 10% w/v polyacrylamide gels. PEI transfected HEK 293T cells served as a negative control. Western blot analysis was performed to confirm the expression of ABCG2 isoforms by probing with primary monoclonal antibody BXP-21 (1:1000). A clear band is visible at approximately 100 kDa for sfGFP_ABCG2 protein.

The mutants, E285K, D292K and N288D did not show the expected immunoreactive band at 100 kDa, which was observed for the WT and other mutants cell lines (figure 6.5). The presence of multiple bands in some lanes was attributed to protein degradation during freeze-thaw cycles (figure 6.5). BXP-21, is an antibody that specifically binds to residues 271-396 of ABCG2, considering this stretch contains the mutated residues, it is likely some mutations reduced the affinity of BXP-21 for the protein. Alternative antibodies available could also have similar impaired binding (e.g. BXP-53 is raised against 221-394) and so were not tested (Halwachs et al., 2016). Anti- GFP blot represented a similar expression pattern as BXP-21 blot, with minimal expression for E285K, N288D and D292K (blot not shown).

In addition to western blot, the stable cell lines generated were screened for sfGFP tag expression *via* confocal microscopy to demonstrate that the mutated proteins were

successfully localised on the cell membrane. Most of the mutants showed clear cell membrane localisation with varying levels of protein expression comparable to the wild type (figure 6.6). This suggested that point mutations were not deleterious to protein folding and translocation.

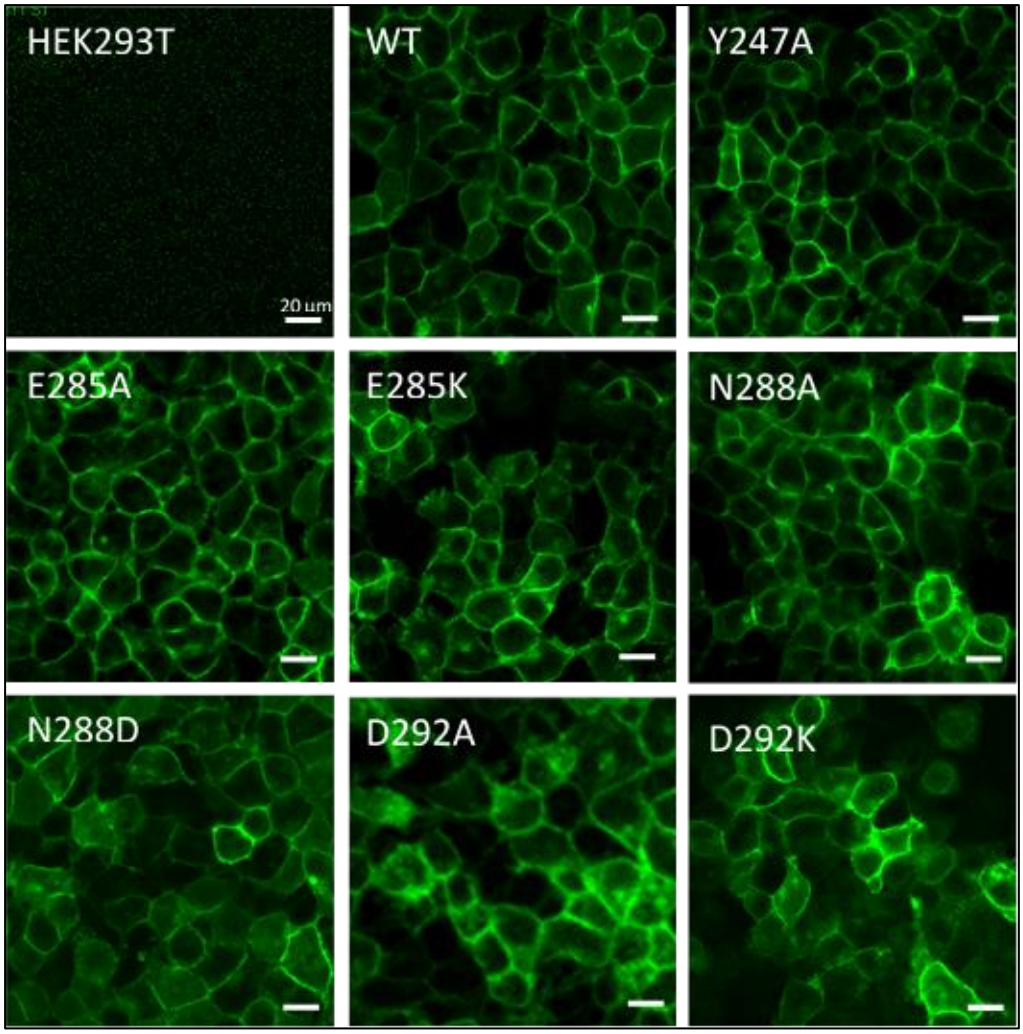


Figure 6.6: Cell surface localisation of NBD interface mutants

Confocal microscopy was performed to visualize cell surface localization of ABCG2 isoforms in stable cell lines. All the mutants were N-terminally sfGFP tagged. Most of the mutant isoforms showed clear cell membrane localization with slightly altered levels of protein expression compared to the wild type. Live cells were imaged using an ImageXpress (IX) Ultra confocal plate reader (plan-apochromat 40X objective, with excitation wavelength of 488nm and emission bandpass filter of 520/50 nm). HEK293T cells represent a negative control (observed under phase contrast microscope, figure not available due to MetaXpress limitation). Scale bars represent 20 µm.

6.5 Cell surface expression and localisation of NBD interface mutants using a two-channel spectrum

As there were some discrepancies between the western blot and the plate reader data (e.g. for N288D there was no expression on the BXP-21 western blot and yet apparent expression in the microplate analysis), two channel flow cytometry was used to monitor expression levels of ABCG2 on the cell surface. HEK293T cells expressing stable NBD interface mutant isoforms were labeled with monoclonal antibody 5D3 which recognises a surface localised epitope of ABCG2 extracellularly. The cells were anlysed in flow cytometry for sfGFP expression as a measure of total sfGFP_ABCG2 expression and 5D3 reactivity as a measure of cell surface expression (figure 6.7).

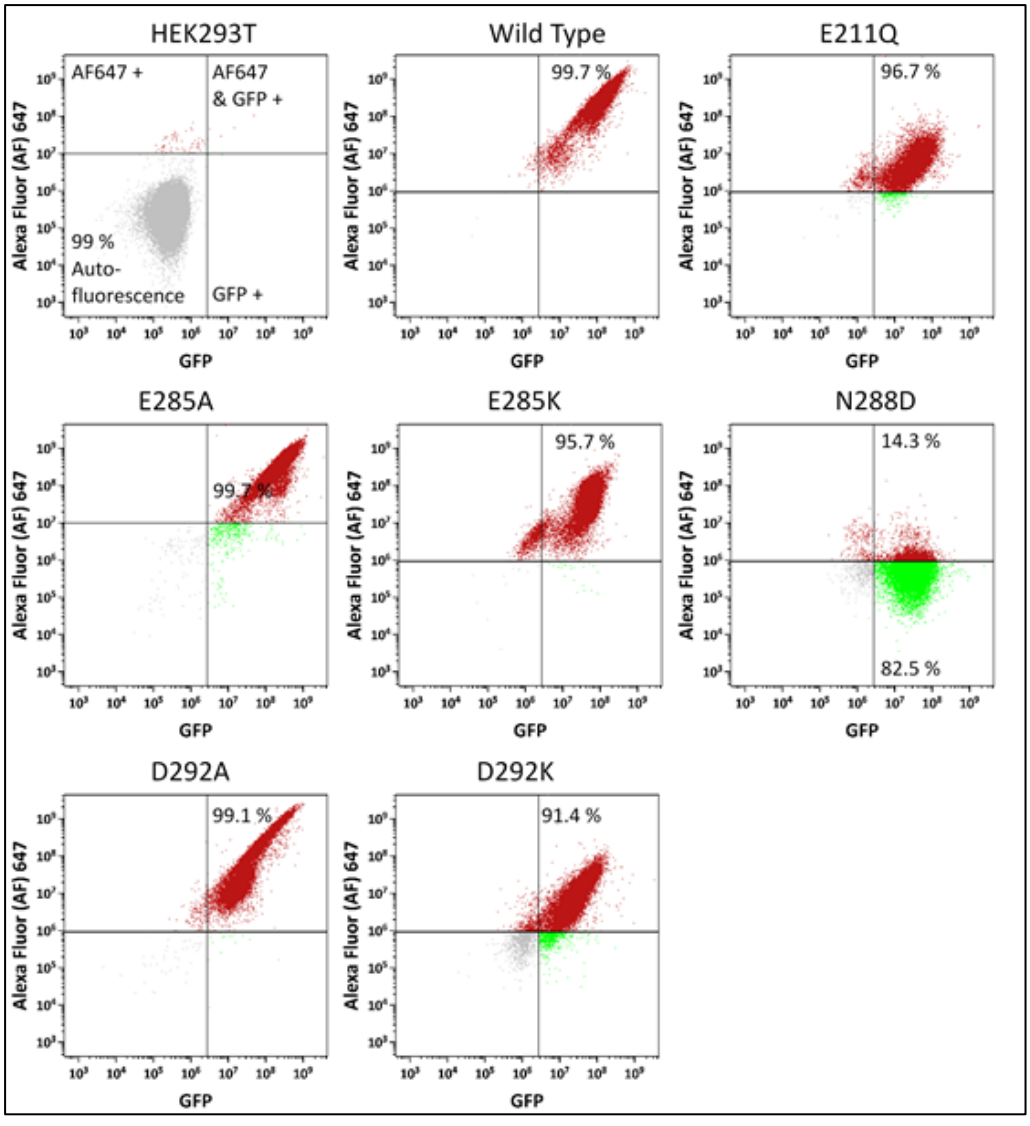


Figure 6.7: Cell surface expression for NBD interface mutant isoforms using a two-channel flow cytometry

The cells were labelled with 5D3 antibody and a secondary antibody conjugated to Alexa Fluor (AF) 647 enabling individual cells to be quantified for cell surface ABCG2 expression (y-axis) and total GFP expression (x-axis). The cells were analysed for GFP and Alexa Fluor 647 (AF647) expression using Astrios (Beckman Coulter). The cells in the upper right corner of the quadrant represent cells with ABCG2 surface expression. The percentage of cell surface expression for HEK293T, wild type and TM3 mutant isoforms have been documented in the quadrant.

In majority of the mutant isoforms investigated for cell surface expression, the percentage of cells positive for GFP and AF647 fluorescence was more than 90%, with wild type depicting nearly 99% cell surface localisation and expression of ABCG2 (figure 6.7). This confirmed that ABCG2 was correctly localised to the plasma membrane in the mutant isoforms. A similar pattern was observed for all the other mutants investigated with the exception of the N288D mutant which showed only 14% of cells having surface localised ABCG2 (figure 6.7). This indicated that N288D mutation prevented proper trafficking of the ABCG2 protein, demonstrating that point mutation facilitating introduction of an acidic charge is deleterious to protein folding and trafficking. Immunohistochemistry using membrane permeabilization to confirm intracellular localisation of the mutant isoform was performed.

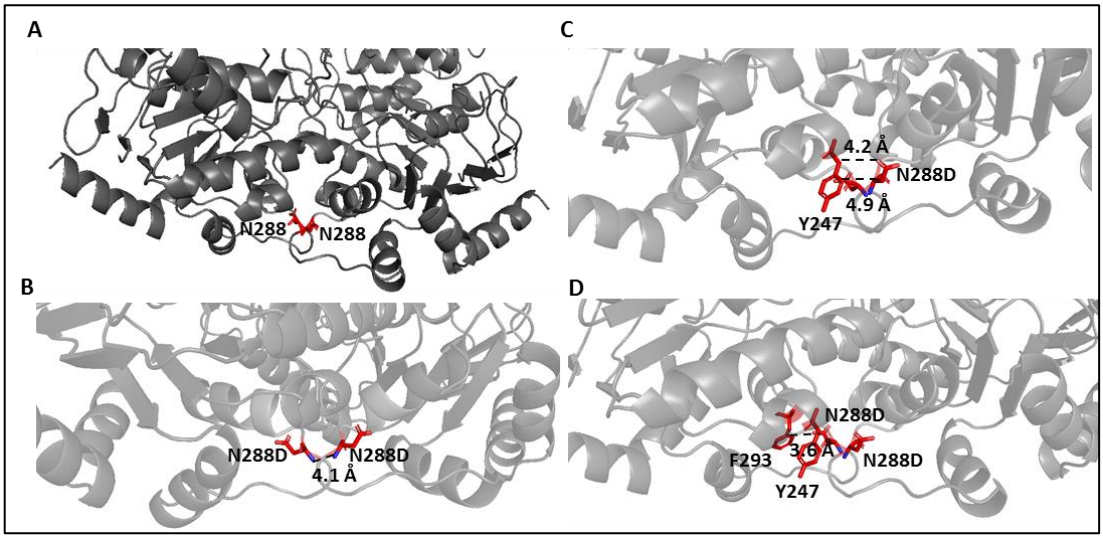


Figure 6.8: Structural insight to N288D mutation

The ABCG2 NBD homodimer cryo-EM structure. A) Mapped N288 residues (red stick representation) on the NBD homodimer. B) Structural mapping of the mutated N288D interface residues (4.1 Å) and its potential interactions (<5 Å, C and D). C) Potential contacts of N288D with Y247 (4.2 Å and 4.9 Å). D) Potential interactions of N288D with F293 (3.9 Å). Figure generated in PyMOL software using PDB: 6ETI; (Jackson et al., 2018).

Structural interpretation of N288D mutation sheds light on its potential interactions (<5 Å) with bulky aromatic amino acids F293 (NPXDF motif) and Y247 (close contact interface residue), that could affect protein expression and trafficking due to addition of a positive charge at residue position 288 (figure 6.8 A, B, C and D).

6.6 Defects in protein folding, trafficking affecting cellular localisation

N288D ABCG2 showed reduced cell surface expression as confirmed by western blot and flow cytometry as shown above. Failure of the protein to reach the cell surface indicated membrane trafficking defect and to support this finding we used immunohistochemistry. Cells were seeded in a 24 well dish as explained in section 2.4.2. Live cell imaging was performed for wild type and N288D mutant to monitor cell surface expression. Phase contrast images are depicted for each condition on the right panel (figure 6.9). In order to detect intracellular localisation, cells were permeabilized using saponin after fixation with cross-linking agent formaldehyde. Cells were subjected to conformational sensitive ABCG2 specific primary antibody 5D3 (monoclonal antibody anti- BCRP1) immunostaining with secondary antibody AF647 to monitor ABCG2 localisation.

Confocal microscopy was used to assess the localisation of mutant protein by exciting the sfGFP fluorophore fused N-terminal to ABCG2. Live cell imaging was performed for wild type and N288D (figure 6.9 A and D). GFP fluorescence was observed on the plasma membrane for wild type ABCG2 compared to N288D that represented intracellular compartmentalisation of GFP fluorescence with an altered cell phenotype. Fixed cells for wild type and N288D mutant were subjected to immunohistochemistry in order to understand ABCG2 localisation (figure 6.9 B, C and E, F; GFP fluorescence, AF647 fluorescence, overlay composite and phase

contrast images). Wild type ABCG2 showed GFP fluorescence on the cell membrane in the non-permeabilised (figure 6.9 B) and permeabilised cells (majorly on the cell surface, figure 6.9 C) compared to N288D (figure 6.9 E and F). Immunostaining using AF647 antibody interacting with ABCG2 specific conformational sensitive primary antibody 5D3 reflected plasma membrane localisation (figure 6.9 B and C) for wild type ABCG2. Immunostaining for N288D represented intracellular localisation, suggesting trafficking defects (figure 6.9 E and F). Visualisation of cells was conducted on an LSM710 confocal laser scanning microscope (Zeiss, Jena, Germany) equipped with a Plan-Apochromat 63x/1.40 Oil Ph3 DIC M27 objective and argon laser (2% argon laser power) with the numerical aperture set at 2 due to low fluorescence intensity of AF647.

Several experimental approaches showed that N288D mutant ABGC2 was exhibits expressed and trafficking defects. Further experimentation is required to elucidate the mechanism causing these defects. In subsequent functional sections this mutant was not included as it presents impaired protein stability.

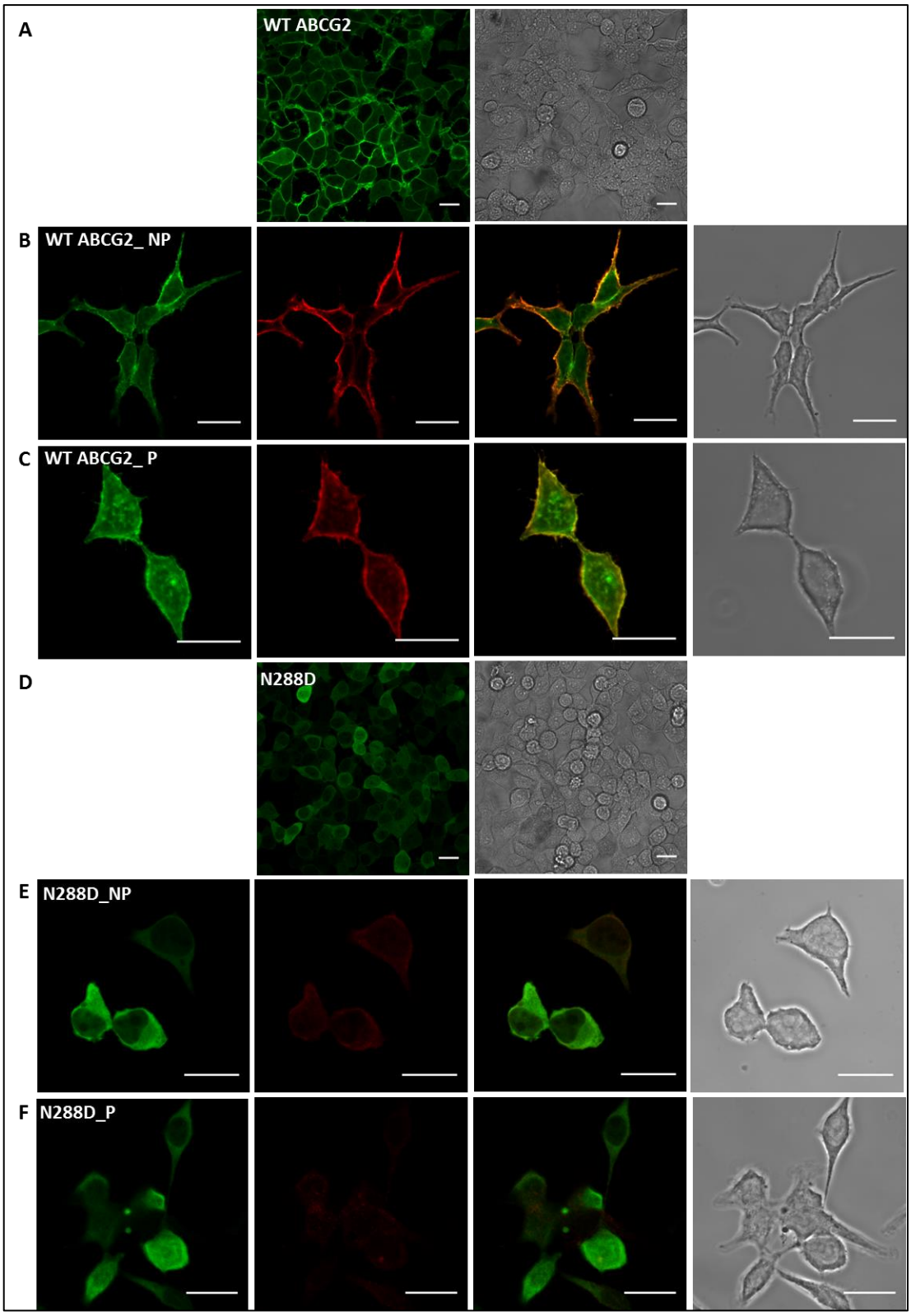

A
WT ABCG2
B
WT ABCG2_ NP
C
WT ABCG2_ P
D
N288D
E
N288D_NP
F
N288D_P

Figure 6.9: Trafficking defect observed for N288D mutant isoform compared to the wild type
HEK293T cells expressing ABCG2 isoforms were visualised for protein localisation by confocal microscopy. GFP (left panel) and AF647 (middle panel) fluorescence were observed as a measure of plasma membrane localisation of ABCG2. Live cell imaging was performed using GFP fluorescence as a measure of plasma membrane localisation for wild type (A) and N288D (D) mutant isoform. Overlay images and phase contrast images are depicted for each condition on the third and fourth right panels respectively. Zoomed images of fixed cells for wild type (B and C) and N288D (E and F) have been depicted here. Permeabilised, denoted as P (C) vs. non-permeabilised, denoted as NP (B) wild type ABCG2; demonstrated membrane localisation as a reflection of GFP fluorescence (left panel) and AF647 fluorescence (middle panel). Permeabilised, denoted as P (F) vs. non-permeabilised, denoted as NP cells (E) N288D cells demonstrated increased intracellular localisation as a reflection of GFP fluorescence and AF647 fluorescence compared to non-permeabilised cells (E). Visualisation of cells was conducted on an LSM710 confocal laser scanning microscope (Zeiss, Jena, Germany) equipped with a Plan-Apochromat 63x/1.40 Oil Ph3 DIC M27 objective and argon laser. For detection of sfGFP-ABCG2 isoforms, a 2% argon laser power was used with excitation set at 488nm and emission collected between 500-530nm (FITC channel). Scale bar is representative of 20μm.

6.7 Functional characterisation of NBD interface mutants

Several lines of evidence clearly suggest plasma membrane localisation of NBD interface mutants based on the confocal microscopy (figure 6.6 and 6.9) and flow cytometry (figure 6.7) based cell surface expression recognising the extracellular 5D3 epitope (ECL3 of ABCG2). Notable exception to this is the mutation N288D that showed reduced cell surface expression, thereby suggesting a trafficking defect. The next step was to investigate the impact of these point mutations on protein localisation and function, i.e. the ability to export the desired substrates (fluorescent wild type and non-wild type). Dual channel flow cytometry was employed to monitor GFP fluorescence (as a measure of total protein expression) and drug fluorescence (as a measure drug efflux).

In this assay, ABCG2 specific transport ability is quantified using the inhibitor Ko143 and three fluorescent substrates; Mx, pheophorbide A and a non-wild type substrate daunorubicin. The data represents the relative efflux of substrate, normalised for GFP expression compared to the wild type (figure 6.10-6.11; table 6.2). The data shows the NBD mutants with normal, impaired or enhanced relative drug efflux compared to the wild type (figure 6.11). Drug efflux assays exposed key residues with significant

differences in the drug efflux phenotype compared to the wild type protein and the negative controls (HEK293T and E211Q; figure 6.11).

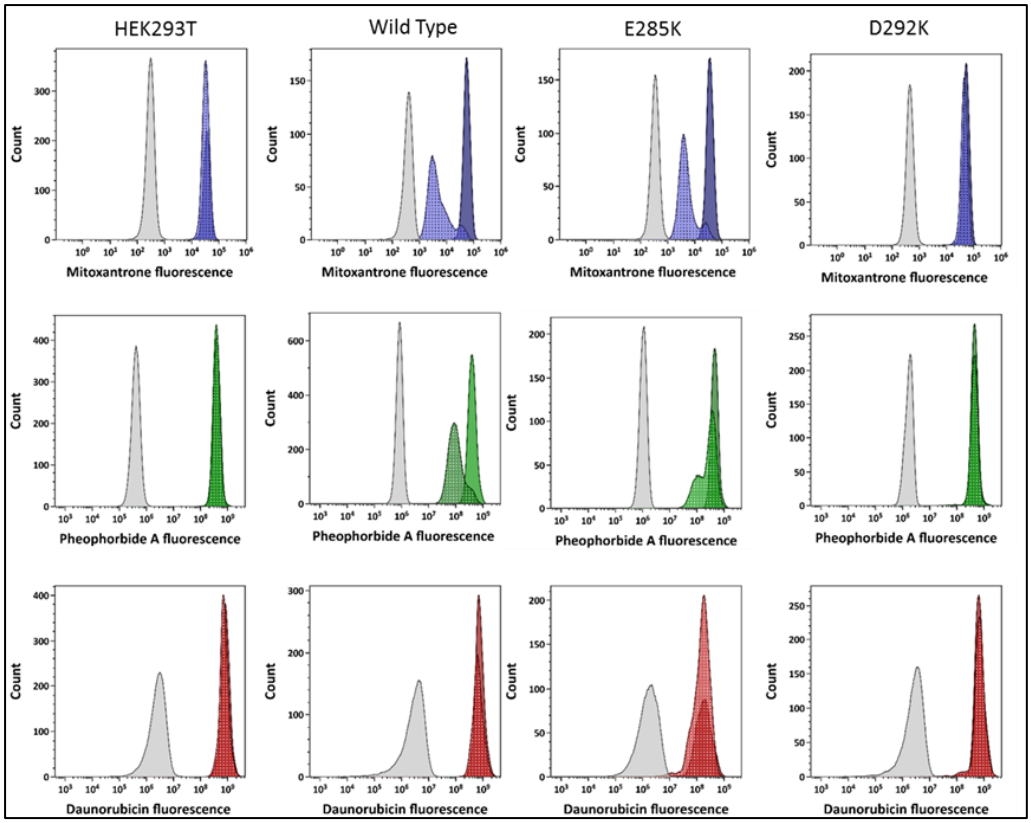


Figure 6.10: Altered transport function in NBD interface mutants

Kaluza single channel histogram plots to monitor mitoxantrone, daunorubicin and pheophorbide A fluorescence based on the drug efflux capacity of the HEK293T cells expressing wild type ABCG2, NBD mutant (D292K) and non-expressing cells (HEK293T). Grey histogram represents the HEK293T cells with inherent fluorescence. The dotted blue, green and red histograms depict equilibrium level of accumulation of mitoxantrone, pheophorbide A and daunorubicin respectively. Quantitative analysis of the rightward shift of ABCG2 specific substrate accumulation in presence of Ko143 is shown by solid colour histograms. The remaining have been displayed in appendix 9.

The negative controls (cells lacking ABCG2 expression; HEK293T and cells expressing an ABCG2 containing the Walker-B motif neutralising mutation; E211Q) displayed no Ko143 mediated inhibition of drug transport of the three fluorescent substrates (figure 6.10). Although, E211Q showed cell surface expression. Positive control expressing wild type ABCG2, behaved as previously described, that is, capable of exporting Mx and pheophorbide A, whereas incapable of exporting daunorubicin (figure 6.10, wild type and 6.11).

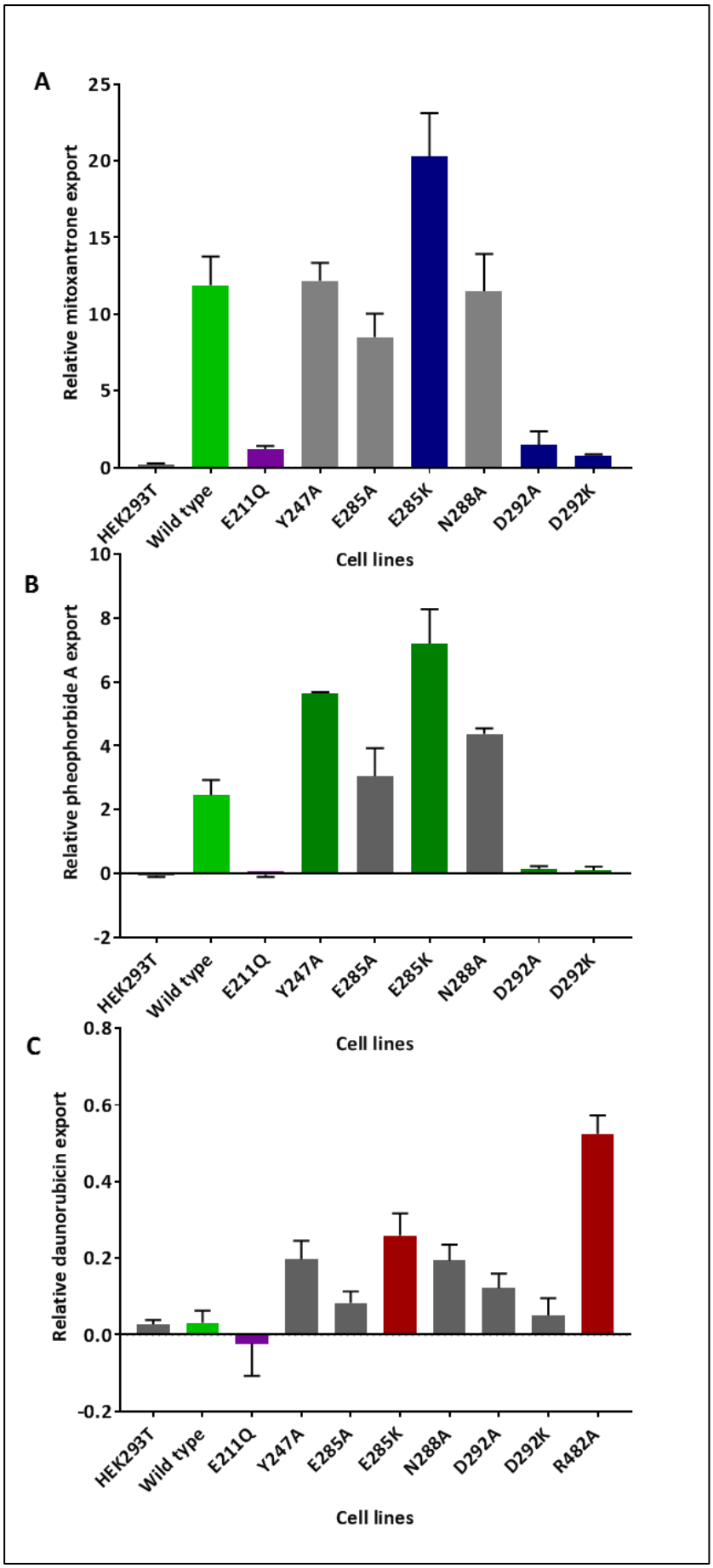

A
Relative mitoxantrone export
25
20
15
10
5
0
HEK293T
Wild type
E211Q
Y247A
E285A
E285K
N288A
D292A
D292K
Cell lines
B
Relative pheophorbide A export
10
8
6
4
2
0
-2
HEK293T
Wild type
E211Q
Y247A
E285A
E285K
N288A
D292A
D292K
Cell lines
C
Relative daunorubicin export
0.8
0.6
0.4
0.2
0.0
-0.2
HEK293T
Wild type
E211Q
Y247A
E285A
E285K
N288A
D292A
D292K
R482A
Cell lines

Figure 6.11: NBD interface mutants show altered phenotypic effects in drug translocation

The bar graphs represent the average fractional difference in substrate accumulation in presence of Ko143, normalised for GFP expression compared to the wild type (green bar). Data represents median fluorescence values for substrate (mitoxantrone (A), pheophorbide A (B) and daunorubicin (C)) accumulation (+/-SEM) for n ≥ 3 independent repeats. The relative efflux by HEK293T cells is represented by the grey bar and the efflux by catalytically inactive mutant, E211Q is represented by the purple bar. The relative efflux of mitoxantrone by the mutant isoforms, with statistically significant (p values < 0.05) ones (E285K, D292A, and D292K); blue (A). Pheophorbide A efflux capacity by the mutant isoforms, with altered phenotypic effects (reduced efflux- D292A, and D292K, enhanced efflux- Y247A), representing the statistically significant isoforms (p values < 0.05); dark green (B). Daunorubicin efflux by the mutant isoforms with gain of function mutations, E285K and R482A; red (C).

The mutants showed drug export function that was statistically different from wild type ABCG2, for the tested drug substrates. E285K differed in its capacity to export mitoxantrone, pheophoribde A and daunorubicin. It showed gain in function for mitoxantrone transport (20.26 ± 2.9), pheophorbide A transport (7.2 ± 1.06) and subtle but statistically significant daunorubicin transport (0.2593 ± 0.06) compared to the wild type (figure 6.11 A, B and C). A stark difference in drug transport was observed by the mutation of residue D292 (to alanine or lysine) within the NPXDF motif. D292A and D292K showed statistically significant impaired function for mitoxantrone and pheophorbide A transport with values indistinguishable from the negative controls (figure 6.11 A and B). It will be interesting to see if the functionally defunct mutant isoforms (D292A and D292K) show impaired effect in ATP hydrolysis. This is investigated and explained in the next section. Mutants E285A and N288A showed transport parameters indistinguishable from wild type ABCG2 (figure 6.11 A- C). The Y247A mutant showed statistically significant enhanced transport for pheophorbide A compared to the wild type.

Cell lines	MITOXANTRONE		PHEOPHORBIDE A		DAUNORUBICIN	
	Mean	SEM	Mean	SEM	Mean	SEM
HEK293T	0.21	0.07	-0.07	0.05	0.03	0.01
Wild type	11.90	1.88	2.45	0.48	0.03	0.03
E211Q	1.22**	0.20	-0.05*	0.07	-0.02	0.08
Y247A	12.19	1.18	5.63**	0.05	0.20	0.05
E285A	8.51	1.53	3.05	0.88	0.08	0.03
E285K	20.26**	2.85	7.20**	1.06	0.26*	0.06
N289A	11.53	2.40	4.37	0.17	0.19	0.04
D292A	1.46**	0.90	0.13*	0.10	0.12	0.04
D292K	0.81**	0.07	0.10*	0.11	0.05	0.05
R482A					0.53**	0.05

Table 6.2: Ko143 inhibited transport of fluorescent drugs by NBD interface mutant isoforms

The data depicts the mean (with SEM) of the fractional difference in Ko143 inhibited drug efflux compared to the wild type. The raw data for mitoxantrone and pheophorbide A were processed using one-way ANOVA and post statistical test (Dunnett's multiple comparison) against the wild type. The data for daunorubicin efflux was subjected to log transformation due to positive skewed data for R482A mutant isoform, prior to analysis of significance. The data are representative of $n \geq 3$ independent repeats. Asterisks indicate the level of significance with $p \leq 0.05$ for * and $p \leq 0.01$ for **.

The coupling of ATP hydrolysis to a conformational switch triggering drug transport is crucial to understand the catalytic cycle. The above data show a spectrum of changes to transport such as alterations to specificity (E285K), alterations to capacity (E285K and Y247A) and loss of function (D292A and D292K). Based on these results, the next step is understanding the ATP consumption at the NBDs and its relation with the drug transport. We demonstrated that ABCG specific NBD interface residues play a pivotal role in drug transportation, next we assessed these mutants for catalytic activity (ATP hydrolysis).

6.8 Functional characterisation of NBD interface mutants using the ATPase assay

It was imperative to determine whether the intrinsic ATPase activity of the protein was affected mutations in the NBD interface residues. An ATPase assay was established in our lab, preliminary work by a colleague (Dr Megan Cox), based on published work

by Ambudkar *et al* (Ambudkar, 1998). This enabled the determination of Pi release from ABCG2-containing membranes in the presence of drug substrate (Lucifer yellow; LY) with or without addition of inhibitor Ko143. Lucifer yellow; a hydrophilic substrate was used to investigate the ATPase activity, a step towards understanding the catalytic cycle (Sjöstedt et al., 2017). Mitoxantrone as a test substrate was not used in the assay as it would interfere with the colorimetric determination of the phosphomolybdate complex. The protocol was further optimised to screen the above mutants to monitor activity using crude membranes in a 96 well plate.

The ATPase activity of ABCG2 is difficult to measure due to presence of endogenous substrates (such as cholesterol) that could stimulate the ATPase activity. Inorganic phosphate release was measured from ABCG2 crude membranes in presence of ABCG2 substrate, LY. The fraction of inorganic phosphate released was measured as both ATP dependent and Ko143 inhibitable. HEK293T cell membranes were used as a negative control to monitor any background ATPase activity observed due to expression of any endogenous ATPases. The data has been normalised for the basal activity measuring the AMP signals. Research has shown no effect of AMP on the ABC transporter catalytic cycle and is therefore used as control for specificity of the interaction (McDevitt et al., 2008). Catalytically inactive E211Q control membranes were also used in the study to characterise ABCG2 specific ATPase activity. The membranes displayed Pi release that was not inhibitable by Ko143 as compared to the wild type membranes (figure 6.12). The assays were carried out in presence of Mg.ATP at highest tolerated level, possibly causing artificially stimulated ATPase activity hence masking any potential substrate stimulated response. Another limitation is the lack of complete inhibition of all the ATPases in the membrane vesicles, using ouabain, thereby suggesting the increased basal activity observed (Hou et al., 2009).

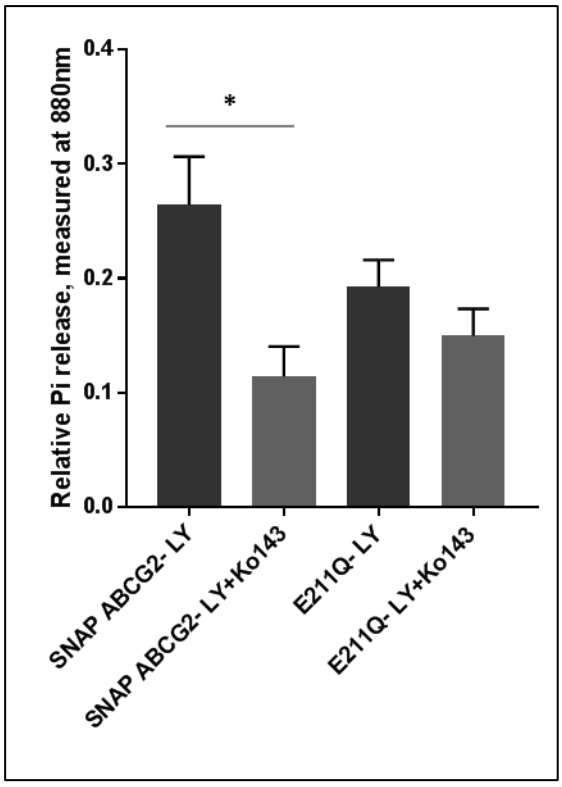


Figure 6.12: ABCG2 specific ATPase activity

Crude membranes (20µg protein) were incubated with lucifer yellow (100µM) in the absence (dark grey) or presence (light grey) of Ko143 (1µM), subjected to 5mM Mg.ATP. The results show ABCG2 specific ATPase activity where inorganic phosphate (Pi) release is measured as a colorimetric determination of phosphomolybdate complex formation. Only wild type ABCG2 shows Ko143 inhibitable Pi release ($p<0.05$).

The assay was further used to screen the mutants for their catalytic properties (figure 6.13). The assay was developed to investigate drug binding and ATP hydrolysis and the cooperativity between the processes in the catalytic cycle. Drug efflux assays of D929A and D292K mutants showed highly reduced relative drug efflux for Mx and pheophorbide A, similar to E211Q (defective in ATP hydrolysis) (section 6.7). The failure to transport substrates by D292A/K could possibly be due to lack of ATP hydrolysis. E285K showed enhanced relative Mx, pheophorbide A and daunorubicin export (section 6.7). Whole cell membranes were prepared for the above-mentioned mutants from large scale cell cultures and investigated for their ATPase activity with a fixed concentration of drug, LY in the presence or absence of Ko143. An ideal control to monitor ABCG2 specific ATP hydrolysis was also used to compare the interesting mutants with the catalytically inactive control E211Q (figure 6.13).

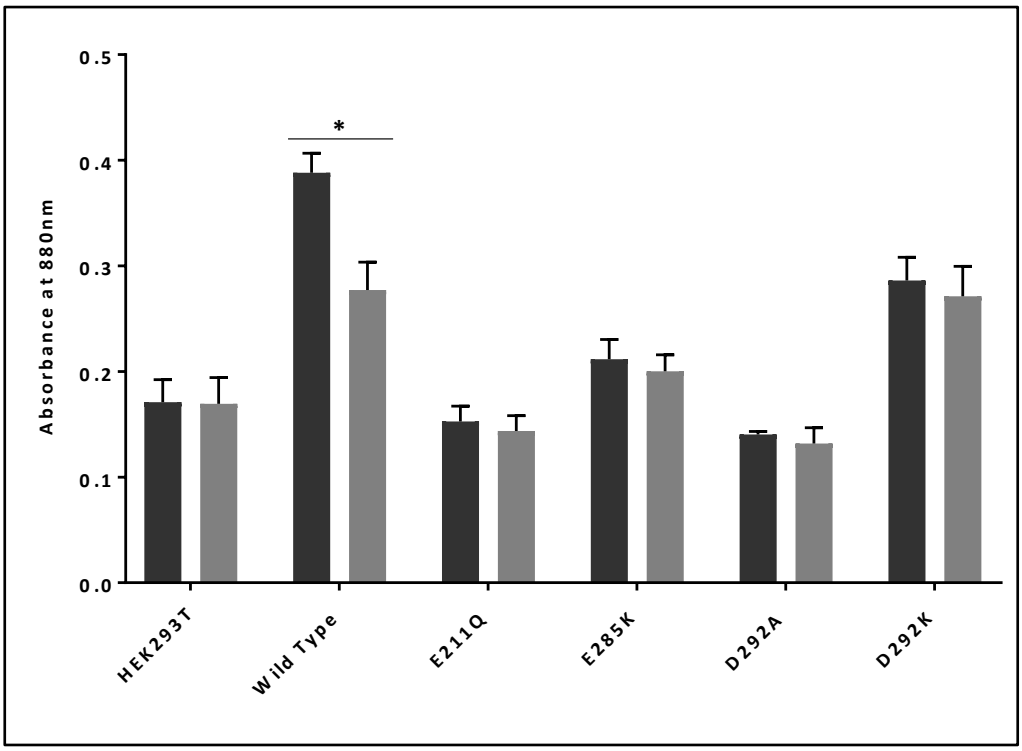


Figure 6.13: ATPase activity for key NBD interface mutants with altered transport capacity
Crude membranes (20µg protein) were incubated with lucifer yellow (100µM) in absence (dark grey) or presence (light grey) of Ko143 (1µM), subjected to 5mM Mg.ATP. The results show ABCG2 specific ATPase activity where inorganic phosphate (Pi) release is measured as a colorimetric determination of phosphomolybdate complex formation. Only wild type ABCG2 shows Ko143 inhibitable Pi release ($p<0.05$), demonstrating ABCG2 specific Pi release.

Membrane preparations from different cell lines displayed different levels of ATPase activity, therefore we tried to identify the mutants with Ko143 inhibitable activity rather than comparing one mutant's activity with the other (figure 6.13). The negative control membranes (HEK293T; membranes not expressing ABCG2 and E211Q; catalytically inactive mutant) showed no Ko143 inhibitable Pi release. HEK 293T membranes expressing ABCG2 (WT) showed much higher relative Pi release compared to the controls which was significantly inhibited by Ko143 (figure 6.13, $p < 0.05$). NBD interface mutants D292A and D292K failed to show any Ko143 inhibition of Pi release, like the well characterised catalytically inactive mutant (figure 6.13). Thus, confirming these two mutations prevent ATP hydrolysis by ABCG2, resulting in abrogation of transport in cell-based assays.

E285K mutant isoform, which has shown to be a gain in function mutation for Mx, pheophorbide A and daunorubicin transport (section 6.7), shows slightly higher Pi

release in presence of LY and LY + Ko143, with very negligible decline in Pi release in presence of Ko143 (figure 6.13). This could be attributed to low turnover of the substrates due to lack of substrate specificity or variability in the expression levels across the membrane preparations.

The ATPase assay can be used to measure differences between wild type and mutant protein, but the variability in expression levels (figure 6.5) of the mutants limits the accurate interpretation and prediction of the ATPase activity.

Due to time constraints, only one potential substrate could be investigated. The assay needs to be optimised further to reduce the background in presence of the vehicle control to screen the mutants, adjusted for their variability in expression. Several drug substrates are known to have a more profound effect on ATPase activity, including the alpha-1 adrenergic receptor antagonist; prazosin (PRA) (Robey et al., 2003). Previous research suggested multiple binding sites within ABCG2 (Glavinas et al., 2007) (Özvegy-Laczka et al., 2005). This results in complex interactions with different substrates and inhibitors, creating diverse kinetic interactions. These findings collectively pose interesting questions regarding effects of different substrates, involving different binding sites, due to the nature of the substrates (hydrophobic to hydrophilic) and investigate whether the catalytic cycle is futile or not? Further investigations are needed to answer these questions.

6.9 Discussion and summary

High resolution structures of ABCG5/G8 and ABCG2 revealed an unexpected constant contact NBD: NBD interface of ABCG family. A conserved motif; NPXDF (residues 289- 293 in ABCG2) and several other residues in close range cross interface interactions has been identified. Here we tested several point mutations for their effects on protein translocation, drug transport and ATP hydrolysis.

N288D showed dramatic effect on cell surface localisation with only 14% of the cells expressing this mutant on the cell surface. Subsequently, confocal microscopy on fixed cells treated with saponin also indicated cytoplasmic retention of the protein, most likely in the endoplasmic reticulum, suggesting that the protein was not being trafficked to the cell surface.

Similar effects have been observed by some other mutant isoforms such as Q141K and I573A (located close to the glycosylated region), which are known to improperly fold and fail to localise on the cell surface (Haider et al., 2015; O. M. Woodward et al., 2009). L633A mutant, (located in the transmembrane helix 6b), demonstrated a reticulated patterning in its localisation, reflecting the altered maturation status of the protein, with effects on protein structure and/or folding (Dr. Megan Cox, PhD thesis, data unpublished). S441N, one of the naturally occurring SNP, expressed in HEK293 cells, transduced with recombinant baculovirus, showed intracellular localisation, based on (BXP-21 conjugated AF488) immunofluorescence staining and wide field microscopy. Presence of proteasomal proteolysis inhibitor increased cell surface protein expression, thereby reflecting on stability (Sjöstedt et al., 2017). This clearly indicated that the destabilisation effect causing a trafficking defect can arise due to direct (improper glycosylation) or indirect (allosteric) effects. The instability observed at the NBD: NBD interface could be due to introduction of two acidic groups very close to the NPXDF motif. Similar effect was observed in ABCG1, where mutating the adjacent N (Asn- Asp) resulted in impaired protein trafficking and function (Wang et al., 2013).

The importance of this unique interface in protein dynamics was further addressed through drug efflux assays. E285K showed higher relative transport for both Mx and pheophorbide A and also a significant transport of the non-wild type substrate, daunorubicin. Only known residues to confer daunorubicin transport are 482 (TM3), 523 (TM5) and 640 (TM6). This indicates the role of several residues on altered substrate specificity, as a result of allosteric communications outside the substrate/ inhibitor binding cavity (Cox et al., 2018; Ejendal et al., 2006; Robey et al., 2003; Taylor et al., 2017). The charge reversal of residue E285K suggests hitherto an unexpected role of the ABCG-family specific NBD interface in transport substrate recognition. Negatively charged residues in ICL1 are known to be critical for regulating ABCG2 function (Khunweeraphong et al., 2017). Mutation studies involving E451A/R and E458A/R/D showed complete abolition of protein expression and Mx efflux. The study proved the importance of E451 located at the membrane-cytoplasmic border after TM2, in ABCG2 ATPase activity and function. (Khunweeraphong et al., 2017). D477A and D477R are also known to show no Mx efflux or ATPase activity, whereas D477E showed normal function and targeting, including the ATPase activity, thereby suggesting the importance of the negative

charge at position 477 for ABCG2 function (Khunweeraphong et al., 2017). We confirmed the D477A mutation reduced Mx and PheoA transport (chapter 5, figure 5.9 A and B).

The phenotypic effects observed for residues Y247 and E285 that reside outside the NPXDF motif indicates that not only residues within the highly conserved G family motif but also residues that reside in short range cross interface contribute towards the constant contact interface.

E285K mutant which has been shown to be a gain in function mutation for Mx, pheophorbide A and daunorubicin transport (section 6.7), showed no Ko143 inhibitable Pi release (figure 6.13). Certain compounds, known to be transported by ABCB1 do not stimulate the vanadate sensitive ATPase activity of the crude membranes, thereby suggesting a low turnover of these compounds that does not reflect a detectable amount of Pi (Glavinas et al., 2007). Therefore, E285K might reflect on the low turnover of the substrates with lack of substrate specificity. This could also reflect on the multiple binding sites observed for ABCG2, as the compound used to study the ATPase activity turnover is a hydrophilic compound; LY as opposed to the hydrophobic compounds used to investigate the drug efflux capacity (Clark et al., 2006) (Ejendal et al., 2006). This might suggest that E285 does not interact with hydrophilic substrates, thereby reflecting on no Ko143 inhibitable Pi release. Alternatively, some ABC transporters (e.g. MsbA and LmrA) have shown substrate transportation in the absence of the nucleotide binding cassettes *via* a proton coupled mechanism (Singh et al., 2016) (Venter et al., 2003). There are certain mutants known in P-gp (for example L339C) that uncouple ATPase activity from substrate transportation (Rothnie et al., 2005). It will be interesting to investigate whether the transport deficient ABCG2 mutant isoforms undergo conformational changes during the catalytic cycle or is the substrate bound but not translocated.

E285 residue, a part of the close contact interface residues shows potential inter and intra molecular interactions (<5 Å) with other close contact interface residues N288 and Y247 and with F293 within the NPXDF motif respectively, which is critical for NBD: NBD interface interactions. E285K shows gain of function for the above tested compounds with basal level ATP hydrolysis. Mutating E285 to amino acids with hydrophobic side chains such as leucine, isoleucine or methionine could help understand the critical role of E285 in the catalytic cycle. A double mutant could be generated with the potential intra molecular interacting residues N288 and F293 or

inter molecular interacting residue Y247 (residues crucial for protein expression, stability and function) to better elucidate the critical role of NBD: NBD interface in allosteric drug transportation to better understand the mechanism of transporter functionality (figure 6.14).

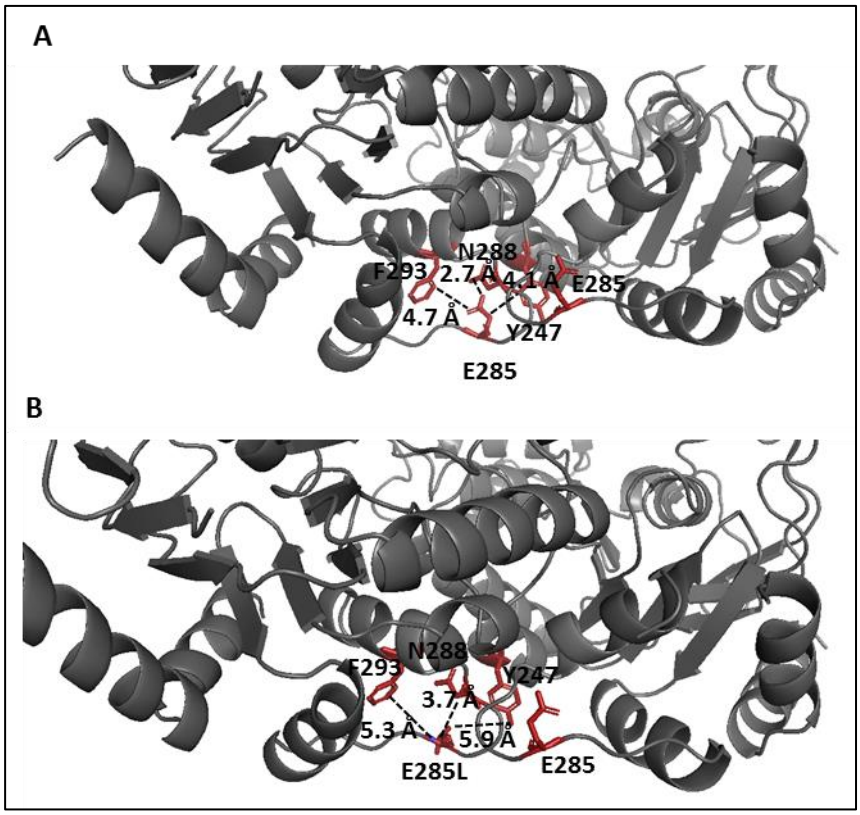


Figure 6.14: NBD close contact residue E285 and its potential intra and inter molecular interactions

The ABCG2 NBD homodimer cryo-EM structure has been depicted. A) Mapped E285 residues (red stick representation) on the NBD homodimer and its potential interactions (<5 Å) with Y247 (4.1 Å), N288 (4.1 Å) and F293 (4.7 Å). B) Potential intra and inter molecular contacts of E285L with Y247 (5.9 Å), N288 (3.7 Å) and F293 (5.3 Å) respectively. Figure generated in PyMOL software using PDB ID: 6ETI; (Jackson et al., 2018).

Mutations within the NPXDF motif are D292A/K that showed cell surface localisation but were defective in drug transport and ATP hydrolysis. This could be attributed to the replacement of acidic functional group affecting the NBD: NBD interaction causing conformational changes, thereby affecting the catalytic cycle. These mutant isoforms did not show Ko143 dependent Pi release, indicating the importance of the NPXDF motif in binding and hydrolysis of nucleotides.

These data suggest that the NBD: NBD constant contact interface is crucial for ATP hydrolysis and NBD: TMD communication. Further structural and functional analyses are critical to better understand the transport mechanism.

Chapter 7: Discussion and future work

7.1 Summary of results

The aim of the project was to understand the molecular mechanism behind drug binding and translocation by ABCG2. ABCG2 transports a diverse array of structurally unrelated compounds. Despite this fact, the structural basis of multidrug transport remains elusive. To understand the mechanism of drug translocation the project was divided into two parts. The first part of the project involved understanding the role of the third TM helix in drug selectivity and translocation. The hypothesis was based on previous research that indicated the importance of R482 and P485 (within the TM3 helix) to drug binding and/ or translocation. The two residues are one helical turn apart, where the nature of the residue at position 482 has shown to alter the substrate repertoire whereas P485 substitution has shown to reduce the substrate transportation (Clark et al., 2006; Haider et al., 2015; Robey et al., 2003). This made us consider whether TM3 helix would harbour further residues of interest that could potentially influence substrate specificity and selectivity.

In this study, 20 TM3 helix point mutations were generated. Mutation to alanine is torsionally neutral, retains the propensity to form alpha helical structures and is therefore unlikely to affect protein folding. None of the mutations dramatically altered protein targeting to the plasma membrane (chapter 4). Chapter 5 shed light on the functional importance of TM3 helix residues using cell-based drug fluorescent assays. The mutant isoforms showed perturbed function for drug transportation compared to the wild type. The data shows that many single alanine mutant isoforms showed altered phenotypic effects for Mx transport. Key residues with altered phenotypic effects included D477 and S486, which showed reduction in Mx and pheophorbide A efflux capacity compared to the wild type, consistent with a simultaneous publication regarding this residue from the Kuchler group (Khunweeraphong et al., 2017). As has already been published in literature, R482A showed a gain in function for transportation of a non-wild type substrate; daunorubicin, supporting a role for TM3

in drug selectivity (Cox et al., 2018; Ejendal et al., 2006; Robey et al., 2003). Three adjacent residues, F489, T490 and C491 all showed perturbation of drug transport when mutated to alanine. The recognition and transport for Mx and pheoA may share structural features as many mutations have been identified to have similar effects on their transport, compared to daunorubicin transport. M496A is the only point mutation that showed a significant increase in drug transportation (Mx). This residue may play a key role in drug recognition as the residue faces the lipid surface and conformational changes may contribute towards the allosteric effects, facilitating hydrophobic drug translocation (Cox et al., 2018). The three fluorescent compounds were subsequently docked on the cryo-EM structure of ABCG2. The study helped identify a putative drug binding site, referred to as a groove site aligned by helices TM1b, 2 and 3 for the three fluorescent substrates.

The next aspect of the project explored a unique element of the ABCG family, namely the NBD: NBD interface. Transport function of the protein minimally requires the interaction of two ABCG2 monomers to form a dimer. Emerging structures of ABCG family proteins showed an apparent constant contact of the NBDs (Jackson et al., 2018; Lee et al., 2016; Manolaridis et al., 2018; Taylor et al., 2017; Zaitseva et al., 2005), brought about by interaction of residues at the C-terminus of the NBD, including, but not restricted to, a highly conserved motif NPXDF (Hopfner, 2003; Jackson et al., 2018; Kerr, 2002; Lee et al., 2016; Manolaridis et al., 2018; Smith et al., 2002; Taylor et al., 2017). The second aspect of the project mutated a selection of residues (alteration of charge or size of the amino acid) at this interface that were involved in short range cross interface interactions.

Cell surface expression using confocal microscopy and flow cytometry proved majority of the mutant isoforms to localise on the cell surface as opposed to N288D isoform. N288D demonstrated immature protein expression with reduced glycosylation, which, when analysed by immunohistochemistry involving confocal microscopy, showed intracellular reticular retention of protein, indicating improper protein trafficking. This destabilisation effect could possibly be due to introduction of two acidic groups in close proximity to the NPXDF motif.

The importance of this interface was further demonstrated by certain residue mutations that showed gain in function in transport for wild type or non-wild type substrates. E285K showed higher relative transport for wild-type substrates Mx and pheophorbide A and also significant gain in transport for a non-wild type substrate daunorubicin.

D292A and D292K showed significant impaired function for Mx and pheophorbide A transport, possibly due to abrogation/ reversal of acidic functional group affecting the NBD: NBD interaction, bringing a drastic conformational change. Functional effects of residues outside of the NPXDF motif (E285, Y247 and N288) confirmed that the NPXDF motif is not the only contributor to the constant contact interface. To better understand the catalytic cycle of ATP hydrolysis and drug translocation, the functionally defunct mutations (D292A and K) were unable to detect Ko143 sensitive ATPase activity, indicating the importance of this interface for binding and hydrolysis of nucleotides. The data suggests that the NBD constant contact interface region contributes towards ATP hydrolysis and NBD: TMD communication and restates the need for further structural and functional elucidations.

7.2 Structural interpretation of drug binding by ABCG2

During the time this thesis was being carried out there was an explosion of structural research for ABCG2, starting with the publication of a structural model of ABCG5-G8, a close protein family member to ABCG2 (Lee et al., 2016). This structure revealed a novel fold for G family proteins and it was not long before the first homology model of ABCG2 based on the ABCG5-G8 structure was produced (Lászloá et al., 2016; Lee et al., 2016). With the advancement in cryo-EM detection systems and processing algorithms, the cryo-EM structural resolution revolution led to the development of ABCG2 structures in presence of cholesterol, Ko143 derivatives and a bona fide substrate estrone-1 sulphate (Jackson et al., 2018; Manolaridis et al., 2018).

The transmembrane domain in ABCG sub-family of transporters exhibits a new transporter fold with no domain swapping, reminiscent of the type II importer (Rice et al., 2014). The cryo-EM structure revealed notable features of TMH organisation. The intracellular loops are shorter, with no crossover from one TMD to opposite NBD. The coupling helix, located between TMH2 and TMH3, is the intracellular loop that couples the motions from ATP binding and hydrolysis in the NBDs to conformational changes in the TMDs. The transmembrane helix 1 is split into a and b; where TMH1a, also known as the connecting/ elbow helix lies interfacial to the lipid bilayer and forms part of a tri-helix bundle ‘connecting’ the TMD to the NBD (Khunweeraphong et al.,

2017; Lee et al., 2016). An interesting new fold is observed on the extracellular loop 3, located between TMH5 and TMH6, exhibiting a V shape, immersed partially in the bilayer, termed as a capping helix. This comprises residues from both TMH5 (b and c) and 6 (a)(Lee et al., 2016; Taylor et al., 2017). How does all this structural data help us to understand drug binding and transport?

To better understand the phenotypic effects observed in ABCG2 substrate translocation by the TM3 helix mutant isoforms, the data are rationalised against the structure, to shed light on the molecular mechanism behind drug recognition/ binding and translocation. Can we identify TM3 helix as the putative gatekeeper in (hydrophobic) drug recognition and translocation? Screening of mutant isoforms with the drug efflux assays established key residues associated with functional importance. The fundamental concept of sequence implying structure and structure implying function underpins the importance of mapping key residues of functional interests to provide a molecular explanation of the transporter functionality phenotypes observed. Molecular dynamic simulations and *in silico* docking by Lászloá et al. demonstrated four putative substrate binding sites, consistent with experimental determination of multiple drug binding sites (figure 7.1) (Clark et al., 2006; Lászloá et al., 2016). The work presented in chapters 4 and 5 is utilised as a framework for interpreting experimental data and designing new experiments. A number of residues investigated here demonstrated partial overlap with the aforementioned sites in the study by Lászloá et al. Site 1 contains D477 (TM3 helix) whereas site 2 contains contributions from residues of the lateral slice hypothesis (postulated that the residues located in the topologically equivalent positions to R482 and P485 of other transmembrane helices would be involved in substrate recognition and/or binding, investigated by Dr. Megan Cox, PhD thesis) and residues from TM3 (D477, L478, M481, R482, P485 and S486) and site 3 contains a large number of lateral slice residues (Cox et al., 2018; Lászloá et al., 2016). Site 2 represents a more defined pocket, contributing towards substrate selectivity. This is partially because of the presence of R482 which is known to exhibit strong effects on substrate selectivity (Clark et al., 2006; Haider et al., 2015; Robey et al., 2003). This also suggests the importance of TM3 and hence direct substrate binding assays could possibly pave the way to understand the key residues involved in drug translocation.

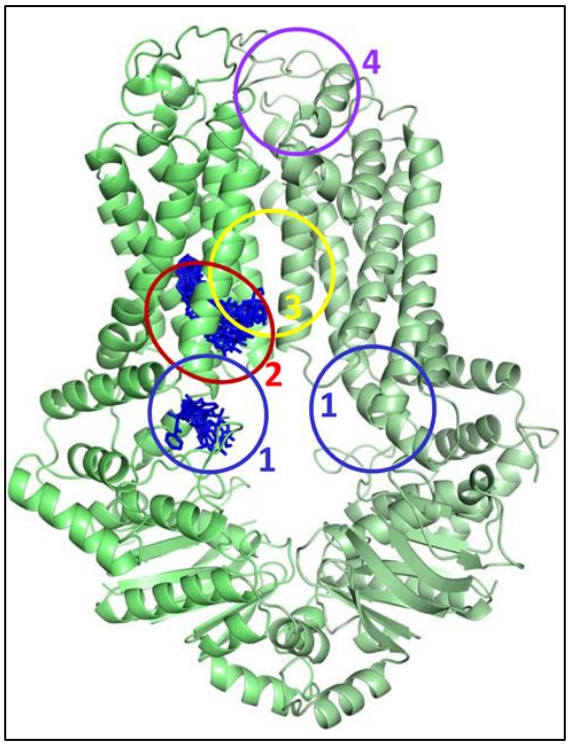


Figure 7.1: *In silico* docking studies reveal the potential substrate binding sites

ABCG2 conformation reflects on the potential docking poses for sulfasalazine (blue sticks) in the potential binding sites (sites 1,2,3 and 4). TM3 helix residues show an overlap with the more pronounced binding site 2 (D477, L478, M481, R482 and S486). Figure adapted from Lászloá, Sarkadi and Hegedüs, 2016.

Cryo-EM structural data of ABCG2, resolved to a near-atomic resolution (overall resolution between 3.1 and 3.8Å) in the presence of Fab complexes bound to the extracellular loop region, initially presented a structure in which cholesterol could be assigned to a region of electron density within a central cavity (figure 7.2B; similar to site 3 presented by Lászloá et al. (Lászloá et al., 2016; Taylor et al., 2017). Later structural publications from the same research group, presented a Ko143 (specific ABCG2 inhibitor) derivative (MZ29) bound in a 2:1 ratio (inhibitor molecule to protein dimer) or a tariquidar derivative (MB136) bound in a 1:1 ratio within the central cavity between TM2 of one monomer and TM5a of the opposing monomer (figure 7.2 A and B; Jackson et al., 2018). The improved structure, and the construction of a panel of Ko143 derivatives, will facilitate the understanding of structure activity relationships for ABCG2 inhibitors.

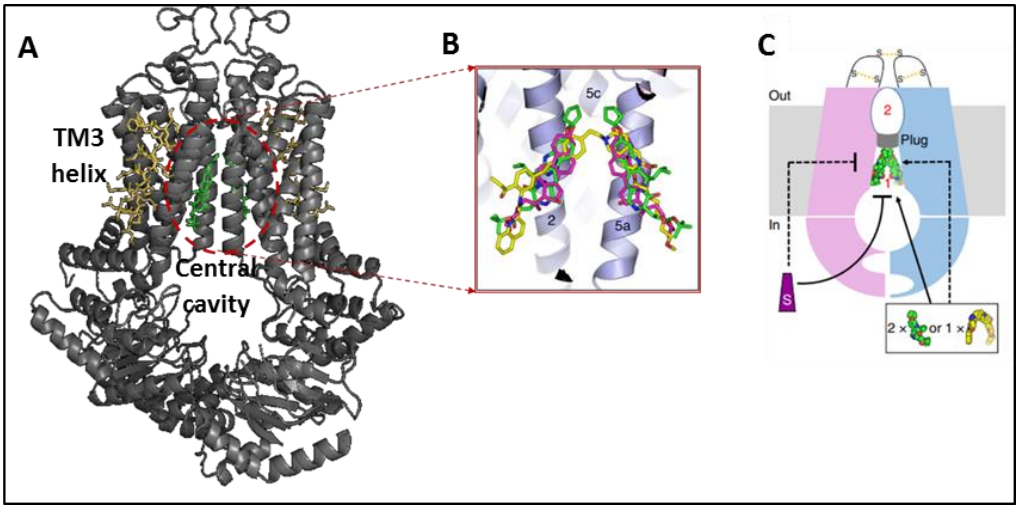


Figure 7.2: Cryo-EM structure of ABCG2 with bound compounds in the central cavity (cavity 1) A) Ribbon representation of ABCG2 homodimer (grey), with bound Ko143 derivative; MZ29 (green stick representation) in the central cavity (cavity 1). The TM3 helix residues facing the membrane periphery have been highlighted (orange yellow stick representation). Figure generated in PyMOL. B) Magnified region of the central cavity showing MZ29 (green) bound in a 2:1 ratio, a tariquidar derivative: MB136 (yellow), bound in a 1:1 ratio, and cholesterol docked (pink) after superposition of ABCG2 TMDs from three structures. Figure adapted from Jackson et al., 2018. C) Schematic representation of ABCG2 homodimer inhibition in a transport cycle. The central cavity 1 and cavity 2 (upper cavity) have been numbered (red). Binding of two MZ29 molecules (green spheres) or one MB136 molecule (yellow spheres) locks the ABCG2 conformation in the inward facing open state. This may prevent the substrate binding/ selectivity to reach cavity 1 and hence be translocated.

Cox et al. proposed the putative binding sites for Mx in two distinct areas of TMD; a surface site, exposed to the inner leaflet of the membrane (encompassing several of the residues investigated as part of the 'lateral slice' hypothesis) and a second buried site (figure 7.3) with a significant contribution from TM3, 1b, 2 and 4 helices (Cox et al., 2018). Our biochemical data (chapter 5) also represents many alanine mutations within TM3 helix that show significant changes to Mx transport (listed above). This is in accordance with Locher et al., where they show the access to the central cavity (cavity 1) through the membrane (dashed arrows), that is the proposed access of hydrophobic sites (surface or buried site, according to Cox et al.) to the cavity 1. The surface or buried site (surrounded by the residues of TM3 helix), proposed by Cox et al. might be a part of the path for the substrates from the membrane to the central cavity (dashed arrow, figure 7.2 C). A number of residues from TM3 helix investigated here have demonstrated partial overlap with the aforementioned sites proposed by Lászloá

et al. (site 2- D477, L478, M481, R482 and S486) and Cox et al. (buried site- D477, L478, M481, R482, P485, S486, I488, F489 and T490).

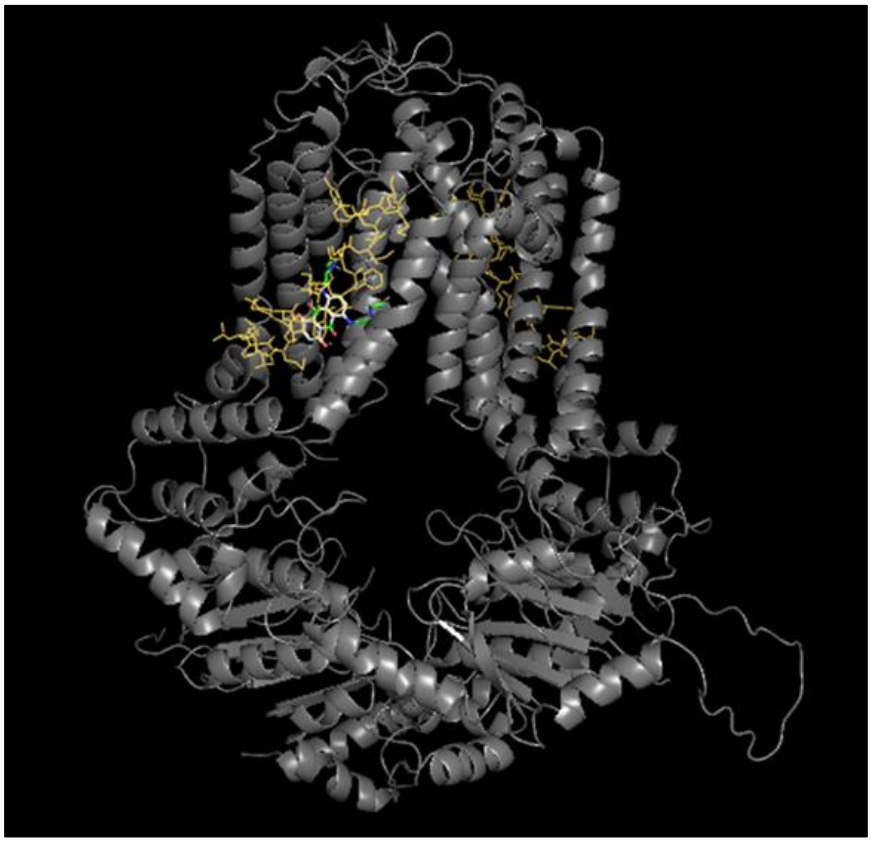


Figure 7.3: TM3 helix as a putative gatekeeper for hydrophobic drugs

A buried site for Mx (stick representation) was identified in close proximity to TM3 (yellow stick representation) using Autodock Vina, TM1b, TM2 and TM4. Figure generated in PyMOL. Figure adapted from Cox et al., 2018.

The distance between the buried site and surface site is estimated to be approximately 15 Å apart, thereby forming a putative translocation pathway (Cox et al., 2018). Is this a potential drug translocation pathway adopted by ABCG2 in lieu of the central cavity and the leucine plug model proposed by the cryo-EM structures? Docking studies have also been performed on the cryo-EM structure that resulted in discovery of a putative drug binding site in close proximity to TM3 helix, referred to as a groove site, aligned by TM helices 1b, 2 and 3. Three key residues (R482, P485 and F489, overlap with the drug binding site 2 identified by Lászloá et al.) have shown potential interactions with the hydrophobic substrates (< 5Å), as described in chapter 5. The putative buried site and the groove site identified based on docking studies could potentially form the translocation pathway for the hydrophobic compounds leading to the central cavity

and subsequent export of the substrates as described by the leucine plug model in the next section.

Advanced biophysical characterisation techniques are needed to identify the exact binding sites, which have been detailed in section 7.4. Could the buried site be the entry point for diverse hydrophobic substrates transported by ABCG2? Is it right to call TM3 helix as the putative gatekeeper for drug entry? There is evidence in the literature that support the access of substrates through the lipid bilayer. ABCB1 and AcrABTolC are known to have access to the potential substrates through the lipid: protein interface (Ferreira et al., 2015; Mittra et al., 2017; Nakashima et al., 2011; Pleban et al., 2005).

7.3 Structural interpretation of drug transport by ABCG2

How substrates are translocated by ABCG2 is open for debate. Our results and structural advances in the ABCG family allow us to formulate a transport mechanism consistent with the available biochemical data. The cryo-EM structure proposes the leucine plug model for substrate translocation. Locher et al. proposed a peristaltic motion model of transport in which substrates bind within the central cavity (occluded from cavity 2; upper cavity) and then translocate to a secondary 'upper' cavity via a 'leucine plug' (L554 and L555), for substrate release (figure 7.2 C). They were able to show electron density consistent with cholesterol and concluded that the central cavity is a multi-drug binding site for ABCG2 (Jackson et al., 2018; Taylor et al., 2017).

Later, a high resolution cryo-EM structure of ABCG2 in a substrate bound, pre-translocation state was identified. The E211Q mutant of ABCG2 was used for conformational trapping of the pre- and post- translocation states. A single molecule of estrone-3-sulfate (E_1S) bound in the central, hydrophobic cavity was observed (Manolaridis et al., 2018). In the ATP bound state, the central cavity is collapsed, facilitating the movement of the substrate through the leucine plug into cavity 2 (Manolaridis et al., 2018).

Leucine at position 555 has been experimentally investigated, as the residue forms part of a putative steroid-binding element (SBE). A leucine to alanine mutation at position 555 did not demonstrate any structural (expression maintained) or functional perturbation (vanadate-sensitive ATPase activity reduced (crude membranes),

however drug transport retained in intact cells, measured using flow cytometry), inconsistent with the results expected for a residue with a key role in structure and transport (Telbisz et al., 2007). In contrast, Locher et al. observed a structural role of L555 in addition to a likely gating function. L555A mutations did not express any functional protein. The L554A mutant showed functional differences compared to the wild type protein (increase in basal ATPase activity, E_1S stimulated ATPase activity (approximately 20%) and an increase in EC_{50}). L554 showed double increase in E_1S transport activity. Therefore, they suggested that leucine plug may act as a check point and facilitate substrate selectivity (Manolaridis et al., 2018).

Based on the above contradictory statements, we still do not understand the role of the leucine plug. The central cavity observed through the cryo-EM data includes some residues demonstrated to affect substrate specificity or transport (e.g. M549 and I543). There are many other residues which have significant effects on transport function but which lie outside of cavity 1 (e.g. R482 and M496 in TM helix 3, and residues 523, 540, 548 and 640 among other TMs) (Cox et al., 2018; Ejendal et al., 2006; Haider et al., 2015; Robey et al., 2003).

Kapoor et al. have proposed a hypothetical mechanism for drug translocation with some parallels to the alternating access models for ABC exporters (figure 7.4). ABCG2 possesses three distinct drug interaction sites; a surface access site (in close proximity to TM3 helix), a binding site (consistent with the structural 'cavity 1') and an extrusion site (consistent with the structural 'cavity 2') (Kapoor et al., 2018). The surface access site includes residues with significant contributions from TM helices 3, 1b, 2 and 4 (Q398, V401, T402, L405, L433, N436, F439, S440, S443, L447, D477, L478, M481, R482, P485, S486, I488, F489, T490, M510, L513, M514, V516, A517 and S521), based on the putative binding site for Mx observed by Cox et al. through docking studies (figure 7.3 and 7.4 E) (Cox et al., 2018). The surface access site shows overlap with the groove site observed through docking studies, explained in section 5.5. The binding site (cavity 1) includes residues from helices 2 (F432 and F439) and 5a (M549, V546, I543 and L539) respectively (figure 7.4 E). The extrusion cavity is the cavity 2 that includes residues from the capping helix (TM 5b, 5c and 6a; figure 7.4 E) (Cox et al., 2018; Jackson et al., 2018; Taylor et al., 2017).

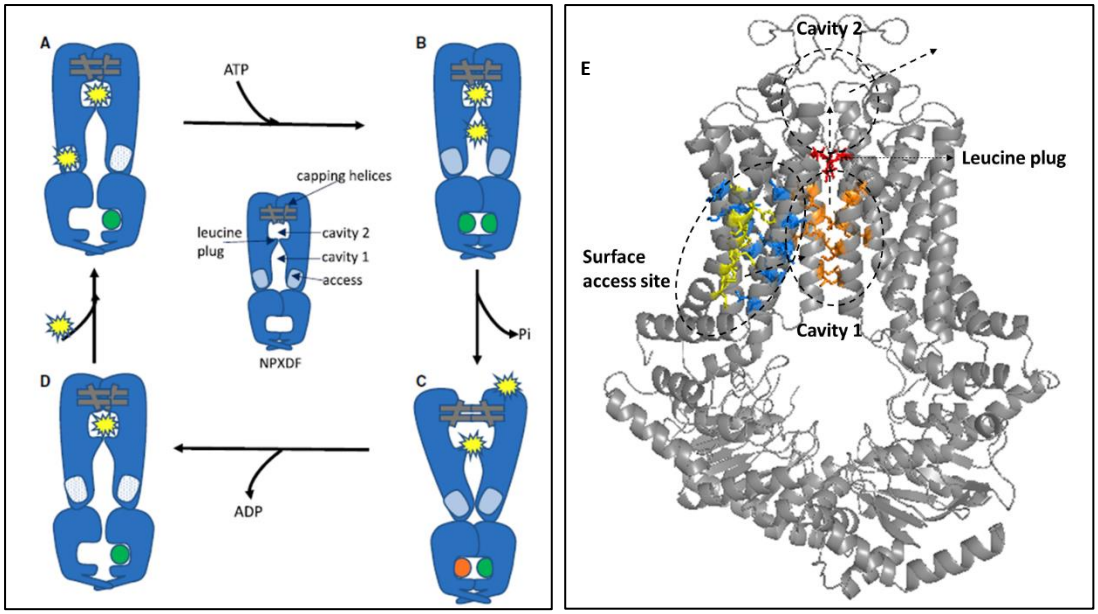


Figure 7.4: ABCG2 catalytic cycle for drug translocation

Schematic representation of the ABCG2 transport catalytic cycle for drug translocation. Drug (yellow) binding to the access site (A) promotes ATP (green) binding and the formation of the classical NBD sandwich dimer (B). The cross talk between the NBDs and TMDs results in the transfer of drug from the access site to cavity 1, and the occlusion of the access sites. ATP hydrolysis (C) promotes an outward open TMD conformation in which the leucine plug and the capping helices undergo structural changes allowing drug extrusion from cavity 2. ADP (orange) release (D) results in resetting of the transporter. Figure adapted from Kapoor et al., 2018. E) ABCG2 structure with the putative translocation site residues mapped, surface access site residues (stick representation; blue and yellow (TM3 helix residues)), cavity 1 (orange stick representation), leucine plug (red stick representation) and cavity 2 (extrusion site), involving the capping helix. The dashed arrow depicts the potential translocation pathway. Figure generated in PyMol (PDB ID: 6ETI).

As stated above, access to cavity 1 for transported substrates may be controlled by the surrounding TM helices TM2 and TM3 which permit access to cavity 1(access sites). As is evident from our biochemical studies, TM3 helix residues show altered phenotypic effects for hydrophobic drug export. Mutations to the intracellular end of TM3 helix show altered substrate specificity (example, R482 for daunorubicin transport). R482 is located 9Å away from the substrate binding pocket (central cavity) and forms hydrogen bonds with S521 (TM4). This might suggest the role of allosteric effects on substrate specificity (Taylor et al., 2017). Recent biochemical and modelling data from Karl Kuchler's laboratory add molecular detail to this hypothesis by proposing that a series of charged and polar residues at the TMD:NBD interface (which includes the ICL1 between TM2 and TM3) act as an allosteric conduit ('polar

relay') between the NBDs and TMDs, with ICL1 acting as a molecular spring to couple the two domains (Khunweeraphong et al., 2017). We are tempted to speculate that the 'molecular spring 'alters the exposure of the access site by changing the angle of kinking in TM3, consistent with the critical role identified for the kink-inducing proline 485 residue (Haider et al., 2015; Ni et al., 2011). Hence, the TM3 helix could act as a putative gatekeeper for drug translocation, but further investigations are needed to substantiate this hypothesis. The altered phenotypic effects observed for drug translocation by NBD interface residues (example, E285K for Mx and daunorubicin transport), also emphasise the importance of allosteric communications during the conformational change leading to substrate translocation.

We still do not understand the mechanism for substrate selectivity. The above hypothesis provides an explanation for hydrophobic substrate recognition and translocation. How are hydrophilic substrates (example, Lucifer yellow) transported? How are certain substrates transported and inhibitors not? More structural data in the presence of transport substrate at various stages of the catalytic cycle are needed to decipher the translocation pathway. This will help comprehend the molecular description of substrate binding and transport by ABCG2. How this data can be used for drug discovery is a whole new chapter. There are still a lot of unanswered questions that require further investigation through mutagenesis studies using the new structures as a framework for the design of new experiments and data interpretation. The development of techniques to monitor direct drug binding interactions are also crucial (section 7.4).

7.4 Deciphering the molecular mechanism of ABCG2 using purified protein

The discussion above indicates further research is needed to fully understand ABCG2 mediated drug transport. At the heart of this is the need to separate out analysis of drug transport, which includes multiple events, and focus purely on drug binding. A number of lines of investigation are on-going, primarily using purified protein to understand the potential drug binding sites. A key step towards achieving this is to use detergent free solubilisation of membrane proteins by styrene maleic acid copolymers (SMA). It inserts into a bilayer and assembles into discrete particles, solubilising the membrane

into small discs of bilayer (native lipid bilayer) encircled by a polymer, known as styrene-maleic acid copolymer lipid particles (SMALPs) (figure 7.5 A) (Gulati et al., 2014; Morrison et al., 2016). SMA 2000 (2:1 ratio of styrene to maleic acid with an average molecular mass of 7.5 kDa) is known to be the best in terms of solubilisation efficiency, purification yield, purity and protein function (Morrison et al., 2016). The Kerr lab has successfully managed to use SMALPs to isolate ABCG2 from a mammalian expression system (HEK293T) and characterise the stoichiometry of ABCG2 complexes and the pharmacology of their substrate binding using fluorescence correlation spectroscopy (FCS). DLS (differential light scattering) and FCS have confirmed ABCG2 was extracted as a dimer into single SMALP particles of 10-20nM diameter with <5% aggregation. (Dr. Aaron Horsey, PhD thesis 2019).

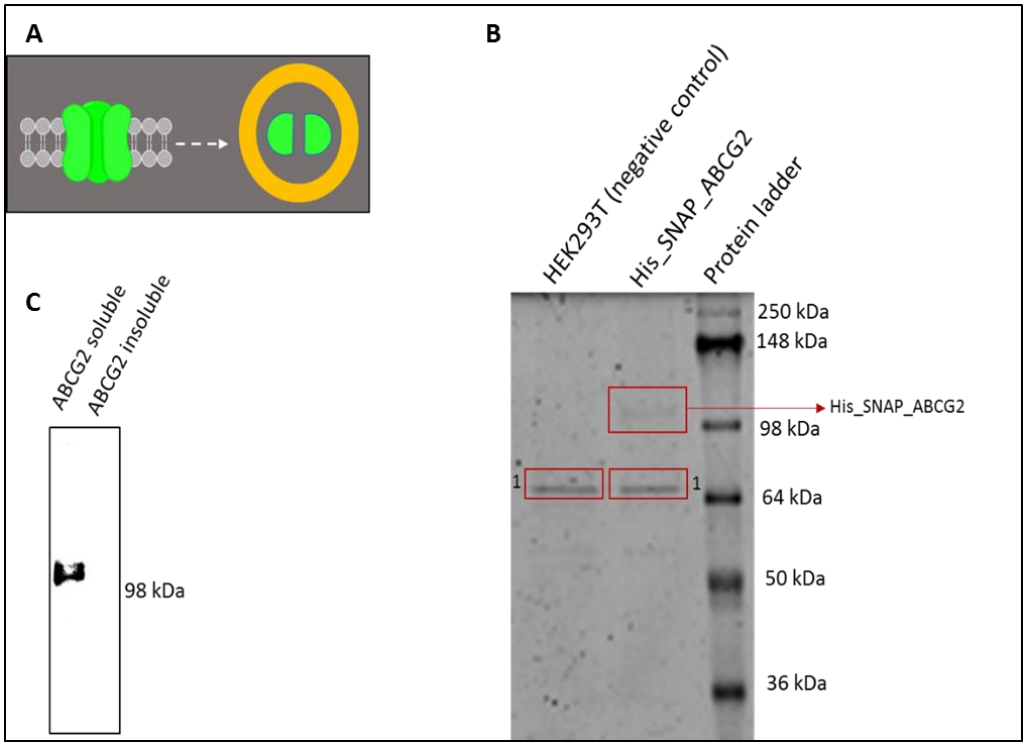


Figure 7.10: ABCG2 SMA solubilisation and purification

A) SMALPS solubilise membrane proteins, isolating them as small discs of lipid bilayer surrounded by the SMA polymer. B) Western blot to depict SMA solubilised ABCG2 membranes. C) ABCG2 (His_SNAP_ABCG2) purified protein run on 10% w/v polyacrylamide gel, with pure protein faintly visible at approximately 100kDa. The gel clearly depicts the presence of a strong contaminant band (red box, 1) in both, the negative control and purified protein.

Extraction of ABCG2 from larger scale HEK293T membrane preparations (HEK293T cells adapted to suspension cell growth by Dr. Aaron Horsey) facilitated purification

of SMALP-ABCG2 by immobilised metal ion affinity chromatography at concentrations of up to 60 nM (figure 7.5 C). The yield of protein obtained was not sufficient to perform direct drug binding assays using intrinsic tryptophan (Trp) quenching. The sole attempt of the assay did not distinguish between ABCG2 and the negative controls (data not shown). The purified protein also showed presence of a strong contaminant protein purified alongside ABCG2 (figure 7.5 C). The contaminant protein was identified using mass spectrometry (Cambridge Centre for Proteomics) to be BSA that could potentially come from the growth medium. The SMALP solubilised and purified ABCG2 protein obtained is not sufficient enough for several of the biophysical and biochemical characterisation studies to better understand the molecular mechanism of drug binding and transport. Hence, further optimisation is needed to increase the total yield of the pure protein using alternative expression strategies such as the Baculovirus mediated gene transduction of mammalian cells (BacMam) for rapid recombinant membrane protein expression, scaling up the suspension culture volume, altering the temperature for protein expression, cell sorting to facilitate the growth and maintenance of high ABCG2 expressing cells. Cell sorting was performed on wild type sfGFP_ABCG2 to separate the mixed population by gating for high GFP_ABCG2 expressors using flow cytometry. Maintenance of top 1% population sfGFP_ABCG2 sorted cells over a couple of passages led to reversion to a mixed population (data not shown). The current optimisation needed is beyond the scope of this PhD. The work is being undertaken by the postdoctoral researcher Dr. James Mitchell (Kerr lab).

SMALPs have solved some issues that have historically afflicted detergent-based systems, yet there are a number of factors that need to be taken care of in order to obtain successful solubilisation of ABCG2. SMA is pH sensitive and an effective chelator of divalent cations (Ca^{2+} and Mg^{2+}) (Dörr et al., 2016; Morrison et al., 2016). This leads to a major drawback as it limits our understanding of the ABCG2 catalytic cycle using the SMALP solubilised and purified ABCG2. Reconstitution from the lipid discs into proteoliposomes, MSPs (membrane scaffold proteins) or using polymers with reduced Mg^{2+} sensitivity (e.g. DIBMALPs) might help address the underlying question on the catalytic cycle.

The key mutant isoforms of ABCG2 (TM3 helix and NBD interface) identified through this project that have shown to contribute towards understanding the translocation pathways and potential multiple drug binding sites can be investigated

further by using SMALP solubilised and purified ABCG2 in direct drug binding assays described below. The application studies would assist in distinguishing changes in transport activity or initial drug binding. The key mutant isoforms can also be screened for drug binding using *in silico* docking studies, involving single point mutation models, which is beyond the scope of this PhD.

This project will facilitate understanding of the direct binding of molecules to the ABCG2 transporter using microscale thermophoresis (MST; Nanotemper technologies) (Jerabek-Willemsen et al., 2014). This technology is a powerful tool used to quantify biomolecular interactions. MST measures the change in the hydration shell of the biomolecule under a microscale temperature gradient generated using infrared lasers. The ABCG2 mutant isoforms will be extracted along with the native lipid environment in SMALPs (Gulati et al., 2014) and further subjected to purification by nickel affinity chromatography. The purified protein still in its native lipid environment will then be subjected to MST technology in order to understand the contribution of individual residues in the drug binding pocket of ABCG2 involved in drug transport. This technique would enable researchers to separate allosteric interactions from direct substrate interactions and gain a better picture of the transport mechanism.

Further attempts are being made in the lab to use fluorescent probes with ABCG2 in lipid nanodiscs using fluorescence correlation spectroscopy. This would enable studying ABCG2 interactions with substrates and inhibitors. It measures fluctuations in fluorescence, based on the movement of fluorescent particles in and out of the defined confocal volume and reveals information on the concentration and diffusion coefficient of the particles in the volume (Elson, 2011). The development of this overall platform would facilitate future studies of the mechanisms of ABCG2 substrate recognition and provide an improved toolset for assessing substrate/inhibitor interactions perhaps in the context of screening and drug design processes. The method development is under way by Dr. James Mitchell (Postdoctoral research).

This project also seeks to establish a novel method for investigating drug binding sites on a membrane transporter through mass spectrometry "footprinting". This part of the research will use wild-type ABCG2 solubilized in SMALPs and purified using affinity chromatography. The purified ABCG2 will then be subjected to a non-specific labelling with diazirine reagent to label expose residues in ABCG2 using near-UV wavelength irradiation (Manzi et al., 2016). Comparison of labelling patterns in the

absence and presence of transported drug substrates will form the basis for the residues that are contributing to the binding site for that substrate.

An intrinsic tryptophan quenching assay can be performed to study substrate binding. A comprehensive study on the intrinsic fluorescence properties of purified, catalytically active ABCG2 in its native state can be used to monitor direct drug binding. Sonveaux et al. have reported data for quenching purified P-gp with iodide ion and used changes in acrylamide quenching susceptibility as an indicator of conformational changes taking place on binding of nucleotides and substrates (Liu et al., 2000).

7.5 Conclusion

This PhD project was set out to investigate the molecular basis of drug binding (specificity and selectivity) and translocation by ABCG2. The project confirmed that several of the investigated residues have significant roles in the transport mechanism of ABCG2, as presented in Cox et al., 2018 and Kapoor et al. 2020. The research study postulates the basis of polyspecific interactions of ABCG2 with diverse hydrophobic compounds which may provide an opportunity, along with structural advancement, to model drugs and inhibitors in the binding cavity and pave the way towards structure-based drug and inhibitor design. There is significant scope for further investigation of the hypotheses developed during this project that is being taken forward by Dr. James Mitchell through the BBSRC funded postdoctoral project "Channelling a path for substrates through a multidrug transporter". Recently, ABCG2 cryo-EM structure revealed the binding mode of chemotherapeutic drugs mitoxantrone, SN38 and imatinib. The study has paved the way to understand the conformational catalytic cycle (Orlando and Liao, 2020). There are still several unanswered questions that require further investigations and hence will be interesting to follow up in future.

References

Abolhoda, A., Wilson, A.E., Ross, H., Danenberg, P. V., Burt, M., Scotto, K.W., 1999. Rapid activation of MDR1 gene expression in human metastatic sarcoma after in vivo exposure to doxorubicin. Clin. Cancer Res. 5, 3352–6.

Adachi, Y., Suzuki, H., Schinkel, A.H., Sugiyama, Y., 2005. Role of Breast Cancer Resistance Protein (Bcrp1/Abcg2) in the Extrusion of Glucuronide and Sulfate Conjugates from Enterocytes to Intestinal Lumen. Mol. Pharmacol. 67, 923–928.

Allen, J.D., Brinkhuis, R.F., Wijnholds, J., Schinkel, A.H., 1999. The mouse Bcrp1/Mxr/Abcp gene: amplification and overexpression in cell lines selected for resistance to topotecan, mitoxantrone, or doxorubicin. Cancer Res. 59, 4237–41.

Allen, J.D., van Loevezijn, A., Lakhai, J.M., van der Valk, M., van Tellingen, O., Reid, G., Schellens, J.H.M., Koomen, G.-J., Schinkel, A.H., 2002. Potent and specific inhibition of the breast cancer resistance protein multidrug transporter in vitro and in mouse intestine by a novel analogue of fumitremorgin C. Mol. Cancer Ther. 1, 417–25.

Aller, S.G., Yu, J., Ward, A., Weng, Y., Chittaboina, S., Zhuo, R., Harrell, P.M., Trinh, Y.T., Zhang, Q., Urbatsch, I.L., Chang, G., 2009. Structure of P-glycoprotein reveals a molecular basis for poly-specific drug binding. Science (80-.). 323, 1718–1722.

Allikmets, R., Schriml, L.M., Hutchinson, A., Romano-Spica, V., Dean, M., 1998. A human placenta-specific ATP-binding cassette gene (ABCP) on chromosome 4q22 that is involved in multidrug resistance. Cancer Res. 58, 5337–9.

Ambudkar, S. V., 1998. [37] Drug-stimulatable ATPase activity in crude membranes of human MDR1-transfected mammalian cells, in: Methods in Enzymology. pp. 504–514.

Ambudkar, S. V., Kim, I.-W., Xia, D., Sauna, Z.E., 2006. The A-loop, a novel conserved aromatic acid subdomain upstream of the Walker A motif in ABC transporters, is critical for ATP binding. FEBS Lett. 580, 1049–1055.

Amin, M.L., 2013. P-glycoprotein Inhibition for Optimal Drug Delivery. Drug Target Insights 7, 27–34.

Ando, T., Kusuhara, H., Merino, G., Alvarez, A.I., Schinkel, A.H., Sugiyama, Y., 2007. Involvement of Breast Cancer Resistance Protein (ABCG2) in the Biliary Excretion Mechanism of Fluoroquinolones. Drug Metab. Dispos. 35, 1873–1879.

Annilo, T., Chen, Z.-Q., Shulenin, S., Costantino, J., Thomas, L., Lou, H., Stefanov, S., Dean, M., 2006. Evolution of the vertebrate ABC gene family: Analysis of gene birth and death. Genomics 88, 1–11.

Aronica, E., Gorter, J.A., Redeker, S., van Vliet, E.A., Ramkema, M., Scheffer, G.L., Scheper, R.J., van der Valk, P., Leenstra, S., Baayen, J.C., Spliet, W.G.M., Troost, D., 2005. Localization of Breast Cancer Resistance Protein (BCRP) in Microvessel Endothelium of Human Control and Epileptic Brain. Epilepsia 46, 849–857.

Azzaria, M., Schurr, E., Gros, P., 1989. Discrete mutations introduced in the predicted nucleotide-binding sites of the mdr1 gene abolish its ability to confer multidrug resistance. Mol. Cell. Biol.

Babenko, A.P., Bryan, J., 2003. SUR Domains That Associate with and Gate K ATP Pores Define a Novel Gatekeeper. J. Biol. Chem. 278, 41577–41580.

Bacso, Z., Nagy, H., Goda, K., Bene, L., Fenyvesi, F., Matkó, J., Szabó, G., 2004. Raft and cytoskeleton associations of an ABC transporter: P-glycoprotein. Cytom. Part A 61A, 105–116.

Bai, X., McMullan, G., Scheres, S.H.W., 2015. How cryo-EM is revolutionizing structural biology. Trends Biochem. Sci. 40, 49–57.

Bailey-Dell, K.J., Hassel, B., Doyle, L.A., Ross, D.D., 2001. Promoter characterization and genomic organization of the human breast cancer resistance protein (ATP-binding cassette transporter G2) gene. Biochim. Biophys. Acta - Gene Struct. Expr. 1520, 234–241.

Bakos, É., Evers, R., Sinkó, E., Váradi, A., Borst, P., Sarkadi, B., 2000. Interactions of the Human Multidrug Resistance Proteins MRP1 and MRP2 with Organic Anions. Mol. Pharmacol. 57, 760–768.

Bakos, É., Evers, R., Szakács, G., Tusnády, G.E., Welker, E., Szabó, K., de Haas, M., van Deemter, L., Borst, P., Váradi, A., Sarkadi, B., 1998. Functional Multidrug Resistance Protein (MRP1) Lacking the N-terminal Transmembrane Domain. J. Biol. Chem. 273, 32167–32175.

Basseville, A., Hall, M.D., Chau, C.H., Robey, R.W., Gottesman, M., Figg, W.D.,

Bates, S.E., 2016a. The ABCG2 Multidrug Transporter, in: ABC Transporters - 40 Years On. Springer International Publishing, Cham, pp. 195–226.

Basseville, A., Hall, M.D., Chau, C.H., Robey, R.W., Gottesman, M., Figg, W.D., Bates, S.E., 2016b. The ABCG2 Multidrug Transporter, in: ABC Transporters - 40 Years On. Springer International Publishing, Cham, pp. 195–226.

Basseville, A., Tamaki, A., Ierano, C., Trostel, S., Ward, Y., Robey, R.W., Hegde, R.S., Bates, S.E., 2012. Histone Deacetylase Inhibitors Influence Chemotherapy Transport by Modulating Expression and Trafficking of a Common Polymorphic Variant of the ABCG2 Efflux Transporter. Cancer Res. 72, 3642–3651.

Beis, K., 2015. Structural basis for the mechanism of ABC transporters. Biochem. Soc. Trans. 43, 889–893.

Benderra, Z., 2005. MRP3, BCRP, and P-Glycoprotein Activities are Prognostic Factors in Adult Acute Myeloid Leukemia. Clin. Cancer Res. 11, 7764–7772.

Bhatia, A., Schäfer, H.-J., Hrycyna, C.A., 2005. Oligomerization of the Human ABC Transporter ABCG2: Evaluation of the Native Protein and Chimeric Dimers †. Biochemistry 44, 10893–10904.

Bodó, A., Bakos, É., Szeri, F., Váradi, A., Sarkadi, B., 2003. Differential Modulation of the Human Liver Conjugate Transporters MRP2 and MRP3 by Bile Acids and Organic Anions. J. Biol. Chem. 278, 23529–23537.

Boussif, O., Lezoualc'h, F., Zanta, M.A., Mergny, M.D., Scherman, D., Demeneix, B., Behr, J.P., 1995. A versatile vector for gene and oligonucleotide transfer into cells in culture and in vivo: polyethylenimine. Proc. Natl. Acad. Sci. U. S. A. 92, 7297–301.

Breedveld, P., Zelcer, N., Pluim, D., Sönmezer, Ö., Tibben, M.M., Beijnen, J.H., Schinkel, A.H., van Tellingen, O., Borst, P., Schellens, J.H.M., 2004. Mechanism of the Pharmacokinetic Interaction between Methotrexate and Benzimidazoles. Cancer Res. 64, 5804–5811.

Brendel, C., Scharenberg, C., Dohse, M., Robey, R.W., Bates, S.E., Shukla, S., Ambudkar, S. V., Wang, Y., Wennemuth, G., Burchert, A., Boudriot, U., Neubauer, A., 2007. Imatinib mesylate and nilotinib (AMN107) exhibit high-affinity interaction with ABCG2 on primitive hematopoietic stem cells. Leukemia 21, 1267–1275.

Brooker, R., Widmaier, E., Graham, L., Stiling, P., 2010. Membrane Structure,

Synthesis and Transport, in: Biology. McGraw-Hill, New York, NY, pp. 97–118.

Burger, H., Foekens, J.A., Look, M.P., Meijer-van Gelder, M.E., Klijn, J.G.M., Wiemer, E.A.C., Stoter, G., Nooter, K., 2003. RNA expression of breast cancer resistance protein, lung resistance-related protein, multidrug resistance-associated proteins 1 and 2, and multidrug resistance gene 1 in breast cancer: correlation with chemotherapeutic response. Clin. Cancer Res. 9, 827–36.

Burger, H., van Tol, H., Boersma, A.W.M., Brok, M., Wiemer, E.A.C., Stoter, G., Nooter, K., 2004. Imatinib mesylate (STI571) is a substrate for the breast cancer resistance protein (BCRP)/ABCG2 drug pump. Blood 104, 2940–2942.

Callaghan, R., 2015. Providing a molecular mechanism for P-glycoprotein; why would I bother? Biochem. Soc. Trans. 43, 995–1002.

Carrier, I., Urbatsch, I.L., Senior, A.E., Gros, P., 2007. Mutational analysis of conserved aromatic residues in the A-loop of the ABC transporter ABCB1A (mouse Mdr3). FEBS Lett. 581, 301–308.

Cascorbi, I., 2011. P-glycoprotein: Tissue Distribution, Substrates, and Functional Consequences of Genetic Variations, in: Handbook of Experimental Pharmacology. pp. 261–283.

Chen, J., Lu, G., Lin, J., Davidson, A.L., Quiocho, F.A., 2003. A Tweezers-like Motion of the ATP-Binding Cassette Dimer in an ABC Transport Cycle. Mol. Cell 12, 651–661.

Chen, Z.-S., Robey, R.W., Belinsky, M.G., Shchaveleva, I., Ren, X.-Q., Sugimoto, Y., Ross, D.D., Bates, S.E., Kruh, G.D., 2003. Transport of methotrexate, methotrexate polyglutamates, and 17beta-estradiol 17-(beta-D-glucuronide) by ABCG2: effects of acquired mutations at R482 on methotrexate transport. Cancer Res. 63, 4048–54.

Cheng, S.H., Rich, D.P., Marshall, J., Gregory, R.J., Welsh, M.J., Smith, A.E., 1991. Phosphorylation of the R domain by cAMP-dependent protein kinase regulates the CFTR chloride channel. Cell 66, 1027–36.

Chifflet, S., Torriglia, A., Chiesa, R., Tolosa, S., 1988. A method for the determination of inorganic phosphate in the presence of labile organic phosphate and high concentrations of protein: Application to lens ATPases. Anal. Biochem. 168, 1–4.

Christian, A.E., Haynes, M.P., Phillips, M.C., Rothblat, G.H., 1997a. Use of

cyclodextrins for manipulating cellular cholesterol content. J. Lipid Res. 38, 2264–72.

Christian, A.E., Haynes, M.P., Phillips, M.C., Rothblat, G.H., 1997b. Use of cyclodextrins for manipulating cellular cholesterol content. J. Lipid Res. 38, 2264–72.

Ciccarone, V.C., Polayes, D.A., Luckow, V.A., 2003. Generation of Recombinant Baculovirus DNA in E. coli Using a Baculovirus Shuttle Vector, in: Molecular Diagnosis of Infectious Diseases. Humana Press, New Jersey, pp. 213–236.

Cisternino, S., Mercier, C., Bourasset, F., Roux, F., Scherrmann, J.-M., 2004. Expression, Up-Regulation, and Transport Activity of the Multidrug-Resistance Protein Abcg2 at the Mouse Blood-Brain Barrier. Cancer Res. 64, 3296–3301.

Clark, R., Kerr, I.D., Callaghan, R., 2006. Multiple drugbinding sites on the R482G isoform of the ABCG2 transporter. Br. J. Pharmacol. 149, 506–515.

Clarke, G., 2003. Practical Statistics for Environmental and Biological Scientists. Fish Fish. 4, 375–376.

Cleophas, M.C., Joosten, L.A., Stamp, L.K., Dalbeth, N., Woodward, O.M., Merriman, T.R., 2017. ABCG2 polymorphisms in gout: insights into disease susceptibility and treatment approaches. Pharmgenomics. Pers. Med. 10, 129–142.

Cole, S.P.C., 2014. Multidrug Resistance Protein 1 (MRP1, ABCC1), a "Multitasking" ATP-binding Cassette (ABC) Transporter. J. Biol. Chem. 289, 30880–30888.

Cole, S.P.C., Bhardwaj, G., Gerlach, J.H., Mackie, J.E., Grant, C.E., Almquist, K.C., Stewart, A.J., Kurz, E.U., Duncan, A.M.V., Deeley, R.G., 1992. Overexpression of a transporter gene in a multidrug-resistant human lung cancer cell line. Science 258, 1650–4.

Cooray, H.C., Blackmore, C.G., Maskell, L., Barrand, M.A., 2002. Localisation of breast cancer resistance protein in microvessel endothelium of human brain. Neuroreport 13, 2059–2063.

Cox, D.W., Moore, S.D.P., 2002. Copper transporting P-type ATPases and human disease. J. Bioenerg. Biomembr. 34, 333–8.

Cox, M.H., Kapoor, P., Briggs, D.A., Kerr, I.D., 2018. Residues contributing to drug transport by ABCG2 are localised to multiple drug-binding pockets. Biochem. J. 475, 1553–1567.

Cusatis, G., Gregorc, V., Li, J., Spreafico, A., Ingersoll, R.G., Verweij, J., Ludovini, V., Villa, E., Hidalgo, M., Sparreboom, A., Baker, S.D., 2006. Pharmacogenetics of ABCG2 and Adverse Reactions to Gefitinib. JNCI J. Natl. Cancer Inst. 98, 1739–1742.

Dai, C. -l., Tiwari, A.K., Wu, C.-P., Su, X. -d., Wang, S.-R., Liu, D. -g., Ashby, C.R., Huang, Y., Robey, R.W., Liang, Y. -j., Chen, L. -m., Shi, C.-J., Ambudkar, S. V., Chen, Z.-S., Fu, L. -w., 2008. Lapatinib (Tykerb, GW572016) Reverses Multidrug Resistance in Cancer Cells by Inhibiting the Activity of ATP-Binding Cassette Subfamily B Member 1 and G Member 2. Cancer Res. 68, 7905–7914.

Dawson, R.J.P., Hollenstein, K., Locher, K.P., 2007. Uptake or extrusion: crystal structures of full ABC transporters suggest a common mechanism. Mol. Microbiol. 65, 250–7.

Dawson, R.J.P., Locher, K.P., 2007. Structure of the multidrug ABC transporter Sav1866 from Staphylococcus aureus in complex with AMP-PNP. FEBS Lett. 581, 935–938.

Dawson, R.J.P., Locher, K.P., 2006. Structure of a bacterial multidrug ABC transporter. Nature 443, 180–185.

Dean, M., Hamon, Y., Chimini, G., 2001. The human ATP-binding cassette (ABC) transporter superfamily. J. Lipid Res. 42, 1007–17.

Deeley, R.G., Westlake, C., Cole, S.P.C., 2006. Transmembrane Transport of Endo- and Xenobiotics by Mammalian ATP-Binding Cassette Multidrug Resistance Proteins. Physiol. Rev. 86, 849–899.

Dehghan, A., Köttgen, A., Yang, Q., Hwang, S.-J., Kao, W.L., Rivadeneira, F., Boerwinkle, E., Levy, D., Hofman, A., Astor, B.C., Benjamin, E.J., van Duijn, C.M., Witteman, J.C., Coresh, J., Fox, C.S., 2008. Association of three genetic loci with uric acid concentration and risk of gout: a genome-wide association study. Lancet 372, 1953–1961.

Demeule, M., Jodoin, J., Gingras, D., Béliveau, R., 2000. P-glycoprotein is localized in caveolae in resistant cells and in brain capillaries. FEBS Lett. 466, 219–224.

Deng, F., Sjöstedt, N., Kidron, H., 2016. The Effect of Albumin on MRP2 and BCRP in the Vesicular Transport Assay. PLoS One 11, e0163886.

Deppe, S., Ripperger, A., Weiss, J., Ergün, S., Benndorf, R.A., 2014. Impact of genetic variability in the ABCG2 gene on ABCG2 expression, function, and

interaction with AT1 receptor antagonist telmisartan. Biochem. Biophys. Res. Commun. 443, 1211–1217.

Dhakshinamoorthy, S., Long, D.J., Jaiswal, A.K., 2001. Antioxidant regulation of genes encoding enzymes that detoxify xenobiotics and carcinogens, in: Current Topics in Cellular Regulation. pp. 201–216.

Diestra, J.E., Scheffer, G.L., Català, I., Maliepaard, M., Schellens, J.H.M., Scheper, R.J., Germà-Lluch, J.R., Izquierdo, M.A., 2002. Frequent expression of the multi-drug resistance-associated protein BCRP/MXR/ABCP/ABCG2 in human tumours detected by the BXP-21 monoclonal antibody in paraffin-embedded material. J. Pathol. 198, 213–219.

Diop, N.K., Hrycyna, C.A., 2005. N-Linked Glycosylation of the Human ABC Transporter ABCG2 on Asparagine 596 Is Not Essential for Expression, Transport Activity, or Trafficking to the Plasma Membrane †. Biochemistry 44, 5420–5429.

Do, T.M., Noel-Hudson, M.-S., Ribes, S., Besengez, C., Smirnova, M., Cisternino, S., Buyse, M., Calon, F., Chimini, G., Chacun, H., Scherrmann, J.-M., Farinotti, R., Bourasset, F., 2012. ABCG2- and ABCG4-Mediated Efflux of Amyloid-β Peptide 1-40 at the Mouse Blood-Brain Barrier. J. Alzheimer's Dis. 30, 155–166.

Dohse, M., Scharenberg, C., Shukla, S., Robey, R.W., Volkmann, T., Deeken, J.F., Brendel, C., Ambudkar, S. V., Neubauer, A., Bates, S.E., 2010. Comparison of ATP-Binding Cassette Transporter Interactions with the Tyrosine Kinase Inhibitors Imatinib, Nilotinib, and Dasatinib. Drug Metab. Dispos. 38, 1371–1380.

Dörr, J.M., Scheidelaar, S., Koorengevel, M.C., Dominguez, J.J., Schäfer, M., van Walree, C.A., Killian, J.A., 2016. The styrene–maleic acid copolymer: a versatile tool in membrane research. Eur. Biophys. J. 45, 3–21.

Doyle, L.A., Yang, W., Abruzzo, L. V., Krogmann, T., Gao, Y., Rishi, A.K., Ross, D.D., 1998a. A multidrug resistance transporter from human MCF-7 breast cancer cells. Proc. Natl. Acad. Sci. U. S. A. 95, 15665–70.

Doyle, L.A., Yang, W., Abruzzo, L. V, Krogmann, T., Gao, Y., Rishi, A.K., Ross, D.D., 1998b. A multidrug resistance transporter from human MCF-7 breast cancer cells. Proc. Natl. Acad. Sci. U. S. A. 95, 15665–70.

DuBridge, R.B., Tang, P., Hsia, H.C., Leong, P.M., Miller, J.H., Calos, M.P., 1987.

Analysis of mutation in human cells by using an Epstein-Barr virus shuttle system. Mol. Cell. Biol. 7, 379–87.

DUNBAR, L., 2000. The cell biology of ion pumps: sorting and regulation. Eur. J. Cell Biol. 79, 557–563.

Eckford, P.D.W., Sharom, F.J., 2008. Interaction of the P-Glycoprotein Multidrug Efflux Pump with Cholesterol: Effects on ATPase Activity, Drug Binding and Transport †. Biochemistry 47, 13686–13698.

Eggensperger, S., Tampé, R., 2015. The transporter associated with antigen processing: a key player in adaptive immunity. Biol. Chem. 396, 1059–1072.

Egido, E., Müller, R., Li-Blatter, X., Merino, G., Seelig, A., 2015. Predicting Activators and Inhibitors of the Breast Cancer Resistance Protein (ABCG2) and P-Glycoprotein (ABCB1) Based on Mechanistic Considerations. Mol. Pharm. 12, 4026–37.

Ejendal, K.F.K., Diop, N.K., Schweiger, L.C., Hrycyna, C.A., 2006. The nature of amino acid 482 of human ABCG2 affects substrate transport and ATP hydrolysis but not substrate binding. Protein Sci. 15, 1597–1607.

Elkind, N.B., Szentpétery, Z., Apáti, Á., Özvegy-Laczka, C., Várady, G., Ujhelly, O., Szabó, K., Homolya, L., Váradi, A., Buday, L., Kéri, G., Német, K., Sarkadi, B., 2005. Multidrug Transporter ABCG2 Prevents Tumor Cell Death Induced by the Epidermal Growth Factor Receptor Inhibitor Iressa (ZD1839, Gefitinib). Cancer Res. 65, 1770–1777.

Ellgaard, L., McCaul, N., Chatsisvili, A., Braakman, I., 2016. Co- and Post-Translational Protein Folding in the ER. Traffic 17, 615–638.

Elson, E.L., 2011. Fluorescence Correlation Spectroscopy: Past, Present, Future. Biophys. J. 101, 2855–2870.

Ferreira, R.J., Ferreira, M.-J.U., dos Santos, D.J.V.A., 2015. Do Drugs Have Access to the P-Glycoprotein Drug-Binding Pocket through Gates? J. Chem. Theory Comput. 11, 4525–4529.

Fujita, Y., Noguchi, K., Suzuki, T., Katayama, K., Sugimoto, Y., 2013. Biochemical interaction of anti-HCV telaprevir with the ABC transporters P-glycoprotein and breast cancer resistance protein. BMC Res. Notes 6, 445.

Garrigues, A., Escargueil, A.E., Orlowski, S., 2002. The multidrug transporter, P-glycoprotein, actively mediates cholesterol redistribution in the cell membrane. Proc. Natl. Acad. Sci. 99, 10347–10352.

George, A.M., Jones, P.M., 2012. Perspectives on the structure–function of ABC transporters: The Switch and Constant Contact Models. Prog. Biophys. Mol. Biol. 109, 95–107.

Gimpl, G., Klein, U., Reilaender, H., Fahrenholz, F., 1995. Expression of the Human Oxytocin Receptor in Baculovirus-Infected Insect Cells: High-Affinity Binding Is Induced by a Cholesterol-Cyclodextrin Complex. Biochemistry 34, 13794–13801.

Giri, N., Agarwal, S., Shaik, N., Pan, G., Chen, Y., Elmquist, W.F., 2009. Substrate-Dependent Breast Cancer Resistance Protein (Bcrp1/Abcg2)-Mediated Interactions: Consideration of Multiple Binding Sites in in Vitro Assay Design. Drug Metab. Dispos. 37, 560–570.

Glavinas, H., Kis, E., Pál, Á., Kovács, R., Jani, M., Vági, E., Molnár, É., Bánsághi, S., Kele, Z., Janáky, T., Báthori, G., von Richter, O., Koomen, G.-J., Krajcsi, P., 2007. ABCG2 (Breast Cancer Resistance Protein/Mitoxantrone Resistance-Associated Protein) ATPase Assay: A Useful Tool to Detect Drug-Transporter Interactions. Drug Metab. Dispos. 35, 1533–1542.

Gonen, T., Sliz, P., Kistler, J., Cheng, Y., Walz, T., 2004. Aquaporin-0 membrane junctions reveal the structure of a closed water pore. Nature 429, 193–197.

Goñi, F.M., 2014. The basic structure and dynamics of cell membranes: An update of the Singer-Nicolson model. Biochim. Biophys. Acta - Biomembr.

Goodell, M.A., Brose, K., Paradis, G., Conner, A.S., Mulligan, R.C., 1996. Isolation and functional properties of murine hematopoietic stem cells that are replicating in vivo. J. Exp. Med. 183, 1797–806.

Gulati, S., Jamshad, M., Knowles, T.J., Morrison, K.A., Downing, R., Cant, N., Collins, R., Koenderink, J.B., Ford, R.C., Overduin, M., Kerr, I.D., Dafforn, T.R., Rothnie, A.J., 2014. Detergent-free purification of ABC (ATP-binding-cassette) transporters. Biochem. J. 461, 269–278.

Gupta, A., Unadkat, J.D., Mao, Q., 2007. Interactions of azole antifungal agents with the human breast cancer resistance protein (BCRP). J. Pharm. Sci. 96, 3226–3235.

Gupta, A., Zhang, Y., Unadkat, J.D., Mao, Q., 2004. HIV Protease Inhibitors Are Inhibitors but Not Substrates of the Human Breast Cancer Resistance Protein (BCRP/ABCG2). J. Pharmacol. Exp. Ther. 310, 334–341.

Gutmann, H., Hruz, P., Zimmermann, C., Beglinger, C., Drewe, J., 2005.

Distribution of breast cancer resistance protein (BCRP/ABCG2) mRNA expression along the human GI tract. Biochem. Pharmacol. 70, 695–699.

Haider, A.J., Briggs, D., Self, T.J., Chilvers, H.L., Holliday, N.D., Kerr, I.D., 2011. Dimerization of ABCG2 analysed by bimolecular fluorescence complementation. PLoS One 6, e25818.

Haider, A.J., Cox, M.H., Jones, N., Goode, A.J., Bridge, K.S., Wong, K., Briggs, D., Kerr, I.D., 2015. Identification of residues in ABCG2 affecting protein trafficking and drug transport, using co-evolutionary analysis of ABCG sequences. Biosci. Rep. 35.

Halwachs, S., Kneuer, C., Gohlsch, K., Müller, M., Ritz, V., Honscha, W., 2016. The ABCG2 efflux transporter from rabbit placenta: Cloning and functional characterization. Placenta 38, 8–15.

Han, J.-Y., Lim, H.-S., Yoo, Y.-K., Shin, E.S., Park, Y.H., Lee, S.Y., Lee, J.-E., Lee, D.H., Kim, H.T., Lee, J.S., 2007. Associations ofABCB1, ABCC2, andABCG2 polymorphisms with irinotecan-pharmacokinetics and clinical outcome in patients with advanced non-small cell lung cancer. Cancer 110, 138–147.

Hanson, P.I., Whiteheart, S.W., 2005. AAA+ proteins: have engine, will work. Nat. Rev. Mol. Cell Biol. 6, 519–529.

Hazai, E., Hazai, I., Ragueneau-Majlessi, I., Chung, S.P., Bikadi, Z., Mao, Q., 2013. Predicting substrates of the human breast cancer resistance protein using a support vector machine method. BMC Bioinformatics 14, 130.

Hediger, M. a., Romero, M.F., Peng, J.B., Rolfs, A., Takanaga, H., Bruford, E. a., 2004. The ABCs of solute carriers: Physiological, pathological and therapeutic implications of human membrane transport proteins. Pflugers Arch. Eur. J. Physiol. 447, 465–468.

Hediger, M.A., Clémençon, B., Burrier, R.E., Bruford, E.A., 2013. The ABCs of membrane transporters in health and disease (SLC series): Introduction. Mol. Aspects Med. 34, 95–107.

Hegedűs, C, Özvegy-Laczka, C., Apáti, Á., Magócsi, M., Német, K., Őrfi, L., Kéri, G., Katona, M., Takáts, Z., Váradi, A., Szakács, G., Sarkadi, B., 2009. Interaction of nilotinib, dasatinib and bosutinib with ABCB1 and ABCG2: implications for altered anti-cancer effects and pharmacological properties. Br. J. Pharmacol. 158, 1153–1164.

Hegedus, C., Szakács, G., Homolya, L., Orbán, T.I., Telbisz, Á., Jani, M., Sarkadi,

B., 2009. Ins and outs of the ABCG2 multidrug transporter: An update on in vitro functional assays. Adv. Drug Deliv. Rev.

Hegedűs, Csilla, Szakács, G., Homolya, L., Orbán, T.I., Telbisz, Á., Jani, M., Sarkadi, B., 2009. Ins and outs of the ABCG2 multidrug transporter: An update on in vitro functional assays. Adv. Drug Deliv. Rev. 61, 47–56.

Henriksen, U., 2005. Effect of Walker A mutation (K86M) on oligomerization and surface targeting of the multidrug resistance transporter ABCG2. J. Cell Sci. 118, 1417–1426.

Henriksen, U., Fog, J.U., Litman, T., Gether, U., 2005. Identification of Intra- and Intermolecular Disulfide Bridges in the Multidrug Resistance Transporter ABCG2. J. Biol. Chem. 280, 36926–36934.

Heyes, N., Kapoor, P., Kerr, I.D., 2018. Polymorphisms of the Multidrug Pump ABCG2: A Systematic Review of Their Effect on Protein Expression, Function, and Drug Pharmacokinetics. Drug Metab. Dispos. 46, 1886–1899.

Higashino, T., Takada, T., Nakaoka, H., Toyoda, Y., Stiburkova, B., Miyata, H., Ikebuchi, Y., Nakashima, H., Shimizu, S., Kawaguchi, M., Sakiyama, M., Nakayama, A., Akashi, A., Tanahashi, Y., Kawamura, Y., Nakamura, T., Wakai, K., Okada, R., Yamamoto, K., Hosomichi, K., Hosoya, T., Ichida, K., Ooyama, H., Suzuki, H., Inoue, I., Merriman, T.R., Shinomiya, N., Matsuo, H., 2017. Multiple common and rare variants of ABCG2 cause gout. RMD Open 3, e000464.

Higgins, C.F., Gottesman, M.M., 1992. Is the multidrug transporter a flippase? Trends Biochem. Sci. 17, 18–21.

Higgins, C.F., Linton, K.J., 2004. The ATP switch model for ABC transporters. Nat. Struct. Mol. Biol. 11, 918–926.

Hinds, M., Deisseroth, K., Mayes, J., Altschuler, E., Jansen, R., Ledley, F.D., Zwelling, L.A., 1991. Identification of a point mutation in the topoisomerase II gene from a human leukemia cell line containing an amsacrine-resistant form of topoisomerase II. Cancer Res. 51, 4729–31.

Hinrichs, J.W.J., Klappe, K., Hummel, I., Kok, J.W., 2004. ATP-binding Cassette Transporters Are Enriched in Non-caveolar Detergent-insoluble Glycosphingolipid-enriched Membrane Domains (DIGs) in Human Multidrug-resistant Cancer Cells. J. Biol. Chem. 279, 5734–5738.

Holland, I.B., A. Blight, M., 1999. ABC-ATPases, adaptable energy generators

fuelling transmembrane movement of a variety of molecules in organisms from bacteria to humans. J. Mol. Biol. 293, 381–399.

Honjo, Y., Hrycyna, C.A., Yan, Q.W., Medina-Pérez, W.Y., Robey, R.W., van de Laar, A., Litman, T., Dean, M., Bates, S.E., 2001. Acquired mutations in the MXR/BCRP/ABCP gene alter substrate specificity in MXR/BCRP/ABCP-overexpressing cells. Cancer Res. 61, 6635–9.

Honjo, Y., Morisaki, K., Huff, L.M., Robey, R.W., Hung, J., Dean, M., Bates, S.E., 2002. Single-nucleotide polymorphism (SNP) analysis in the ABC half-transporter ABCG2 (MXR/BCRP/ABCP1). Cancer Biol. Ther. 1, 696–702.

Hopfner, K.-P., Karcher, A., Craig, L., Woo, T.T., Carney, J.P., Tainer, J.A., 2001. Structural Biochemistry and Interaction Architecture of the DNA Double-Strand Break Repair Mre11 Nuclease and Rad50-ATPase. Cell 105, 473–485.

Hopfner, K., 2003. Rad50/SMC proteins and ABC transporters: unifying concepts from high-resolution structures. Curr. Opin. Struct. Biol. 13, 249–255.

Hou, Y., Li, C.-Z., Palaniyandi, K., Magtibay, P.M., Homolya, L., Sarkadi, B., Chang, X., 2009. Effects of Putative Catalytic Base Mutation E211Q on ABCG2-Mediated Methotrexate Transport. Biochemistry 48, 9122–9131.

Housman, G., Byler, S., Heerboth, S., Lapinska, K., Longacre, M., Snyder, N., Sarkar, S., 2014. Drug resistance in cancer: an overview. Cancers (Basel). 6, 1769–92.

Hu, W., Liu, W., 2010. Side populations of glioblastoma cells are less sensitive to HSV-TK/GCV suicide gene therapy system than the non-side population. Vitr. Cell. Dev. Biol. - Anim. 46, 497–501.

Huls, M., Brown, C.D.A., Windass, A.S., Sayer, R., van den Heuvel, J.J.M.W., Heemskerk, S., Russel, F.G.M., Masereeuw, R., 2008. The breast cancer resistance protein transporter ABCG2 is expressed in the human kidney proximal tubule apical membrane. Kidney Int. 73, 220–225.

Hung, L.-W., Wang, I.X., Nikaido, K., Liu, P.-Q., Ames, G.F.-L., Kim, S.-H., 1998. Crystal structure of the ATP-binding subunit of an ABC transporter. Nature 396, 703–707.

Hyde, Stephen C, Emsley, P., Hartshorn, M.J., Mimmack, M.M., Gileadi, U., Pearce, S.R., Gallagher, M.P., Gill, D.R., Hubbard, R.E., Higgins, C.F., 1990. Structural model of ATP-binding proteing associated with cystic fibrosis, multidrug resistance and bacterial transport. Nature 346, 362–365.

Hyde, S C, Emsley, P., Hartshorn, M.J., Mimmack, M.M., Gileadi, U., Pearce, S.R., Gallagher, M.P., Gill, D.R., Hubbard, R.E., Higgins, C.F., 1990. Structural model of ATP-binding proteins associated with cystic fibrosis, multidrug resistance and bacterial transport. Nature 346, 362–5.

Imai, Y., Asada, S., Tsukahara, S., Ishikawa, E., Tsuruo, T., Sugimoto, Y., 2003. Breast Cancer Resistance Protein Exports Sulfated Estrogens but Not Free Estrogens. Mol. Pharmacol. 64, 610–618.

Imai, Y., Ishikawa, E., Asada, S., Sugimoto, Y., 2005. Estrogen-mediated post transcriptional down-regulation of breast cancer resistance protein/ABCG2. Cancer Res. 65, 596–604.

International Transporter Consortium, Giacomini, K.M., Huang, S.-M., Tweedie, D.J., Benet, L.Z., Brouwer, K.L.R., Chu, X., Dahlin, A., Evers, R., Fischer, V., Hillgren, K.M., Hoffmaster, K.A., Ishikawa, T., Keppler, D., Kim, R.B., Lee, C.A., Niemi, M., Polli, J.W., Sugiyama, Y., Swaan, P.W., Ware, J.A., Wright, S.H., Yee, S.W., Zamek-Gliszczynski, M.J., Zhang, L., 2010. Membrane transporters in drug development. Nat. Rev. Drug Discov. 9, 215–36.

Jackson, S.M., Manolaridis, I., Kowal, J., Zechner, M., Taylor, N.M.I., Bause, M., Bauer, S., Bartholomaeus, R., Bernhardt, G., Koenig, B., Buschauer, A., Stahlberg, H., Altmann, K.-H., Locher, K.P., 2018. Structural basis of small-molecule inhibition of human multidrug transporter ABCG2. Nat. Struct. Mol. Biol. 25, 333–340.

Jandu, H., Aluzaite, K., Fogh, L., Thrane, S.W., Noer, J.B., Proszek, J., Do, K.N., Hansen, S.N., Damsgaard, B., Nielsen, S.L., Stougaard, M., Knudsen, B.R., Moreira, J., Hamerlik, P., Gajjar, M., Smid, M., Martens, J., Foekens, J., Pommier, Y., Brünner, N., Schrohl, A.-S., Stenvang, J., 2016. Molecular characterization of irinotecan (SN-38) resistant human breast cancer cell lines. BMC Cancer 16, 34.

JANVILISRI, T., SHAHI, S., VENTER, H., BALAKRISHNAN, L., van VEEN, H.W., 2005. Arginine-482 is not essential for transport of antibiotics, primary bile acids and unconjugated sterols by the human breast cancer resistance protein (ABCG2). Biochem. J. 385, 419–426.

Jaroszeski, M.J., Radcliff, G., 1999. Fundamentals of flow cytometry. Mol. Biotechnol. 11, 37–53.

Jerabek-Willemsen, M., André, T., Wanner, R., Roth, H.M., Duhr, S., Baaske, P.,

Breitsprecher, D., 2014. MicroScale Thermophoresis: Interaction analysis and beyond. J. Mol. Struct. 1077, 101–113.

Johnson, Z.L., Chen, J., 2017. Structural Basis of Substrate Recognition by the Multidrug Resistance Protein MRP1. Cell 168, 1075-1085.e9.

Jones, P., 1999. Subunit interactions in ABC transporters: towards a functional architecture. FEMS Microbiol. Lett. 179, 187–202.

Jonker, J.W., 2000. Role of Breast Cancer Resistance Protein in the Bioavailability and Fetal Penetration of Topotecan. J. Natl. Cancer Inst. 92, 1651–1656.

Jonker, J.W., Buitelaar, M., Wagenaar, E., van der Valk, M.A., Scheffer, G.L., Scheper, R.J., Plosch, T., Kuipers, F., Elferink, R.P.J.O., Rosing, H., Beijnen, J.H., Schinkel, A.H., 2002. Nonlinear partial differential equations and applications: The breast cancer resistance protein protects against a major chlorophyll-derived dietary phototoxin and protoporphyria. Proc. Natl. Acad. Sci. 99, 15649–15654.

Jonker, J.W., Merino, G., Musters, S., van Herwaarden, A.E., Bolscher, E., Wagenaar, E., Mesman, E., Dale, T.C., Schinkel, A.H., 2005. The breast cancer resistance protein BCRP (ABCG2) concentrates drugs and carcinogenic xenotoxins into milk. Nat. Med. 11, 127–129.

Juliano, R.L., Ling, V., 1976. A surface glycoprotein modulating drug permeability in Chinese hamster ovary cell mutants. Biochim. Biophys. Acta - Biomembr. 455, 152–162.

Kage, K., Fujita, T., Sugimoto, Y., 2005. Role of Cys-603 in dimer/oligomer formation of the breast cancer resistance protein BCRP/ABCG2. Cancer Sci. 96, 866–872.

Kapoor, P., Briggs, D.A., Cox, M.H., Kerr, I.D., 2020. Disruption of the unique ABCG-family NBD:NBD interface impacts both drug transport and atp hydrolysis. Int. J. Mol. Sci.

Kapoor, P., Horsey, A.J., Cox, M.H., Kerr, I.D., 2018. ABCG2: does resolving its structure elucidate the mechanism? Biochem. Soc. Trans. 46, 1485–1494.

Kasza, I., Várady, G., Andrikovics, H., Koszarska, M., Tordai, A., Scheffer, G.L., Németh, A., Szakács, G., Sarkadi, B., 2012. Expression Levels of the ABCG2 Multidrug Transporter in Human Erythrocytes Correspond to Pharmacologically Relevant Genetic Variations. PLoS One 7, e48423.

Katayama, K., Yoshioka, S., Tsukahara, S., Mitsuhashi, J., Sugimoto, Y., 2007.

Inhibition of the mitogen-activated protein kinase pathway results in the down-regulation of P-glycoprotein. Mol. Cancer Ther. 6, 2092–2102.

Kerr, I.D., 2002. Structure and association of ATP-binding cassette transporter nucleotide-binding domains. Biochim. Biophys. Acta - Biomembr. 1561, 47–64.

Kerr, I.D., Haider, A.J., Gelissen, I.C., 2011. The ABCG family of membrane-associated transporters: you don't have to be big to be mighty. Br. J. Pharmacol. 164, 1767–1779.

Kerr, I.D., Jones, P.M., George, A.M., 2010. Multidrug efflux pumps: The structures of prokaryotic ATP-binding cassette transporter efflux pumps and implications for our understanding of eukaryotic P-glycoproteins and homologues. FEBS J. 277, 550–563.

Khunweeraphong, N., Stockner, T., Kuchler, K., 2017. The structure of the human ABC transporter ABCG2 reveals a novel mechanism for drug extrusion. Sci. Rep. 7.

Kim, H.-S., Sunwoo, Y.E., Ryu, J.Y., Kang, H.-J., Jung, H.-E., Song, I.-S., Kim, E.-Y., Shim, J.-C., Shon, J.-H., Shin, J.-G., 2007. The effect of ABCG2 V12M, Q141K and Q126X, known functional variants in vitro, on the disposition of lamivudine. Br. J. Clin. Pharmacol. 64, 645–654.

Kim, I.-S., Kim, H.-G., Kim, D.C., Eom, H.-S., Kong, S.-Y., Shin, H.-J., Hwang, S.-H., Lee, E.-Y., Lee, G.-W., 2008. ABCG2 Q141K polymorphism is associated with chemotherapy-induced diarrhea in patients with diffuse large B-cell lymphoma who received frontline rituximab plus cyclophosphamide/doxorubicin/ vincristine/prednisone chemotherapy. Cancer Sci. 99, 2496–2501.

Kim, Y., Chen, J., 2018. Molecular structure of human P-glycoprotein in the ATP-bound, outward-facing conformation. Science (80-.). 359, 915–919.

Kitamura, S., Maeda, K., Wang, Y., Sugiyama, Y., 2008. Involvement of Multiple Transporters in the Hepatobiliary Transport of Rosuvastatin. Drug Metab. Dispos. 36, 2014–2023.

Krishnamurthy, P., Ross, D.D., Nakanishi, T., Bailey-Dell, K., Zhou, S., Mercer, K.E., Sarkadi, B., Sorrentino, B.P., Schuetz, J.D., 2004. The Stem Cell Marker Bcrp/ABCG2 Enhances Hypoxic Cell Survival through Interactions with Heme. J. Biol. Chem. 279, 24218–24225.

Kuroda, T., Tsuchiya, T., 2009. Multidrug efflux transporters in the MATE family.

Biochim. Biophys. Acta - Proteins Proteomics 1794, 763–768.

LAEMMLI, U.K., 1970. Cleavage of Structural Proteins during the Assembly of the Head of Bacteriophage T4. Nature 227, 680–685.

Lagas, J.S., van der Kruijssen, C.M.M., van de Wetering, K., Beijnen, J.H., Schinkel, A.H., 2009. Transport of diclofenac by breast cancer resistance protein (ABCG2) and stimulation of multidrug resistance protein 2 (ABCC2)-mediated drug transport by diclofenac and benzbromarone. Drug Metab. Dispos. 37, 129–36.

László, L., Sarkadi, B., Hegedüs, T., 2016. Jump into a new fold-A homology based model for the ABCG2/BCRP multidrug transporter. PLoS One 11.

Lawson, J., O'Mara, M.L., Kerr, I.D., 2008. Structure-based interpretation of the mutagenesis database for the nucleotide binding domains of P-glycoprotein. Biochim. Biophys. Acta - Biomembr.

Lee, A.G., 2004. How lipids affect the activities of integral membrane proteins. Biochim. Biophys. Acta - Biomembr.

Lee, J.Y., Kinch, L.N., Borek, D.M., Wang, Jin, Wang, Junmei, Urbatsch, I.L., Xie, X.S., Grishin, N. V., Cohen, J.C., Otwinowski, Z., Hobbs, H.H., Rosenbaum, D.M., 2016. Crystal structure of the human sterol transporter ABCG5/ABCG8. Nature 533, 561–564.

Lefevre, F., 1997. Alanine-stretch scanning mutagenesis: a simple and efficient method to probe protein structure and function. Nucleic Acids Res. 25, 447–448.

Leier, I., Jedlitschky, G., Buchholz, U., Cole, S.P.C., Deeley, R.G., Keppler, D., 1994. The MRP gene encodes an ATP-dependent export pump for leukotriene C4 and structurally related conjugates. J. Biol. Chem. 269, 27807–10.

Leslie, E.M., Deeley, R.G., Cole, S.P.C., 2005. Multidrug resistance proteins: role of P-glycoprotein, MRP1, MRP2, and BCRP (ABCG2) in tissue defense. Toxicol. Appl. Pharmacol. 204, 216–237.

Linton, K.J., 2007. Structure and function of ABC transporters. Physiology.

Linton, K.J., Higgins, C.F., 2007a. Structure and function of ABC transporters: The ATP switch provides flexible control. Pflugers Arch. Eur. J. Physiol.

Linton, K.J., Higgins, C.F., 2007b. Structure and function of ABC transporters: The ATP switch provides flexible control. Pflugers Arch. Eur. J. Physiol.

Liscovitch, M., Lavie, Y., 2000. Multidrug resistance: A role for cholesterol efflux

pathways? Trends Biochem. Sci.

Litman, T., Brangi, M., Hudson, E., Fetsch, P., Abati, A., Ross, D.D., Miyake, K., Resau, J.H., Bates, S.E., 2000. The multidrug-resistant phenotype associated with overexpression of the new ABC half-transporter, MXR (ABCG2). J. Cell Sci.

Liu, R., Siemiarczuk, A., Sharom, F.J., 2000. Intrinsic fluorescence of the P-glycoprotein multidrug transporter: Sensitivity of tryptophan residues to binding of drugs and nucleotides. Biochemistry.

Liu, Y., Yang, Y., Qi, J., Peng, H., Zhang, J.-T., 2008. Effect of Cysteine Mutagenesis on the Function and Disulfide Bond Formation of Human ABCG2. J. Pharmacol. Exp. Ther.

Locher, K.P., 2016. Mechanistic diversity in ATP-binding cassette (ABC) transporters. Nat. Struct. Mol. Biol.

Locher, K.P., Lee, A.T., Rees, D.C., 2002. The E. coli BtuCD structure: A framework for ABC transporter architecture and mechanism. Science (80-.).

LOWRY, O.H., ROSEBROUGH, N.J., FARR, A.L., RANDALL, R.J., 1951. Protein measurement with the Folin phenol reagent. J. Biol. Chem. 193, 265–75.

Luckow, V.A., Lee, S.C., Barry, G.F., Olins, P.O., 1993. Efficient generation of infectious recombinant baculoviruses by site-specific transposon-mediated insertion of foreign genes into a baculovirus genome propagated in Escherichia coli. J. Virol. 67, 4566–4579.

Lugli, E., Roederer, M., Cossarizza, A., 2010. Data analysis in flow cytometry: The future just started. Cytom. Part A 77A, 705–713.

Maier, P., Spier, I., Laufs, S., Veldwijk, M.R., Fruehauf, S., Wenz, F., Zeller, W.J., 2010. Chemoprotection of human hematopoietic stem cells by simultaneous lentiviral overexpression of multidrug resistance 1 and O6-methylguanine-DNA methyltransferaseP140K. Gene Ther. 17, 389–399.

Maliepaard, M., Scheffer, G.L., Faneyte, I.F., van Gastelen, M.A., Pijnenborg, A.C., Schinkel, A.H., van De Vijver, M.J., Scheper, R.J., Schellens, J.H., 2001a. Subcellular localization and distribution of the breast cancer resistance protein transporter in normal human tissues. Cancer Res. 61, 3458–64.

Maliepaard, M., van Gastelen, M.A., Tohgo, A., Hausheer, F.H., van Waardenburg, R.C., de Jong, L.A., Pluim, D., Beijnen, J.H., Schellens, J.H.M., 2001b. Circumvention of breast cancer resistance protein (BCRP)-mediated resistance

to camptothecins in vitro using non-substrate drugs or the BCRP inhibitor GF120918. Clin. Cancer Res. 7, 935–41.

Manolaridis, I., Jackson, S.M., Taylor, N.M.I., Kowal, J., Stahlberg, H., Locher, K.P., 2018. Cryo-EM structures of a human ABCG2 mutant trapped in ATP-bound and substrate-bound states. Nature 563, 426–430.

Manzi, L., Barrow, A.S., Scott, D., Layfield, R., Wright, T.G., Moses, J.E., Oldham, N.J., 2016. Carbene footprinting accurately maps binding sites in protein–ligand and protein–protein interactions. Nat. Commun. 7, 13288.

Mao, Q., Unadkat, J.D., 2015. Role of the Breast Cancer Resistance Protein (BCRP/ABCG2) in Drug Transport—an Update. AAPS J. 17, 65–82.

Marheineke, K., Grünewald, S., Christie, W., Reiländer, H., 1998. Lipid composition of Spodoptera frugiperda (Sf9) and Trichoplusia ni (Tn) insect cells used for baculovirus infection. FEBS Lett. 441, 49–52.

Marie, J., Zittoun, R., Sikic, B., 1991. Multidrug resistance (mdr1) gene expression in adult acute leukemias: correlations with treatment outcome and in vitro drug sensitivity. Blood 78, 586–592.

März, L., Altmann, F., Staudacher, E., Kubelka, V., 1995. Chapter 10 Protein Glycosylation in Insects, in: New Comprehensive Biochemistry. pp. 543–563.

McDevitt, C.A., Collins, R., Kerr, I.D., Callaghan, R., 2009. Purification and structural analyses of ABCG2. Adv. Drug Deliv. Rev. 61, 57–65.

McDevitt, C.A., Collins, R.F., Conway, M., Modok, S., Storm, J., Kerr, I.D., Ford, R.C., Callaghan, R., 2006. Purification and 3D Structural Analysis of Oligomeric Human Multidrug Transporter ABCG2. Structure 14, 1623–1632.

McDevitt, C.A., Crowley, E., Hobbs, G., Starr, K.J., Kerr, I.D., Callaghan, R., 2008. Is ATP binding responsible for initiating drug translocation by the multidrug transporter ABCG2? FEBS J. 275, 4354–4362.

Merino, G., Álvarez, A.I., Pulido, M.M., Molina, A.J., Schinkel, A.H., Prieto, J.G., 2006. BREAST CANCER RESISTANCE PROTEIN (BCRP/ABCG2) TRANSPORTS FLUOROQUINOLONE ANTIBIOTICS AND AFFECTS THEIR ORAL AVAILABILITY, PHARMACOKINETICS, AND MILK SECRETION. Drug Metab. Dispos. 34, 690–695.

Merino, G., Jonker, J.W., Wagenaar, E., van Herwaarden, A.E., Schinkel, A.H., 2005. The Breast Cancer Resistance Protein (BCRP/ABCG2) Affects Pharmacokinetics, Hepatobiliary Excretion, and Milk Secretion of the

Antibiotic Nitrofurantoin. Mol. Pharmacol. 67, 1758–1764.

Mikkaichi, T., Suzuki, T., Tanemoto, M., Ito, S., Abe, T., 2004a. The organic anion transporter (OATP) family. Drug Metab. Pharmacokinet. 19, 171–179.

Mikkaichi, T., Suzuki, T., Tanemoto, M., Ito, S., Abe, T., 2004b. The organic anion transporter (OATP) family. Drug Metab. Pharmacokinet. 19, 171–9.

Mishra, J., Simonsen, R., Kumar, N., 2019. Intestinal breast cancer resistance protein (BCRP) requires Janus kinase 3 activity for drug efflux and barrier functions in obesity. J. Biol. Chem. 294, 18337–18348.

MITOMO, H., KATO, R., ITO, A., KASAMATSU, S., IKEGAMI, Y., KII, I., KUDO, A., KOBATAKE, E., SUMINO, Y., ISHIKAWA, T., 2003. A functional study on polymorphism of the ATP-binding cassette transporter ABCG2: critical role of arginine-482 in methotrexate transport. Biochem. J. 373, 767–774.

Mittra, R., Pavy, M., Subramanian, N., George, A.M., O'Mara, M.L., Kerr, I.D., Callaghan, R., 2017. Location of contact residues in pharmacologically distinct drug binding sites on P-glycoprotein. Biochem. Pharmacol. 123, 19–28.

Miwa, M., Tsukahara, S., Ishikawa, E., Asada, S., Imai, Y., Sugimoto, Y., 2003. Single amino acid substitutions in the transmembrane domains of breast cancer resistance protein (BCRP) alter cross resistance patterns in transfectants. Int. J. Cancer 107, 757–763.

Miyake, K., Mickley, L., Litman, T., Zhan, Z., Robey, R., Cristensen, B., Brangi, M., Greenberger, L., Dean, M., Fojo, T., Bates, S.E., 1999. Molecular cloning of cDNAs which are highly overexpressed in mitoxantrone-resistant cells: demonstration of homology to ABC transport genes. Cancer Res. 59, 8–13.

Mlejnek, P., Kosztyu, P., Dolezel, P., Bates, S.E., Ruzickova, E., 2017. Reversal of ABCB1 mediated efflux by imatinib and nilotinib in cells expressing various transporter levels. Chem. Biol. Interact. 273, 171–179.

Mohrmann, K., van Eijndhoven, M.A.J., Schinkel, A.H., Schellens, J.H.M., 2005. Absence of N-linked glycosylation does not affect plasma membrane localization of breast cancer resistance protein (BCRP/ABCG2). Cancer Chemother. Pharmacol. 56, 344–350.

Moody, J.E., Millen, L., Binns, D., Hunt, J.F., Thomas, P.J., 2002. Cooperative, ATP-dependent Association of the Nucleotide Binding Cassettes during the Catalytic Cycle of ATP-binding Cassette Transporters. J. Biol. Chem. 277,

21111–21114.

Morisaki, K., Robey, R.W., Özvegy-Laczka, C., Honjo, Y., Polgar, O., Steadman, K., Sarkadi, B., Bates, S.E., 2005. Single nucleotide polymorphisms modify the transporter activity of ABCG2. Cancer Chemother. Pharmacol. 56, 161–172.

Morrison, K.A., Akram, A., Mathews, A., Khan, Z.A., Patel, J.H., Zhou, C., Hardy, D.J., Moore-Kelly, C., Patel, R., Odiba, V., Knowles, T.J., Javed, M.-H., Chmel, N.P., Dafforn, T.R., Rothnie, A.J., 2016. Membrane protein extraction and purification using styrene–maleic acid (SMA) copolymer: effect of variations in polymer structure. Biochem. J. 473, 4349–4360.

Müller, M., Bakos, É., Welker, E., Váradi, A., Germann, U.A., Gottesman, M.M., Morse, B.S., Roninson, I.B., Sarkadi, B., 1996. Altered Drug-stimulated ATPase Activity in Mutants of the Human Multidrug Resistance Protein. J. Biol. Chem. 271, 1877–1883.

Mutoh, K., Tsukahara, S., Mitsuhashi, J., Katayama, K., Sugimoto, Y., 2006. Estrogen-mediated post transcriptional down-regulation of P-glycoprotein in MDR1-transduced human breast cancer cells. Cancer Sci. 97, 1198–1204.

Nakanishi, T., Ross, D.D., 2012. Breast cancer resistance protein (BCRP/ABCG2): its role in multidrug resistance and regulation of its gene expression. Chin. J. Cancer 31, 73–99.

Nakashima, R., Sakurai, K., Yamasaki, S., Nishino, K., Yamaguchi, A., 2011. Structures of the multidrug exporter AcrB reveal a proximal multisite drug-binding pocket. Nature 480, 565–569.

Nakatomi, K., Yoshikawa, M., Oka, M., Ikegami, Y., Hayasaka, S., Sano, K., Shiozawa, K., Kawabata, S., Soda, H., Ishikawa, T., Tanabe, S., Kohno, S., 2001. Transport of 7-Ethyl-10-hydroxycamptothecin (SN-38) by Breast Cancer Resistance Protein ABCG2 in Human Lung Cancer Cells. Biochem. Biophys. Res. Commun. 288, 827–832.

Natarajan, K., Xie, Y., Baer, M.R., Ross, D.D., 2012. Role of breast cancer resistance protein (BCRP/ABCG2) in cancer drug resistance. Biochem. Pharmacol.

Ni, Z., Bikadi, Z., Shuster, D.L., Zhao, C., Rosenberg, M.F., Mao, Q., 2011. Identification of Proline Residues in or near the Transmembrane Helices of the Human Breast Cancer Resistance Protein (BCRP/ABCG2) That Are Important for Transport Activity and Substrate Specificity. Biochemistry 50, 8057–8066.

Ni, Z., Mark, M.E., Cai, X., Mao, Q., 2010. Fluorescence resonance energy transfer (FRET) analysis demonstrates dimer/oligomer formation of the human breast cancer resistance protein (BCRP/ABCG2) in intact cells. Int. J. Biochem. Mol. Biol. 1, 1–11.

Nicolson, G.L., 2014. The Fluid—Mosaic Model of Membrane Structure: Still relevant to understanding the structure, function and dynamics of biological membranes after more than 40years. Biochim. Biophys. Acta - Biomembr. 1838, 1451–1466.

Nies, A.T., Koepsell, H., Damme, K., Schwab, M., 2011. Organic cation transporters (OCTs, MATEs), in vitro and in vivo evidence for the importance in drug therapy. Handb. Exp. Pharmacol.

Nigam, S.K., Bush, K.T., Martovetsky, G., Ahn, S.-Y., Liu, H.C., Richard, E., Bhatnagar, V., Wu, W., 2015. The Organic Anion Transporter (OAT) Family: A Systems Biology Perspective. Physiol. Rev. 95, 83–123.

Nikaido, K., Ames, G.F.-L., 1999. One Intact ATP-binding Subunit Is Sufficient to Support ATP Hydrolysis and Translocation in an ABC Transporter, the Histidine Permease. J. Biol. Chem. 274, 26727–26735.

Nishikawa, M., Nojima, S., Akiyama, T., Sankawa, U., Inoue, K., 1984. Interaction of digitonin and its analogs with membrane cholesterol. J. Biochem. 96, 1231–1239.

Oldham, M.L., Chen, J., 2011. Snapshots of the maltose transporter during ATP hydrolysis. Proc. Natl. Acad. Sci. 108, 15152–15156.

Oldham, M.L., Hite, R.K., Steffen, A.M., Damko, E., Li, Z., Walz, T., Chen, J., 2016. A mechanism of viral immune evasion revealed by cryo-EM analysis of the TAP transporter. Nature 529, 537–540.

Oldham, M.L., Khare, D., Quiocho, F.A., Davidson, A.L., Chen, J., 2007. Crystal structure of a catalytic intermediate of the maltose transporter. Nature 450, 515–521.

Orbán, T.I., Seres, L., Özvegy-Laczka, C., Elkind, N.B., Sarkadi, B., Homolya, L., 2008. Combined localization and real-time functional studies using a GFP-tagged ABCG2 multidrug transporter. Biochem. Biophys. Res. Commun. 367, 667–673.

Orlando, B.J., Liao, M., 2020. ABCG2 transports anticancer drugs via a closed-to-open switch. Nat. Commun. 11, 2264.

Oswald, C., Holland, I.B., Schmitt, L., 2006. The motor domains of ABC-transporters. Naunyn. Schmiedebergs. Arch. Pharmacol. 372, 385–399.

Otsuka, M., Matsumoto, T., Morimoto, R., Arioka, S., Omote, H., Moriyama, Y., 2005. A human transporter protein that mediates the final excretion step for toxic organic cations. Proc. Natl. Acad. Sci. U. S. A. 102, 17923–17928.

Özvegy-Laczka, C., Köblös, G., Sarkadi, B., Váradi, A., 2005. Single amino acid (482) variants of the ABCG2 multidrug transporter: major differences in transport capacity and substrate recognition. Biochim. Biophys. Acta - Biomembr. 1668, 53–63.

Özvegy-Laczka, C., Laczkó, R., Hegedűs, C., Litman, T., Várady, G., Goda, K., Hegedűs, T., Dokholyan, N. V., Sorrentino, B.P., Váradi, A., Sarkadi, B., 2008. Interaction with the 5D3 Monoclonal Antibody Is Regulated by Intramolecular Rearrangements but Not by Covalent Dimer Formation of the Human ABCG2 Multidrug Transporter. J. Biol. Chem. 283, 26059–26070.

Özvegy, C., Litman, T., Szakács, G., Nagy, Z., Bates, S., Váradi, A., Sarkadi, B., 2001. Functional Characterization of the Human Multidrug Transporter, ABCG2, Expressed in Insect Cells. Biochem. Biophys. Res. Commun. 285, 111–117.

Özvegy, C., Váradi, A., Sarkadi, B., 2002. Characterization of Drug Transport, ATP Hydrolysis, and Nucleotide Trapping by the Human ABCG2 Multidrug Transporter. J. Biol. Chem. 277, 47980–47990.

Pál, Á., Méhn, D., Molnár, É., Gedey, S., Mészáros, P., Nagy, T., Glavinas, H., Janáky, T., von Richter, O., Báthori, G., Szente, L., Krajcsi, P., 2007. Cholesterol Potentiates ABCG2 Activity in a Heterologous Expression System: Improved in Vitro Model to Study Function of Human ABCG2. J. Pharmacol. Exp. Ther. 321, 1085–1094.

Palmberg, C., Koivisto, P., Hyylinen, E., Isola, J., Visakorpi, T., Kallioniemi, O.-P., Tammela, T., 1997. Androgen Receptor Gene Amplification in a Recurrent Prostate Cancer after Monotherapy with the Nonsteroidal Potent Antiandrogen Casodex (Bicalutamide) with a Subsequent Favorable Response to Maximal Androgen Blockade. Eur. Urol. 31, 216–219.

Palmgren, M.G., Nissen, P., 2011. P-Type ATPases. Annu. Rev. Biophys. 40, 243–266.

Pan, G., Giri, N., Elmquist, W.F., 2007. Abcg2/Bcrp1 Mediates the Polarized

Transport of Antiretroviral Nucleosides Abacavir and Zidovudine. Drug Metab. Dispos. 35, 1165–1173.

Pavek, P., Merino, G., Wagenaar, E., Bolscher, E., Novotna, M., Jonker, J.W., Schinkel, A.H., 2005. Human Breast Cancer Resistance Protein: Interactions with Steroid Drugs, Hormones, the Dietary Carcinogen 2-Amino-1-methyl-6-phenylimidazo(4,5- b)pyridine, and Transport of Cimetidine. J. Pharmacol. Exp. Ther. 312, 144–152.

Pédelacq, J.-D., Cabantous, S., Tran, T., Terwilliger, T.C., Waldo, G.S., 2006. Engineering and characterization of a superfolder green fluorescent protein. Nat. Biotechnol. 24, 79–88.

Perez, M., Blazquez, A.G., Real, R., Mendoza, G., Prieto, J.G., Merino, G., Alvarez, A.I., 2009. In vitro and in vivo interaction of moxidectin with BCRP/ABCG2. Chem. Biol. Interact. 180, 106–112.

Pleban, K., Kopp, S., Csaszar, E., Peer, M., Hrebicek, T., Rizzi, A., Ecker, G.F., Chiba, P., 2005. P-Glycoprotein Substrate Binding Domains Are Located at the Transmembrane Domain/Transmembrane Domain Interfaces: A Combined Photoaffinity Labeling-Protein Homology Modeling Approach. Mol. Pharmacol. 67, 365–374.

PULIDO, M.M., MOLINA, A.J., MERINO, G., MENDOZA, G., PRIETO, J.G., ALVAREZ, A.I., 2006. Interaction of enrofloxacin with breast cancer resistance protein (BCRP/ABCG2): influence of flavonoids and role in milk secretion in sheep. J. Vet. Pharmacol. Ther. 29, 279–287.

Quandt, N., Stindl, A., Keller, U., 1993. Sodium Dodecyl Sulfate-Polyacrylamide Gel Electrophoresis for Mr Estimations of High-Molecular-Weight Polypeptides. Anal. Biochem. 214, 490–494.

Rabindran, S.K., He, H., Singh, M., Brown, E., Collins, K.I., Annable, T., Greenberger, L.M., 1998. Reversal of a novel multidrug resistance mechanism in human colon carcinoma cells by fumitremorgin C. Cancer Res. 58, 5850–8.

Rice, A.J., Park, A., Pinkett, H.W., 2014. Diversity in ABC transporters: Type I, II and III importers. Crit. Rev. Biochem. Mol. Biol. 49, 426–437.

Robey, R.W., Honjo, Y., Morisaki, K., Nadjem, T.A., Runge, S., Risbood, M., Poruchynsky, M.S., Bates, S.E., 2003. Mutations at amino-acid 482 in the ABCG2 gene affect substrate and antagonist specificity. Br. J. Cancer 89, 1971–1978.

Robey, R.W., Honjo, Y., van de Laar, A., Miyake, K., Regis, J.T., Litman, T., Bates, S.E., 2001a. A functional assay for detection of the mitoxantrone resistance protein, MXR (ABCG2). Biochim. Biophys. Acta - Biomembr. 1512, 171–182.

Robey, R.W., Medina-Pérez, W.Y., Nishiyama, K., Lahusen, T., Miyake, K., Litman, T., Senderowicz, A.M., Ross, D.D., Bates, S.E., 2001b. Overexpression of the ATP-binding cassette half-transporter, ABCG2 (Mxr/BCrp/ABCP1), in flavopiridol-resistant human breast cancer cells. Clin. Cancer Res. 7, 145–52.

Robey, R.W., Steadman, K., Polgar, O., Morisaki, K., Blayney, M., Mistry, P., Bates, S.E., 2004. Pheophorbide a Is a Specific Probe for ABCG2 Function and Inhibition. Cancer Res. 64, 1242–1246.

Romsicki, Y., Sharom, F.J., 1999. The Membrane Lipid Environment Modulates Drug Interactions with the P-Glycoprotein Multidrug Transporter †. Biochemistry 38, 6887–6896.

Rosenberg, M.F., 2001. Repacking of the transmembrane domains of P-glycoprotein during the transport ATPase cycle. EMBO J. 20, 5615–5625.

Rosenberg, M.F., Bikadi, Z., Chan, J., Liu, X., Ni, Z., Cai, X., Ford, R.C., Mao, Q., 2010. The human breast cancer resistance protein (BCRP/ABCG2) shows conformational changes with mitoxantrone. Structure 18, 482–93.

Rosenberg, M.F., Bikadi, Z., Hazai, E., Starborg, T., Kelley, L., Chayen, N.E., Ford, R.C., Mao, Q., 2015. Three-dimensional structure of the human breast cancer resistance protein (BCRP/ABCG2) in an inward-facing conformation. Acta Crystallogr. Sect. D Biol. Crystallogr. 71, 1725–1735.

Rosenberg, M.F., Kamis, A.B., Callaghan, R., Higgins, C.F., Ford, R.C., 2003. Three-dimensional Structures of the Mammalian Multidrug Resistance P-glycoprotein Demonstrate Major Conformational Changes in the Transmembrane Domains upon Nucleotide Binding. J. Biol. Chem. 278, 8294–8299.

Ross, D.D., Karp, J.E., Chen, T.T., Doyle, L.A., 2000. Expression of breast cancer resistance protein in blast cells from patients with acute leukemia. Blood 96, 365–8.

Roth, M., Obaidat, A., Hagenbuch, B., 2012. OATPs, OATs and OCTs: The organic anion and cation transporters of the SLCO and SLC22A gene superfamilies. Br. J. Pharmacol.

Rothnie, A., Callaghan, R., Deeley, R.G., Cole, S.P.C., 2006. Role of GSH in

Estrone Sulfate Binding and Translocation by the Multidrug Resistance Protein 1 (MRP1/ABCC1). J. Biol. Chem. 281, 13906–13914.

Rothnie, A., Storm, J., McMahon, R., Taylor, A., Kerr, I.D., Callaghan, R., 2005. The coupling mechanism of P -glycoprotein involves residue L339 in the sixth membrane spanning segment. FEBS Lett. 579, 3984–3990.

Rothnie, A., Theron, D., Soceneantu, L., Martin, C., Traikia, M., Berridge, G., Higgins, C.F., Devaux, P.F., Callaghan, R., 2001. The importance of cholesterol in maintenance of P-glycoprotein activity and its membrane perturbing influence. Eur. Biophys. J. 30, 430–442.

Russel, F.G.M., 2010. Transporters: Importance in Drug Absorption, Distribution, and Removal, in: Enzyme- and Transporter-Based Drug-Drug Interactions. Springer New York, New York, NY, pp. 27–49.

Russell, W.C., Graham, F.L., Smiley, J., Nairn, R., 1977. Characteristics of a Human Cell Line Transformed by DNA from Human Adenovirus Type 5. J. Gen. Virol. 36, 59–72.

Ryan, A.J., 1993. Baculoviruses on the bench. Baculovirus expression vectors: A laboratory manual (1992). By D <scp>AVID</scp> R. O'R <scp>EILLY</scp> , L <scp>OIS</scp> K. M <scp>ILLER AND</scp> V <scp>ERNE A</scp> . L <scp>UCKNOW</scp> W. H. Freeman and Co., New York. 34. BioEssays 15, 217–217.

Sabnis, D.H., Storer, L.C.D., Liu, J.-F., Jackson, H.K., Kilday, J.P., Grundy, R.G., Kerr, I.D., Coyle, B., 2019. A role for ABCB1 in prognosis, invasion and drug resistance in ependymoma. Sci. Rep. 9, 10290.

Sai, K., Saito, Y., Maekawa, K., Kim, S.-R., Kaniwa, N., Nishimaki-Mogami, T., Sawada, J., Shirao, K., Hamaguchi, T., Yamamoto, N., Kunitoh, H., Ohe, Y., Yamada, Y., Tamura, T., Yoshida, T., Matsumura, Y., Ohtsu, A., Saijo, N., Minami, H., 2010. Additive effects of drug transporter genetic polymorphisms on irinotecan pharmacokinetics/pharmacodynamics in Japanese cancer patients. Cancer Chemother. Pharmacol. 66, 95–105.

Saison, C., Helias, V., Ballif, B.A., Peyrard, T., Puy, H., Miyazaki, T., Perrot, S., Vayssier-Taussat, M., Waldner, M., Le Pennec, P.-Y., Cartron, J.-P., Arnaud, L., 2012. Null alleles of ABCG2 encoding the breast cancer resistance protein define the new blood group system Junior. Nat. Genet. 44, 174–177.

Sarkadi, B., Price, E.M., Boucher, R.C., Germann, U.A., Scarborough, G.A., 1992.

Expression of the human multidrug resistance cDNA in insect cells generates a high activity drug-stimulated membrane ATPase. J. Biol. Chem. 267, 4854–8.

Sauna, Z.E., Ambudkar, S. V., 2000. Evidence for a requirement for ATP hydrolysis at two distinct steps during a single turnover of the catalytic cycle of human P-glycoprotein. Proc. Natl. Acad. Sci. 97, 2515–2520.

Scharenberg, C.W., Harkey, M.A., Torok-Storb, B., 2002. The ABCG2 transporter is an efficient Hoechst 33342 efflux pump and is preferentially expressed by immature human hematopoietic progenitors. Blood 99, 507–512.

Senior, A.E., Al-Shawi, M.K., Urbatsch, I.L., 1995. The catalytic cycle of P-glycoprotein. FEBS Lett. 377, 285–289.

Sharom, Frances J., 2011. The P-glycoprotein multidrug transporter. Essays Biochem. 50, 161–78.

Sharom, Frances J, 2011. The P-glycoprotein multidrug transporter. Essays Biochem. 50, 161–178.

Shi, X., Jarvis, D.L., 2007. Protein N-glycosylation in the baculovirus-insect cell system. Curr. Drug Targets 8, 1116–25.

Shigeta, J., Katayama, K., Mitsuhashi, J., Noguchi, K., Sugimoto, Y., 2010. BCRP/ABCG2 confers anticancer drug resistance without covalent dimerization. Cancer Sci. 101, 1813–1821.

Shyamala, V., Baichwal, V., Beall, E., Ames, G.F.L., 1991. Structure-function analysis of the histidine permease and comparison with cystic fibrosis mutations. J. Biol. Chem.

Simons, K., Ikonen, E., 1997. Functional rafts in cell membranes. Nature 387, 569–72.

Singer, S.J., Nicolson, G.L., 1972. The fluid mosaic model of the structure of cell membranes. Science 175, 720–31.

Singh, H., Velamakanni, S., Deery, M.J., Howard, J., Wei, S.L., van Veen, H.W., 2016. ATP-dependent substrate transport by the ABC transporter MsbA is proton-coupled. Nat. Commun. 7, 12387.

Sjöstedt, N., van den Heuvel, J.J.M.W., Koenderink, J.B., Kidron, H., 2017. Transmembrane Domain Single-Nucleotide Polymorphisms Impair Expression and Transport Activity of ABC Transporter ABCG2. Pharm. Res. 34, 1626–1636.

Slot, A.J., Molinski, S. V., Cole, S.P.C., 2011. Mammalian multidrug-resistance

proteins (MRPs). Essays Biochem. 50, 179–207.

Smith, P.C., Karpowich, N., Millen, L., Moody, J.E., Rosen, J., Thomas, P.J., Hunt, J.F., 2002. ATP binding to the motor domain from an ABC transporter drives formation of a nucleotide sandwich dimer. Mol. Cell 10, 139–49.

Sobek, K.M., Cummings, J.L., Bacich, D.J., O'Keefe, D.S., 2017. Contrasting roles of the ABCG2 Q141K variant in prostate cancer. Exp. Cell Res. 354, 40–47.

Sparreboom, A., Gelderblom, H., Marsh, S., Ahluwalia, R., Obach, R., Principe, P., Twelves, C., Verweij, J., McLeod, H.L., 2004. Diflomotecan pharmacokinetics in relation to ABCG2 421C>A genotype. Clin. Pharmacol. Ther. 76, 38–44.

Steinbach, D., Sell, W., Voigt, A., Hermann, J., Zintl, F., Sauerbrey, A., 2002. BCRP gene expression is associated with a poor response to remission induction therapy in childhood acute myeloid leukemia. Leukemia 16, 1443–1447.

Storch, C.H., Ehehalt, R., Haefeli, W.E., Weiss, J., 2007a. Localization of the Human Breast Cancer Resistance Protein (BCRP/ABCG2) in Lipid Rafts/Caveolae and Modulation of Its Activity by Cholesterol in Vitro. J. Pharmacol. Exp. Ther. 323, 257–264.

Storch, C.H., Ehehalt, R., Haefeli, W.E., Weiss, J., 2007b. Localization of the human breast cancer resistance protein (BCRP/ABCG2) in lipid rafts/caveolae and modulation of its activity by cholesterol in vitro. J. Pharmacol. Exp. Ther. 323, 257–64.

SZAKÁCS, G., ÖZVEGY, C., BAKOS, É., SARKADI, B., VÁRADI, A., 2001. Role of glycine-534 and glycine-1179 of human multidrug resistance protein (MDR1) in drug-mediated control of ATP hydrolysis. Biochem. J. 356, 71.

Szilagyi, J.T., Vetrano, A.M., Laskin, J.D., Aleksunes, L.M., 2017. Localization of the placental BCRP/ ABCG2 transporter to lipid rafts: Role for cholesterol in mediating efflux activity. Placenta 55, 29–36.

Szymanski, W.G., Zauber, H., Erban, A., Gorka, M., Wu, X.N., Schulze, W.X., 2015. Cytoskeletal Components Define Protein Location to Membrane Microdomains. Mol. Cell. Proteomics 14, 2493–2509.

Tamura, A., Wakabayashi, K., Onishi, Y., Takeda, M., Ikegami, Y., Sawada, S., Tsuji, M., Matsuda, Y., Ishikawa, T., 2007. Re-evaluation and functional classification of non-synonymous single nucleotide polymorphisms of the human ATP-binding cassette transporter ABCG2. Cancer Sci. 98, 231–239.

Tamura, A., Watanabe, M., Saito, H., Nakagawa, H., Kamachi, T., Okura, I.,

Ishikawa, T., 2006. Functional Validation of the Genetic Polymorphisms of Human ATP-Binding Cassette (ABC) Transporter ABCG2: Identification of Alleles That Are Defective in Porphyrin Transport. Mol. Pharmacol. 70, 287–296.

Tan, K.P., Wang, B., Yang, M., Boutros, P.C., MacAulay, J., Xu, H., Chuang, A.I., Kosuge, K., Yamamoto, M., Takahashi, S., Wu, A.M.L., Ross, D.D., Harper, P.A., Ito, S., 2010. Aryl Hydrocarbon Receptor Is a Transcriptional Activator of the Human Breast Cancer Resistance Protein (BCRP/ABCG2). Mol. Pharmacol. 78, 175–185.

Taylor, N.M.I., Manolaridis, I., Jackson, S.M., Kowal, J., Stahlberg, H., Locher, K.P., 2017. Structure of the human multidrug transporter ABCG2. Nature 546, 504–509.

Telbisz, Á., Müller, M., Özvegy-Laczka, C., Homolya, L., Szente, L., Váradi, A., Sarkadi, B., 2007. Membrane cholesterol selectively modulates the activity of the human ABCG2 multidrug transporter. Biochim. Biophys. Acta - Biomembr. 1768, 2698–2713.

Telbisz, Á., Özvegy-Laczka, C., Hegedűs, T., Váradi, A., Sarkadi, B., 2013. Effects of the lipid environment, cholesterol and bile acids on the function of the purified and reconstituted human ABCG2 protein. Biochem. J. 450, 387–395.

ter Beek, J., Guskov, A., Slotboom, D.J., 2014. Structural diversity of ABC transporters. J. Gen. Physiol. 143, 419–435.

Theodoulou, F.L., Kerr, I.D., 2015. ABC transporter research: going strong 40 years on. Biochem. Soc. Trans. 43, 1033–1040.

Tietz, P., Jefferson, J., Pagano, R., LaRusso, N.F., 2005. Membrane microdomains in hepatocytes: potential target areas for proteins involved in canalicular bile secretion. J. Lipid Res. 46, 1426–1432.

To, K.K.W., Zhan, Z., Litman, T., Bates, S.E., 2008. Regulation of ABCG2 Expression at the 3′ Untranslated Region of Its mRNA through Modulation of Transcript Stability and Protein Translation by a Putative MicroRNA in the S1 Colon Cancer Cell Line. Mol. Cell. Biol. 28, 5147–5161.

Tombline, G., Bartholomew, L., Gimi, K., Tyndall, G.A., Senior, A.E., 2004. Synergy between Conserved ABC Signature Ser Residues in P-glycoprotein Catalysis. J. Biol. Chem. 279, 5363–5373.

Trock, B.J., Leonessa, F., Clarke, R., 1997. Multidrug Resistance in Breast Cancer: a

Meta-analysis of MDR1/gp170 Expression and Its Possible Functional Significance. JNCI J. Natl. Cancer Inst. 89, 917–931.

Troost, J., Albermann, N., Emil Haefeli, W., Weiss, J., 2004a. Cholesterol modulates P-glycoprotein activity in human peripheral blood mononuclear cells. Biochem. Biophys. Res. Commun. 316, 705–711.

Troost, J., Lindenmaier, H., Haefeli, W.E., Weiss, J., 2004b. Modulation of Cellular Cholesterol Alters P-Glycoprotein Activity in Multidrug-Resistant Cells. Mol. Pharmacol. 66, 1332–1339.

Trott, O., Olson, A.J., 2010. AutoDock Vina: improving the speed and accuracy of docking with a new scoring function, efficient optimization, and multithreading. J. Comput. Chem. 31, 455–61.

Urbatsch, I.L., Gimi, K., Wilke-Mounts, S., Senior, A.E., 2000a. Conserved Walker A Ser Residues in the Catalytic Sites of P-glycoprotein Are Critical for Catalysis and Involved Primarily at the Transition State Step. J. Biol. Chem. 275, 25031–25038.

Urbatsch, I.L., Gimi, K., Wilke-Mounts, S., Senior, A.E., 2000b. Investigation of the Role of Glutamine-471 and Glutamine-1114 in the Two Catalytic Sites of P-Glycoprotein †. Biochemistry 39, 11921–11927.

Van Der Does, C., Tampé, R., 2004. How do ABC transporters drive transport? Biol. Chem. 385, 927–933.

van der Heijden, J., 2004. Acquired resistance of human T cells to sulfasalazine: stability of the resistant phenotype and sensitivity to non-related DMARDs. Ann. Rheum. Dis. 63, 131–137.

van Herwaarden, A.E., Jonker, J.W., Wagenaar, E., Brinkhuis, R.F., Schellens, J.H.M., Beijnen, J.H., Schinkel, A.H., 2003. The breast cancer resistance protein (Bcrp1/Abcg2) restricts exposure to the dietary carcinogen 2-amino-1-methyl-6-phenylimidazo[4,5-b]pyridine. Cancer Res. 63, 6447–52.

van Herwaarden, A.E., Wagenaar, E., Merino, G., Jonker, J.W., Rosing, H., Beijnen, J.H., Schinkel, A.H., 2007. Multidrug Transporter ABCG2/Breast Cancer Resistance Protein Secretes Riboflavin (Vitamin B2) into Milk. Mol. Cell. Biol. 27, 1247–1253.

van Veen, H.W., 2000. The homodimeric ATP-binding cassette transporter LmrA mediates multidrug transport by an alternating two-site (two-cylinder engine) mechanism. EMBO J. 19, 2503–2514.

Vasiliou, V., Vasiliou, K., Nebert, D.W., 2008. Human ATP-binding cassette (ABC) transporter family. Hum. Genomics 3, 281.

Velamakanni, S., Janvilisri, T., Shahi, S., van Veen, H.W., 2008. A Functional Steroid-Binding Element in an ATP-Binding Cassette Multidrug Transporter. Mol. Pharmacol. 73, 12–17.

Venter, H., Shilling, R.A., Velamakanni, S., Balakrishnan, L., van Veen, H.W., 2003. An ABC transporter with a secondary-active multidrug translocator domain. Nature 426, 866–870.

Volk, E.L., Farley, K.M., Wu, Y., Li, F., Robey, R.W., Schneider, E., 2002. Overexpression of wild-type breast cancer resistance protein mediates methotrexate resistance. Cancer Res. 62, 5035–40.

Volk, E.L., Schneider, E., 2003. Wild-type breast cancer resistance protein (BCRP/ABCG2) is a methotrexate polyglutamate transporter. Cancer Res. 63, 5538–43.

von Stetten, D., Noirclerc-Savoye, M., Goedhart, J., Gadella, T.W.J., Royant, A., 2012. Structure of a fluorescent protein from Aequorea victoria bearing the obligate-monomer mutation A206K. Acta Crystallogr. Sect. F Struct. Biol. Cryst. Commun. 68, 878–882.

Wakabayashi-Nakao, K., Tamura, A., Furukawa, T., Nakagawa, H., Ishikawa, T., 2009. Quality control of human ABCG2 protein in the endoplasmic reticulum: Ubiquitination and proteasomal degradation. Adv. Drug Deliv. Rev. 61, 66–72.

Walker, J.E., Saraste, M., Runswick, M.J., Gay, N.J., 1982. Distantly related sequences in the alpha- and beta-subunits of ATP synthase, myosin, kinases and other ATP-requiring enzymes and a common nucleotide binding fold. EMBO J. 1, 945–951.

Wang, F., Li, G., Gu, H., Zhang, D., 2013. Characterization of the Role of a Highly Conserved Sequence in ATP Binding Cassette Transporter G (ABCG) Family in ABCG1 Stability, Oligomerization, and Trafficking. Biochemistry 52, 9497–9509.

Wang, H., Lee, E.-W., Cai, X., Ni, Z., Zhou, L., Mao, Q., 2008. Membrane Topology of the Human Breast Cancer Resistance Protein (BCRP/ABCG2) Determined by Epitope Insertion and Immunofluorescence †. Biochemistry 47, 13778–13787.

Wang, X., Furukawa, T., Nitanda, T., Okamoto, M., Sugimoto, Y., Akiyama, S.-I.,

Baba, M., 2003. Breast cancer resistance protein (BCRP/ABCG2) induces cellular resistance to HIV-1 nucleoside reverse transcriptase inhibitors. Mol. Pharmacol. 63, 65–72.

Wasilko, D., Lee, S.E., 2006. TIPS: Titerless Infected-Cells Preservation and Scale-Up. Bioprocess. J. 5, 29–32.

Watson, H., 2015. Biological membranes. Essays Biochem. 59, 43–69.

Weidner, L.D., Zoghbi, S.S., Lu, S., Shukla, S., Ambudkar, S. V., Pike, V.W., Mulder, J., Gottesman, M.M., Innis, R.B., Hall, M.D., 2015. The Inhibitor Ko143 Is Not Specific for ABCG2. J. Pharmacol. Exp. Ther. 354, 384–393.

Weiss, J., Rose, J., Storch, C.H., Ketabi-Kiyanvash, N., Sauer, A., Haefeli, W.E., Efferth, T., 2006. Modulation of human BCRP (ABCG2) activity by anti-HIV drugs. J. Antimicrob. Chemother. 59, 238–245.

Wilkens, S., 2015. Structure and mechanism of ABC transporters. F1000Prime Rep. 7, 14.

Wong, K., Briddon, S.J., Holliday, N.D., Kerr, I.D., 2016. Plasma membrane dynamics and tetrameric organisation of ABCG2 transporters in mammalian cells revealed by single particle imaging techniques. Biochim. Biophys. Acta - Mol. Cell Res. 1863, 19–29.

Wong, K., Ma, J., Rothnie, A., Biggin, P.C., Kerr, I.D., 2014. Towards understanding promiscuity in multidrug efflux pumps. Trends Biochem. Sci. 39, 8–16.

Woodward, O.M., 2015. ABCG2: The molecular mechanisms of urate secretion and gout. Am. J. Physiol. - Ren. Physiol.

Woodward, Owen M., Kottgen, A., Coresh, J., Boerwinkle, E., Guggino, W.B., Kottgen, M., 2009. Identification of a urate transporter, ABCG2, with a common functional polymorphism causing gout. Proc. Natl. Acad. Sci. 106, 10338–10342.

Woodward, O. M., Kottgen, A., Coresh, J., Boerwinkle, E., Guggino, W.B., Kottgen, M., 2009. Identification of a urate transporter, ABCG2, with a common functional polymorphism causing gout. Proc. Natl. Acad. Sci. 106, 10338–10342.

Woodward, O.M., Tukaye, D.N., Cui, J., Greenwell, P., Constantoulakis, L.M., Parker, B.S., Rao, A., Köttgen, M., Maloney, P.C., Guggino, W.B., 2013. Gout-causing Q141K mutation in ABCG2 leads to instability of the nucleotide-

binding domain and can be corrected with small molecules. Proc. Natl. Acad. Sci. U. S. A. 110, 5223–5228.

Xie, Y., Xu, K., Linn, D.E., Yang, X., Guo, Z., Shimelis, H., Nakanishi, T., Ross, D.D., Chen, H., Fazli, L., Gleave, M.E., Qiu, Y., 2008. The 44-kDa Pim-1 Kinase Phosphorylates BCRP/ABCG2 and Thereby Promotes Its Multimerization and Drug-resistant Activity in Human Prostate Cancer Cells. J. Biol. Chem. 283, 3349–3356.

Yang, N.J., Hinner, M.J., 2015. Getting across the cell membrane: an overview for small molecules, peptides, and proteins. Methods Mol. Biol.

Yoshikawa, M., Ikegami, Y., Hayasaka, S., Ishii, K., Ito, A., Sano, K., Suzuki, T., Togawa, T., Yoshida, H., Soda, H., Oka, M., Kohno, S., Sawada, S., Ishikawa, T., Tanabe, S., 2004. Novel camptothecin analogues that circumvent ABCG2-associated drug resistance in human tumor cells. Int. J. Cancer 110, 921–927.

Yoshioka, S., Katayama, K., Okawa, C., Takahashi, S., Tsukahara, S., Mitsuhashi, J., Sugimoto, Y., 2007. The Identification of Two Germ-line Mutations in the Human Breast Cancer Resistance Protein Gene that Result in the Expression of a Low/Non-functional Protein. Pharm. Res. 24, 1108–1117.

Yuan, Y.-R., Blecker, S., Martsinkevich, O., Millen, L., Thomas, P.J., Hunt, J.F., 2001. The Crystal Structure of the MJ0796 ATP-binding Cassette. J. Biol. Chem. 276, 32313–32321.

Zacharias, D.A., 2002. Partitioning of Lipid-Modified Monomeric GFPs into Membrane Microdomains of Live Cells. Science (80-.). 296, 913–916.

Zaitseva, J., Jenewein, S., Jumpertz, T., Holland, I.B., Schmitt, L., 2005. H662 is the linchpin of ATP hydrolysis in the nucleotide-binding domain of the ABC transporter HlyB. EMBO J. 24, 1901–1910.

Zelcer, N., Huisman, M.T., Reid, G., Wielinga, P., Breedveld, P., Kuil, A., Knipscheer, P., Schellens, J.H.M., Schinkel, A.H., Borst, P., 2003. Evidence for Two Interacting Ligand Binding Sites in Human Multidrug Resistance Protein 2 (ATP Binding Cassette C2). J. Biol. Chem. 278, 23538–23544.

Zelinski, T., Coghlan, G., Liu, X.-Q., Reid, M.E., 2012. ABCG2 null alleles define the Jr(a−) blood group phenotype. Nat. Genet. 44, 131–132.

Zhang, Y., Gupta, A., Wang, H., Zhou, L., Vethanayagam, R.R., Unadkat, J.D., Mao, Q., 2005. BCRP Transports Dipyridamole and is Inhibited by Calcium Channel Blockers. Pharm. Res. 22, 2023–2034.

Zhang, Y., Wang, H., Unadkat, J.D., Mao, Q., 2007. Breast cancer resistance protein 1 limits fetal distribution of nitrofurantoin in the pregnant mouse. Drug Metab. Dispos.

Zhang, Z., Chen, J., 2016. Atomic Structure of the Cystic Fibrosis Transmembrane Conductance Regulator. Cell 167, 1586-1597.e9.

Zhou, L., Naraharisetti, S.B., Wang, H., Unadkat, J.D., Hebert, M.F., Mao, Q., 2008. The Breast Cancer Resistance Protein (Bcrp1/Abcg2) Limits Fetal Distribution of Glyburide in the Pregnant Mouse: An Obstetric-Fetal Pharmacology Research Unit Network and University of Washington Specialized Center of Research Study. Mol. Pharmacol. 73, 949–959.

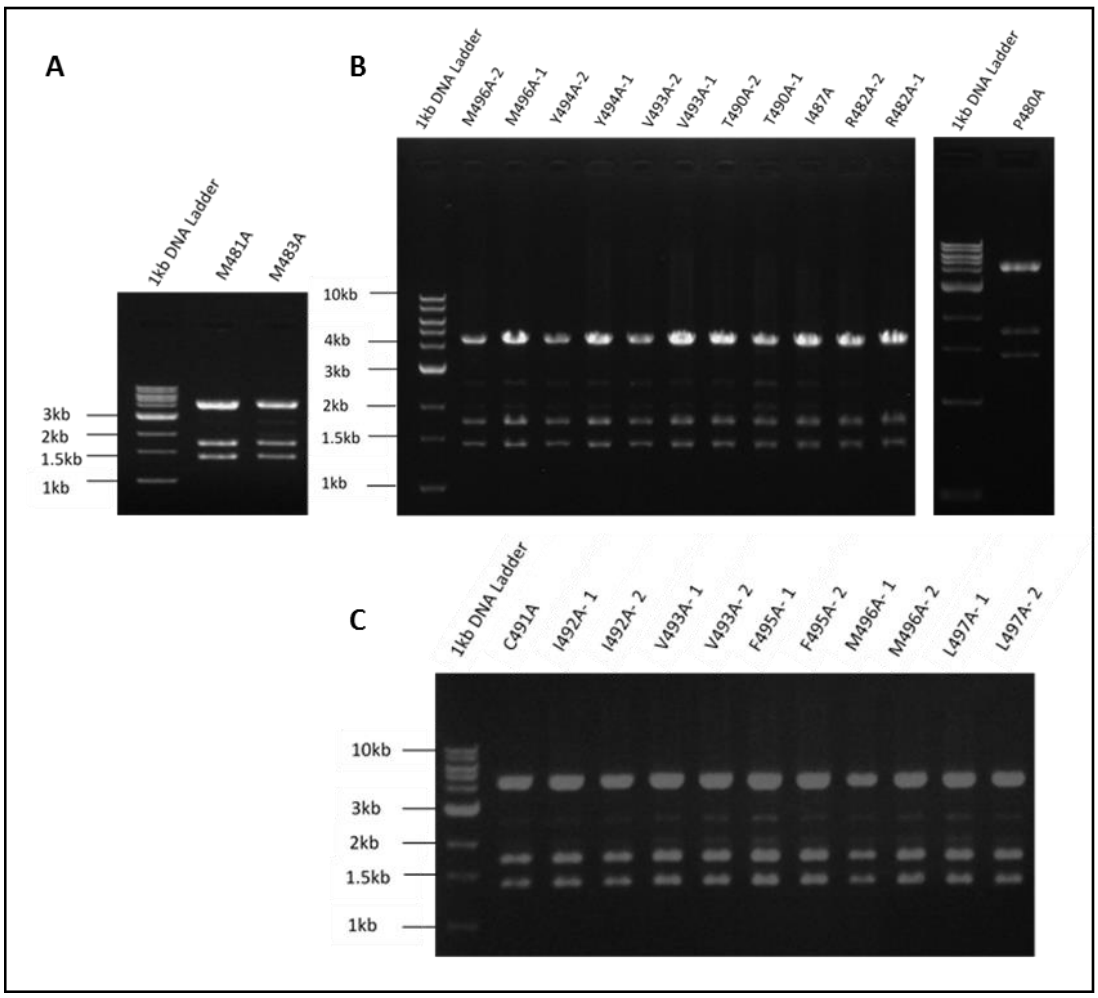
Zhou, S., Morris, J.J., Barnes, Y., Lan, L., Schuetz, J.D., Sorrentino, B.P., 2002. Bcrp1 gene expression is required for normal numbers of side population stem cells in mice, and confers relative protection to mitoxantrone in hematopoietic cells in vivo. Proc. Natl. Acad. Sci. 99, 12339–12344.

Zhou, S., Schuetz, J.D., Bunting, K.D., Colapietro, A.-M., Sampath, J., Morris, J.J., Lagutina, I., Grosveld, G.C., Osawa, M., Nakauchi, H., Sorrentino, B.P., 2001. The ABC transporter Bcrp1/ABCG2 is expressed in a wide variety of stem cells and is a molecular determinant of the side-population phenotype. Nat. Med. 7, 1028–1034.

Zhou, Y., Ojeda-May, P., Pu, J., 2013. H-loop histidine catalyzes ATP hydrolysis in the E. coli ABC-transporter HlyB. Phys. Chem. Chem. Phys. 15, 15811.

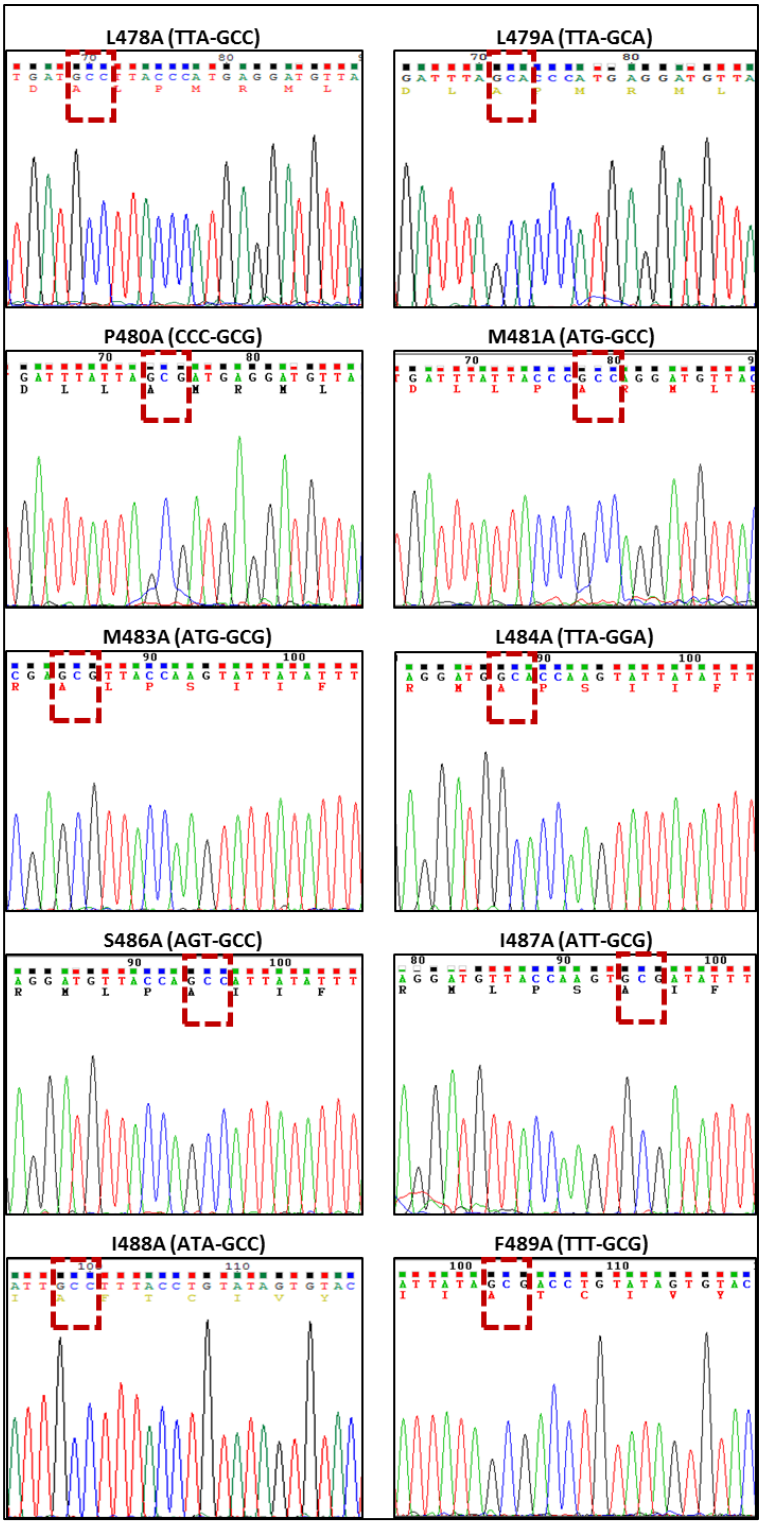
Zolnerciks, J.K., Wooding, C., Linton, K.J., 2007. Evidence for a Sav1866-like architecture for the human multidrug transporter P-glycoprotein. FASEB J.

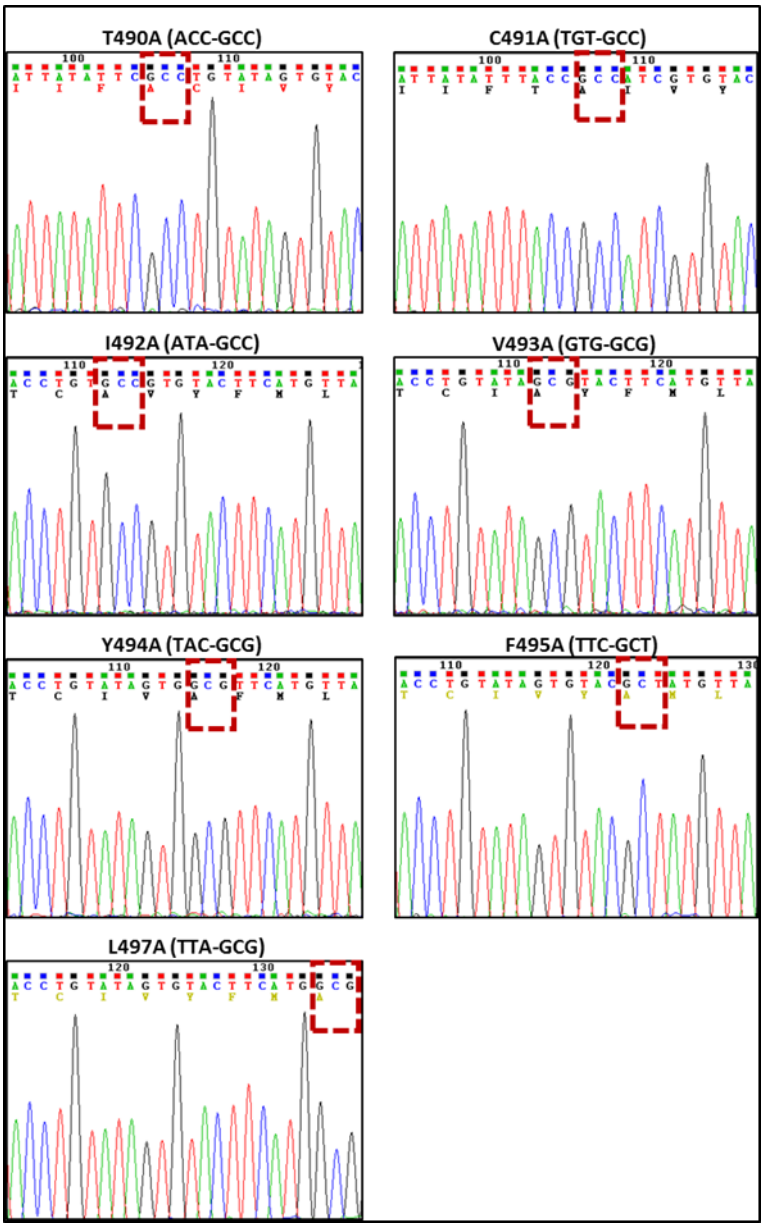
Appendices



Appendix 1: PvuII restriction digest profile of ABCG2 mutant isoforms

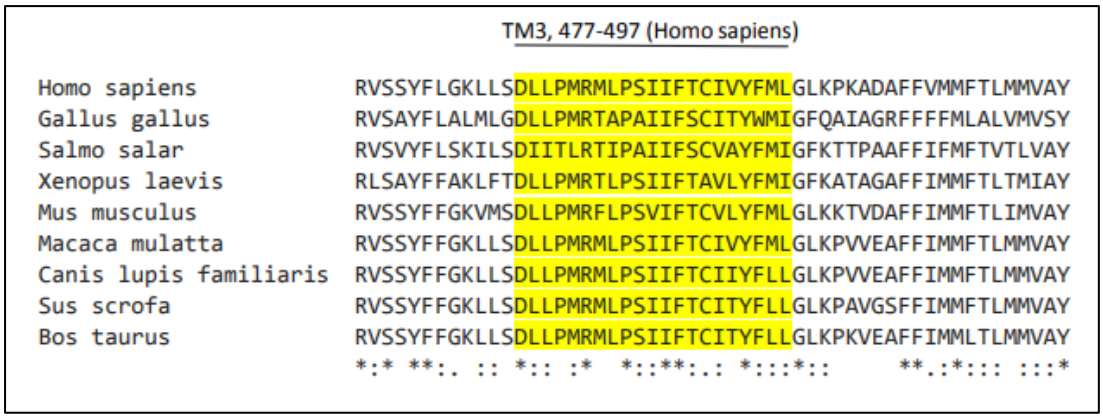
Restriction digestion with PvuII confirms the presence of p3.1zeo_sfGFP_ABCG2 vector in the variant forms. It cuts the vector at 3 positions (two in the plasmid backbone and one in the ABCG2 gene sequence (indicated with yellow lightning) with a recognition sequence of CAGCTG. The plasmid DNA for each mutant isoform was subjected to restriction digestion profile using the PvuII enzyme and analysed on 0.7% w/v agarose gel to confirm the presence of p3.1Zeo_sf_GFP_ABCG2 vector in each isoform. A) Depicts the agarose gel loaded with isoforms of p3.1Zeo_sf_GFP_ABCG2 vector (M481 and M483A). B) Depicts the agarose gel loaded with isoforms of p3.1Zeo_sf_GFP_ABCG2 vector (R482A, I487A, T490A, V493A, Y494A, M496A and P480A). C) Depicts the agarose gel loaded with isoforms of p3.1Zeo_sf_GFP_ABCG2 vector (C491A, I492A, V493A, F495A, M496A and L497A). 1 kb DNA ladder is used as the marker. Vector presence in all the isoforms is confirmed by the 3 bands of sizes 4.5 kb, 1.7kb and 1.4 kb obtained after the restriction digestion using PvuII enzyme.


L478A (TTA-GCC)
L479A (TTA-GCA)
P480A (CCC-GCG)
M481A (ATG-GCC)
M483A (ATG-GCG)
L484A (TTA-GGA)
S486A (AGT-GCC)
I487A (ATT-GCG)
I488A (ATA-GCC)
F489A (TTT-GCG)



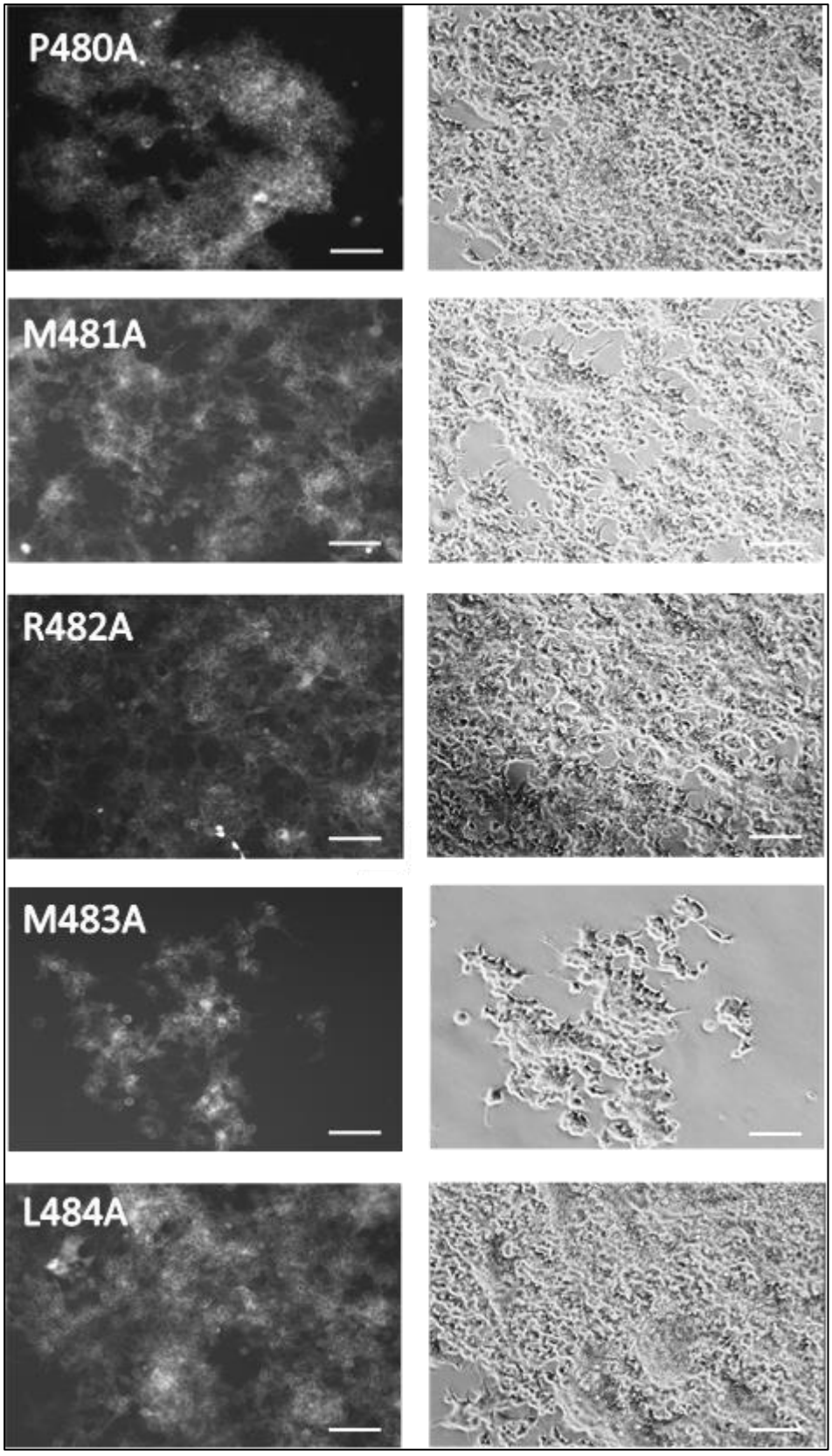
Appendix 2: Sequencing chromatograms (analysed through Chromas) to confirm the desired mutation

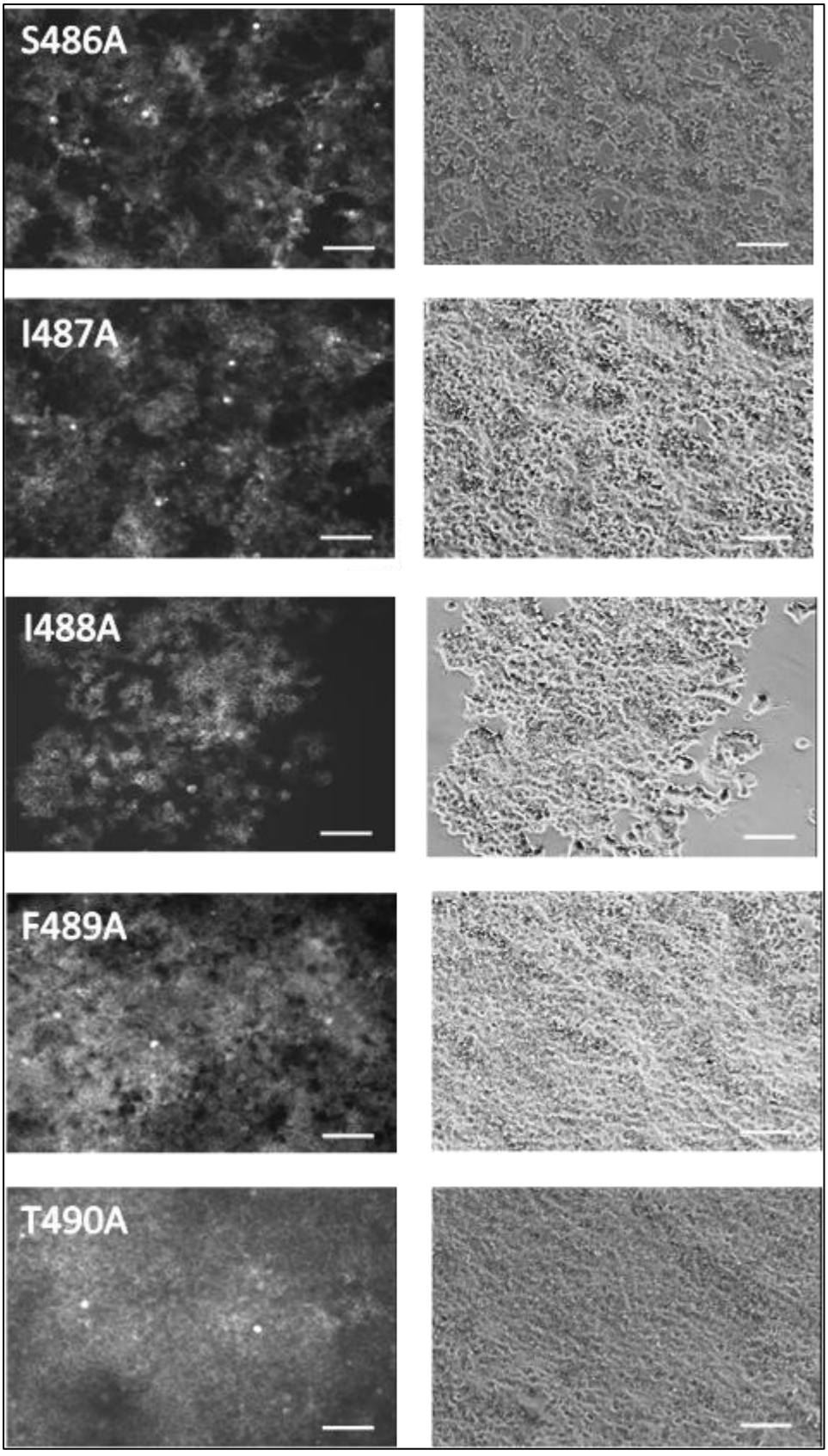
The sequence was obtained for the ABCG2 trans-membrane 3 helix using the Seq482 primer. The mutations in the above depicted chromatograms are highlighted in a red box. The sequence analysis for the amino acid D477 is depicted in figure 4.6B. Point mutations for amino acids R482 and M496 were analysed using the restriction digestion screen (figures 4.4 and 4.5).

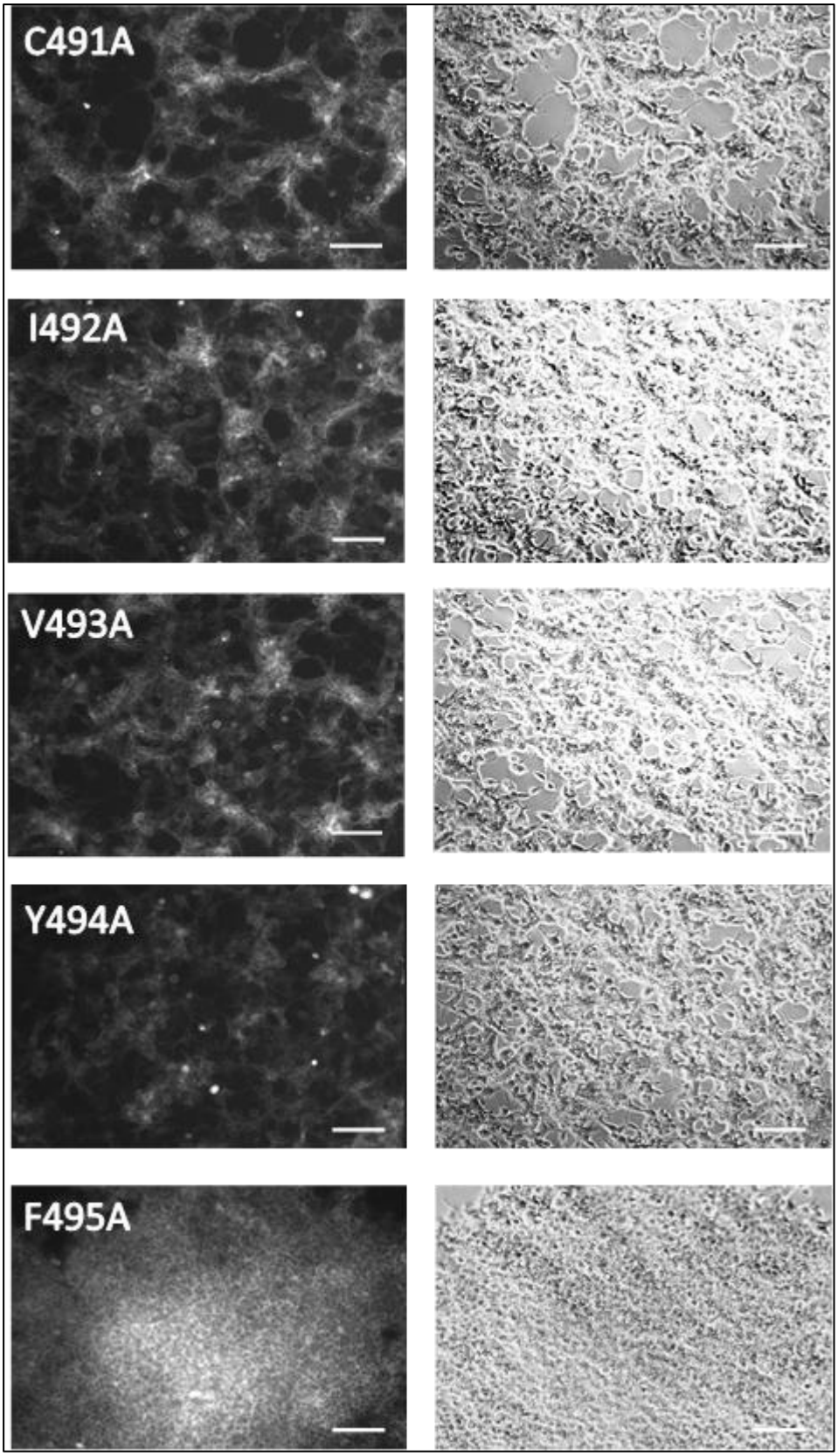


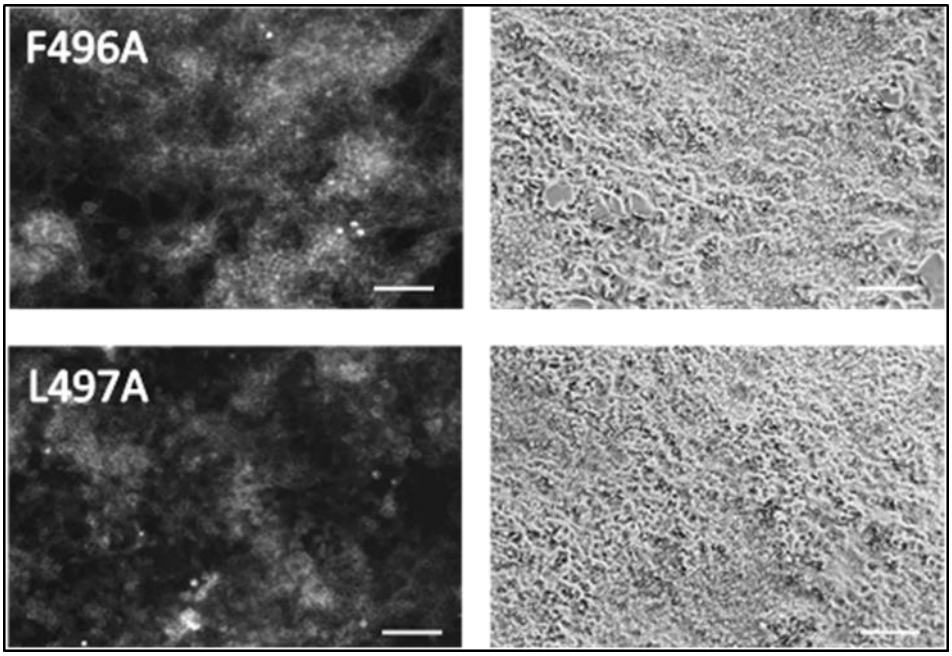
Appendix 3: Transmembrane helix 3 conservation across species

The yellow highlighted area depicts the TM3 helix residues highly across species. Sequence alignment was performed using ClustalO. Conservation is denoted by "*" and similarity by ":" or ".". Figure adapted from Cox et al., 2018.


P480A
M481A
R482A
M483A
L484A

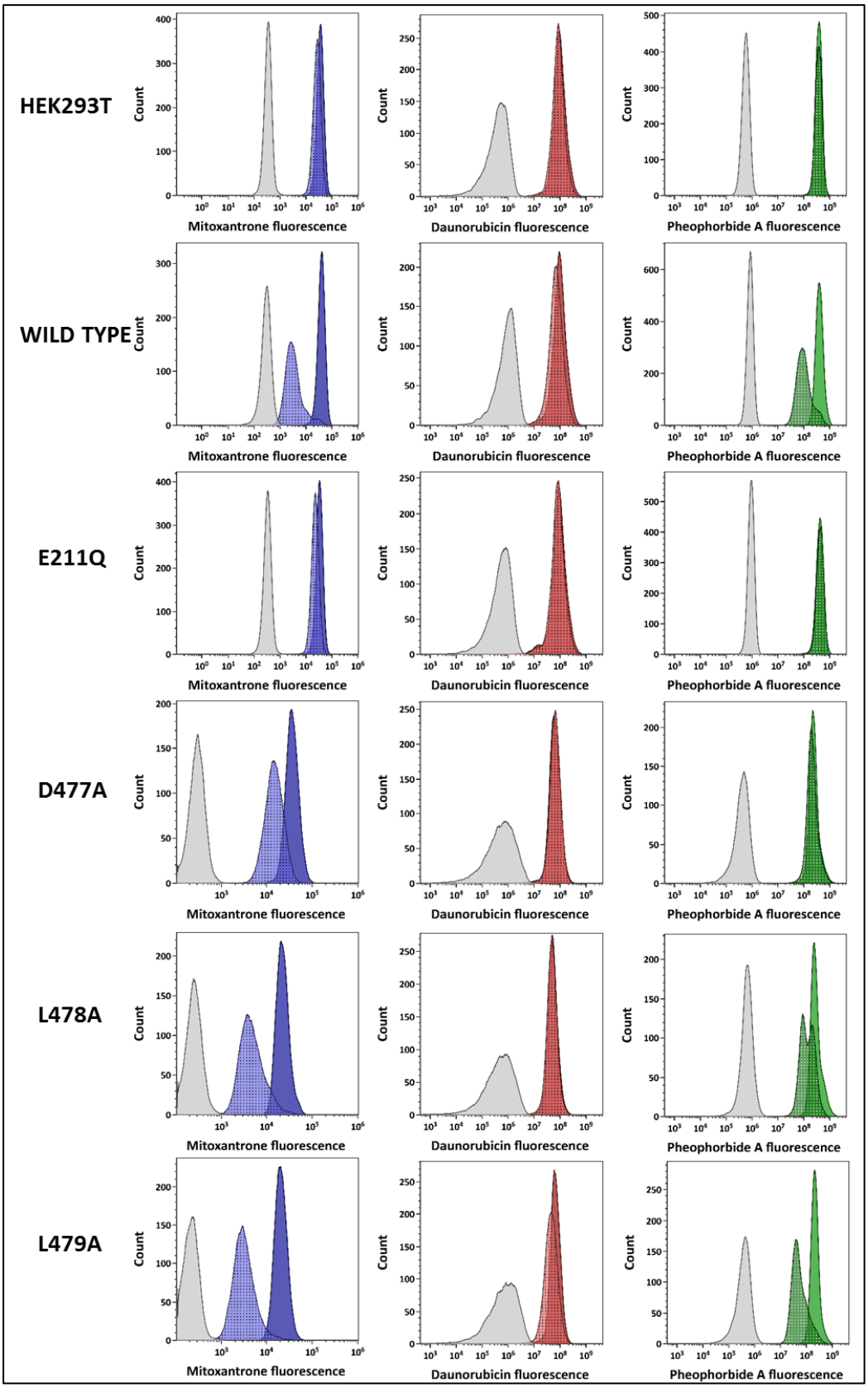

S486A
I487A
I488A
F489A
T490A

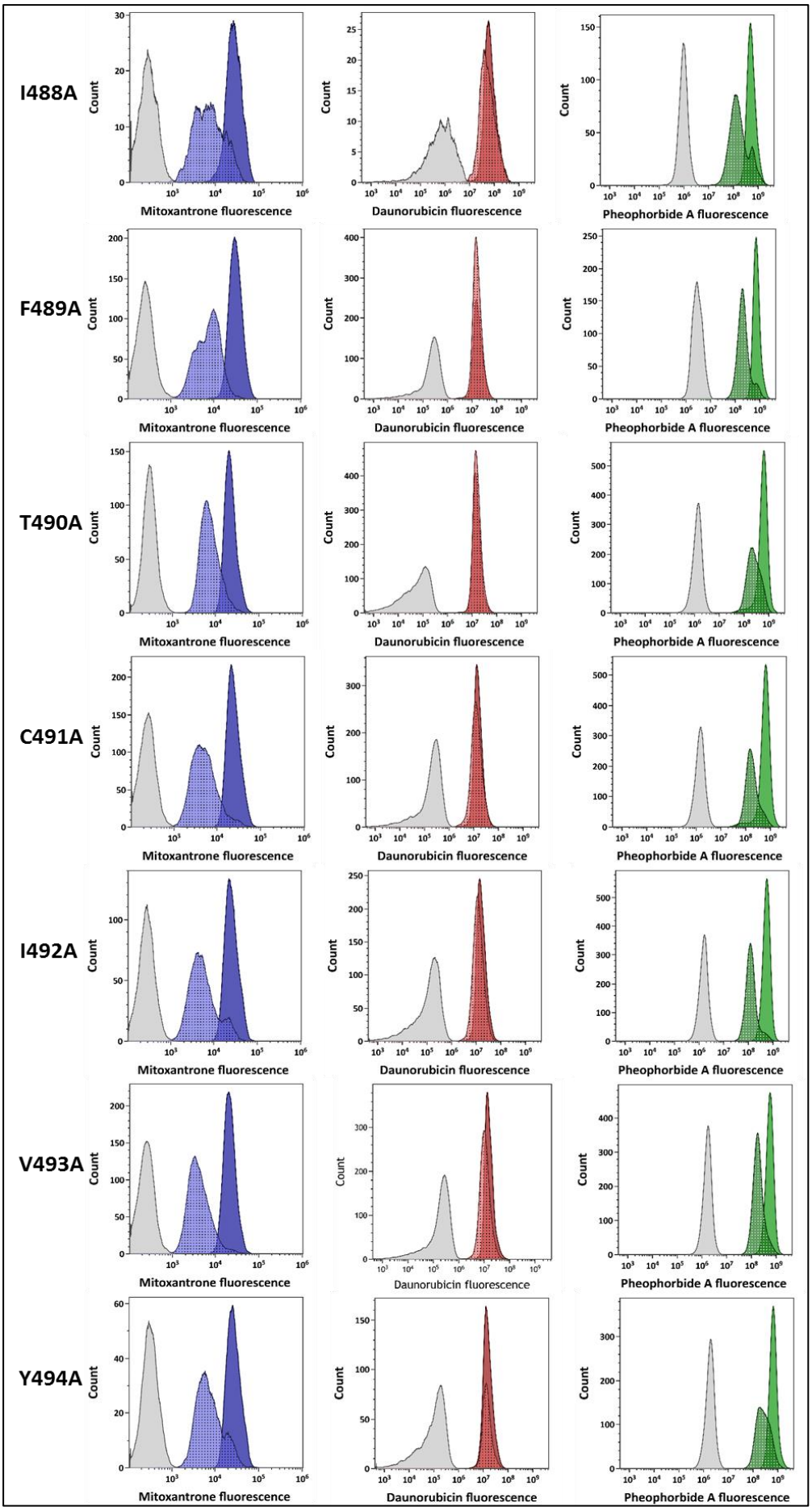

C491A
I492A
V493A
Y494A
F495A

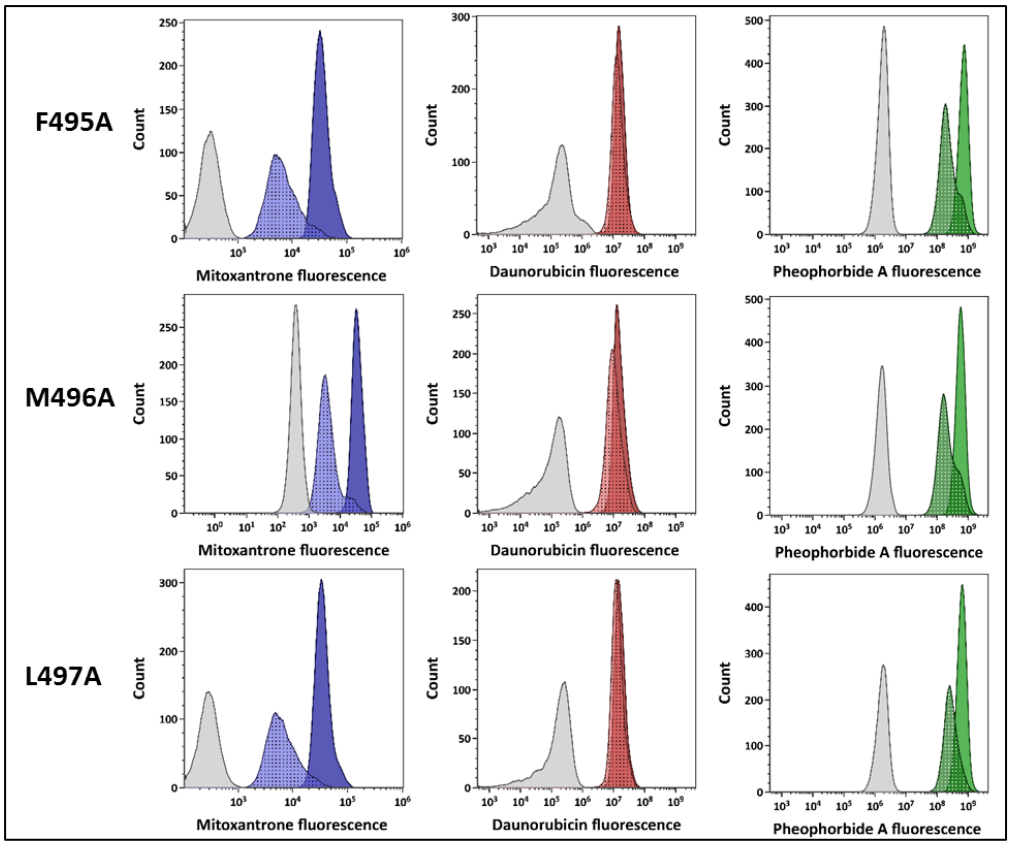


Appendix 4: Expression analysis for p3.1Zeo_sfGFP_ABCG2 transfected stable cell lines (wild type and mutants) indicated through fluorescence microscope

HEK293T cells transfected with the vector p3.1Zeo_sf_GFP_ABCG2 (wild type and mutant forms) were observed for GFP fluorescence under an epifluorescent microscope (phase 1, 10 X objective; Carl Zeiss, Birmingham, UK) connected to an inbuilt camera (AxioCam MRm, Zeiss) and analysed using the software Axio Vision release 4.8.2 SP3. Fluorescent (left panel) and phase contrast (right panel) images for all the mutants have been documented. Scale bars represent 10 µm.

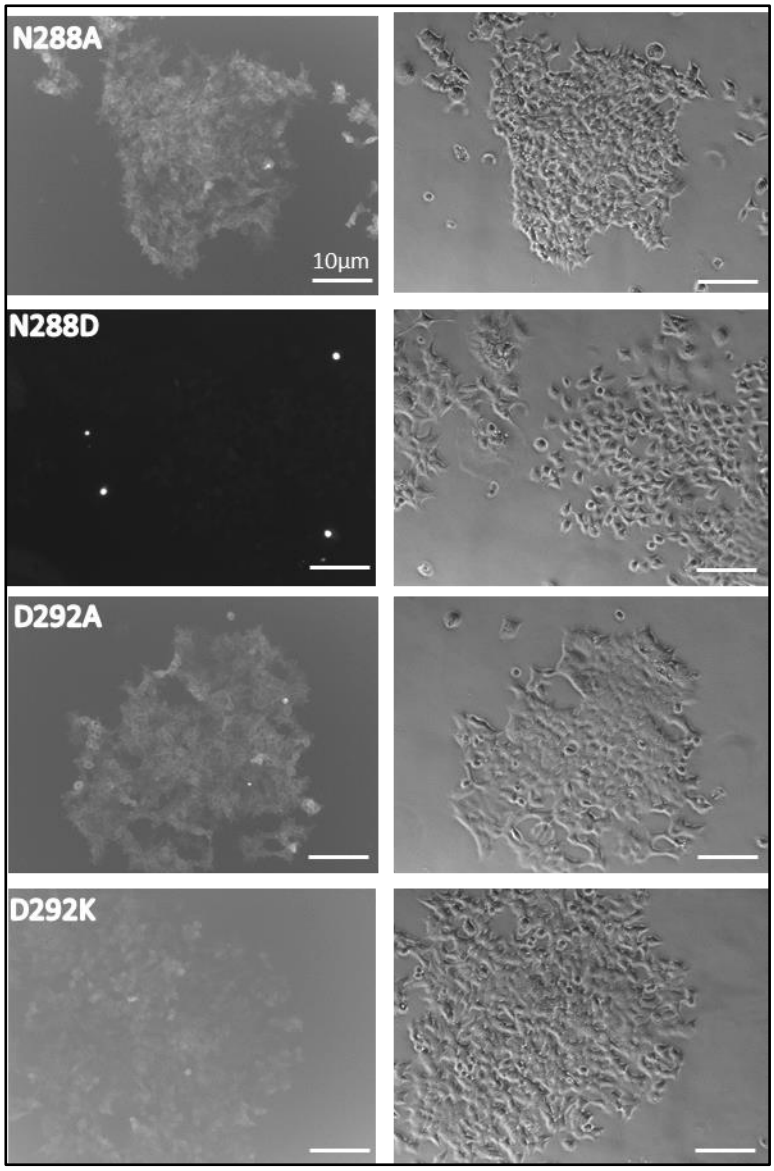

HEK293T
WILD TYPE
E211Q
D477A
L478A
L479A
Count
Mitoxantrone fluorescence
Daunorubicin fluorescence
Pheophorbide A fluorescence


I488A
F489A
T490A
C491A
I492A
V493A
Y494A
Count
Mitoxantrone fluorescence
Daunorubicin fluorescence
Pheophorbide A fluorescence



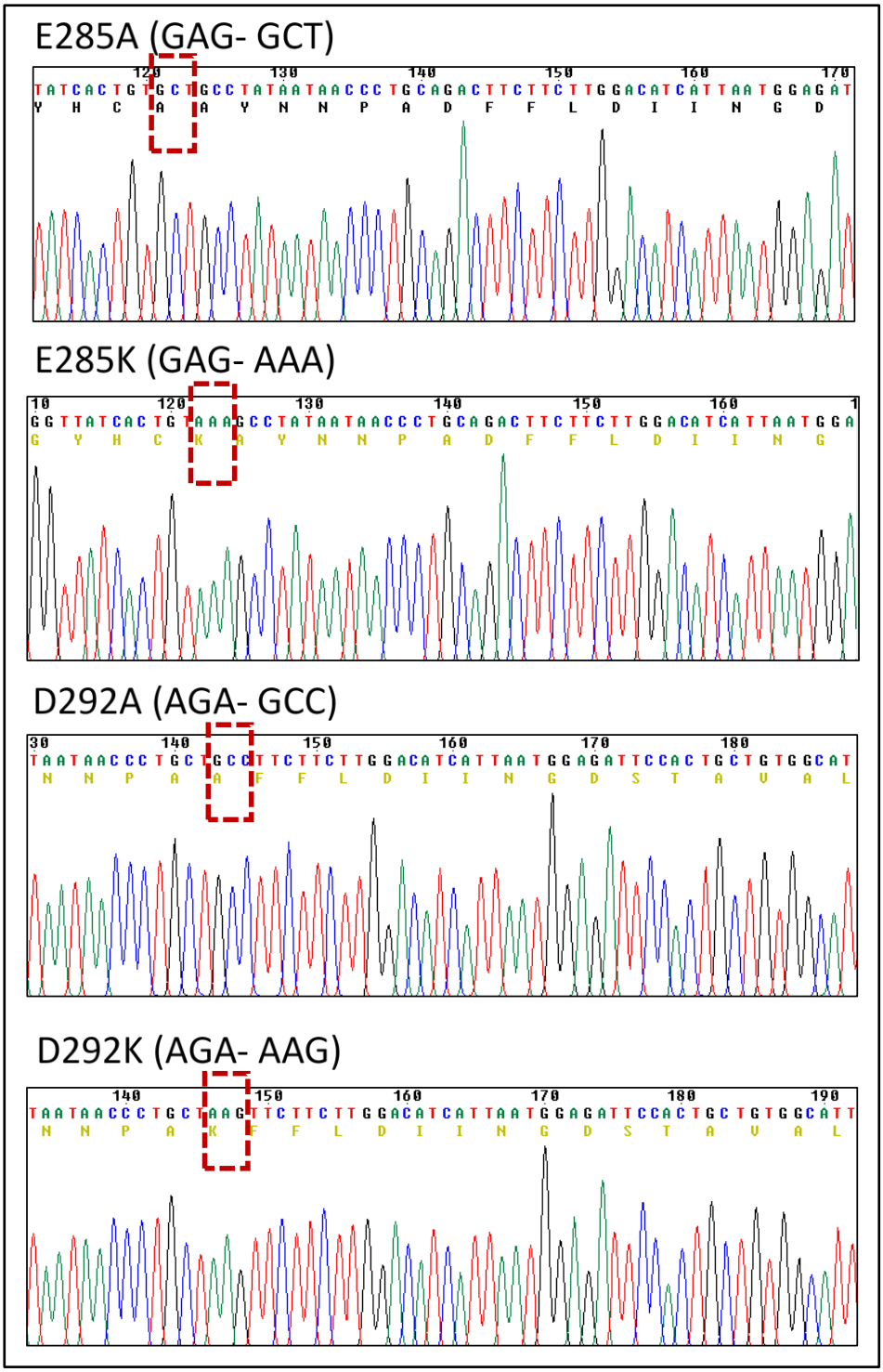
Appendix 5: ABCG2 TM3 helix mutant isoforms and their role in function

HEK293T cell lines expressing the TM3 mutant isoforms were incubated with the fluorescent substrates in the presence and absence of ABCG2 specific inhibitor Ko143. Kaluza single channel histogram plots for mitoxantrone, pheophorbide A and daunorubicin transport. The grey histograms for all the mutant isoforms depict auto-fluorescence. Equilibrium level of substrate accumulation is depicted by the dotted blue histogram (mitoxantrone), dotted green (pheophorbide A) and dotted red (daunorubicin) for all the mutant isoforms. Quantitative analysis of the rightward shift in substrate accumulation (fluorescence) in presence of ABCG2 specific inhibitor Ko143 is depicted by the dark blue histogram for mitoxantrone, dark green for pheophorbide A and dark red for daunorubicin in all the mutant isoforms. The data is representative of n=1. Data n=3 omitted for clarity.



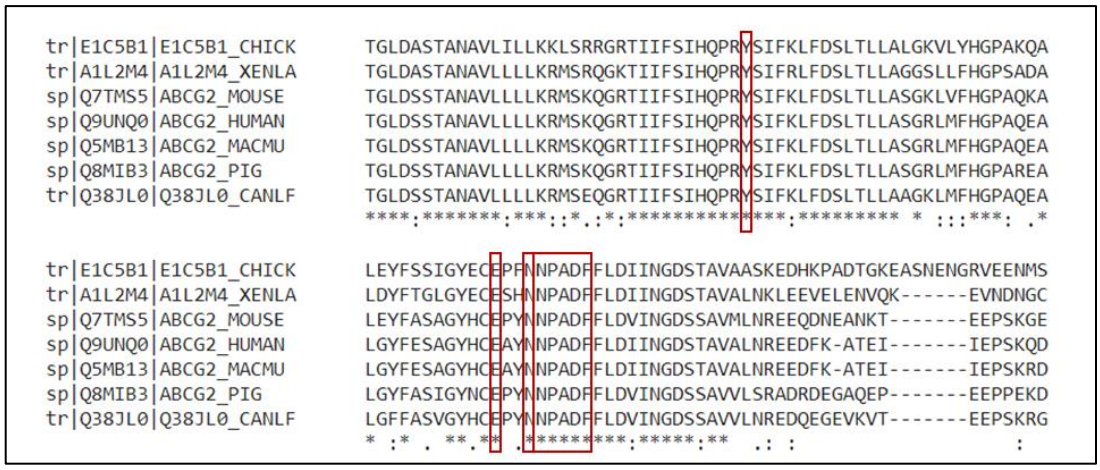
Appendix 6: Expression analysis for p3.1Zeo_sfGFP_ABCG2 transfected stable cell lines (wild type and mutants) indicated through fluorescence microscope

HEK293T cells transfected with the vector p3.1Zeo_sf_GFP_ABCG2 (wild type and mutant forms) were observed for GFP fluorescence under an epifluorescent microscope (phase 1, 10 X objective; Carl Zeiss, Birmingham, UK) connected to an inbuilt camera (AxioCam MRm, Zeiss) and analysed using the software Axio Vision release 4.8.2 SP3. Fluorescent (left panel) and phase contrast (right panel) images for all the mutants have been documented. Scale bars represent 10 µm.



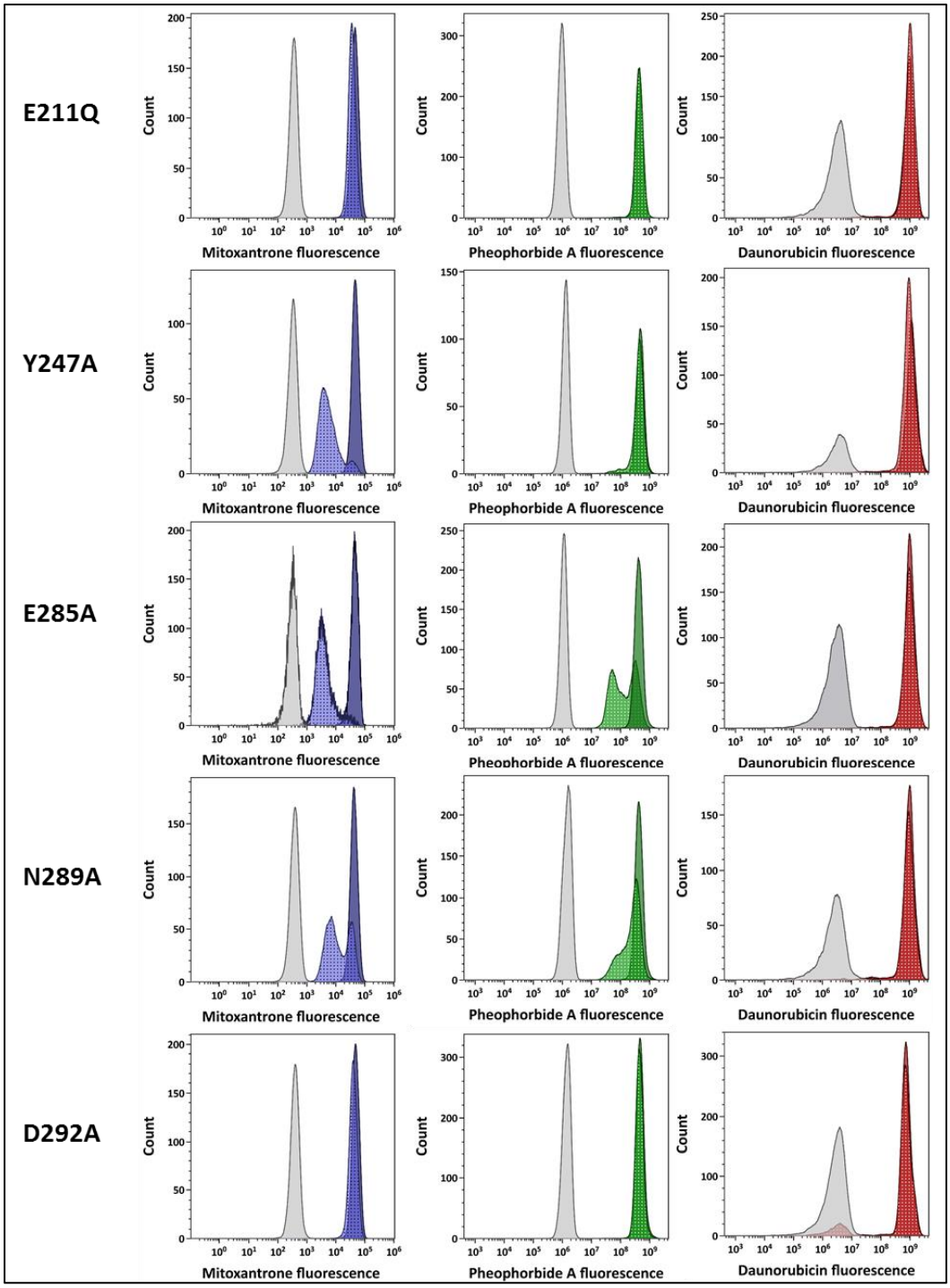
Appendix 7: Sequencing chromatograms (analysed through Chromas) to confirm the desired mutation

The sequence was obtained for the ABCG2 NBD interface residues using the SeqF2 primer. The mutations in the above depicted chromatograms are highlighted in a red box.



Appendix 8: Multiple sequence alignment for NBD interface residues across species

The NBD interface mutants (red box) were screened for conservation across the species. Only part of sequence alignment across the G subfamily that includes the conserved sequence NPXDF motif and the NBD interface residues within the cross-range interactions have been depicted here. Sequence alignment has been performed using Clustal O. Conservation is denoted by "*" and similarity by ":" or ".".



Appendix 9: Altered transport function in NBD interface mutants

Kaluza single channel histogram plots to monitor mitoxantrone, daunorubicin and pheophorbide A fluorescence based on the drug efflux capacity of the HEK293T cells expressing catalytically inactive mutant E211Q, NBD interface mutants (Y247A, E285A, N289A and D292A). Grey histogram represents the HEK293T cells with inherent fluorescence. The dotted blue, green and red histograms depict equilibrium level of substrate accumulation (mitoxantrone, pheophorbide A and daunorubicin respectively). Quantitative analysis of the rightward shift of ABCG2 specific substrate accumulation in presence of Ko143 is shown by solid colour histograms.